申报	系列：教师系列教学科研并重型
	专业：动物营养与饲料科学
	职称：副教授

业绩成果材料

（申报人的业绩成果材料包括论文、科研项目、获奖以及其他成果等）

单　位（二级单位）　动物科学学院

姓　名　**李龚**

材料核对人：　　单位盖章：

核对时间：

华南农业大学制

目　录

一、科研项目

1.主持：关于国家自然科学基金青C项目有关佐证材料.. 5
2.主持：关于广东省基础与应用基础研究基金面上项目有关佐证材料 7
3.主持：关于中国博士后科学基金面上项目有关佐证材料 18
4.主参：关于国家自然科学基金面上项目有关佐证材料. 19
5.主参：关于山东省教育厅“青创团队计划”团队项目相关佐证材料 22
6.主参：关于广东省农业厅项目相关佐证材料..... 26

二、论文、著作等

1.检索证明 43
2.以第一作者发表本专业论文情况
2.1. CRISPR-AMRtracker: A novel toolkit to monitor the antimicrobial resistance gene transfer in fecal microbiota 46
2.2.Waterborne polyurethane nanoparticles incorporating linoleic acid as a potential strategy for controlling antibiotic resistance spread in the mammalian intestine 61
2.3.Acquisition of a novel conjugative multidrug-resistant hypervirulent plasmid leads to hypervirulence in clinical carbapenem-resistant *Klebsiella pneumoniae* strains 73
2.4.Mechanisms of gastrointestinal toxicity in neuromyelitis optica spectrum disorder patients treated with mycophenolate mofetil: insights from a

mouse model and human study 84
2.5.Linoleic acid and α-linolenic acid inhibit conjugative transfer of an IncX4 plasmid carrying *mcr-1* 99
2.6.Integrative analysis of purine metabolites and gut microbiota in patients with neuromyelitis optica spectrum disorders after mycophenolate mofetil treatment 108

三、科研成果

1.知识产权

1.1.专利授权证书：一种监测细菌生长的设备及监测方法 116
1.2.专利授权证书：一种荧光菌株 E.coli C600 及构建方法与应用 117
1.3.专利授权证书：基于 mariner 转座子构建自杀型质粒及耐药突变菌株的方法 118
1.4.专利授权证书：一株供体菌、其构建方法与应用以及质粒抑制剂筛选方法 119
1.5.专利授权证书：基于 IS26 插入序列构建能表达荧光的自杀型质粒及菌株的方法 120
1.6.专利授权证书：基于 ISApl1 插入序列构建能表达荧光的自杀型质粒及菌株的方法 121
1.7.专利授权证书：一种基于 IncQ 型质粒泛宿主的功能基因递送载体、构建方法和应用 122
1.8.专利授权证书：一种抑制耐药质粒水平转移的复合材料及其制备方法和应用 123
1.9.专利授权证书：肉桂酸在制备耐药质粒接合转移抑制剂

中的应用 124
1.10.专利授权证书：一种靶向肠道菌群筛选影响黄嘌呤氧化酶活性药物的方法 125

四、其他业绩

1.个人荣誉
1.1.中国畜牧兽医学会兽医药理与毒理学分会“优秀论文” 126
1.2.中国畜牧兽医学会动物营养学分会“优秀报告” 127
2.社会服务
2.1 期刊任职：One Health 编委 128
3.应用转化
3.1 广东农垦应用证明 129

【佐证材料切记与目录页所列页码对应，不要用图片格式的材料进行打印。】

国家自然科学基金资助项目批准通知

（包干制项目）

李龚　先生/女士：

根据《国家自然科学基金条例》、相关项目管理办法规定和专家评审意见，国家自然科学基金委员会（以下简称自然科学基金委）决定资助您申请的项目。项目批准号：32402943，项目名称：Pi1Q蛋白I375T突变增强IncI2质粒接合转移能力的分子机制，资助经费：30.00万元，项目起止年月：2025年01月至 2027年 12月，有关项目的评审意见及修改意见附后。

请您尽快登录科学基金网络信息系统（https://grants.nsfc.gov.cn），**认真阅读《国家自然科学基金资助项目计划书填报说明》并按要求填写《国家自然科学基金资助项目计划书》（以下简称计划书）**。对于有修改意见的项目，请您按修改意见及时调整计划书相关内容；如您对修改意见有异议，须在电子版计划书报送截止日期前向相关科学处提出。

请您将电子版计划书通过科学基金网络信息系统（https://grants.nsfc.gov.cn）提交，由依托单位审核后提交至自然科学基金委。自然科学基金委审核未通过者，将退回的电子版计划书修改后再行提交；审核通过者，打印纸质版计划书（一式两份，双面打印）并在项目负责人承诺栏签字，由依托单位在承诺栏加盖依托单位公章，且将申请书纸质签字盖章页订在其中一份计划书之后，一并报送至自然科学基金委项目材料接收工作组。纸质版计划书应当保证与审核通过的电子版计划书内容一致。**自然科学基金委将对申请书纸质签字盖章页进行审核，对存在问题的，允许依托单位进行一次修改或补齐。**

向自然科学基金委提交电子版计划书、报送纸质版计划书并补交申请书纸质签字盖章页截止时间节点如下：

1. **2024年9月9日16点：**提交电子版计划书的截止时间；

2. **2024年9月16日16点：**提交修改后电子版计划书的截止时间；

3. **2024年9月23日：**报送纸质版计划书（一式两份，其中一份包含申请书纸质签字盖章页）的截止时间。

4. **2024年10月8日：**报送修改后的申请书纸质签字盖章页的截止时间。

请按照以上规定及时提交电子版计划书，并报送纸质版计划书和申请书纸质签字盖章页，逾期不报计划书或申请书纸质签字盖章页且未说明理由的，视为自动放弃接受资助；未按要求修改或逾期提交申请书纸质签字盖章页者，将视情况给予暂缓拨付经费等处理。

附件：项目评审意见及修改意见表

国家自然科学基金委员会

2024年8月23日

受理编号：c25140500002644

项目编号：2025A1515012412

文件编号：粤基金字〔2025〕10号

广东省基础与应用基础研究基金项目

任务书

项目名称： PilQ氨基酸突变驱动IncI2质粒接合转移的分子机制

项目类别： 广东省自然科学基金-面上项目

项目起止时间： 2025-01-01　至　2027-12-31

管理单位（甲方）： 广东省基础与应用基础研究基金委员会

依托单位（乙方）： 华南农业大学

通讯地址： 广东省广州市天河区五山路483号

邮政编码： 510642　　**单位电话：** 020-85283435

项目负责人： 李龚　　**联系电话：** 15089893236

2025A1515012412

（广东科技微信公众号）　　（查看任务书信息）　　（受理纸质材料二维码）

广东省基础与应用基础研究
基金委员会
二〇二〇年制

填写说明

一、项目任务书内容原则上要求与申报书相关内容保持一致，不得无故修改。

二、项目承担单位通过广东省科技业务管理阳光政务平台下载项目任务书，按要求完成签名盖章后扫描上传到广东省科技业务管理阳光政务平台。

三、签名盖章说明。请分别在单位工作分工及经费分配情况页、人员信息页、签约各方页等地方按要求签字或盖章，签章不合规或错漏将不予受理。其中，人员信息页要求所有参与人员本人亲笔签名，代签或印章无效，漏签将不予受理。

四、本任务书自签字并加盖公章之日起生效，各方均应负本任务书的法律责任，不应受机构、人事变动影响。

五、根据《广东省科学技术厅广东省财政厅关于深入推进省基础与应用基础研究基金项目经费使用“负面清单+包干制”改革试点工作的通知》(粤科规范字〔2022〕2号)，2022年度及以后立项资助的全部省基金项目(包括省自然科学基金、省市联合基金、省企联合基金项目等)均适用“负面清单+包干制”，项目提交申请书和任务书时无需编制费用明细科目预算。

2025A1515012[illegible]

一、主要研究内容和要达到的目标

研究内容

（1）RpoS在PilQ蛋白I375T突变增强IncI2质粒接合转移能力中的作用

比较PilQ蛋白I375T突变株、野生株IncI2质粒的接合转移频率以及T4SS基因的相对表达量，获得PilQ蛋白I375T突变增强IncI2质粒接合转移能力的证据；构建PilQ敲除株、PilQ回补株、PilQ I375T回补株，并比较IncI2质粒接合转移频率，明确PilQ蛋白I375T突变的功能；比较PilQ蛋白I375T突变株及其野生株rpoS基因的相对表达量，并构建rpoS荧光报告系统，测定细菌胞内rpoS启动子转录活性，从而分析PilQ蛋白I375T突变是否激活rpoS的表达；在PilQ I375T突变株中敲除rpoS基因，构建rpoS敲除株，并通过功能回补实验构建rpoS回补株，进一步通过比较rpoS野生株，rpoS敲除株，rpoS回补株IncI2质粒接合转移频率，以揭示RpoS在PilQ蛋白I375T突变增强IncI2质粒接合转移能力中的作用。

（2）ROS响应的sRNA对RpoS介导IncI2质粒接合转移能力增强的调控机制

已有研究表明ROS响应的sRNA调控RpoS的表达，为阐明PilQ I375T突变导致rpoS表达的激活是否依赖于ROS响应sRNA的调控，申请人拟：比较PilQ蛋白I375T突变株及其野生株胞内ROS含量，以及dsrA，arcZ，hfq等sRNA基因的相对表达量，初步建立PilQ I375T突变和胞内氧化水平的联系；在PilQ I375T突变株的接合体系中加入ROS猝灭剂，并测定rpoS基因的相对表达量以及IncI2质粒接合转移频率，进一步揭示ROS在质粒接合转移能力增强中的角色；在PilQ I375T突变株中分别敲除相对表达量显著增高的sRNA基因，从而得到sRNA基因敲除株，分别测定野生株、PilQ I375T突变株以及sRNA基因敲除株质粒接合转移能力，rpoS的相对表达量，以阐明ROS响应的sRNA对RpoS介导IncI2质粒接合转移增强的调控机制。

（3）PilQ蛋白I375T突变诱导ROS产生的内在机制

在上述基础上，通过构建PilQ和PilQ I375T表达载体，表达纯化PilQ和PilQ I375T蛋白，并比较两者水解ATP的能力，以揭示PilQ I375T对能量代谢的影响；比较PilQ蛋白I375T突变株及其野生株胞内ATP含量，细胞膜通透性，质子驱动力（PMF），电子呼吸链相关酶活性以及ubiD、nuoC、cyoD等电子呼吸链基因的相对表达量，建立PilQ蛋白I375T突变与电子呼吸链活性的联系；以PilQ敲除株、PilQ回补株、PilQ I375T回补株为对象，开展上述电子呼吸链表征明显的实验，进一步分析PilQ I375T对电子呼吸链的影响；敲除PilQ蛋白I375T突变株中电子呼吸链基因表达量显著增高的基因，并比较呼吸链基因敲除株、PilQ I375T突变株胞内ROS含量，从而揭示PilQ蛋白I375T突变导致ROS产生的内在机制，最终构建起PilQ蛋白I375T突变增强IncI2质粒接合转移能力的调控网络。

研究目标

（1）揭示RpoS在PilQ蛋白I375T突变增强IncI2质粒接合转移能力中的作用；

（2）阐明ROS响应的sRNA对RpoS介导IncI2质粒接合转移能力增强的调控机制；

（3）解析PilQ蛋白I375T突变诱导ROS产生的内在机制。

2025A1515012412

二、项目预期获得的研究成果及形式

<table>
<tr><td rowspan="3">论文及专著情况</td><td colspan="2">国家统计源刊物以上刊物发表论文（篇）</td><td colspan="2">2</td><td colspan="2">科技报告（篇）</td><td colspan="2">1</td></tr>
<tr><td colspan="2">其中被SCI/EI/ISTP收录论文数（篇）</td><td colspan="2">1</td><td colspan="2">培养人才（人）</td><td colspan="2">1</td></tr>
<tr><td colspan="2">专著（册）</td><td colspan="2"></td><td colspan="2">引进人才（人）</td><td colspan="2">0</td></tr>
<tr><td rowspan="3">专利情况(项)</td><td colspan="2">发明专利</td><td colspan="2">实用新型专利</td><td colspan="2">外观设计专利</td><td colspan="2">国外专利</td></tr>
<tr><td>申请</td><td>授权</td><td>申请</td><td>授权</td><td>申请</td><td>授权</td><td>申请</td><td>授权</td></tr>
<tr><td></td><td></td><td></td><td></td><td></td><td></td><td></td><td></td></tr>
</table>

2025A1515012412

三、项目进度和阶段目标

（一）项目起止时间： 2025-01-01 至 2027-12-31		
（二）项目实施进度及阶段主要目标:		
开始日期	结束日期	主要工作内容
2025-01-01	2025-12-31	（1）验证PilQ I375T对IncI2质粒接合转移的作用； （2）分析PilQ蛋白I375T突变株内rpoS的表达是否激活； （3）验证RpoS在IncI2质粒接合转移能力增强中的作用； （4）整理数据，撰写年终报告。
2026-01-01	2026-12-31	（1）分析PilQ蛋白I375T突变株内ROS及sRNA是否激活； （2）验证ROS在IncI2质粒接合转移频率增强中的作用； （3）鉴定激活RpoS的关键sRNA； （4）参加中国畜牧兽医学会兽医药理毒理学分会学术研讨会； （5）整理数据，撰写年终报告。
2027-01-01	2027-12-31	（1）比较PilQ I375T和PilQ的酶活力； （2）分析PilQ蛋白I375T突变株内ETC功能是否紊乱； （3）鉴定PilQ蛋白I375T突变株内ETC诱导ROS产生的关键基因； （4）整理数据，总结课题，撰写发表研究论文。

2025A1515012412

四、项目总经费及省基金委经费预算

1.省基金委经费下达总额： （大写）壹拾万圆整；（小写 ）10万元；					
2.省基金委经费年度下达计划：					
年度	2025 年	年	年	年	年
经费(万元)	10.00				

2025A1515012412

五、人员信息

项目负责人								
姓名	证件号码	年龄	性别	职称	学历	在项目中承担的任务	所在单位	签名
李龚	612324199402057012	31	男	未取得	博士研究生	项目负责人	华南农业大学	

项目组主要成员								
姓名	证件号码	年龄	性别	职称	学历	在项目中承担的任务	所在单位	签名
夏丽娟	360122199508172126	30	女	未取得	硕士研究生	接合实验及氧化应激研究	华南农业大学	
周士迎	372923199511015651	30	男	未取得	硕士研究生	基因编辑相关工作	华南农业大学	
高昂	412722200006120013	25	男	未取得	本科	能量代谢研究	华南农业大学	

2025A1515012412

六、工作分工及财政经费分配

承担/参与单位名称（盖章）	工作分工	省级财政科技资金分配（万元）
华南农业大学	负责项目所涉及的研究内容：（1）揭示RpoS在PilQ蛋白I375T突变增强IncI2质粒接合转移能力中的作用；（2）阐明ROS响应的sRNA对RpoS介导IncI2质粒接合转移能力增强的调控机制；（3）解析PilQ蛋白I375T突变诱导ROS产生的内在机制。	10.00
	合计	10.00

2025A1515012412

七、任务书条款

第一条 甲方与乙方根据《中华人民共和国民法典》及国家有关法规和规定，按照《广东省自然科学基金及联合基金项目管理实施细则》（粤科规范字〔2024〕5号）《省级科技计划项目任务书管理细则》（粤科规范字〔2022〕8号）等规定，为顺利完成（2025）年PilQ氨基酸突变驱动IncI2质粒接合转移的分子机制专项项目（项目编号：2025A1515012412）经协商一致，特订立本任务书，作为甲乙双方在项目实施管理过程中共同遵守的依据。

第二条 甲方的权利义务：1.按任务书规定进行经费核拨的有关工作协调。2.根据甲方需要，在不影响乙方工作的前提下，定期或不定期对乙方项目的实施情况和经费使用情况进行检查或抽查。3.根据《广东省科学技术厅科技计划项目科研诚信管理办法》（粤科规范字〔2024〕2号）《广东省基础与应用基础研究基金项目科研不端行为调查处理实施细则（试行）》（粤科规范字〔2023〕1号）等规定对乙方进行科技计划信用管理。

第三条 乙方的权利义务：1.确保落实自筹经费及有关保障条件。2.按任务书规定，对甲方核拨的经费实行专款专用，单独列账，并随时配合甲方进行监督检查。3.经费使用按照广东省级财政科研项目经费使用及省基金项目经费使用“负面清单+包干制”等有关规定进行管理。4.项目依托单位应制定经费使用“负面清单+包干制”内部管理制度并报甲方备案。5.使用财政资金采购设备、原材料等，按照《广东省实施〈中华人民共和国招标投标法〉办法》有关规定，符合招标条件的须进行招标。6.项目任务书任务完成后，或任务书规定的任务、指标及经费投入等提前完成的，乙方可提出验收结题申请，并按甲方要求做好项目验收结题工作。7.若项目发生需要终止结题的情况，乙方须提出终止结题申请，并按甲方要求做好项目终止结题工作。8.在每年规定时间内向甲方如实提交上年度工作情况报告，报告内容包含上年度项目进展情况、经费决算和取得的成果等。9.按照国家和省有关规定，提交科技报告及其他材料。10.利用甲方的经费获得的研究成果，项目负责人和参与者应当注明获得“广东省基础与应用基础研究基金（英文：Guangdong Basic and Applied Basic Research Foundation）（项目编号）”资助或作有关说明。11.乙方要恪守科学道德准则，遵守科研活动规范，践行科研诚信要求，不得抄袭、剽窃他人科研成果或者伪造、篡改研究数据、研究结论；不得购买、代写、代投论文，虚构同行评议专家及评议意见；不得违反论文署名规范，擅自标注或虚假标注获得科技计划（专项、基金等）等资助；不得弄虚作假，骗取科技计划（专项、基金等）项目、科研经费以及奖励、荣誉等；不得有其他违背科研诚信要求的行为。12.确保本项目开展的研究工作符合我国科技伦理管理相关规定。

第四条 在履行本任务书的过程中，如出现广东省相关政策法规重大改变等不可抗力情况，甲方有权对所核拨经费的数量和时间进行相应调整。

第五条 在履行本任务书的过程中，当事人一方发现可能导致项目整体或部分失败的情形时，应及时通知另一方，并采取适当措施减少损失，没有及时通知并采取适当措施，致使损失扩大的，应当就扩大的损失承担责任。

第六条 本项目技术成果的归属、转让和实施技术成果所产生的经济利益的分享，除双方另有约定外，按国家和广东省有关法规执行。

2025A1515012412

第七条 根据项目具体情况，经双方另行协商订立的附加条款，作为本任务书正式内容的一部分，与本任务书具有同等效力。

第八条 本任务书一式三份，各份具有同等效力。甲、乙方及项目负责人各执一份，三方签字、盖章后即生效，有效期至项目结题后一年内。各方均应负任务书的法律责任，不应受机构、人事变动的影响。

第九条 乙方必须接受甲方聘请的本项目任务书监理单位的监督和管理。监理单位按照甲方赋予的权利对本项目任务书的履行进行审核、进度调查，对项目任务书变更、经费使用情况进行监督管理及组织项目验收。

说明：1.本任务书中，凡是当事人约定无需填写的内容，应在空白处划（/）。

2.委托代理人签订本任务书的，应出具合法、有效的委托书。

2025A1515012412

八、本任务书签约各方

管理单位（甲方）：　　广东省基础与应用基础研究基金委员会 （盖章）

法定代表人（或法人代理）：　　曾路　　（签章）

2025 年　03 月　21 日

依托单位（乙方）：　华南农业大学　　（盖章）

法定代表人（或法人代理）：　薛红卫　　（签章）

联系人（项目主管）姓名：　夏杰　　（签章）

Email：kjcgxk@scau.edu.cn

电话：　020-85283435　/　13711345768

开户单位名称：　华南农业大学

开户银行名称：　广东广州工行五山支行

开户银行账号：　3602002609000310520

年　月　日

联系人（项目负责人）姓名：　李龚　（签名）

Email：ligong@scau.edu.cn

电话：15089893236

年　月　日

2025A1515012412

资助证书

华南农业大学　李龚　（博士后编号：342690 ）获得中国博士后科学基金第74批面上资助。 资助编号：2023M741221

特颁此证。

This certificate verifies that its holder has been awarded a fellowship from the China Postdoctoral Science Foundation(Certificate Number: 2023M741221).

中国博士后科学基金会

2023 年 11 月 27 日

国家自然科学基金资助项目批准通知

（预算制项目）

方亮星　先生/女士：

根据《国家自然科学基金条例》、相关项目管理办法规定和专家评审意见，国家自然科学基金委员会（以下简称自然科学基金委）决定资助您申请的项目。项目批准号：32373063，项目名称：ArcA调控TCA循环和氧化应激介导多重耐药IncHI2质粒与鼠伤寒沙门菌补偿性进化的机制研究，直接费用：50.00万元，项目起止年月：2024年01月至 2027年 12月，有关项目的评审意见及修改意见附后。

请您尽快登录科学基金网络信息系统（https://grants.nsfc.gov.cn），**认真阅读《国家自然科学基金资助项目计划书填报说明》并按要求填写《国家自然科学基金资助项目计划书》（以下简称计划书）**。对于有修改意见的项目，请您按修改意见及时调整计划书相关内容；如您对修改意见有异议，须在电子版计划书报送截止日期前向相关科学处提出。

请您将电子版计划书通过科学基金网络信息系统（https://grants.nsfc.gov.cn）提交，由依托单位审核后提交至自然科学基金委。自然科学基金委审核未通过者，将退回的电子版计划书修改后再行提交；审核通过者，打印纸质版计划书（一式两份，双面打印）并在项目负责人承诺栏签字，由依托单位科研、财务管理等部门审核、签章并在承诺栏加盖依托单位公章，且将申请书纸质签字盖章页订在其中一份计划书之后，一并报送至自然科学基金委项目材料接收工作组。纸质版计划书应当保证与审核通过的电子版计划书内容一致。**自然科学基金委将对申请书纸质签字盖章页进行审核，对存在问题的，允许依托单位进行一次修改或补齐。**

向自然科学基金委提交电子版计划书、报送纸质版计划书并补交申请书纸质签字盖章页截止时间节点如下：

1. **2023年9月7日16点：**提交电子版计划书的截止时间；

2. **2023年9月14日16点：**提交修改后电子版计划书的截止时间；

3. **2023年9月21日：**报送纸质版计划书（一式两份，其中一份包含申请书纸质签字盖章页）的截止时间。

4. **2023年10月7日：**报送修改后的申请书纸质签字盖章页的截止时间。

请按照以上规定及时提交电子版计划书，并报送纸质版计划书和申请书纸质签字盖章页，逾期不报计划书或申请书纸质签字盖章页且未说明理由的，视为自动放弃接受资助；未按要求修改或逾期提交申请书纸质签字盖章页者，将视情况给予暂缓拨付经费等处理。

附件：项目评审意见及修改意见表

国家自然科学基金委员会

2023年8月24日

主要参与者（注：主要参与者不包括项目申请人）

编号	姓名	出生年月	性别	职 称	学 位	工作单位	项目分工	办公电话	证件号码
1	李龚	1994-02-05	男	无	博士	华南农业大学	基因编辑与生信分析		6**********2

总人数统计（注：包括项目申请人、主要参与者及其他参与人员；勿重复计数）

总人数	高级职称	中级职称	初级职称	博士后	博士生	硕士生	本科生及其他学生	其他
7	1	0	0	1	1	4	0	0

NSFC 2023

山 东 省 教 育 厅

鲁教科函〔2024〕58号

山东省教育厅
关于公布2024年度山东省高等学校
“青创团队计划”团队立项名单的通知

各有关高等学校:

经各高校推荐、专家评审、省教育厅厅长办公会审议和公示，决定认定山东大学“肿瘤微环境响应性超分子治疗创新团队”等部属高校团队、山东科技大学“工矿环境气溶胶污染溯源基础研究创新团队”等省属高校团队为2024年度山东省高等学校“青创团队计划”团队（见附件），现将立项名单予以公布。

各依托高校和团队要根据《山东省教育厅关于印发<山东省高等学校青年创新团队发展计划实施方案>的通知》（鲁教科字〔2022〕1号）要求，登录“山东省高等学校优秀青年创新团队申报管理系统”（以下简称“系统”，网址为：https:\\kygl.sdei.edu.cn\qncxtd），认真编制《山东省高等学校青年创新团队发展计划任务合同书》（以下简称《任务合同书》），团队牵头人（乙方）签字并经依托高校（丙方）审核后加

盖依托高校公章，以依托高校为单位将本校团队的《任务合同书》纸质版一式三份送至教育厅科学技术处（济南市市中区舜耕路60号614房间）审核盖章，于2025年1月10日前，将盖章完毕的《任务合同书》PDF版本上传至系统，每份《任务合同书》均以“编号+学校名称+团队名称”的形式命名。经审核备案后的《任务合同书》，将作为团队支持和管理的依据。支持经费由各高校统筹安排，支持标准由学校视项目开展情况自行确定。

联系人：石金雨，联系电话：0531-51793859。

技术支持：王睿晨、赵同祥，联系电话：0531-89701233、89701715。

附件：2024年度山东省高等学校“青创团队计划”团队立项名单

山东省教育厅

2024年12月19日

附件

2024年度山东省高等学校“青创团队计划”团队立项名单

序号	所在单位	编号	团队名称	研究课题名称	团队带头人	团队核心成员
1	聊城大学	2024KJH132	6G通信太赫兹光子技术与应用创新团队	6G高速太赫兹探测器件研发与应用	宋琦	王晓伟,张帆,李校博,戴子杰,吴志洋
2	聊城大学	2024KJH174	海洋能源岩土工程创新团队	新型海上风电基础研发及承载机理研究	吴宇旗	边江,任玉宾,栾鲁宝,李珊珊,翟汉波,朱彬
3	聊城大学	2024KJG064	高分子生物医用材料创新团队	凝胶基多酶柔性传感器件的有序构筑及其对慢性伤口的智能诊疗研究	张琦	吴越,尚英辉,赵加民,魏俊杰,王巧芝,张玉珏
4	聊城大学	2024KJH145	先进电介质材料研究与应用创新团队	高性能低损耗无铅压电陶瓷设计及能量收集与转换技术研究	李朋	黄海华,周旭峰,杜姗姗,王阳波,白海瑞,高潇逸

序号	所在单位	编号	团队名称	研究课题名称	团队带头人	团队核心成员
5	聊城大学	2024KJN032	艺术治疗青年创新团队	艺术治疗对提高乡村自闭性障碍儿童社会性能力的干预研究	潘佩佩	袁秀鸣,李傲翼,桑发德,李文哲,丁浩东,徐海鸽
6	聊城大学	2024KJD010	中华优秀传统文化助推社会治理创新团队	儒家文化价值观推动铸牢中华民族共同体意识的心理学取径研究	亓立东	闫琳,李雅宁,许文涛,王玲晓,辛聪,王鹏飞
7	聊城大学	2024KJJ047	胶质瘤代谢及靶向治疗精准医学创新团队	WDR82 促进胶质瘤谷氨酰胺代谢及其靶向治疗的功能和机制研究	杨睿	于亚慧,王冉,张珊珊,高亿茹
8	聊城大学	2024KJN042	脑信号解码与分析创新团队	被动式认知负荷解码研究	周月莹	徐达,姜筱,孙丝雨,刘诗涛
9	聊城大学	2024KJN040	康养旅居创新团队	复杂自适应系统视域下康养旅居体系构建与地方响应研究	唐若菡	张云飞,宋永林,苏泽明,刘晓临,田耘
10	聊城大学	2024KJI019	动物细菌性疾病绿色防控技术创新团队	禽致病菌的噬菌体筛选改造及制剂研发	王民歌	赵霞,李龚,周国栋,杨耀森,张鸿焱

附件

合同编号：2025-WPY-00-001

2025年省级财政专项种业振兴行动项目

合 同 书

项目名称：猪肠道关键微生物种质资源挖掘、培养与高效利用

项目管理单位（甲方）：广东省农业农村厅

项目牵头承担单位（乙方）：华南农业大学

项目推荐(主管)单位(丙方)：

项目负责人：赵江潮　　联系电话：15918006508

项目联系人：全建平　　联系电话：15102030907

广东省农业农村厅制

第一条　为保障2025年省级财政专项种业振兴行动项目顺利实施，按时保质保量完成项目任务，根据《中华人民共和国民法典》《广东省省级财政专项资金管理办法（2025年修订）》（粤府〔2025〕56号）、《广东省农业农村厅种业振兴行动专项资金管理办法（试行）》等文件有关规定，经甲、乙、丙三方协商一致，签署本合同书。

第二条 甲方的权利义务：本合同履行过程中，甲方有权对乙方项目的实施情况和资金到位、使用情况进行监督、检查，提出改进要求。

第三条　乙方的权利义务：

1.按财政资金管理规定，对甲方核拨的资金做到专款专用，单独列账，并随时配合甲方进行监督检查。

2.认真填写本合同书附件1《项目任务书》，《项目任务书》的内容应与乙方的《项目申报书》保持一致。

3.严格按照本合同书及附件1《项目任务书》的要求及时完成项目建设内容，项目实施完成后，按照本合同附件2《验收报告》模版要求提交验收报告。

4.按照《广东省农业农村厅种业振兴行动专项资金管理办法（试行）》规定，按期（每年6月30日、12月31日）向甲方、丙方书面报告项目实施进展及资金使用情况等内容。

5.乙方需保留与所有参与单位的合作实施协议和相关财务凭证，并向甲方备案。

第四条　丙方的权利义务：

1.为乙方项目实施提供必要的条件保障。

2.负责对项目承担单位的实施条件、能力以及财务管理规范进行审查，对推荐项目的实施场地、申报资料等进行真实性审核，并监督项目实施、资金预算执行情况。

3. 协助甲方完成对财政资金投资500万元（含）以上【科研项目财政资金在200万元（含）以上】项目验收等工作；负责完成对财政资金投资500万元以下（科研项目财政资金200万元以下）项目验收工作，并及时向甲方报告情况。

第五条　本项目资金不得用于以下方向：1. 行政事业单位基本支出；2. 各项奖金、津贴、福利补助、职工工资、奖励绩效等；3. 企业担保金和弥补企业亏损；4. 修缮楼堂馆所以及建造职工住宅；5. 弥补单位预算支出缺口和偿还债务；6. 购买交通工具及通讯设备；7. 形成地方政府债务的支出；8. 购买理财产品、发放借款及平衡预算等。

第六条　项目验收。项目验收及结果处理严格执行《广东省农业农村厅专项资金项目验收管理办法（试行）》（粤农农办〔2023〕73号）的规定。乙方应在项目完成后3个月内，提出验收申请。申请验收除了规定材料外，还应该提交项目审计报告或者经费决算表，其中财政专项资金50万元以下的项目，需提交由项目承担单位财务部门出具的经费决算表，财政专项资金50万元（含）以上的项目，需提交由项目承担单位委托会计师事务所出具的审计报告。对财政资金投资500万元（含）以上【科研项目财政资金在200万元（含）以上】的项目，及乙方直接向甲方申报的项目，由甲方负责组织验收；对财政资金投资500万元以下（科研项目财政资金200万元以下）的项目，由项目推荐（主管）单位（丙方）负责验收，验收单位向甲方提交验收材料，甲方对验收材料进行审核确认。

第七条　在履行本合同的过程中，如出现相关政策法规重大改变等不可抗力情况，甲方有权对所核拨经费的数量和时间进行相应调整。因非不可抗力因素导致的项目未履行或未履行完毕，或因乙方责任造成项目不能继续开展的，甲方有权终止项目合同，收回尚未使用和使用不符合规定的财政经费。

第八条　在履行本合同的过程中，乙方发现可能导致项目整体或部分失败的情形时，应及时通知甲方，并采取适当措施减少损失，没有及时通知并采取适当措施，致使损失扩大的，应当就扩大的损失承担责任。

第九条　实施项目所获得的科技成果(项目成果)归属、成果转让和实施技术成果所产生的经济利益的分享，按照国家和广东省有关规定执行。项目研究成果应向省农业农村厅进行登记、备案，对外发布前应征求省农业农村厅的意见。

第十条　本合同在履行过程中发生的任何争议，由甲乙丙三方友好协商解决。

第十一条　本合同未尽事宜，各方同意按照《广东省省级财政专项资金管理办法（2025 年修订）》（粤府〔2025〕56 号）、《广东省农业农村厅种业振兴行动专项资金管理办法（试行）》履行。

项目管理单位(甲方)　(盖章)：广东省农业农村厅

法定代表人(或授权代表)　(签章)：

签订日期：2025年12月5日

项目牵头承担单位(乙方)　(盖章)：

法定代表人(或授权代表)　(签章)：

项目负责人(签章)：

签订日期：2025年10月27日

乙方推荐（主管）单位(丙方)　(盖章)：

法定代表人(或授权代表)　(签章)：

签订日期：　　年　月　日

附件 1

项 目 任 务 书

填 写 说 明

一、本项目任务书由乙方填写。

二、本项目任务书所列内容应实事求是填写，表达要明确、严谨。对填写不符合要求的，或填报内容出现虚报夸大、不切实际的，将退回项目承担单位修改。

三、项目任务书规定的项目考核指标、建设内容和绩效目标必须依据《项目申报书》填写，应遵循明确、量化、可考核的原则，其中技术指标应明确项目完成时达到的关键技术参数及预期可以形成的发明专利、标准、新技术、新产品、新装置、论文、专著等的数量。项目申报指南对项目技术、经济和成果等指标有明确要求的，应符合项目申报指南的要求，相关专项管理办法有特别规定的，应符合相关规定。

四、《项目申报书》及申报指南是本项目任务书填报的重要依据，项目任务书填报不得修改考核指标、绩效目标、资金预算等内容。《项目申报书》、申报指南和本项目任务书将共同作为项目过程管理、综合绩效评价（验收）和监督评估的重要依据。

五、省财政资金支出的预算计划应按照国家及省相关规定执行。

六、表格栏目不够可自行增加。

一、目的及意义

主要说明项目的建设目的、研究价值和意义。

本项目将围绕猪肠道微生物智能培养体系构建、菌株资源保藏与功能挖掘、促生长与节粮型微生态制剂研制及示范推广等核心任务，建立涵盖功能菌株精准识别、高通量筛选、协同配伍、规模化制备与应用推广的完整技术体系。项目拟率先建立针对猪肠道微生物种质资源挖掘的智能化技术平台与菌种资源库，实现猪肠道代表性菌株（如肠道优势菌株：高丰度菌株；核心菌株：高覆盖率菌株；基石菌株：高调控能力菌株）高覆盖，解决功能菌种培养难、菌株功能复配难、菌株潜力转化难等关键瓶颈，开发提升猪饲料利用效率、缩短出栏周期的功能微生态制剂，并在规模化猪场开展推广示范。该项目有望系统整合我国猪源微生物种质资源，显著提升生猪养殖效率，降低饲料等主要生产成本，为我国生猪产业转型升级提供创新路径，对保障国家肉类安全和推动现代畜牧业种业振兴具有重要现实意义与战略价值。

二、项目建设内容

详细说明项目建设内容和技术路线（项目需求或项目建设任务，包含各项目参与单位的建设内容）。

1、牵头单位：华南农业大学

（1）研制菌株培养条件智能设计系统。基于公共数据库中猪肠道菌株参考基因组序列等先验信息，运用代谢通路预测算法（如 CarveMe、ModelSEED 等），识别具有代表性的猪源肠道细菌，包括肠道优势菌株、核心菌株与基石菌株等在内的重要菌株对碳源、氮源、维生素、微量元素等营养因子的依赖与代谢偏好，构建菌株-培养条件匹配矩阵；设计定制化培养基组合库，采用多通道微量反应体系进行培养条件的高通量筛选与验证，探索培养低丰度微生物的特异性生长所需温度、pH 与氧气含量。

（2）构建基于图谱融合（AI 图像识别与光谱表型指纹分析）的智能识别系统。通过自动采集不同菌落的形态图像、光谱图像与光谱曲线，利用人工智能识别算法（如 YOLO，Transformer 等）。整合菌株代谢偏好数据、培养条件库、图像识别模型与表型数据库，实现从代谢预测、培养条件优化、菌落识别与筛选、菌株归档的自动化工作流程。

（3）构建“微生物—宿主表型”数据库与多组学整合分析。采集不同生长阶段猪只的粪便与肠道样本，记录猪只的日增重、采食量、料重比、粪便形态等表型数据；开展肠道菌群 16S/宏基因组测序、肠道转录组和代谢组数据获取，建立“微生物—宿主表型”一体化数据集；运用机器学习和网络分析（如随机森林、网络分析、LASSO 等）识别与促生长、提高饲料利用率相关的关键微生物群体，为目标菌群筛选提供候选微生物资源清单及菌株间共现关系。

（4）目标菌群的高通量筛选与营养功能机制预测。对筛选出的核心微生物群体开展高通量培养、鉴定以及全基因组测序，注释菌株参与营养物质分解、吸收转运、短链脂肪酸合成等关键代谢通路；基于代谢模型分析菌株对蛋白质、脂类、非淀粉多糖等主要饲料成分的消化利用贡献，结合文献与数据库预测促进快速生长与提高饲料利用率相关

的潜在分子机制与靶点，为代表性功能菌株的验证与产品开发提供理论支撑。

（5）猪源益生菌促生长的作用机制解析。围绕已筛选获得的促生长核心功能菌株，系统解析其调控猪只生长性能的作用机制，重点从菌株定植能力、代谢功能、宿主响应和分子信号通路四个层面展开，构建益生菌调控猪生长与营养利用的理论体系和机制模型。研究内容包括：1）菌株在肠道各部位的定植动力学及代谢特征研究：分别在小肠（空肠、回肠）和大肠（盲肠、结肠、直肠）中开展核心功能菌株的定植动态跟踪，结合代谢组学分析其关键代谢产物（如短链脂肪酸、胆汁酸、色氨酸代谢产物等），明确其在不同肠段的功能优势与贡献机制。2）体外模型联合灌胃实验验证其对宿主生理的调控效应：利用空肠上皮细胞、原代肝细胞、肠道类器官等体外模型，分别评价菌株在以下方面的功能：生长性能相关模型：促进细胞增殖、营养吸收、激素轴调控（如 GH/IGF-1），增强抗氧化与抗炎能力；饲料利用相关模型：增强非淀粉多糖、纤维素、蛋白质等营养物质的降解能力，维持肠道屏障完整性，调控轻微炎症状态，促进代谢物有效利用；结合猪只灌胃试验，综合评估菌株对动物表型的直接影响与其体内分布。3）生长性能相关的关键信号通路解析：通过组织病理学、多组学联合分析，系统揭示菌株通过 mTOR、AhR、Wnt/β-catenin 等信号通路调控肠道干细胞“干性”、上皮细胞更新、免疫平衡（Th1/Th2）及能量代谢调控等过程，从而影响猪的生长速度。

2、参与单位：佛山大学

（1）构建猪源肠道菌株信息库。入库菌株开展基因组测序，解析菌株毒力基因、耐药基因、代谢功能基因和定植相关因子，综合评估菌株的益生潜力、安全性和应用价值。通过标准化的菌株保存、命名和分类体系，建立结构清晰、可共享、可查询的猪源肠道微生物信息库。

（2）开发菌株复配潜力评估模型。收集群体样本的宏基因组数据，构建菌群共发生网络图，识别具有稳定共现关系的协同微生物模块，绘制“交叉喂养网络图谱”。基于代谢通路互补性与生态协同性，开发菌株复配潜力评估模型，预测不同菌株之间的协同增效潜力，筛选可用于不同生长阶段、营养场景的复配菌组合，为后续精准干预产品开发提供理论支撑与菌种资源基础，实现菌株的系统保藏、功能注释、网络关系可视化和复配信息整合，推动肠道微生物资源向高效利用与工程化方向转化。

3、参与单位：广东省农业科学院农业生物基因研究中心

（1）构建猪源肠道微生物种质资源库。收集健康状态下不同品种、生长阶段（如哺乳期、断奶期、保育期、生长期、育肥期）以及不同肠段（如空肠、回肠、盲肠、结肠、直肠）内容物样本，全面覆盖猪肠道各微生物区系，精准刻画微生物的空间分布和功能特征。依托高通量培养分离与智能化鉴定技术，分离保藏具有代表性的猪源肠道细菌，覆盖肠道优势菌株、核心菌株与基石菌株，入库菌株数量不少于 3000 株。数据来源与资源体系可为项目提供高价值的关键菌群来源、微生态功能解析支撑及菌株分离培养平台。

4、参与单位：广东省农业科学院动物科学研究所

（1）猪源益生菌提高饲料利用率的作用机制解析。围绕已筛选获得的节粮型核心功能菌株，系统解析其调控猪只饲料利用效率的作用机制，重点从菌株定植能力、代谢功能、宿主响应和分子信号通路四个层面展开，构建益生菌调控猪生长与营养利用的理论

体系和机制模型。研究内容包括：1）菌株在肠道各部位的定植动力学及代谢特征研究：分别在小肠（空肠、回肠）和大肠（盲肠、结肠、直肠）中开展核心功能菌株的定植动态跟踪，结合代谢组学分析其关键代谢产物（如短链脂肪酸、胆汁酸、色氨酸代谢产物等），明确其在不同肠段的功能优势与贡献机制。2）体外模型联合灌胃实验验证其对宿主生理的调控效应：利用空肠上皮细胞、原代肝细胞、肠道类器官等体外模型，分别评价菌株在以下方面的功能：生长性能相关模型：促进细胞增殖、营养吸收、激素轴调控（如 GH/IGF-1），增强抗氧化与抗炎能力；饲料利用相关模型：增强非淀粉多糖、纤维素、蛋白质等营养物质的降解能力，维持肠道屏障完整性，调控轻微炎症状态，促进代谢物有效利用；结合猪只灌胃试验，综合评估菌株对动物表型的直接影响与其体内分布。3）饲料转化效率相关的关键信号通路解析：通过组织病理学、多组学联合分析，系统揭示菌株通过 mTOR、AhR、Wnt/β-catenin 等信号通路调控肠道干细胞“干性”、上皮细胞更新、免疫平衡（Th1/Th2）及能量代谢调控等过程，从而影响猪的饲料利用效率。

5、参与单位：肇庆大北农农牧食品有限公司

（1）促生长、节粮型猪源益生菌的功能验证与微生态制剂开发。在明确促生长型与节粮型核心功能菌株作用机制的基础上，开展协同增效型复配微生态制剂的开发与中试验证。重点围绕猪生长速度提升、饲料转化效率优化两个方向，系统开展以下研究内容：1）菌株复配与协同筛选：基于菌株共现网络、代谢通路互补性及生态互作模型，结合饲料中主要组分（如纤维素、非淀粉多糖、蛋白质等）的降解能力，分别筛选与促生长或节粮核心菌株具有代谢协同与互补作用的候选菌株，构建两类功能导向型复配菌群（各不少于两组）。2）发酵工艺优化：在现有高密度发酵平台基础上，分别针对促生长型与节粮型菌群，优化菌株共培养和混合发酵工艺，调控温度、pH、C/N 比、溶氧水平、氧化还原电位等核心参数，提升菌体产量、芽孢形成率与关键代谢产物积累；节粮型工艺将引入 Mn^{2+} 、K^{+} 、Zn^{2+} 等促进酶活的微量元素，结合生物传感与自动补料系统，实现精准调控。3）冻干与制粒工艺开发：针对不同菌群特性，优化冻干保护剂配方与干燥参数，提升菌株存活率与复苏能力；筛选兼容性高、可饲用的载体材料，优化制粒与造粒参数，提升制剂在饲料加工过程中的适配性与耐热稳定性。4）复配比例与功能效率优化：通过正交设计优化不同菌株之间的复配比例，提升整体代谢效率与功能协同性；构建从制剂稳定性、饲料适配性到动物体内功能效果的三级质量评价体系，确保产品在实际应用中的稳定性与一致性。5）中试验证与动物实验：开展 300 L 级中试验证与工艺放大，分别在小规模猪只群体中进行动物试验，系统评估不同制剂对日增重、采食量、料重比、饲料转化率、粪便特征及消化道健康等表型指标的影响，明确促生长与节粮机制。6）产品开发与成果转化：分别开发 1 种具商品化潜力的促生长型与节粮型复配微生态制剂，完成关键工艺备案、知识产权申报和配方标准化，具备在规模化养殖场中推广应用的技术基础与产业可行性。

（2）微生态制剂应用效果评估与推广示范。围绕已开发的节粮型与促生长型微生态制剂，系统推进中试验证、多场景评估与商品化转化。1）选取 3-5 个以上具有代表性的规模化养殖场，设立试验组与对照组，在保育期至育肥阶段连续开展 150 天饲喂试验，系统采集日增重、采食量、料重比、健康评分、粪便特征等数据，定量评估制剂对猪只饲料利用率、出栏周期和抗应激能力的影响；2）开展多品种、不同日龄与气候条件下的多场景应用试验，构建多因素响应模型，明确制剂的适配边界与应用优势；3）

与市售同类微生态产品开展对比试验，从性能提升、成本效益比、稳定性等方面评估项目产品的市场竞争力；4）在中试工艺基础上，搭建年产100吨的微生态制剂生产线，制定涵盖菌株批次管理、载体标准、制粒工艺、包装运输与贮藏条件等环节的标准化生产流程，形成可推广复制的工艺体系；5）完成2个以上制剂的安全性、有效性与稳定性评估，开展急性毒性、耐药基因转移、靶器官影响等试验，整理登记资料，推动产品注册；6）依托企业平台，开展面向养殖企业的技术培训与应用示范，推动微生态制剂在实际养殖中的应用，示范推广规模达50万头猪，为规模化推广与产业化奠定基础。

备注：项目建设内容（项目需求或项目建设任务）按《项目申报书》内容填写。

三、项目绩效目标

主要说明项目实施后，预期达到的总体目标和当年度目标产生的效果，相关表述应量化。

1、总体绩效目标如下:

（1）构建猪肠道菌群高通量智能培养体系 1 套，实现菌落原位识别与自动化挑取。

（2）建立猪源肠道菌株种质资源库 1 个，入库保藏 3000 株以上具有代表性的猪源肠道细菌，覆盖肠道优势菌株（高丰度菌株）、核心菌株（高覆盖率菌株）与基石菌株（高调控能力菌株），具备冷冻长期保存及复苏验证功能。

（3）建立菌株种质资源库配套的信息库 1 个，涵盖入库菌株的基础分类信息、参考基因组、代谢通路预测结果、培养条件记录、功能标签数据等，整体信息覆盖率不低于 50%，核心菌群与基石菌群的信息覆盖率不低于 80%，数据结构化、可检索、可共享。

（4）开发菌株复配潜力评估模型 1 套，具备猪源菌株的复配兼容性、功能互补性进行智能打分与组合推荐的能力。

（5）筛选鉴定具备促进猪快速生长、提高猪饲料利用率的功能菌株各 10 株，每类菌株与猪日增重、饲料转化率等核心表型性状的相关性在至少 5 个独立动物实验和至少三种不同算法都表现一致。

（6）培养开发促进猪快速生长、提高饲料利用率功能菌株各 1 株，通过动物实验验证其对猪日增重、饲料转化率的显著提升效果（$P < 0.05$），明确作用机制包含至少各 1 条核心调控通路。

（7）研制促进猪快速生长的微生态制剂产品 1 种，在生猪规模化饲养试验中（猪只数量 ＞400），处理组商品猪出栏周期缩短不少于 5 天。

（8）研制提高猪饲料利用率的微生态制剂产品 1 种，在生猪试验测定群体中，处理组商品猪饲料利用效率 5%以上（猪个体数 ＞400）。

（9）建立促生长、节粮型微生态制剂生产的标准化工艺流程，开展微生态制剂在规模化猪场的应用示范基地 3-5 个，技术推广辐射商品猪达不少于 50 万头。

（10）申请国家发明专利 1-2 件，软件著作权 1-2 项；发表高水平论文 2-3 篇；培养人才 5-10 名。

2、年度绩效目标

（1）2025 年 11 月 至 2026 年 10 月：建立猪肠道菌群高通量智能培养体系 1 套；筛选促进猪快速生长、提高饲料利用率的关键功能微生物各 10 种；构建猪肠道微生物种质资源库 1 个，入库保藏重要细菌 400 种（株）以上；建立菌株种质资源库配套的信息库 1 个，实现入库保藏菌株的信息可共享、可查询。

四、项目进度安排

详细说明各阶段的工作内容、时间安排情况。

1、2025 年 11 月 至 2026 年 1 月：建立猪肠道菌群高通量智能培养体系：基于公共数据库中猪肠道菌株参考基因组序列等先验信息，运用代谢通路预测算法（如 CarveMe、ModelSEED 等），识别菌株对碳源、氮源、维生素、微量元素等营养因子的依赖与代谢偏好，构建菌株-培养条件匹配矩阵；设计定制化培养基组合库，采用多通道微量反应体系进行培养条件的高通量筛选与验证，探索培养盲区微生物的特异性生长所需温度、pH 与氧气含量。

2、2026 年 2 月 至 2026 年 5 月：构建基于图谱融合（AI 图像识别与光谱表型指纹分析）的智能识别系统：通过自动采集不同菌落的形态图像、光谱图像及光谱曲线，利用人工智能识别算法（如 YOLO，Transformer 等）实现菌落微观水平的原位去重复、快速归类与初步功能判别，提升培养效率与菌株多样性覆盖。整合菌株代谢偏好数据、培养条件库、图像识别模型与表型数据库，实现从代谢预测、培养条件优化、菌落识别与筛选、菌株归档的自动化工作流程。

3、2026 年 6 月 至 2026 年 8 月：筛选促生长、节粮型猪源益生菌：采集不同生长阶段猪只的粪便与肠道样本，记录猪只的日增重、采食量、料重比、粪便形态等表型数据；开展肠道菌群 16S/宏基因组测序、肠道转录组和代谢组数据获取，建立“微生物—宿主表型”一体化数据集；运用机器学习和网络分析（如随机森林、网络分析、LASSO 等）识别与促生长、提高饲料利用率相关的关键微生物群体，为目标菌群筛选提供候选微生物资源清单及菌株间共现关系。

4、2026 年 9 月 至 2026 年 10 月：建立菌株种质资源库与配套的菌株信息库：收集健康状态下不同品种、生长阶段（如哺乳期、断奶期、保育期、生长期、育肥期）以及不同肠段（如空肠、回肠、盲肠、结肠、直肠）内容物样本，全面覆盖猪肠道各微生物区系，精准刻画微生物的空间分布和功能特征。依托高通量培养分离与智能化鉴定技术，分离保藏具有代表性的猪源肠道细菌，覆盖肠道优势菌株（高丰度菌株）、核心菌株（高覆盖率菌株）与基石菌株（高调控能力菌株），入库菌株数量不少于 400 株；入库菌株开展基因组测序，解析菌株毒力基因、药基因、代谢功能基因和定植相关因子，综合评估菌株的益生潜力、安全性和应用价值。通过标准化的菌株保存、命名和分类体系，建立结构清晰、可共享、可查询的猪源肠道微生物信息库。

备注：项目绩效目标按《项目申报书》内容填写。

五、项目主要合作、参与单位(含牵头承担单位)

单位名称	单位性质	统一社会信用代码	通讯地址
华南农业大学	大专院校	124400004554165634	广东省广州市天河区五山路483号华南农业大学
佛山大学	大专院校	1244060045607389XC	广东省佛山市南海区狮山镇广云路33号
广东省农业科学院农业生物基因研究中心	科研院所	1244000005680362XU	广州市天河区金颖路20号
广东省农业科学院动物科学研究所	科研院所	124400000651519695	广东省广州市天河区五山路大丰一街1号
肇庆大北农农牧食品有限公司	企业	91441223MA4WTUW58D	肇庆市广宁县南街街道南东三路103号

六、项目组主要成员(含项目负责人)

姓名	性别	身份证号	单位	职称/职务	电话
赵江潮	男	110108197703289335	华南农业大学	正高级	15918006508
王晓帆	女	220282198903136527	华南农业大学	正高级	18819392566
杨杰	男	430721198706211333	华南农业大学	正高级	18602020087
谭成全	男	430223198505113513	华南农业大学	副高级	13922348414
邓海东	男	362201197608216014	华南农业大学	副高级	15920359682
全建平	男	420281199206128 05X	华南农业大学	副高级	15102030907
李龚	男	612324199402057012	华南农业大学	其他	15089893236
左斌	男	130481199011241994	华南农业大学	其他	18688208381
李英	女	532527197510210 02X	佛山大学	正高级	18782044091
邓飞龙	男	511602199002065439	佛山大学	副高级	13208101080

宋博	男	421281199510214519	佛山大学	其他	15970405937
柴建民	男	13043519880501191X	佛山大学	中级	17688296650
姜辉	女	370686199302074142	佛山大学	中级	18296155676
董博	男	421125198209210032	广东省农业科学院农业生物基因研究中心	副高级	18028604208
俞婷	女	362322198710063968	广东省农业科学院农业生物基因研究中心	副高级	15692436670
魏文康	男	441423197105151018	广东省农业科学院农业生物基因研究中心	正高级	13808879089
曹舒婷	女	652324199311032829	广东省农业科学院动物科学研究所	副高级	13967196255
胡胜兰	女	420606198405173520	广东省农业科学院动物科学研究所	副高级	13609757189
何威	男	220722199508111616	广东省农业科学院动物科学研究所	其他	17072967136
吴凡	男	422301198611058519	肇庆大北农农牧食品有限公司	副高级	15002001599
文婷	女	460033199301141784	肇庆大北农农牧食品有限公司	副高级	18826487452
张益焘	男	352229199009286014	肇庆大北农农牧食品有限公司	副高级	17688863256
朱泽欣	女	445122199106225912	肇庆大北农农牧食品有限公司	中级	15322511305
张文飞	男	412824199104140 31X	肇庆大北农农牧食品有限公司	其他	15920991476
陈伟	男	152502199103183352	肇庆大北农农牧食品有限公司	其他	18819474991

七、资金使用预算

主要说明资金使用的范围或方向及资金使用进度安排（包含参与单位内容），明确各项目单位资金分配和预计支出进度。

本项目第一年度省级财政专项资金、其他渠道资金具体分匹配情况如下：

单位名称	省级财政专项资金分配比例	省级财政专项资金（万元）	直接经费（万元）	间接经费（万元）	其他渠道资金（万元）
华南农业大学	30.00%	45.00	40.50	4.50	0.00
佛山大学	10.00%	15.00	13.50	1.50	0.00
广东省农业科学院农业生物基因研究中心	5.00%	7.50	6.75	0.75	0.00
广东省农业科学院动物科学研究所	5.00%	7.50	6.75	0.75	0.00
肇庆大北农农牧食品有限公司	50.00%	75.00	75.00	0.00	300.00

其中省级财政专项资金、其他渠道资金具体使用范围如下：

预算科目名称	省级财政专项资金第一年度（万元）	其他渠道资金第一年度（万元）
合计	150.00	300.00
（一）直接费用	142.50	300.00
1.设备费	0.00	0.00
2.材料费	34.50	150.00
3.测试化验加工费	67.50	50.00
4.燃料动力费	0.00	25.00
5.出版/文献/信息传播/知识产权事务费	8.00	10.00
6.会议/差旅/国际合作交流费	8.00	15.00
7.培训费	0.00	0.00
8.劳务费	22.50	50.00
10.专家咨询费	2.00	0.00

11.基本建设费	0.00	0.00
（1）房屋建筑物构建	0.00	0.00
（2）专用设备购置	0.00	0.00
（3）基础设施建设	0.00	0.00
（4）大型修缮	0.00	0.00
（5）信息网络建设	0.00	0.00
（6）其他基本建设支出	0.00	0.00
12.其他费用	0.00	0.00
（二）间接费用	7.50	0.00

省级财政专项资金150.00万元主要使用的范围：

（1）直接费用：142.50万元

①材料费：34.50万元，用于采样及运输耗材、检测试剂盒、建库试剂盒、菌株分离培养与保藏耗材、实验室常规耗材。

②测试化验加工费：67.50万元，用于支付肠道菌群16S扩增子测序、宏基因组测序、核心菌株全基因组测序费用。

③出版/文献/信息传播/知识产权事务费：8.00万元，用于论文出版、专利和软件著作权等相关费用。

④会议/差旅/国际合作交流费：8.00万元，用于样品采集、技术交流、科研试验、外出调研、工作检查和指导、技术咨询、参加学术会议等的差旅费和注册费。

⑤劳务费：22.50万元，用于支付参与项目的聘用研究人员、研究生等劳务费。

⑥专家咨询费：2.00万元，用于聘请专家参与培训、会议等的专家咨询费。

（2）间接费用：7.50 万元

用于单位科研管理费等。

其他渠道资金300.00万元主要使用的范围：

（1）直接费用：300.00万元

①材料费：150.00万元，用于购买发酵原料、待筛选的保护剂、制剂载体材料、正交试验与响应面法优化所需耗材、造粒模拟与干燥工艺的辅料、消化道环境模拟试剂、生物传感器专用检测芯片、高温处理包材、商业化包装材料、运输模拟耗材、贮存稳定性测试样品、养殖场试验耗材及竞品对比试验的对照制剂。

②测试化验加工费：50.00万元，用于支付第三方机构或校内平台进行的各项关键指标检测费用，包括菌体活性计数、制剂稳定性测试、制剂物理特性分析、制粒后颗粒特性与稳定性评估、代谢产物定量检测、安全性评估、有效性认证及竞品成分与功效对比检测。

③燃料动力费：25.00万元，用于支撑实验室和车间在工艺开发、优化及放大试验期间，进行大规模发酵、冻干、制粒等设备长时间运行所产生的水、电等能源消耗费用，及样品冷链运输成本。

④出版/文献/信息传播/知识产权事务费：10.00万元，用于支付专利申请、产品登记、技术标准发布、市场准入文件、竞品专利分析、推广应用手册/宣传资料设计印刷等费用。

⑤会议/差旅/国际合作交流费：15.00 万元，用于项目组成员参加国内外相关学术会议、技术研讨会、行业展会进行交流学习的差旅费、注册费；赴合作单位进行技术对接、工艺验证或现场调研的差旅费。

⑥劳务费：50.00 万元，用于支付直接参与本项目工艺开发、优化及检测分析工作的项目聘用研究人员、研究生以及聘请的领域内专家顾问的劳务报酬。

（2）间接费用：0.00 万元

省级财政专项资金 150.00 万元使用进度安排：

时间段	进度占比	金额（万元）
2025.11-2026.01	20%	30.00
2026.02-2026.04	20%	30.00
2026.05-2026.07	30%	45.00
2026.08-2026.10	30%	45.00
合计	100%	150.00

其他渠道资金 300.00 万元使用进度安排：

时间段	进度占比	金额（万元）
2025.11-2026.01	20%	60.00
2026.02-2026.04	20%	60.00
2026.05-2026.07	30%	90.00
2026.08-2026.10	30%	90.00
合计	100%	300.00

八、保障措施

说明围绕完成项目任务、目标所要采取的具体措施。

1、组织方式:

为保障项目的顺利推进，课题的组织管理实行由项目领导小组统一领导下的课题主持人负责制。组建由项目牵头单位牵头成立的项目管理小组、技术攻关小组、产业推广小组和成果转化小组，统一协调项目进度与任务落实，保障项目高效推进。

（1）管理小组：由牵头单位项目负责人担任组长，负责项目整体规划、重大事项决策、年度目标制定与多方协作协调。

（2）技术攻关小组：由各单位骨干专家组成，围绕菌株筛选、复配优化、智能系统构建等关键技术开展协同攻关。

（3）成果转化与示范小组：重点负责筛选出的核心技术在企业端的应用验证与推广，组织产品应用评价、用户反馈收集及推广材料整理。

（4）培训与交流小组：负责组织技术培训、学术交流和成果推广活动，提升养殖企业的技术应用能力与科研单位的成果影响力。

2、管理机制

本项目将建立科学规范的管理制度与监控制度，确保技术路线清晰、任务分工明确、资金使用规范、成果产出高效，形成良好的组织运行机制。

立项与评估机制：设立由行业内专家组成的项目技术委员会，对项目的关键节点、研究计划和技术路线进行评估与技术指导。

经费管理机制：实行专项经费独立账户管理，由项目牵头单位统筹，接受财政与主管单位审计监管，严格执行“专款专用、专账管理、绩效导向”。

年度评审机制：项目每年开展一次进展评估，由第三方专家或主管部门组织年度绩效考核，评估研究进度与阶段成果质量。

量化考核机制：将项目成果（包括功能菌株数、软件著作权、专利授权、微生态制剂推广示范规模等）与各单位及个人绩效直接挂钩，调动科研人员积极性。

进度控制机制：各项任务设定具体时间表与量化指标，实行月度检查、季度通报、半年督导的分级跟踪制度，强化项目过程管理与风险应对。

成果转化与激励机制：项目形成的菌种资源库、智能筛选系统和微生态制剂产品优先向合作企业许可使用，推动建立技术入股、成果收益共享等机制，激发产学研联合创新活力。

SCAULIB202514374

检索证明

根据委托人提供的论文材料，委托人**华南农业大学兽医学院 李龚** 5 篇论文收录情况如下表：

序号	论文名称	发表刊物及发表的年月卷期/页码等	作者排名	论文等级	作者文中单位、收录情况		影响因子	中科院大类分区	引用
1	CRISPR-AMRtracker: A novel toolkit to monitor the antimicrobial resistance gene transfer in fecal microbiota	DRUG RESISTANCE UPDATES 出版年：2024 出版日期：NOV 卷期：77 页码：- 文献号：101142 文献类型：Article	第一作者	T2 类	华南农业大学兽医学院	SCI	IF2-year=15.8 IF5-year=18.1 （2023）	医学 1 区 Top 期刊：否 （2023）	SCI 核心合集 总引：0
2	Waterborne polyurethane nanoparticles incorporating linoleic acid as a potential strategy for controlling antibiotic resistance spread in the mammalian intestine	MATERIALS TODAY BIO 出版年：2024 出版日期：OCT 卷期：28 页码：- 文献号：101181 文献类型：Article	第一作者	T2 类	华南农业大学兽医学院	SCI	IF2-year=8.7 IF5-year=8.8 （2023）	医学 1 区 Top 期刊：否 （2023）	SCI 核心合集 总引：0
3	Mechanisms of gastrointestinal toxicity in neuromyelitis optica spectrum disorder patients	MICROBIOLOGY SPECTRUM 出版年：2024 出版日期：AUG 6 卷期：12 8 页码：-	第一作者	A 类	华南农业大学兽医学院	SCI	IF2-year=3.7 IF5-year=4.2 （2023）	生物学 2 区 Top 期刊：否 （2023）	SCI 核心合集 总引：0

华南农业大学图书馆SCAULIB202514374

	treated with mycophenolate mofetil: insights from a mouse model and human study	文献号： 文献类型：Article							
4	Acquisition of a novel conjugative multidrug-resistant hypervirulent plasmid leads to hypervirulence in clinical carbapenem-resistant Klebsiella pneumoniae strains	mLife 出版年：2023 出版日期： 卷期： 页码：- 文献号： 文献类型：	第一作者	普刊类	华南农业大学兽医学院	在线发表	无	无	SCI 核心合集总引：
5	Integrative analysis of purine metabolites and gut microbiota in patients with neuromyelitis optica spectrum disorders after mycophenolate mofetil treatment	BMC NEUROLOGY 出版年：2023 出版日期：DEC 16 卷期：23 1 页码：- 文献号：444 文献类型：Article	第一作者	B 类	华南农业大学兽医学院	SCI	IF2-year=2.2 IF5-year=2.5 （2023）	医学 3 区 Top 期刊：否 （2023）	SCI 核心合集总引：1

说明：论文等级和中科院大类分区按《华南农业大学学术论文评价方案（试行）》划分。

华南农业大学图书馆SCAU[R]20251437

报告免责声明:如未盖章,报告无效

华南农业大学图书馆 信息检索专用章

检索员：刘汉忠

华南农业大学图书馆

2025-01-03

SCAULIB202514375

检索证明

根据委托人提供的论文材料，委托人华南农业大学兽医学院 李龚 1 篇论文收录情况如下表。

序号	论文名称	发表刊物及发表的年月卷期/页码等	作者排名	论文等级	作者文中单位	收录情况	影响因子	中科院大类分区	引用
1	Linoleic acid and α-linolenic acid inhibit conjugative transfer of an IncX4 plasmid carrying mcr-1	JOURNAL OF APPLIED MICROBIOLOGY 出版年：2021 出版日期：JUN 卷期：130 6 页码：1893--1901 文献号： 文献类型：Article	第一作者	B 类	华南农业大学兽医学院	SCI	IF2-year=4.059 IF5-year=4.438 （2021）	生物学 3 区 Top 期刊：否 （2021）	SCI 核心合集 总引：5

说明：论文等级和中科院大类分区按《华南农业大学学术论文评价方案（试行）》划分。

华南农业大学图书馆SCAULIB202514375

报告免责声明:如未盖章,报告无效

检索员：刘汉忠

华南农业大学图书馆

2025-01-03

华南农业大学图书馆 信息检索专用章

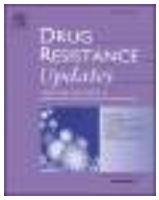
Drug Resistance Updates 77 (2024) 101142



Contents lists available at ScienceDirect

Drug Resistance Updates

journal homepage: www.elsevier.com/locate/drup



CRISPR-AMRtracker: A novel toolkit to monitor the antimicrobial resistance gene transfer in fecal microbiota

Gong Li [a,b,c,1,2], Teng-Fei Long [a,c,1,2], Shi-Ying Zhou [a,c,2], Li-Juan Xia [a,c,2], Ang Gao [a,c,2], Lei Wan [a,c,2], Xiao-Yuan Diao [a,c,2], Yu-Zhang He [a,c,2], Ruan-Yang Sun [a,c,2], Jin-Tao Yang [a,c,2], Sheng-Qiu Tang [b], Hao Ren [a,c,2], Liang-Xing Fang [a,c,2], Xiao-Ping Liao [a,c,2], Ya-Hong Liu [a,c,2], Liang Chen [d,*], Jian Sun [a,c,2,**]

[a] State Key Laboratory for Animal Disease Control and Prevention, College of Veterinary Medicine, South China Agricultural University, Guangzhou 510642, PR China
[b] Guangdong Provincial Key Laboratory of Utilization and Conservation of Food and Medicinal Resources in Northern Region, Shaoguan University, Shaoguan, PR China
[c] Guangdong Provincial Key Laboratory of Veterinary Pharmaceutics Development and Safety Evaluation, South China Agricultural University, Guangzhou 510642, PR China
[d] Department of Pharmacy Practice, School of Pharmacy and Pharmaceutical Sciences, University at Buffalo, Buffalo, NY 14214, United States

ARTICLE INFO

Keywords:
Conjugation
Antibiotic resistance genes
Horizontal gene transfer
mcr-1
CRISPR/Cas9
Fluorescently labelling

ABSTRACT

The spread of antibiotic resistance genes (ARGs), particularly those carried on plasmids, poses a major risk to global health. However, the extent and frequency of ARGs transfer in microbial communities among human, animal, and environmental sectors is not well understood due to a lack of effective tracking tools. We have developed a novel fluorescent tracing tool, CRISPR-AMRtracker, to study ARG transfer. It combines CRISPR/Cas9 fluorescence tagging, fluorescence-activated cell sorting, 16S rRNA gene sequencing, and microbial community analysis. CRISPR-AMRtracker integrates a fluorescent tag immediately downstream of ARGs, enabling the tracking of ARG transfer without compromising the host cell's antibiotic susceptibility, fitness, conjugation, and transposition. Notably, our experiments demonstrate that *sfGFP*-tagged plasmid-borne *mcr-1* can transfer across diverse bacterial species within fecal samples. This innovative approach holds the potential to illuminate the dynamics of ARG dissemination and provide valuable insights to shape effective strategies in mitigating the escalating threat of antibiotic resistance.

1. Introduction

Antimicrobial resistance (AMR) is a growing concern that poses a significant threat to the global health (Iregbu et al., 2022). To effectively combat the emergence and spread of AMR, it is crucial to understand the mechanisms, spectrum, and frequency by which antibiotic resistance genes (ARGs) are disseminated. Horizontal gene transfer (HGT) is one of the most significant routes for the spread of ARGs, particularly when mediated by conjugative plasmids (Arnold et al., 2021; Brito, 2021). Conjugative plasmid transfer is a process through which bacteria can horizontally transfer genes to other strains, species, genera, phyla and even domains. Besides ARGs, these plasmids often carry other accessory genes, such as those involved in metal resistances, catabolic pathways or virulence factors. HGT is a common event in the human and animal gut microbiome as well as environmental microbiome, encompassing a collection of all microbes from various bacterial species, fungi and viruses (Li et al., 2018; Shen et al., 2022). Conjugative plasmids serve as the main vessels of gene flow in microbial communities, connecting

* Correspondence author.
** Corresponding author at: State Key Laboratory for Animal Disease Control and Prevention, College of Veterinary Medicine, South China Agricultural University, Guangzhou 510642, PR China.
E-mail addresses: liangch@buffalo.edu (L. Chen), jiansun@scau.edu.cn (J. Sun).
[1] Gong Li and Teng-Fei Long are co-first authors of the article.
[2] Guangdong Laboratory for Lingnan Modern Agriculture, National Risk Assessment Laboratory for Antimicrobial Resistance of Animal Original Bacteria, College of Veterinary Medicine, South China Agricultural University, Guangzhou 510642, PR China.

https://doi.org/10.1016/j.drup.2024.101142
Received 4 November 2023; Received in revised form 4 August 2024; Accepted 17 August 2024
Available online 24 August 2024
1368-7646/© 2024 Elsevier Ltd. All rights are reserved, including those for text and data mining, AI training, and similar technologies.

distinct genetic pools among different biological sectors. Despite their importance, the dynamics of conjugative gene transfer in complex microbial communities, such as the gut microbiome, are still poorly understood.

Previous methods for monitoring plasmid-mediated HGT in natural environments have primarily focused on identifying specific plasmid-encoded traits and phenotypes, such as antibiotic resistance or catabolic pathways that impose plasmid selection in new hosts (Pinilla-Redondo et al., 2018). However, these approaches are predominantly cultivation-dependent, thereby inherently limiting the range of bacterial host profiling (Pinilla-Redondo et al., 2018). Recent advancements in the field, such as the utilization of fluorescently-labelled plasmids, have broadened the spectrum of host plasmids that can be studied. These experiments have been conducted in various microcosms, including soil (Brophy et al., 2018), water (Cyriaque et al., 2020), activated sludge (Qiu et al., 2018) and the gut (Ronda et al., 2019). Nonetheless, these studies have often focused on a few plasmid types, such as RP4 or pKJK5, whereas clinically significant plasmids, such as those harboring carbapenemase genes or mobile colistin resistance gene (*mcr*), are rarely explored. Other techniques, like transposition with Mu (Bahl et al., 2009), Tn*5* (Herrero et al., 1990) and Tn*7* (McKenzie and Craig, 2006), have been employed to introduce fluorescent gene markers into plasmids. However, these insertions are often random, potentially leading to unintended consequences.

The CRISPR/Cas9 system is a highly efficient tool for introducing a double-strand break (DSB) at a target site (Ryan and Cate, 2014). This system comprises the Cas9 protein and a guide RNA (gRNA). By utilizing a specific single guide RNA (sgRNA), the Cas9 endonuclease can make precise incisions (He et al., 2021) (Wang et al., 2021). The Lambda Red recombination system facilitates recombination between the bacterial genome and exogenous double-stranded DNA (dsDNA) through the coordinated action of several proteins, including the 5′→3′exonuclease (Exo), the single-stranded DNA (ssDNA)-binding protein (Beta), and the degradation-inhibiting protein (Gam) (Murphy, 1998). This method requires the presence of homologous arms of approximately 40 base pairs or longer on either side of the intended modification (Yang et al., 2014). Combing the CRISPR/Cas9 and Lambda Red systems represents a highly efficient methodology for generating precisely defined insertions (Wang et al., 2021), potentially enabling the specific integration of a fluorescent gene into a plasmid.

In this study, we employed the CRISPR/Cas9 and lambda Red system to integrate an *sfGFP* gene into the conserved regions of plasmids containing clinically significant ARGs, including *mcr-1*, $bla_{\text{NDM-1}}$, $bla_{\text{KPC-2}}$, and $bla_{\text{OXA-48}}$, in their clinical bacterial hosts such as *Escherichia coli*, *Salmonella* Typhimurium, and *Klebsiella pneumoniae*. We conducted a comparison between antibiotic resistance, growth patterns, conjugation and transposition abilities of the tagged strains and their wild-type counterparts. Subsequently, the fluorescently tagged strains were used to monitor the dissemination of the *mcr-1* gene in fecal microbiota. Our study introduces a highly effective method for tracking ARG transfer in microbial populations.

2. Material and methods

2.1. Bacterial strains, plasmids, primers and growth conditions

The strains used in this study are detailed in Table S1, while the plasmids employed are outlined in Table S2. A comprehensive list of the primers used can be found in Table S3. Cultures of *E. coli*, *S.* Typhimurium, *K. pneumoniae*, *A. baylyi*, and *E. faecalis* were cultivated at 37°C in LB medium. Diaminopimelic acid (DAP) was supplemented at 50 mg/L for *E. coli* WM3064 growth. Antibiotics were used at the following concentrations as needed: chloramphenicol (CHL) 25 mg/L, meropenem (MEM) 1 mg/L, Ampicillin (AMP) 100 mg/L, apramycin (APR) 30 mg/L, kanamycin (KAN) 30 mg/L, rifampin (RIF) 50 mg/L, streptomycin (STR) 2000 mg/L and colistin (CS) 2 mg/L.

2.2. Plasmid construction

The plasmids used in this study, namely pCasKP-oriT (cas9 plasmid with an *oriT* site), pSGKP-Tmcr-500GFP, pSGKP-arr2-TNDM500GFP, pSGKP-arr2-TKPC500GFP, and pSGKP-arr2-TOXA500GFP (guide RNA plasmids containing *sfGFP* gene and repair template targeting downstream ARGs), as well as pJS05, pJS06 (suicide plasmids harboring *mcr-1* transposon without and with sfGFP tag), and pMQ (a plasmid incorporating $lacI^q$ gene to inhibit the P_{trc} promoter of sfGFP), were all constructed using standard molecular cloning techniques (Supplementary data, Appendix 1).

2.3. Fluorescently labelling ARG plasmids

The target sites for insertion of the *sfGFP* gene were selected within the regions immediately downstream of ARGs, which are typically conserved for the same resistance genes across different plasmid types. Additional details regarding the target site selection and gRNA design were present in the Supplementary data, Appendix 2. This was achieved using a two-plasmid CRISPR/Cas9 system (Hao et al., 2020; Wang et al., 2018). The Cas9 plasmid, pCasKP-oriT, was transferred via conjugation to clinical isolates of *E. coli* CSZ4, *S.* Typhimurium 14E1050, *S.* Typhimurium LS3479, *E. coli* HZE22, *K. pneumoniae* 50700 and *K. pneumoniae* 49210(Additional details were present in the Supplementary data, Appendix 3). The pCasKP-oriT recipient strains were incubated overnight at 30°C in LB-APR medium and then subcultured at 30°C in LB-APR, followed by 0.1 M L-arabinose induction, to make competent cells. The pSGKP-gfp plasmid vectors, including the gRNA and the repaired template, were transferred by electroporation as previously described (Datsenko and Wanner, 2000). Electroporants were selected on LB plates supplemented with RIF and APR, followed by PCR confirmation. Single colonies were transferred onto LB agar plates containing 5 % sucrose and incubated at 37°C to remove pSGKP-gfp and pCasKP-oriT vectors. Macroscopic green colonies were screened and confirmed by PCR and Sanger sequencing using primers MF and OR. The removal of pCasKP-oriT was confirmed using primers CasKP-F and CasKP-R in PCR reactions, while primers SGKP-F and SGKP-R were used to verify the removal of pSGKP-gfp. The labelling efficiency (%) was calculated as the percentage of *sfGFP*-labelled clones out of the total tested clones.

2.4. Donor strain construction

Reporter donor strains were constructed from *sfGFP* gene-labelled clinical AMR strains. To do this, 100 ng of plasmid pMQ was electroporated into *sfGFP* gene-labelled strain and selected on LB-KAN plates. Red colonies were then selected and confirmed by PCR using primers Kan-F and Kan-R.

2.5. Conjugation assays

Both the donor and recipient strains were grown to the log phase in their respective media, and the cell suspensions were adjusted to OD_{600} ~0.3 (~10^8 CFU/mL cells). The cells were then washed in the media prior to mating. For broth mating, equal volumes of donor: recipient (500 μL each) cells were mixed and incubated at 37°C for 8 h. For agar mating, equal amounts of donor: recipient cells (10 μL) were transferred onto 0.45 μm nitrocellulose membrane filters on LB agar. The mixtures were then incubated at 37°C for 8 h. The cells were then suspended in sterile PBS and used for flow cytometry, fluorescence microscopy, or serially-diluted and spotted on LB plates containing appropriate antibiotics for bacterial enumeration. The conjugation frequency was calculated as the number of transconjugants per output recipients. The experiment was performed with 3 biological replicates. The coefficient of variation (CV) is calculated as standard deviation (SD) / mean × 100 %.

2.6. Antimicrobial susceptibility testing

The minimum inhibitory concentrations (MICs) of meropenem, ampicillin and colistin were determined using the broth dilution method and the results were interpreted according to the guideline of Clinical and Laboratory Standards Institute (CLSI, 2018). The assay was performed using 3 biological replicates. *E. coli* ATCC 25922 was used as the quality control strain.

2.7. Bacterial growth curve assay

The overnight cultures of bacterial strains were adjusted to an OD_{600} ~0.3 and then diluted 10 times with LB broth. 100 μL cells (~10^6 CFU) were then transferred into 10 mL LB and cultured at 37°C at 180 rpm. The growth was monitored by measuring OD_{600} for 24 hours, and growth curves were constructed using Prism 8 (GraphPad, San Diego, Ca, USA).

2.8. Transposition assays

Transposition assays were performed as previously described with minor modifications (YZ et al., 2019). In brief, suicide plasmids pJS05 and pJS06, each harboring the RK2 replicons and *mcr-1* transposon while pJS06 contains an additional *sfGFP* gene inserted downstream of *mcr-1*, were electroporated into *E. coli* WM3064 to generate the donors WM3064/pJS05 and WM3064/pJS06. *E. coli* MG1655 was used as a recipient in the transposition assays. The donor strain was grown for 8 h at 37°C in LB supplemented with DAP until an OD_{600} of ~0.3. The recipient strains were cultivated in LB at 37°C until an OD_{600} of ~0.3 was reached. Both donor and recipient strains were centrifuged for 5 min at 6000 rpm, and 10 μL donor and recipient cells were mixed by pipetting and placed on membrane filters on LB agar plates supplemented with DAP, followed by incubation at 37°C for 8 h. Membranes were then transferred to microcentrifuge tubes containing 900 μL PBS and vortexed to release the cells. Transposons were then identified as colonies growing on selective agar plates containing CS without DAP. The transposition frequency was calculated as transposons per recipient, and conjugation assays were performed using 6 biological replicates.

2.9. Fluorescence imaging of bacteria

Bacteria were washed by PBS and centrifuged at 6000 rpm, then resuspended in PBS. A 1 μL suspension was dropped onto a microscope slide and covered with a glass coverslip. The bacteria were imaged using a laser scanning confocal microscope (LSCM, LEICA, TCS SP8) with the BF (bright field), FITC and TRITC channels.

2.10. Animal ethics statement

Female C57BL/6 mice, 6 weeks old, were housed at the Laboratory Animal Center of Southern Medical University, Guangzhou, China. Animal care was conducted in accordance with the guidelines of the American Association for Accreditation of Laboratory Animal Care criteria. All animal experiments were carried out in compliance with institution's guidelines for animal use and the Guide for the Care and use of Laboratory Animals at laboratory animal center of South China Agricultural University (Guangzhou, China).

2.11. Isolation of live bacteria from mouse gut

Live gut bacteria from mice were isolated using a previously established protocol with minor modifications(Ronda et al., 2019). Briefly, 250 μl of PBSC (pH 7.4 PBS containing 0.1 % (w/v) L-cysteine) was added to pre-weighed stool samples in microcentrifuge tubes. The samples were mechanically disrupted using a motorized pestle, and 750 μL PBSC was added, followed by vortex mixing and centrifugation at 1000 rpm for 30 s. 750 μL of supernatant was then transferred into a new tube. The above step was repeated three more times to obtain a total ~3 mL supernatant. The resulting 3 mL of isolated cells were pelleted by centrifugation at 6000 rpm for 5 min, and the supernatant was discarded. The cells were then resuspended in 0.5–1.0 mL of PBSC.

2.12. Conjugation in natural recipient community

Donor strain MQCSZ4GFP was streaked onto LB agar plates with 2 mg/L colistin and incubated at 37°C overnight. Single colonies were incubated into 4 mL LB broth media and grown for 4 h at 37°C. The recipient community was isolated anaerobically from fresh mouse feces immediately before conjugation as described above. The donor cells were washed twice in PBSC and adjusted to OD_{600}~0.5. 10 μL aliquots were mixed 1:1 with recipient cells onto 0.45 μM membrane filters on BHI agar. The mating cultures were incubated at 37°C for 8 h. The cells were harvested from plates by scraping, suspended in 1 mL PBS, and used for downstream experiments.

2.13. Flow cytometry and FACS(fluorescence-activated cell sorting) measurements

The BD FACSAria III (Becton Dickinson Biosciences, San Jose, CA, USA), equipped with BD FACSDiva software, was utilized to quantify the numbers of donor and transconjugants(Klümper et al., 2015). The analysis employed the following settings and voltages: forward scatter=37 V, side scatter=208 V, and detectors for green (bandpass filter 530/30 nm) and red fluorescence (bandpass filter 582/15 nm) were set at 373 and 571 V, respectively. The threshold for the side scatter parameter was set at 300. Sorting was performed using a 70 μm nozzle at a sheath fluid pressure of 70 psi. The BD FACSDiva software version 6.1.3 was used for both operational and analytical purposes. Prior to FACS, all samples were diluted about 100-fold in PBS to ensure optimal detection of donor material ($GFP^-mCherry^+$), gut microbiota without a transferred vector ($GFP^-mCherry^-$), and transconjugants ($GFP^+mCherry^-$). The populations selected for sorting transconjugants consisted of a minimum of 4000,000 cells. The donor strain and recipient strains (gut bacteria) served as mCherry positive control and GFP negative controls, respectively. The FACS plots were generated using the BD FACSDiva software. Plating of approximately 200 isolated transconjugants on BHI agar containing 2 mg/L colistin resulted in the detection of green fluorescence in all colonies by Colony Screening Suite (Singer Instrument, UK). In addition, we also verified the GFP-expressing transconjugants by PCR using primers mcr-1-F-ZSY and mcr-1-R-ZSY from these colonies. Among the isolated transconjugants, 8 colonies were randomly selected and subject to whole genome sequencing (WGS).

2.14. Metagenomic 16S rRNA sequencing and analysis

The microbial DNA from the FACS-sorted transconjugants and recipients was extracted using the E.Z.N.A. stool DNA Kit (Omega Bio-Tek, Norcross, GA, USA) following the manufacturer's instructions. The V3-V4 hypervariable regions of the bacteria 16S rRNA genes were amplified using PCR, and the amplicons were sequenced using the Illumina MiSeq platform. The raw data was quality filtered using Trimmomatic (version 0.33)(Bolger et al., 2014). Primer sequences were identified and removed using Cutadapt (version 1.9.1)(Kechin et al., 2017), followed by the merging of paired-end reads and removal of chimeras using USEARCH (version 10)(Edgar, 2013) and employing UCHIME (version 8.1)(Edgar et al., 2011). High-quality sequences were obtained for subsequent analysis. Sequence clustering was performed using USEARCH (version 10.0)(Edgar, 2013). DADA2 method from QIIME2 (version 2020.6) was used to denoise the quality-controlled data(Bolyen et al., 2019). Abundance and diversity analysis of operational taxonomic units (OTUs) was conducted for the samples. Representative OTUs were

aligned using the GeneBank (NCBI) databases.

2.15. WGS and phylogenetic analysis

Whole genome sequencing (WGS) was performed on a subset of chosen isolates using the Illumina MiSeq system (Illumina, San Diego, CA, USA). The resulting paired-end Illumina reads were assembled using SPAdes v3.6.2 (Bankevich et al., 2012) and genome annotation was conducted via the Prokaryotic Genome Annotation Pipeline server. Bacterial species and potential contamination were examined by Mash 2.2 using NCBI RefSeq genome database(Ondov et al., 2019). For sequence comparisons(Alikhan et al., 2011), the BLASTn algorithm integrated within BLAST Ring Image Generator (BRIG) Version 0.95 was employed. Additionally, EasyFig2.1 was utilized for linear plasmid comparisons using the BLASTn default settings(Sullivan et al., 2011).

2.16. Statistical analysis

The statistical analysis was performed using GraphPad Prism 8 software. The results are presented as the mean ± standard deviation obtained from at least three independent experiments. To determine significant differences between groups, unpaired t-tests or one-way analysis of variance (ANOVA) were used, and a p-value of less than 0.05 was considered significant.

3. Results

3.1. Two plasmid CRISPR/Cas9 system was used for fluorescence tagging

In this study, we have introduced a novel tool that utilizes the sfGFP fluorescence tag to track the spread of clinically important ARGs harbouring plasmid in bacterial communities. Unlike previous studies, in which a fluorescence tag was either inserted in a gene or integrated randomly into a plasmid (Buckner et al., 2020; Hardiman et al., 2016; Shintani et al., 2014), our approach targets the conserved regions associated with different ARGs. These earlier techniques were limited in their ability to quickly label diverse plasmids containing the same ARG. Moreover, they could pose a risk of causing unintended biological consequences due to the stochastic nature of the insertions.

To overcome these limitations, we have developed this novel fluorescence plasmid tagging system, specifically targeting the conserved regions associated with different ARGs. ARGs are often linked to different mobile genetic elements (MGEs), such as the carbapenemase genes bla_{KPC}, bla_{NDM} and bla_{OXA-48}, associated with Tn*4401*/NTM$_{KPC}$ (Chen et al., 2012), Tn*125* (Chen et al., 2015) and Tn*1999* (Potron et al., 2014), respectively. The mobile colistin resistance *mcr-1* gene is often situated in complete or partial Tn*6330* with a core *mcr-1-pap2* cassette (He et al., 2019; Snesrud et al., 2018). Our analysis of NCBI database genomes of bla_{KPC}, bla_{NDM}, bla_{OXA-48} and *mcr-1* genes has revealed conserved regions within these gene cassettes across diverse plasmid types (Fig S1a). For instance, the *mcr-1-pap2* cassette (approx. 2000 bp) in Tn*6330* is highly conserved in *mcr-1*-containing IncX4, IncI2 and IncHI2 plasmids. The above in silico analysis suggested that the regions flanking the AMR genes could be transferred together with the AMR genes during horizontal gene transfer. This characteristic renders these regions prime candidates for fluorescence-based tracking. Our system targets the conserved regions associated with specific ARGs, such as bla_{KPC}, bla_{NDM}, bla_{OXA-48} and *mcr-1*. This capability allows us to label different clinically significant plasmids containing the same ARGs, regardless of the plasmid background, using the same fluorescence tagging system. If the ARGs are located on the chromosome, our design also facilitates the insertion of the *sfGFP* gene into the chromosome.

Six clinical isolates, each harboring different ARGs, were selected for fluorescence tagging. These isolates were obtained from *E. coli*, *S.* Typhimurium and *K. pneumoniae* and carried *mcr-1* (CSZ4, 14E1050 and LS3479), bla_{KPC-2} (50700), bla_{NDM-1} (HZE22), and bla_{OXA-48} (49210). The *mcr-1* gene was located on plasmids pCSZ4 (IncX4), p14E1050 (IncI2), and pLS3479 (IncHI2), while bla_{NDM-1}, bla_{KPC-2} and bla_{OXA-48} were located on plasmids pHZE22 (IncHI2), p50700 (IncF) and p49210 (IncL), respectively (Table S2 and Fig S1b).

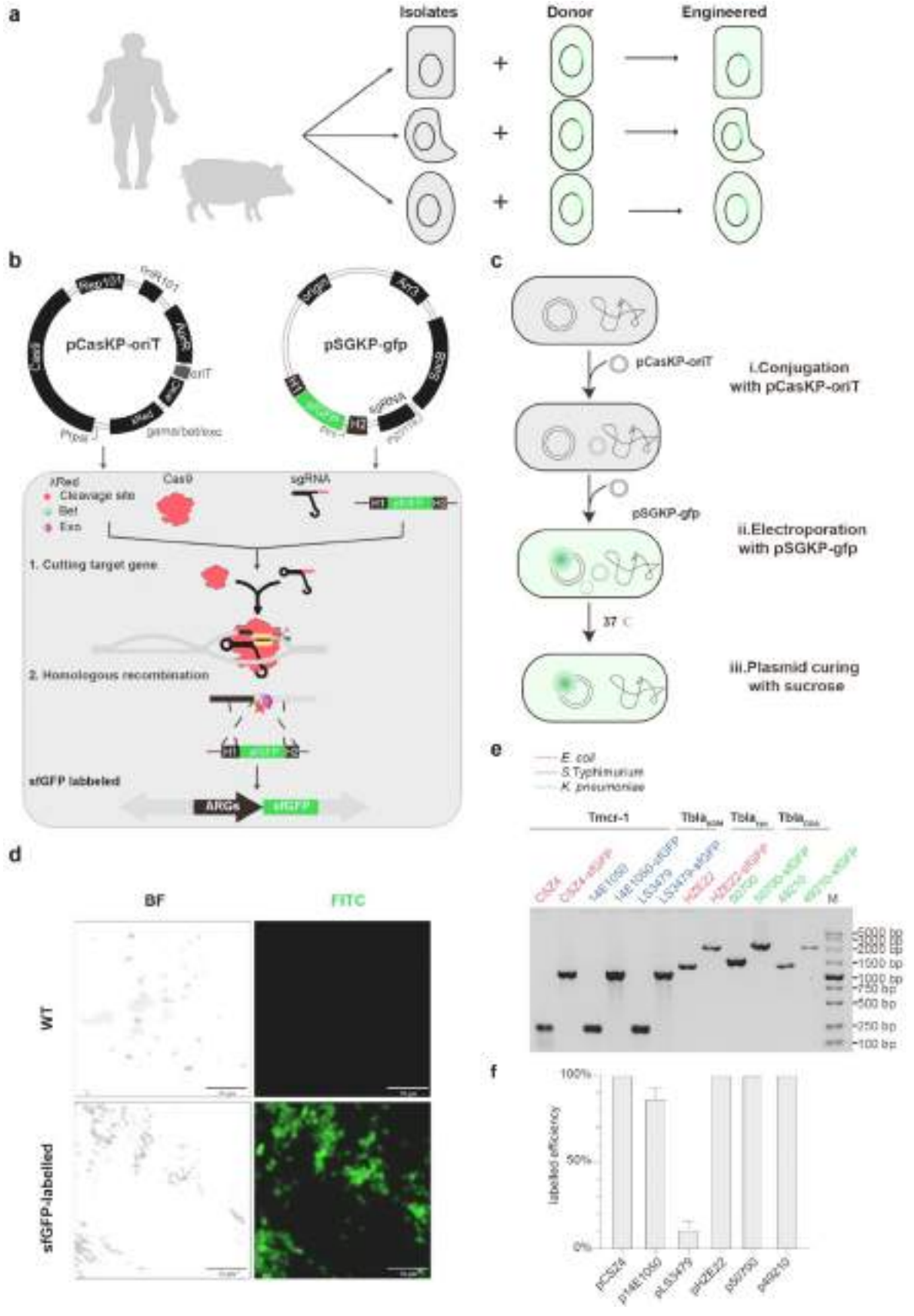
Subsequently, a two plasmids CRISPR/Cas9 system (consisting of plasmid pCas9-oriT and pSGKP-gfp) was utilized for fluorescence tagging (Table S2 , Fig. 1a). Plasmid pCas9-oriT was engineered by the addition of an *oriT* region to the thermosensitive plasmid pCas9-apr, which provides Cas9 and lambda Red proteins (Qi et al., 2012). This plasmid enabled the transfer of Cas9 and lambda Red genes to clinical isolates through conjugation. The plasmid pSGKP-gfp encoded the sgRNA under the control of the J23119 promoter (Qi et al., 2012), the superfolder green fluorescent protein gene (*sfGFP*) under the control of the pTrc promoter, the sucrose-sensitive gene *sacB* (Quandt and Hynes, 1993) as well as a homologous DNA fragment targeting the AMR gene. Upstream and downstream elements of approximately 500 bp flanking the sfGFP insertion site were PCR amplified and ligated to pSGKP-gfp at the *Xba*I site. The *sfGFP* gene on the plasmid pSGKP-gfp is regulated by a modified pTrc promoter, which can be repressed by the LacI^{q} protein (Fig. 1b).

Four pSGKP-gfp plasmids (pSGKP-arr2-TKPC500GFP, pSGKP-arr2-TNDM500GFP, pSGKP-arr2-TOXA500GFP and pSGKP-Tmcr-500GFP) were constructed, each targeting the bla_{KPC}, bla_{NDM}, bla_{OXA-48} and *mcr-1* gene cassettes, respectively. To tag *sfGFP* gene in the conserved downstream region of the ARGs, the pCasKP-oriT plasmid was transferred into the clinical isolates *E. coli* CSZ4, S. Typhimurium 14E1050, *S.* Typhimurium LS3479, *K. pneumoniae* 50700, *E. coli* HZE22 and *K. pneumoniae* 49210, respectively, through conjugation, achieving a 100 % success rate for each strain. Subsequently, the plasmid pSGKP-gfp with different homologous templates (e.g. pSGKP-arr2-TKPC500GFP, pSGKP-arr2-TNDM500GFP, pSGKP-arr2-TOXA500GFP and pSGKP-Tmcr-500GFP) was electrotransformed into the aforementioned strains harboring pCasKP-oriT. Following induction with L-arabinose, the sfGFP fluorescent tag was successfully inserted into the region downstream of *mcr-1*, bla_{NDM-1}, bla_{KPC-2}, bla_{OXA-48} in the strains *E. coli* CSZ4, S. Typhimurium14E1050, S. Typhimurium LS3479, *E. coli* HZE22, *K. pneumoniae* 50700 and *K. pneumoniae* 49210, respectively (Fig. 1c). By increasing the cultivation temperature of the strains to 37°C and subjecting them to selection on 5 % sucrose plates, PCR results confirmed the complete elimination of plasmids pSGKP-gfp and pCas9-oriT from the sfGFP labelled strains (Fig S2). Further PCR screening and laser scanning confocal microscope (LSCM) showed that all of these strains were successfully labelled with *sfGFP* at the targeted sites (Fig. 1d-e). The labeling efficiency ranged from 11.09 % (pLS3479) to 100 % (85.85 % for p14E1050, and 100 % for pCSZ4, pHZE22, p50700 and p49210), as shown in Fig. 1f.

3.2. Fluorescence labeling did not interfere normal functions of the bacterial strains

To assess the effects of fluorescent labeling on host strains, we compared the minimum inhibitory concentration (MIC) values and growth curves of *sfGFP*-labelled strains with those of their parent strains. The results showed no differences in the MIC values of CS, MEM, or AMP in *E. coli* CSZ4, *S.* Typhimurium 14E1050, *S.* Typhimurium LS3479, *E. coli* HZE22, *K. pneumoniae* 50700, and *K. pneumoniae* 49210 between the *sfGFP*-labelled strains and their parent strains (Fig. 2a). Additionally, the growth kinetics of the *sfGFP*-labelled and parent strains were found to be the same (Fig. 2b and Fig S3). These findings suggested that the fluorescent labeling did not alter the antimicrobial susceptibility of the AMR genes or impose any significant fitness costs on the bacterial hosts.

We then examined whether the fluorescent tagging would impact the plasmid conjugation frequency. The coefficient of variation (CV) of conjugation frequency (logarithmically transformed) among replicates ranged from −0.53 % to −23.25 %. No significant differences in conjugation frequency were observed between *sfGFP*-labelled strains



(caption on next page)

Fig. 1. Two plasmid CRISPR/Cas9 system was used for fluorescence tagging. (a) The two-plasmid CRISPR/Cas9 system was employed to tag the *sfGFP* gene at the downstream conserved-region of ARGs in clinical isolates. (b) Schematic representation of the procedures involved in the fluorescence tagging process using the two-plasmid CRISPR/Cas9 system. (c) Schematic representation of the two-plasmid CRISPR/Cas9 system utilized to tag the *sfGFP* gene at the downstream conserved-region of ARGs in clinical isolates. The sgRNA-Cas9 complex is responsible for cleaving the double-strand DNA adjacent to a PAM site, thereby generating a double-stranded DNA break. The double-stranded DNA break is repaired through the process of lambda Red-mediated homologous recombination. (d) Laser scanning confocal microscope (LSCM) of the *sfGFP*-labelled strains along with their parent strains. BF, bright-field. (e) Genotyping PCR results of the *sfGFP*-labelled *E. coli* CSZ4-sfGFP, *S.* Typhimurium 14E1050-sfGFP, *S.* Typhimurium LS3479-sfGFP, *E. coli* HZE22-sfGFP, *K. pneumoniae* 50700-sfGFP, *K. pneumoniae* 49210-sfGFP, and their respective parent strains. (f) The labelled efficiency of *E. coli* CSZ4, *S.* Typhimurium 14E1050, *S.* Typhimurium LS3479, *E. coli* HZE22, *K. pneumoniae* 50700, and *K. pneumoniae* 49210. The calculation of labeling efficiency (%) involved determining the percentage of *sfGFP*-labelled clones out of all the clones that were tested.

and their parent strains ($P > 0.05$, Fig. 2c-d).

We also examined if the insertion with *sfGFP* element would impact the transposition frequency. We cloned the *mcr-1* or *mcr-1-sfGFP* into the suicide plasmid pJS01 (He et al., 2019; He et al., 2020), resulting in the plasmid pJS05 (containing a 4673 bp Tn) and pJS06 (containing a 5582 bp Tn) (Fig. 2e-g), respectively. The transposition frequencies into *E. coli* MG1655 were $1.48\pm0.66 \times 10^{-6}$ and $1.98\pm0.21 \times 10^{-6}$ per transformed cell for pJS05 and pJS06, respectively. No significant transposition frequency differences were observed between pJS05 and pJS06 ($P > 0.05$, Fig. 2h). These results indicated that labeling the *sfGFP* gene at the downstream conserved region of ARGs did not impact antibiotic susceptibility, growth characteristics, conjugation frequency, or transposition frequency.

3.3. Monitoring the horizontal transfer of ARGs using a dual-fluorescence reporter system

To improve the detection of ARGs transfer from clinical isolated isolates to complex microbiota, we constructed a non-transferable ColE1 plasmid pMQ. The plasmid pMQ expresses mCherry fluorescence protein and $LacI^q$, which inhibits the sfGFP promoter pTrc. The concept behind this design is to introduce the pMQ into sfGFP tagged clinical isolates, and the presence of pMQ will inhibit the sfGFP expression, resulting in the manifestation of only red fluorescence due to the expression of *mCherry* gene in pMQ. However, when the sfGFP labeled ARG plasmid is transferred to other recipients, the inhibition of sfGFP promoter is removed, thereby enabling the emission of green fluorescence (Fig. 3a). This dual-fluorescence reporter system facilitates a straightforward differentiation and quantification of transconjugant cells, which can be accomplished through flow cytometry or rapid detection using a confocal microscope.

We then experimentally validated the design. The plasmid pMQ was transformed into *E. coli* CSZ4-sfGFP, *K. pneumoniae* 49210-sfGFP, *E. coli* HZE22-sfGFP to track the transfer of IncX4-*mcr-1*, IncL-bla_{OXA-48} and IncHI2-bla_{NDM-1} plasmids, respectively. As shown in Fig. 3b, *E. coli* CSZ4-sfGFP, *K. pneumoniae* 49210-sfGFP, *E. coli* HZE22-sfGFP showed green fluorescence. Upon introduction of pMQ into *E. coli* CSZ4-sfGFP, *K. pneumoniae* 49210-sfGFP *or E. coli* HZE22-sfGFP, only red fluorescence was observed.

In the conjugation system, both red and green fluorescence were observed, representing donor pMQ/AMR plasmids-harboring strains and *E. coli* C600 transconjugants, respectively (Fig. 3b). To confirm the fluorescence detecting results, we randomly selected ~10 green and red colonies, and subsequently conducted PCR, Sanger sequencing, Enterobacterial Repetitive Intergenic Consensus PCR (ERIC PCR) and found that the red colonies were all from donors, while the green colonies were all from the *E. coli* C600 transconjugants (Fig S4). These results confirmed that our dual-fluorescence reporter system can effectively detect the AMR plasmid transfer *in vitro*.

The high conjugation frequency of the *mcr-1*-carrying IncX4 plasmid pCSZ4 (31,229 bp, Fig S5) from *E. coli* CSZ4 to *E. coli* C600 strain prompted us to select it for further studies. To investigate the potential of IncX4-*mcr-1* transfer from dual-fluorescence reporter system *E. coli* MQCSZ4GFP to mixed bacterial populations, we firstly established recipient populations with the addition of three other Gram-negative species: *S.* Typhimurium 14028, *K. pneumoniae* 700603 and *A. baylyi* ADP1. Using our above described pMQ/AMR-sfGFP system, we examined the IncX4-*mcr-1* transfer in the bacterial populations using LSCM. The conjugation frequency obtained through fluorescence-based assay was presented in a normalized context with transconjugants (green) per donor counts (red). Our results revealed the fluorescence of both red and green cells in the conjugation cultures of *E. coli* C600, *S.* Typhimurium 14028 and *K. pneumoniae* 700603, with transfer frequencies (TCs/donors) of $(2.21\pm1.40) \times 10^{-1}$, $(3.70\pm2.34) \times 10^{-4}$ and $(6.00\pm1.61) \times 10^{-4}$, respectively. However, no *A. baylyi* ADP1 transconjugants were observed using LSCM (Fig. 3c-d). To validate the fluorescence tracking results, we further conducted conjugation assay using culture-based approach. The results showed that IncX4-*mcr-1* transferred successfully from donor to the recipient strains, including *E. coli* C600, *S.* Typhimurium 14028 and *K. pneumoniae* 700603, with frequencies (TCs/donors) of $(1.37\pm0.57) \times 10^{-1}$, $(3.27\pm0.92) \times 10^{-4}$ and $(5.53\pm2.14) \times 10^{-4}$, respectively. Notably, transfer to *A. baylyi* ADP1 was not observed (Fig. 3d). The transfer frequency of IncX4-*mcr-1* to different bacteria exhibited no significant difference between culture-based and fluorescence-based assays ($P > 0.05$). The fluorescence-based assays produced consistent results with the culture-based findings, reinforcing the potential applicability of our system in monitoring plasmid-mediated ARG transfer within natural bacterial populations, such as the fecal microbiota.

3.4. Plasmid pCSZ4-sfGFP transfer in natural fecal microbiota community

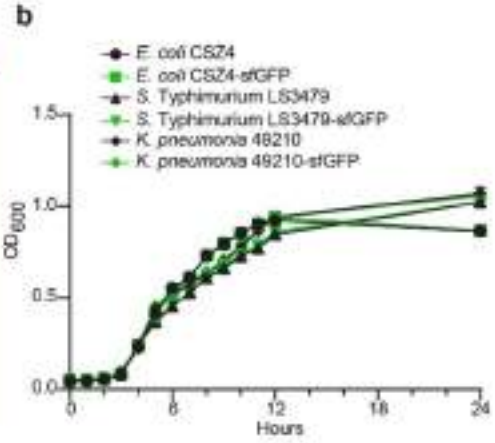
Next, we explored the plasmid-mediated ARGs transfer within fecal microbiota community using the IncX4-*mcr-1* dual-fluorescence reporter system. The generated transconjugants were isolated via cell sorting (FACS) and characterized by 16S rRNA gene amplicon sequencing (Fig. 4a). Initially , we optimized the gating stringency of FACS with donor (MQCSZ4GFP), GFP positive control (CSZ4-sfGFP) and fecal microbiota. In the FACS analysis, zone Q1 represents mCherry fluorescent donor cells, Q2 represents both positive signals, Q3 indicates both negative signals without fluorescence, and the Q4 region defines the sorted $GFP^+mCherry^-$ transconjugant populations (Fig. 4b). Subsequently, we introduced GFP-tagged bacteria into a synthetic community comprising equimolar concentrations of donor bacteria and fecal microbiota.

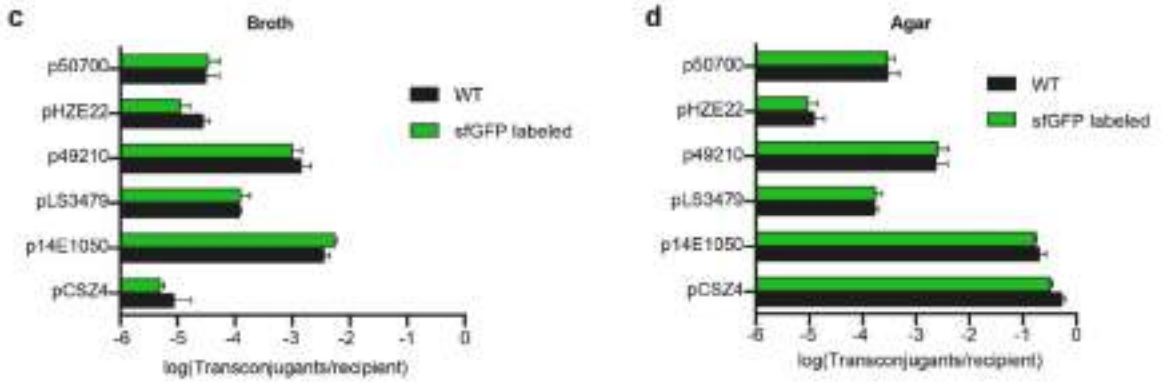
By comparing the GFP-tagged bacteria ratio with the observed $GFP^+mCherry^-$ cell ratio, we established standard curves for the $GFP^+mCherry^-$ cell ratio (y) and GFP-tagged bacteria ratio (x) for recipients and donors with the equations : $y=0.9835x-8E-05$ ($R^2=1$, TCs/Recipients) and $y=0.9996x-0.001$ ($R^2=1$, TCs/Donors , Fig S6), respectively. Following this, we conducted in vitro conjugation experiments with fecal microbiota, which confirmed the successful transfer of the payload from donors to fecal microbiota. This resulted in the generation of $GFP^+mCherry^-$ transconjugants that could be selectively enriched using FACS (Fig. 4b).

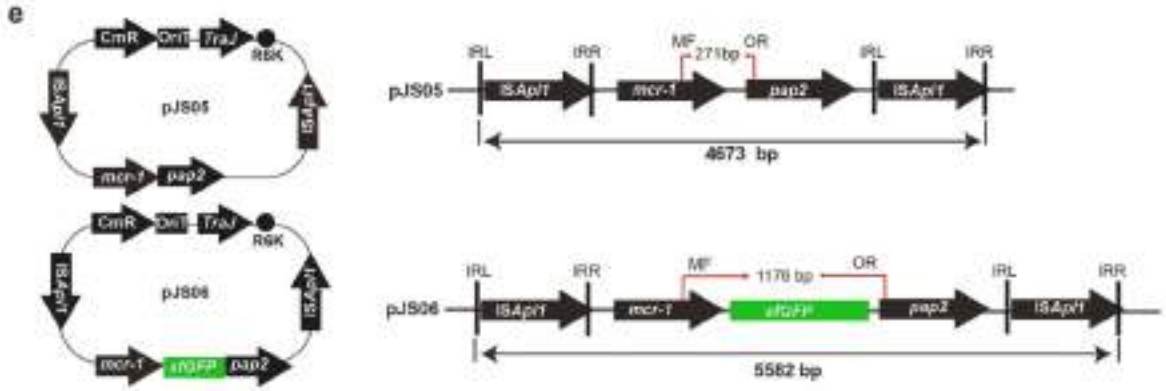
Subsequent 16S rRNA sequencing analysis was performed on the FACS-enriched transconjugant populations. Our observations revealed that the recipient (fecal microbiota, RPs) comprised a total of 294 core OTUs. The FACS-enriched transconjugant populations (TCs) had 69 core OTUs (Fig. 4c). At the phylum level, 8 bacteria phyla were detected in the RPs group, with *Bacteroidota*, *Firmicutes*, *Patescibacteria*, and

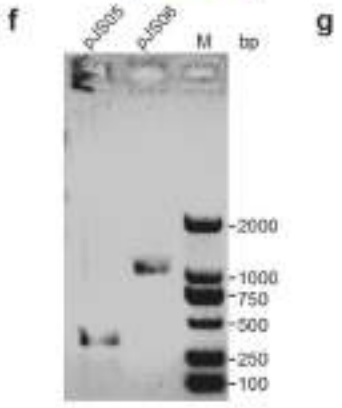
a

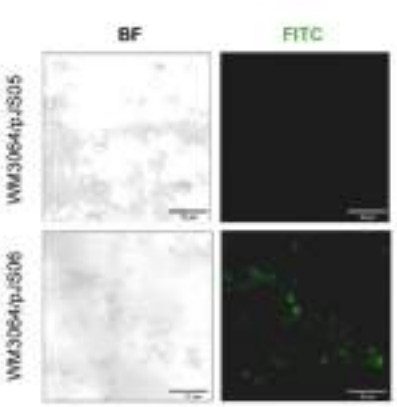
Strains	CS (mg/L)	MEM (mg/L)	AMP (mg/L)
E. coli CSZ4	4	-	-
E. coli CSZ4-sfGFP	4	-	-
S. Typhimurium 14E1050	4	-	-
S. Typhimurium 14E1050-sfGFP	4	-	-
S. Typhimurium LS3479	4	-	-
S. Typhimurium LS3479-sfGFP	4	-	-
E. coli HZE22	-	32	>256
E. coli HZE22-sfGFP	-	32	>256
K. pneumoniae 50700	-	256	>256
K. pneumoniae 50700-sfGFP	-	256	>256
K. pneumoniae 49210	-	2	>256
K. pneumoniae 49210-sfGFP	-	2	>256

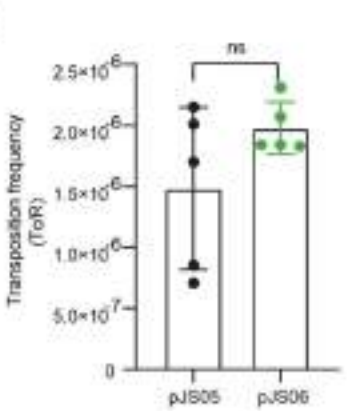












(caption on next page)

Fig. 2. Fluorescence labeling did not interfere normal functions of the bacterial strains. (a) The minimum inhibitory concentrations (MICs) of strains labelled with *sfGFP* gene were compared to those of the parental strains. (b) Growth curves of strains labelled with *sfGFP* gene and their parental strains were observed over a period of 24 hours. (c) The conjugation frequencies of plasmids labelled with *sfGFP* gene were compared to those of the parental plasmids using both broth mating. (d) The conjugation frequencies of plasmids labelled with *sfGFP* gene were compared to those of the parental plasmids using agar mating. The experiment was conducted with three biological replicates. (e) The plasmids pJS05 and pJS06 were depicted in maps, illustrating the presence of a 4673 bp transposon (Tn) in pJS05 and a 5582 bp Tn with *sfGFP* gene in pJS06. The figure displayed the R6K replication, RP4 *oriT*, *traJ, cmR*, IS*Apl1*, *mcr-1*, and *pap2* genes. The *mcr-pap2* cassette was flanked by two IS*Apl1* elements, forming a composite transposon (Tn). To assess pJS05 and pJS06, primers MF and OR were utilized, resulting in the generation of a 271 bp fragment (pJS05) or a 1176 bp fragment (pJS06). IRL, inverted repeat left. IRR, inverted repeat right. (f) The genotyping PCR results of plasmid pJS05 and pJS06 were analyzed using primers MF and OR. (g) The laser scanning confocal microscope (LSCM) was used to examine WM3064/pJS05 and WM3064/pJS06. BF, bright-field. (h) The transposition frequencies in pJS05 or pJS06 were determined by calculating the number of transposons per recipient, n=6. ns, $P > 0.05$. * , $P < 0.05$.

Proteobacteria being the top four bacterial phyla. However, in the TCs group, the predominant phylum of bacteria is *Proteobacteria*, followed by *Firmicutes*, *Bacteroidota*, and others (Fig. 4d). At the genus level, the relative abundance of the most abundant genera in RPs were *Muribaculaceae* (0.228), unclassified_*Lachnospiraceae* (0.165), *Lachnospiraceae*_NK4A136_group (0.093), *Alistipes* (0.075), uncultured_*Bacteroidales*_bacterium (0.073), *Bacteroides* (0.066), *Muribaculum* (0.05), *Candidatus_Saccharimonas* (0.030), *Escherichia_Shigella* (0.030). In contrast, the relative abundance of the most abundant genera at genus level in TCs were *Escherichia_Shigella* (0.867), *Enterococcus* (0.068), unclassified_*Muribaculaceae* (0.0002), *Lachnospiraceae*_NK4A136_group (0.00003), uncultured_*Bacteroidales*_bacterium (0.00001), unclassified_*Lachnospiraceae* (0.000009) (Fig. 4e). Simultaneously, the patterns of transconjugants were displayed on a heatmap (Fig S7), revealing that transconjugant OTUs were classified into two main clusters. Notably, we observed substantial reproducible enrichment of Proteobacteria and Firmicutes, particularly *Escherichia_Shigella* and *Enterococcus*, among successful transconjugants across multiple independent experiments (Fig. 4e and Fig S7). The most abundant taxa in TCs/RPs at the genus level included *Escherichia_Shigella*, *Enterobacter*, *Pseudomonas*, and *Enterococcus*, followed by *Ligilactobacillus* and *Lactobacillus* (Fig. 4f). The 16S rRNA sequencing of these transconjugant populations unveiled a broad spectrum of phylogenetic diversity.

3.5. Identification of transconjugants from the mice with whole genome sequencing

In parallel to FACS metagenomic studies, we isolated individual transconjugants from sorted library, containing potential distinct transconjugants, by selectively plating the library with a colistin concentration of 2 mg/L as payload. Confirmation of transconjugants was achieved through UV imaging and PCR. Across the experiments, the majority of colonies that grown on the plate were green (Fig. 5a). We successfully isolated and validated over 60 *mcr-1* positive transconjugants, encompassing three genera within the Phylum Proteobacteria (Fig. 5b-c). Eight transconjugants carrying the *mcr-1* gene and displaying distinct colony morphologies were selected for whole-genome sequencing (WGS). Genomic analysis revealed that two of these transconjugants originated from *C. freundii* (W14–1 and W13–4), five from *S. sonnei* (W17–2, R2–1, R6–1, R1–1, and R7–1), and one from *E. cloacae* (440−2) (Fig. 5d). Further blastn based comparative genomic analysis confirmed the presence of pCSZ4-sfGFP and the lack of *mCherry* among all the genomes (Fig. 5e), indicating that *mcr-1 was* successfully transferred to the recipient microbiota bacteria along with the IncX4 plasmid through conjugation.

To investigate the potential of transconjugants within the microbiota to serve as intermediate donors, initiating secondary plasmid transfers, we conducted conjugation experiments via agar mating. FACS-sorted transconjugants were employed as donors, with *E. coli* C600 as the recipient. The results illustrated that the IncX4-*mcr-1* plasmid could be effectively transferred to *E. coli* C600. This implies that specific gut bacteria are able to act as intermediate hosts for subsequent plasmid transfer.

4. Discussion

HGT plays a crucial role in driving the dissemination of ARGs among bacteria. Gaining insight into the specific bacteria that are more inclined to accept plasmids, along with identifying potential factors influencing their susceptibility, is pivotal for achieving a thorough understanding of plasmid dissemination mechanisms and their ecological ramifications. However, a lack of a robust tracking system has hindered our comprehensive comprehension of ARG transfer within complex bacterial ecosystems. The implementation of CRISPR-AMRtracker, capable of distinguishing between donor, recipient and transconjugant populations, offers a distinct advantage in investigating HGT. Our study established a novel toolkit to enhance the investigation of clinical plasmid transfer.

In this study, the *sfGFP* gene driven by the promoter (Ptrc) was employed as a reporter for the plasmid. The Plac promoter is a commonly used inducible promoter that governs gene expression. Sanin Musovic et al. detected Plac::gfp expression in Proteobacteria and Bacteroides (Musovic et al., 2014). Masaki Shintani et al. further extended this finding, showing Plac promoter-derived $P_{A1/04/03}$-induced gfp expression in Proteobacteria, Actinobacteria, Bacteroidetes, and Firmicutes (Shintani et al., 2014). Derived from Plac (lac) promoter, Ptrc promoter has been optimized for increased flexibility and efficiency in gene regulation. It effectively controls gene expression in Gram-negative bacteria like *E. coli*, *Salmonella spp*, *Klebsiella spp*, and some Gram-positive bacteria such as *Bacillus subtilis* (Musovic et al., 2014). The sfGFP emits green fluorescence upon exposure to blue to ultraviolet light. Notably, sfGFP expression has been documented not only in eukaryotic organisms (Zhang et al., 2020), but also in a variety of prokaryotic organisms, including *A. baumannii* (Godeux et al., 2018), *L. lactis* (Hernández-Ortega et al., 2022), *B. subtilis* (Xu et al., 2022). Furthermore, Carlotta Ronda et al. employed the *sfGFP* gene to directly modify various taxa within the mouse gut microbiome (Ronda et al., 2019). We also observed the expressions of Ptrc-controlled sfGFP in bacteria of *E. coli*, *Salmonella spp*, *Klebsiella spp*, *C. freundii*, *S. sonnei, and E. cloacae*. These findings indicate its potential functionality across diverse bacterial species. In this study, the implementation of Ptrc-controlled sfGFP in our design allows for real-time detection of AMR plasmid transfer among different microbiota species using flow cytometry or fluorescent microscopy techniques.

Previous dual-fluorescence tracking systems were limited to the examination of plasmid transmission for a few specific types (e.g., RP4, pKJK5) (Qiu et al., 2018). However, clinical plasmids possess a more intricate genetic context due to the inclusion of MGEs and recombination events, potentially leading to distinct transmission behaviors when compared to the aforementioned plasmids. For example, the *mcr-1-pap2* structure predominates as the carrier of *mcr-1* genes (Lu et al., 2023). Common Tn*4401* genetic elements include *tnpA* and *tnpR*, which are Tn*3*-based transposases inserted upstream of bla_{KPC}. Additionally, IS*Kpn6* and IS*Kpn7* are inserted downstream and upstream of bla_{KPC}, respectively (Chen et al., 2014). Similarly, IS*Aba125* is positioned upstream of bla_{NDM}, while the bleomycin resistance gene, ble_{MBL}, is reliably located downstream (Wu et al., 2019). The dissemination of bla_{OXA-48} is primarily facilitated by the composite transposon Tn*1999* (Manageiro

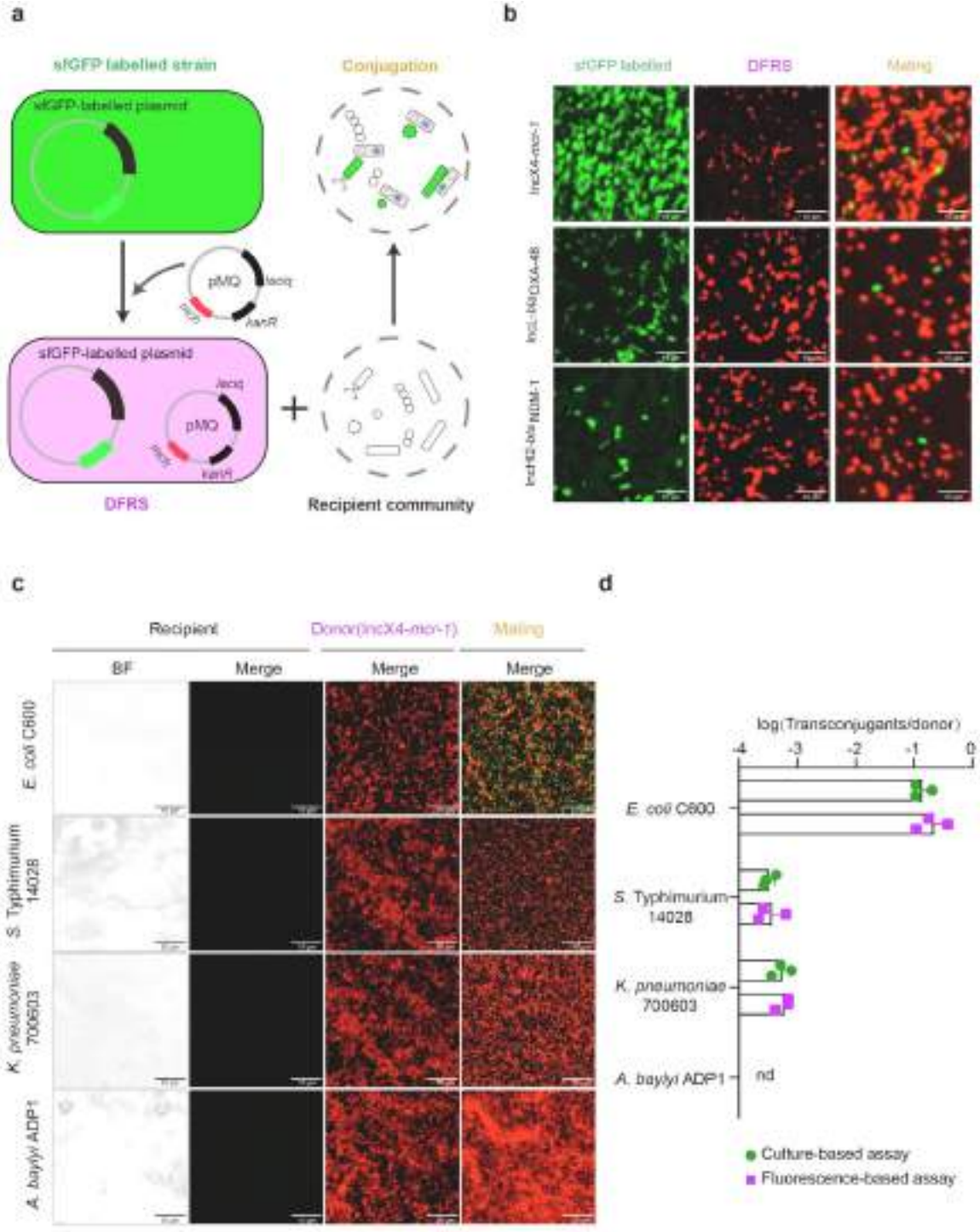


Fig. 3. Monitoring the horizontal transfer of ARGs using a dual-fluorescence reporter system. (a) Development of new dual-fluorescence reporter system (DFRS) to monitor transfer of ARGs within complex microbiota. The donor cells were equipped with two plasmids, including a *sfGFP*-labelled plasmid and a non-transferable ColE1 plasmid pMQ that was tagged with *mCh* and *lacI*^{q} gene. The expression of *sfGFP* gene is repressed by LacIq, resulting in the production of red fluorescence in the donor cell. The plasmid carrying the sfGFP tag was introduced into either an individual recipient cell or a bacterial community, leading to the generation of transconjugants. Following this, the sfGFP protein was produced in the transconjugant cells. (b) The analysis of the sfGFP-labeled strains, DFRS, and the mating cultures of DFRS with the recipient *E. coli* C600 was conducted using a laser scanning confocal microscope (LSCM). The plasmid pMQ was transformed into *E. coli* CSZ4-sfGFP, *K. pneumoniae* 49210-sfGFP, and *E. coli* HZE22-sfGFP to monitor the transfer of IncX4-*mcr-1*, IncL-*bla*$_{\text{OXA-48}}$, and IncHI2-*bla*$_{\text{NDM-1}}$, respectively. (c) The mating cultures of pCSZ4-sfGFP contained *E. coli* MQCSZ4GFP, along with *E. coli*, *S.* Typhimurium, *K. pneumoniae*, and *A. baylyi*, respectively. These cultures were observed using LSCM. (d) The conjugation frequencies of plasmid pCSZ4-sfGFP transfers into *E. coli, S.* Typhimurium, *K. pneumoniae*, and *A. baylyi* strains were determined using both culture-based and fluorescence-based assays. The conjugation frequency obtained through the culture-based assay was calculated by counting the colonies of transconjugant and donor. The conjugation frequency obtained through the fluorescence-based assay was presented in a normalized context, with the number of transconjugants (green) per donor (red). The assay was performed in triplicate, and all data points were included, along with the mean and standard deviation (represented by error bars). nd, no data. ns, $P > 0.05$. * , $P < 0.05$.

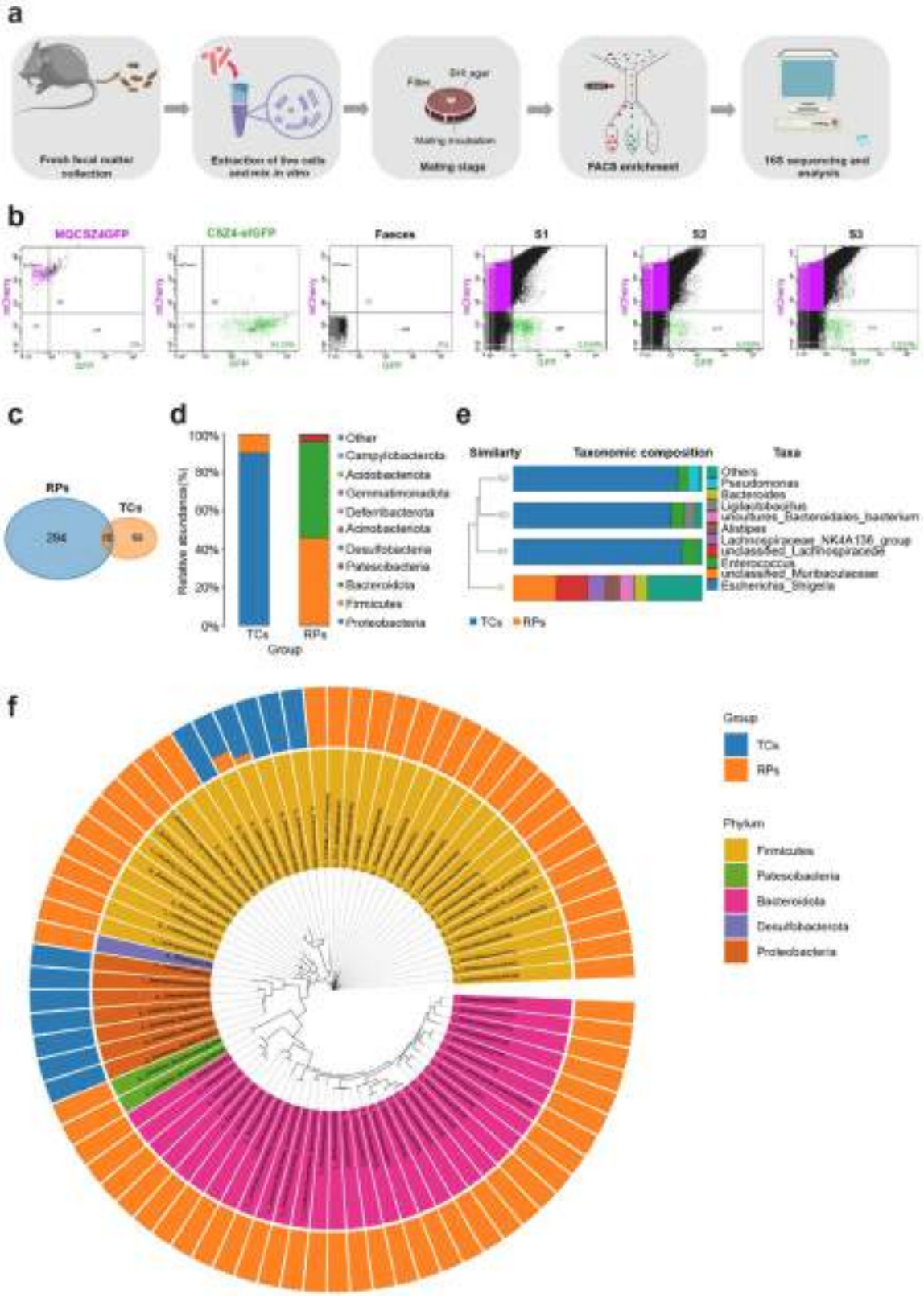


Fig. 4. Plasmid pCSZ4-sfGFP transfer in natural fecal microbiota community. (a) The pCSZ4-sfGFP plasmid was conjugative transfer from the donor strain into fecal bacteria obtained from mice feces. This was followed by the use of FACS and 16S rRNA gene amplicon sequencing. (b) FACS was used to count the donor (MQCSZ4GFP), GFP positive control (CSZ4-sfGFP), mice feces, and mating cultures. The mCherry fluorescent donor cells were represented in Zone Q1, while both positive signals were represented in Zone Q2. Zone Q3 indicated both negative signals without fluorescence, and the sorted GFP+mCherry– transconjugant populations were defined in the Q4 region. (c) The operational taxonomic units (OTUs) representing the microbial composition were analyzed for both the recipient group (RPs) and the transconjugants group (TCs). (d) The genus level analysis was conducted for both RPs and TCs. (e) The microbiota from RPs and TCs were subjected to unweighted UniFrac principal coordinate analysis. (f) The species abundance profile of RPs and TCs. RPs, recipient group. TCs, transconjugants group.

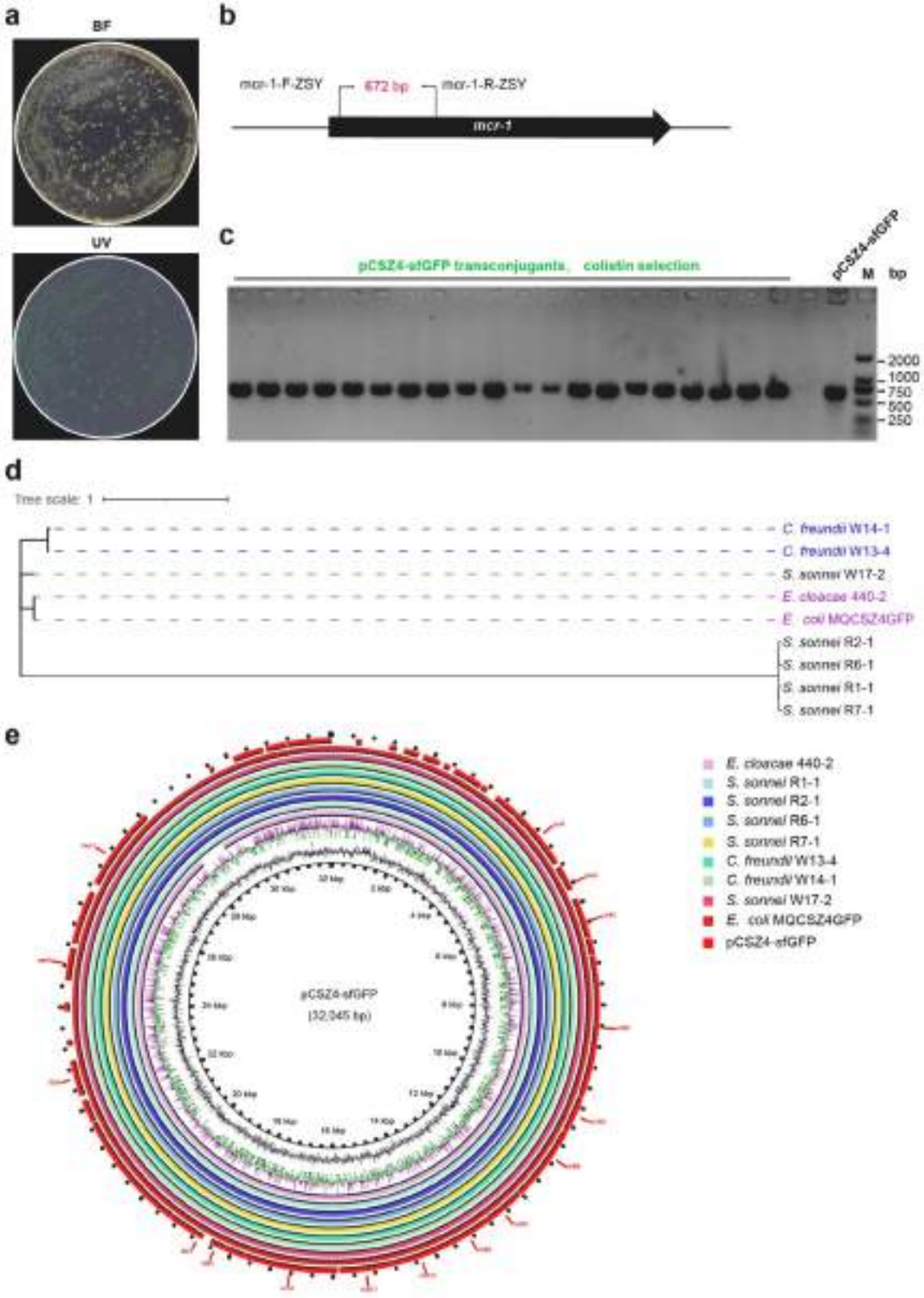


Fig. 5. Identification of transconjugants from the mice with whole genome sequencing. (a) Sorted GFP+ cells were plated on selective media and grown at 37 °C for 24 h. Subsequently, the plates were subjected to imaging using both bright-field (BF) and ultraviolet (UV). (b) The primers mcr-1-F-ZSY and mcr-1-R-ZSY were employed to amplify the *mcr-1* gene, resulting in the generation of a 672 bp fragment. (c) Genotyping PCR results of *mcr-1* gene. (d) The phylogenetic structures, genus types, and names of the *mcr-1* positive isolates. (e) Sequence alignment of sorted *mcr-1* positive isolates. The 32,045 bp plasmid pCSZ4-sfGFP was used as a reference and genetic regions. The donor *E. coli* MQCSZ4GFP was used as positive control.

et al., 2015). The horizontal transfer of these genes involves not only the transfer of plasmids between different strains but may also encompass transposon-mediated transposition within the same cell. Consequently, an ideal tracking system should be capable of capturing both of these scenarios.

In this study, we targeted the conserved downstream regions of *mcr-1*, bla_{NDM-1}, bla_{KPC-1} and bla_{OXA-48} in clinical isolates to integrate the *sfGFP* gene using the CRISPR/Cas9 and Lambda Red system. We successfully labeled these clinically significant ARGs carried by IncX4, IncI2, IncHI2, IncF, and IncL type plasmids, achieving a 100 % labeling success rate with relatively higher labeling efficiency. By selecting conserved sequences surrounding the ARGs as targets, we maximized the labeling potential of distinct plasmid variants bearing ARGs. This study provides effective sgRNA target sequences for effective labeling clinical plasmids carrying *mcr-1*, bla_{NDM-1}, bla_{KPC-2} or bla_{OXA-48}. The labeling strategy employed here directly focused on ARGs, enabling the labeling of diverse Inc plasmid variants and facilitating the monitoring of plasmid transfer across various clinical bacterial strains. In addition, our innovative design, featuring the positioning of the *sfGFP* gene downstream within the conserved region of the ARGs, makes it possible to effectively track the transfer of ARGs facilitated by diverse MGEs, encompassing plasmids, transposons, integrons, and others.

Furthermore, the fluorescently labeled strains demonstrated comparable antibiotic susceptibilities, growth characteristics, conjugation, and transposition behaviors to their parent strains. These findings affirm that fluorescence tagging preserves the normal functionality of the bacterial host, highlighting the applicability of this approach for labeling diverse ARGs-bearing plasmids in clinical strains.

Notably, our results showed that plasmids of IncX4, IncI2, IncF, and IncL types exhibited heightened transfer rates on agar compared to those in broth, possibly due to the promotion of bacterial biofilm formation on solid surfaces (Partridge et al., 2018). It's known that conjugation events in aquatic environments primarily take place in liquid media, whereas gut-based conjugation simulates conditions similar to solids (Neil et al., 2020). Therefore, the employing agar-based mating in our study could more accurately mimic conjugation incidents occurring within the gastrointestinal tract. We selected the *mcr-1*-carrying IncX4 type plasmid pCSZ4, which exhibits a relatively higher conjugation frequency, as a representative model to investigate the versatility of this tool. The IncX4-*mcr-1* plasmid was transferred to *E. coli* C600, *S.* Typhimurium 14028, and *K. pneumoniae* 700603 using both fluorescence-based assays and culture-based methods. The consistent results from these approaches suggest the utility of this system for investigating plasmid transfer within bacterial populations. *A. baylyi* ADP1 has been employed to investigate the potential risks associated with HGT (Fu et al., 2012; Zhang et al., 2021). In a previous study, GFP facilitated the direct in situ visualization of natural transformation in *A. baylyi* (Rizzi et al., 2008). Our observations indicate that the IncX4-*mcr-1* plasmid was not successfully transferred into *A. baylyi* ADP1, as evidenced by both fluorescence-based assays and culture-based methods. Currently, only a few plasmids, such as RSF1010 (IncQ), pQ-mini (IncQ) and pWH1277 (a cryptic plasmid originally isolated from *A. calcoaceticus*), have demonstrated efficient replication and stability within *A. baylyi* ADP1 (Long et al., 2024; Lucidi et al., 2018; Santala and Santala, 2021). We speculate the inability of IncX4-*mcr-1* plasmid transfer into *A. baylyi* ADP1 may be due to specific characteristics related to plasmid replication and maintenance in different bacterial species.

The results of FACS and 16S rRNA sequencing reveal that, at the genus level, the taxa within the $GFP^{+}mCherry^{-}$ population (transconjugants) mainly includes *Escherichia_Shigella*, *Enterobacter*, *Pseudomonas*, *Enterococcus*, *Ligilactobacillus* and *Lactobacillus*. Specifically, a preference for transfer to Enterobacteriaceae bacteria is evident, highlighting diverse preferences and compatibilities among different bacterial types in plasmid transfer. Certain bacteria readily accept and maintain plasmids, leading to higher transfer frequencies, while others exhibit lower receptivity. The variability in recipient bacterial communities, encompassing diversity and abundance, plays a crucial role in influencing plasmid transfer preferences. Bacteria with high abundance and specific mechanisms for plasmid acceptance may serve as primary recipients for efficient plasmid acquisition. As a result, the composition and structure of recipient bacterial communities are key factors influencing the study of plasmid dissemination and receptivity. Some dual-fluorescence reporter systems have been employed for exploring specific plasmid dissemination within microbial communities residing in soil, sediment, and the gut (Brophy et al., 2018; Cyriaque et al., 2020; Fan et al., 2019; Klümper et al., 2015; Ronda et al., 2019). Our results suggest that microbial communities abundant in Enterobacteriaceae, especially those containing high levels of Enterobacteriaceae bacteria, are likely to facilitate more efficient AMR plasmid dissemination (e.g. pCSZ4), particularly for plasmids characterized by narrow-host, such as IncI2 or IncHI2. Upon successful validation of this novel dual-fluorescence reporter system, our focus will shift towards investigating the transfer dynamics of the sfGFP-labeled clinical plasmid. This exploration will encompass the journey from its natural bacterial host to diverse recipients within the bacterial population, with the overarching objective of comprehending plasmid transfer efficiency and its spectrum within a bacterial collective boasting varying relative abundances.

Interestingly, in addition to *Escherichia_Shigella*, our investigation revealed the presence of other species among the sorted IncX4-*mcr-1* transconjugants, including *Enterobacter*, *Pseudomonas*, *Enterococcus*, *Ligilactobacillus*, and *Lactobacillus*. This finding was consistent with molecular epidemiological reports. As evidence, *mcr-1*-harboring IncX4 plasmids are predominantly detected in *E. coli*, *K. pneumoniae*, *S. enterica*, and *E. cloacae* from human, animal and environmental sections (Bustamante and Iredell, 2017; Stokes et al., 2013). The *mcr-1* gene has also been reported in other Gram-negative bacteria such as *P. aeruginosa* and *Acinetobacter* species (Mmatli et al., 2022). A keyword search using "*mcr-1*" in the NCBI database yielded a total of 854,400 nucleic acid sequences. Among the bacteria carrying the *mcr-1* gene, predominant species included *E. coli* (549,177), *K. pneumoniae* (15,647), *S. enterica* (9760), *K. quasipneumoniae* (2805), *S. sonnei* (923), *P. mirabilis* (377), *A. variabilis* (298), *M. morganii* (254), *A. baumannii* (194), *C. freundii* (179), *P. aeruginosa* (20), among others (Fig S8), indicating the broad host of *mcr-1* gene. The WGS data from isolated transconjugants provided further confirmation of the horizontal gene transfer of IncX4-*mcr-1* plasmid to *C. freundii*, *S. sonnei*, and *E. cloacae* within the fecal microbiota.

The results obtained from FACS and 16S rRNA sequencing in our study provide additional support to the notion that bacteria belonging to the Enterobacteriaceae family, notably *Escherichia coli* and *Shigella* species, have a greater tendency to acquire the IncX4-*mcr-1* plasmid. This finding could potentially explain the extensive prevalence of IncX4 plasmids carrying the *mcr-1* gene within Enterobacteriaceae bacteria worldwide. Additionally, an *mcr-1*-carrying *Bacillus cereus* strain was detected in tap water, and subsequent experimentation demonstrated the transfer of *mcr-1* to *Enterococcus hirae* within a BALB/c female mouse through HGT subsequent to the inoculation of the *B. cereus* parent strain (Khan et al., 2020). Interestingly, in our study, we observed consistent and significant enrichment of *Enterococcus* among successful transconjugants across multiple independent experiments. This observation, combined with aforementioned *E. hirae* report, suggests that the inter-specific transfer of *mcr-1* may occur within the mouse gut. However, despite our efforts, obtaining *mcr-1*-positive *Enterococcus* clones from sorted transconjugant populations remained elusive. This could be attributed to the relatively lower abundance of *Enterococcus* when compared to *Escherichia_Shigella* within the population or, alternatively, to a transient nature of *mcr-1* plasmid transfer in *Enterococcus*, where the plasmid fails to maintain stable replication. Subsequently, we directly co-cultured the donor bacteria with *E. faecalis* ATCC 29212, followed by a repetition of FACS assays. Regrettably, significant signals corresponding to the transconjugants were not detected. We speculate that

this could be due to the relatively lower conjugation frequency of the IncX4-*mcr-1* plasmid when transferring from the donor to *E. faecalis* ATCC 29212 or that an intermediate host (e.g. *B. cereus*) is needed for the plasmid transfer into *Enterococcus*. Further studies are needed to unravel the nature of IncX4-*mcr-1* plasmid transfer between Gram negative (e.g. *E. coli*) and Gram positive (e.g. *Enterococcus* species) strains.

However, the CRISPR-AMRtracker introduced in this study exhibits certain limitations that warrant consideration. Firstly, it is important to acknowledge that in instances where the conjugation frequency is at an exceedingly low level, falling beneath the detection threshold of the FACS methodology (TCs/Donors, 0.0002), our system's capacity to accurately reflect the true conjugation frequency might be compromised. This predicament could also exert an adverse influence on subsequent sorting procedures. To address this challenge, a spectrum of innovative methodologies has emerged. Among these, OIL-PCR stands out as the latest breakthrough in investigating plasmid hosts (Diebold et al., 2021), especially those enigmatic taxa that necessitate a molecular linkage between plasmid-encoded genes and the bacterial 16S rRNA gene through fusion PCR performed within an emulsion. The combination of the CRISPRAMR-tracker with OIL-PCR holds promising prospects to monitor the transfer of ARGs within complex microbiota. Secondly, although the deployment of the Ptrc promoter enhances the expression of the *sfGFP* gene, yielding robust green fluorescence across diverse bacterial strains with commendable sensitivity, uncertainties persist regarding the heterologous expression of *sfGFP* in all conceivable recipient bacteria. Although we observe robust *sfGFP* expression in numerous bacterial species, further investigations are necessary to delineate the promoter's activity within other microbiota species. Lastly, employing the CRISPRAMR-tracker system to explore in vivo plasmid conjugative transfer presents its own set of challenges. Our endeavors to employ CRISPRAMR-tracker for monitoring *mcr-1* dissemination within the mouse gut underscore these challenges. We conducted experiments using the oral administration of 10^8 CFU tagged bacteria *E. coli* MQCSZ4GFP to mice, followed by the collection of fecal samples after 24 hours for subsequent FACS and sequencing analysis. Regrettably, our observations revealed not only a scarcity of $GFP^+mCherry^-$ cells within the fecal samples but also a substantial decline in the abundance of donor bacteria (data not shown), indicating inadequate colonization by the donor bacteria or constrained plasmid conjugation dissemination in situ. Consequently, the identification of bacterial donors exhibiting increased gut colonization levels or the implementation of a more efficacious colonization model emerges as imperative for yielding more substantive in vivo findings.

5. Conclusions

In summary, the development of CRISPR-AMRtracker introduces a powerful tool for monitoring the transfer of ARGs within complex microbiota. With its straightforward construction process and high efficiency, the future applications of CRISPR-AMRtracker hold the potential to significantly advance various research endeavors, including the identification of plasmid host ranges, exploration of driving factors, and the development of novel strategies to combat antimicrobial resistance.

Ethics approval

Animal experimentation was approved by the by the ethics Committee of the Laboratory Animal Center of South China Agricultural University (Guangzhou, China), approval number 2020B041.

Consent for publication

Not applicable.

Funding

This work was supported by the Foundation for Innovative Research Groups of the National Natural Science Foundation of China (32121004), Local Innovative and Research Teams Project of Guangdong Pearl River Talents Program (2019BT02N054), China Postdoctoral Science Foundation (2023M741221), National key research and development program of China (2022YFD1800400), Guangdong Major Project of Basic and Applied Basic Research (2020B0301030007), Double First-class Discipline Promotion Project (2023B10564003), and the 111 Center (D20008).

Authors contributions

LC, JS conceived and designed the experiments. GL, TF-L, SY-Z, LJ-X, AG, LW, XY-D, YZ-H, RY-S, JT-Y and SQ-T performed the experiments and analyzed the data. JS, XP-L, YH-L supervised the project. GL wrote the manuscript. LC, HR, and LX-F revised manuscript. The authors have read and approved the manuscript.

CRediT authorship contribution statement

Ang Gao: Investigation. **Yu-Zhang He:** Investigation, Methodology, Validation, Writing – review & editing. **Lei Wan:** Investigation. **Liang Chen:** Conceptualization, Methodology, Writing – review & editing. **Xiao-Yuan Diao:** Investigation, Validation, Writing – review & editing. **Jian Sun:** Conceptualization, Funding acquisition, Project administration, Supervision, Validation, Writing – review & editing. **Ruan-Yang Sun:** Data curation, Formal analysis, Resources, Software, Validation. **Jin-Tao Yang:** Formal analysis, Validation, Visualization. **Sheng-Qiu Tang:** Funding acquisition. **Shi-Ying Zhou:** Investigation. **Xiao-Ping Liao:** Supervision. **Li-Juan Xia:** Investigation. **Ya-Hong Liu:** Supervision. **Gong li:** Conceptualization, Formal analysis, Funding acquisition, Software, Validation, Visualization, Writing – original draft, Writing – review & editing. **Hao Ren:** Writing – review & editing. **Teng-Fei Long:** Formal analysis, Investigation, Methodology, Validation, Writing – review & editing. **Liang-Xing Fang:** Methodology, Writing – review & editing.

Declaration of Competing Interest

The authors declare that they have no known competing financial interests or personal relationships that could have appeared to influence the work reported in this paper.

Data availability

The complete nucleotide sequence of pCasKp-oriT (ON988038), pSGKP-arr2-TKPC500GFP (ON988039), pSGKP-arr2-TNDM500GFP (ON988040), pSGKP-arr2-TOXA500GFP (ON988041), pSGKP-Tmcr-500GFP (OP009361) and pMQ (OP009360) were deposited in GenBank. The Whole genome sequencing data have been deposited in GenBank under the BioProject accession number PRJNA1004258. The raw 16S rRNA gene amplicon sequencing data from the fecal microbiota in this paper were uploaded to the Sequence Read Archive (SRA) data (https://www.ncbi.nlm.nih.gov/sra) under the accession number PRJNA1004061.

Appendix A. Supporting information

Supplementary data associated with this article can be found in the online version at doi:10.1016/j.drup.2024.101142.

References

Alikhan, N., Petty, N., Ben Zakour, N., Beatson, S., 2011. BLAST Ring Image Generator (BRIG): simple prokaryote genome comparisons. BMC Genom. 12, 402.

Arnold, B.J., Huang, I.T., Hanage, W.P., 2021. Horizontal gene transfer and adaptive evolution in bacteria. Nat. Rev. Microbiol.

Bahl, M., Oregaard, G., Sørensen, S., Hansen, L., 2009. Construction and use of flow cytometry optimized plasmid-sensor strains. Methods Mol. Biol. (Clifton, N. J.) 532, 257–268.

Bankevich, A., Nurk, S., Antipov, D., Gurevich, A., Dvorkin, M., Kulikov, A., Lesin, V., Nikolenko, S., Pham, S., Prjibelski, A., Pyshkin, A., Sirotkin, A., Vyahhi, N., Tesler, G., Alekseyev, M., Pevzner, P., 2012. SPAdes: a new genome assembly algorithm and its applications to single-cell sequencing. J. Comput. Biol.: a J. Comput. Mol. Cell Biol. 19, 455–477.

Bolger, A.M., Lohse, M., Usadel, B., 2014. Trimmomatic: a flexible trimmer for Illumina sequence data. Bioinformatics 30, 2114–2120.

Bolyen, E., Rideout, J.R., Dillon, M.R., Bokulich, N.A., Abnet, C.C., Al-Ghalith, G.A., Alexander, H., Alm, E.J., Arumugam, M., Asnicar, F., Bai, Y., Bisanz, J.E., Bittinger, K., Brejnrod, A., Brislawn, C.J., Brown, C.T., Callahan, B.J., Caraballo-Rodríguez, A.M., Chase, J., Cope, E.K., Da Silva, R., Diener, C., Dorrestein, P.C., Douglas, G.M., Durall, D.M., Duvallet, C., Edwardson, C.F., Ernst, M., Estaki, M., Fouquier, J., Gauglitz, J.M., Gibbons, S.M., Gibson, D.L., Gonzalez, A., Gorlick, K., Guo, J., Hillmann, B., Holmes, S., Holste, H., Huttenhower, C., Huttley, G.A., Janssen, S., Jarmusch, A.K., Jiang, L., Kaehler, B.D., Kang, K.B., Keefe, C.R., Keim, P., Kelley, S.T., Knights, D., Koester, I., Kosciolek, T., Kreps, J., Langille, M.G.I., Lee, J., Ley, R., Liu, Y.X., Loftfield, E., Lozupone, C., Maher, M., Marotz, C., Martin, B.D., McDonald, D., McIver, L.J., Melnik, A.V., Metcalf, J.L., Morgan, S.C., Morton, J.T., Naimey, A.T., Navas-Molina, J.A., Nothias, L.F., Orchanian, S.B., Pearson, T., Peoples, S.L., Petras, D., Preuss, M.L., Pruesse, E., Rasmussen, L.B., Rivers, A., Robeson 2nd, M.S., Rosenthal, P., Segata, N., Shaffer, M., Shiffer, A., Sinha, R., Song, S.J., Spear, J.R., Swafford, A.D., Thompson, L.R., Torres, P.J., Trinh, P., Tripathi, A., Turnbaugh, P.J., Ul-Hasan, S., van der Hooft, J.J.J., Vargas, F., Vázquez-Baeza, Y., Vogtmann, E., von Hippel, M., Walters, W., Wan, Y., Wang, M., Warren, J., Weber, K.C., Williamson, C.H.D., Willis, A.D., Xu, Z.Z., Zaneveld, J.R., Zhang, Y., Zhu, Q., Knight, R., Caporaso, J.G., 2019. Reproducible, interactive, scalable and extensible microbiome data science using QIIME 2. Nat. Biotechnol. 37, 852–857.

Brito, I.L., 2021. Examining horizontal gene transfer in microbial communities. Nat. Rev. Microbiol.

Brophy, J.A.N., Triassi, A.J., Adams, B.L., Renberg, R.L., Stratis-Cullum, D.N., Grossman, A.D., Voigt, C.A., 2018. Engineered integrative and conjugative elements for efficient and inducible DNA transfer to undomesticated bacteria. Nat. Microbiol. 3, 1043–1053.

Buckner, M.M.C., Ciusa, M.L., Meek, R.W., Moorey, A.R., McCallum, G.E., Prentice, E.L., Reid, J.P., Alderwick, L.J., Maio, A.D., Piddock, L.J.V., 2020. HIV drugs inhibit transfer of plasmids carrying extended-spectrum β-lactamase and carbapenemase genes. mBio 11, e03355–03319.

Bustamante, P., Iredell, J.R., 2017. Carriage of type II toxin-antitoxin systems by the growing group of IncX plasmids. Plasmid 91, 19–27.

Chen, L., Chavda, K., Mediavilla, J., Jacobs, M., Levi, M., Bonomo, R., Kreiswirth, B., 2012. Partial excision of blaKPC from Tn4401 in carbapenem-resistant Klebsiella pneumoniae. Antimicrob. Agents Chemother. 56, 1635–1638.

Chen, Z., Li, H., Feng, J., Li, Y., Chen, X., Guo, X., Chen, W., Wang, L., Lin, L., Yang, H., Yang, W., Wang, J., Zhou, D., Liu, C., Yin, Z., 2015. NDM-1 encoded by a pNDM-BJ01-like plasmid p3SP-NDM in clinical Enterobacter aerogenes. Front. Microbiol. 6, 294.

Chen, L., Mathema, B., Chavda, K.D., DeLeo, F.R., Bonomo, R.A., Kreiswirth, B.N., 2014. Carbapenemase-producing Klebsiella pneumoniae: molecular and genetic decoding. Trends Microbiol. 22, 686–696.

CLSI. Performance Standards for Antimicrobial Susceptibility Testing—Twenty-Eighth Edition: M100. 2018.

Cyriaque, V., Jacquiod, S., Riber, L., Abu Al-Soud, W., Gillan, D.C., Sorensen, S.J., Wattiez, R., 2020. Selection and propagation of IncP conjugative plasmids following long-term anthropogenic metal pollution in river sediments. J. Hazard Mater. 382, 121173.

Datsenko, K.A., Wanner, B.L., 2000. One-step inactivation of chromosomal genes in Escherichia coli K-12 using PCR products. Proc. Natl. Acad. Sci. USA 97, 6640–6645.

Diebold, P.J., New, F.N., Hovan, M., Satlin, M.J., Brito, I.L., 2021. Linking plasmid-based beta-lactamases to their bacterial hosts using single-cell fusion PCR. eLife 10.

Edgar, R.C., 2013. UPARSE: highly accurate OTU sequences from microbial amplicon reads. Nat. Methods 10, 996–998.

Edgar, R.C., Haas, B.J., Clemente, J.C., Quince, C., Knight, R., 2011. UCHIME improves sensitivity and speed of chimera detection. Bioinformatics 27, 2194–2200.

Fan, X.T., Li, H., Chen, Q.L., Zhang, Y.S., Ye, J., Zhu, Y.G., Su, J.Q., 2019. Fate of antibiotic resistant Pseudomonas putida and broad host range plasmid in natural soil microcosms. Front. Microbiol. 10, 194.

Fu, Y., Du, X., Ji, J., Chen, Y., Jiang, Y., Yu, Y., 2012. Epidemiological characteristics and genetic structure of blaNDM-1 in non-baumannii Acinetobacter spp. in China. J. Antimicrob. Chemother. 67, 2114–2122.

Godeux, A.S., Lupo, A., Haenni, M., Guette-Marquet, S., Wilharm, G., Laaberki, M.H., Charpentier, X., 2018. Fluorescence-based detection of natural transformation in drug-resistant acinetobacter baumannii. J. Bacteriol. 200.

Hao, M., He, Y., Zhang, H., Liao, X., Liu, Y., Sun, J., Du, H., Kreiswirth, B., Chen, L., 2020. EnterobacteriaceaeCRISPR-Cas9-mediated carbapenemase gene and plasmid curing in carbapenem-resistant. Antimicrob. Agents Chemother. 64.

Hardiman, C.A., Weingarten, R.A., Conlan, S., Khil, P., Dekker, J.P., Mathers, A.J., Sheppard, A.E., Segre, J.A., Frank, K.M., 2016. Horizontal transfer of carbapenemase-encoding plasmids and comparison with hospital epidemiology data. Antimicrob. Agents Chemother. 60, 4910–4919.

He, Y.-Z., Kuang, X., Long, T.-F., Li, G., Ren, H., He, B., Yan, J.-R., Liao, X.-P., Liu, Y.-H., Chen, L., Sun, J., 2021. Re-engineering a mobile-CRISPR/Cas9 system for antimicrobial resistance gene curing and immunization in Escherichia coli. J. Antimicrob. Chemother. 77, 74–82.

He, Y.Z., Li, X.P., Miao, Y.Y., Lin, J., Sun, R.Y., Wang, X.P., Guo, Y.Y., Liao, X.P., Liu, Y. H., Feng, Y., Sun, J., 2019. The ISApl1 (2) Dimer circular intermediate participates in mcr-1 transposition. Front. Microbiol. 10, 15.

He, Y.Z., Long, T.F., Chen, C.P., He, B., Li, X.P., Schuyler, J., Chen, L., Liao, X.P., Liu, Y. H., Sun, J., 2020. ISKpn40-mediated mobilization of the colistin resistance gene mcr-3.11 in Escherichia coli. Antimicrob. Agents Chemother. 64.

Hernández-Ortega, E.P., van der Meulen, S., Kuijpers, L.J., Kok, J., 2022. Riboswitch RS (thiT) as a molecular tool in Lactococcus lactis. Appl. Environ. Microbiol. 88, e0176421.

Herrero, M., de Lorenzo, V., Timmis, K., 1990. Transposon vectors containing non-antibiotic resistance selection markers for cloning and stable chromosomal insertion of foreign genes in gram-negative bacteria. J. Bacteriol. 172, 6557–6567.

Iregbu, K., Dramowski, A., Milton, R., Nsutebu, E., Howie, S.R.C., Chakraborty, M., Lavoie, P.M., Costelloe, C.E., Ghazal, P., 2022. Global health systems' data science approach for precision diagnosis of sepsis in early life. Lancet Infect. Dis. 22, e143–e152.

Kechin, A., Boyarskikh, U., Kel, A., Filipenko, M., 2017. cutPrimers: a new tool for accurate cutting of primers from reads of targeted next generation sequencing. J. Comput. Biol. 24, 1138–1143.

Khan, H., Miao, X., Liu, M., Ahmad, S., Bai, X., 2020. Behavior of last resort antibiotic resistance genes (mcr-1 and bla) in a drinking water supply system and their possible acquisition by the mouse gut flora. Environ. Pollut. 259, 113818.

Klümper, U., Riber, L., Dechesne, A., Sannazzarro, A., Hansen, L., Sørensen, S., Smets, B., 2015. Broad host range plasmids can invade an unexpectedly diverse fraction of a soil bacterial community. ISME J. 9, 934–945.

Li, X., Tong, W., Wang, L., Rahman, S.U., Wei, G., Tao, S., 2018. A novel strategy for detecting recent horizontal gene transfer and its application to rhizobium strains. Front. Microbiol. 9, 973.

Long, T.-F., Zhou, S.-Y., Huang, Z.-L., Li, G., Zhong, Q., Zhang, X.-J., Li, Y.-Y., Chen, C.-P., Xia, L.-J., Wei, R., 2024. Innovative delivery system combining CRISPR-Cas12f for combatting antimicrobial resistance in gram-negative bacteria. ACS Synth. Biol.

Lu, X., Zhang, P., Du, P., Zhang, X., Wang, J., Yang, Y., Sun, H., Wang, Z., Cui, S., Li, R., Bai, L., 2023. Prevalence and genomic characteristics of mcr-Positive Escherichia coli strains isolated from humans, pigs, and foods in China. Microbiol. Spectr. 11, e0456922.

Lucidi, M., Runci, F., Rampioni, G., Frangipani, E., Leoni, L., Visca, P., 2018. New Shuttle Vectors for Gene Cloning and Expression in Multidrug-Resistant Acinetobacter Species. Antimicrob. Agents Chemother. 62, 10.1128/aac.02480-02417.

Manageiro, V., Pinto, M., Caniça, M., 2015. Complete sequence of a blaOXA-48-harboring IncL plasmid from an enterobacter cloacae clinical isolate. Genome Announc. 3.

McKenzie, G., Craig, N., 2006. Fast, easy and efficient: site-specific insertion of transgenes into enterobacterial chromosomes using Tn7 without need for selection of the insertion event. BMC Microbiol. 6, 39.

Mmatli, M., Mbelle, N.M., Osei Sekyere, J., 2022. Global epidemiology, genetic environment, risk factors and therapeutic prospects of mcr genes: a current and emerging update. Front. Cell. Infect. Microbiol. 12, 941358.

Murphy, K.C., 1998. Use of bacteriophage lambda recombination functions to promote gene replacement in Escherichia coli. J. Bacteriol. 180, 2063–2071.

Musovic, S., Klümper, U., Dechesne, A., Magid, J., Smets, B.F., 2014. Long-term manure exposure increases soil bacterial community potential for plasmid uptake. Environ. Microbiol Rep. 6, 125–130.

Neil, K., Allard, N., Grenier, F., Burrus, V., Rodrigue, S., 2020. Highly efficient gene transfer in the mouse gut microbiota is enabled by the Incl2 conjugative plasmid TP114. Commun. Biol. 3, 523.

Ondov, B.D., Starrett, G.J., Sappington, A., Kostic, A., Koren, S., Buck, C.B., Phillippy, A. M., 2019. Mash Screen: high-throughput sequence containment estimation for genome discovery. Genome Biol. 20, 232.

Partridge, S.R., Kwong, S.M., Firth, N., Jensen, S.O., 2018. Mobile genetic elements associated with antimicrobial resistance. Clin. Microbiol. Rev. 31, 10.1128/cmr.00088-00017.

Pinilla-Redondo, R., Cyriaque, V., Jacquiod, S., Sorensen, S.J., Riber, L., 2018. Monitoring plasmid-mediated horizontal gene transfer in microbiomes: recent advances and future perspectives. Plasmid.

Potron, A., Poirel, L., Nordmann, P., 2014. Derepressed transfer properties leading to the efficient spread of the plasmid encoding carbapenemase OXA-48. Antimicrob. Agents Chemother. 58, 467–471.

Qi, L., Haurwitz, R.E., Shao, W., Doudna, J.A., Arkin, A.P., 2012. RNA processing enables predictable programming of gene expression. Nat. Biotechnol. 30, 1002–1006.

Qiu, Y., Zhang, J., Li, B., Wen, X., Liang, P., Huang, X., 2018. A novel microfluidic system enables visualization and analysis of antibiotic resistance gene transfer to activated sludge bacteria in biofilm. Sci. Total Environ. 642, 582–590.

Quandt, J., Hynes, M.F., 1993. Versatile suicide vectors which allow direct selection for gene replacement in gram-negative bacteria. Gene 127, 15–21.

Rizzi, A., Pontiroli, A., Brusetti, L., Borin, S., Sorlini, C., Abruzzese, A., Sacchi, G.A., Vogel, T.M., Simonet, P., Bazzicalupo, M., Nielsen, K.M., Monier, J.-M., Daffonchio, D., 2008. Strategy for in situ detection of natural transformation-based horizontal gene transfer events. Appl. Environ. Microbiol. 74, 1250–1254.

Ronda, C., Chen, S.P., Cabral, V., Yaung, S.J., Wang, H.H., 2019. Metagenomic engineering of the mammalian gut microbiome in situ. Nat. Methods 16, 167–170.

Ryan, O., Cate, J., 2014. Multiplex engineering of industrial yeast genomes using CRISPRm. Methods Enzymol. 546, 473–489.
Santala, S., Santala, V., 2021. Acinetobacter baylyi ADP1-naturally competent for synthetic biology. Essays Biochem 65, 309–318.
Shen, Z., Tang, C.M., Liu, G.Y., 2022. Towards a better understanding of antimicrobial resistance dissemination: what can be learnt from studying model conjugative plasmids? Mil. Med Res 9, 3.
Shintani, M., Matsui, K., Inoue, J.-i, Hosoyama, A., Ohji, S., Yamazoe, A., Nojiri, H., Kimbara, K., Ohkuma, M., 2014. Single-cell analyses revealed transfer ranges of IncP-1, IncP-7, and IncP-9 plasmids in a soil bacterial community. Appl. Environ. Microbiol. 80, 138–145.
Snesrud, E., McGann, P., Chandler, M., 2018. The birth and demise of the ISApl1-mcr-1-ISApl1 Composite transposon: the vehicle for transferable colistin resistance. mBio 9.
Stokes, M.O., AbuOun, M., Umur, S., Wu, G., Partridge, S.R., Mevius, D.J., Coldham, N. G., Fielder, M.D., 2013. Complete sequence of pSAM7, an IncX4 plasmid carrying a novel blaCTX-M-14b transposition unit isolated from escherichia coli and enterobacter cloacae from cattle. Antimicrob. Agents Chemother. 57, 4590–4594.
Sullivan, M.J., Petty, N.K., Beatson, S.A., 2011. Easyfig: a genome comparison visualizer. Bioinformatics 27, 1009–1010.
Wang, R., Luo, S., Clarke, B.B., Belanger, F.C., 2021. The Epichloë festucae antifungal protein Efe-AfpA Is also a possible effector protein required for the interaction of the fungus with its host grass Festuca rubra subsp. rubra. Microorganisms 9.
Wang, Y., Wang, S., Chen, W., Song, L., Zhang, Y., Shen, Z., Yu, F., Li, M., Ji, Q., 2018. CRISPR-Cas9 and CRISPR-assisted cytidine deaminase enable precise and efficient genome editing in Klebsiella pneumoniae. Appl. Environ. Microbiol. 84.
Wu, W., Feng, Y., Tang, G., Qiao, F., McNally, A., Zong, Z., 2019. NDM metallo-β-lactamases and their bacterial producers in health care settings. Clin. Microbiol. Rev. 32.
Xu, K., Tong, Y., Li, Y., Tao, J., Rao, S., Li, J., Zhou, J., Liu, S., 2022. Autoinduction expression modules for regulating gene expression in Bacillus subtilis. ACS Synth. Biol. 11, 4220–4225.
Yang, J., Sun, B., Huang, H., Jiang, Y., Diao, L., Chen, B., Xu, C., Wang, X., Liu, J., Jiang, W., Yang, S., 2014. High-efficiency scarless genetic modification in Escherichia coli by using lambda red recombination and I-SceI cleavage. Appl. Environ. Microbiol. 80, 3826–3834.
YZ, H., XP, L., YY, M., J, L., RY, S., XP, W., YY, G., XP, L., YH, L., Y, F., J, S., 2019. Apl1The IS dimer circular intermediate participates in transposition. Front. Microbiol. 10, 15.
Zhang, L., Liu, W.Q., Li, J., 2020. Establishing a Eukaryotic Pichia pastoris cell-free protein synthesis system. Front. Bioeng. Biotechnol. 8, 536.
Zhang, S., Wang, Y., Lu, J., Yu, Z., Song, H., Bond, P.L., Guo, J., 2021. Chlorine disinfection facilitates natural transformation through ROS-mediated oxidative stress. ISME J. 15, 2969–2985.

Materials Today Bio 28 (2024) 101181

Contents lists available at ScienceDirect

Materials Today Bio

journal homepage: www.journals.elsevier.com/materials-today-bio

Waterborne polyurethane nanoparticles incorporating linoleic acid as a potential strategy for controlling antibiotic resistance spread in the mammalian intestine

Gong Li [a,b,c,1], Lu Han [a,b,c,1], Li-Juan Xia [a,c], Ang Gao [a,c], Zhi-Peng Li [a,c], Shi-Ying Zhou [a,c], Lei Wan [a,c], Yao Deng [a,c], Tian-Hong Zhou [a,c], Xin-Yi Lu [a,c], Yang Luo [a,c], Dun-Sheng Liang [a,c], Gui-Ting Wu [a,c], Sheng-Qiu Tang [b], Xin-Lei Lian [a,c], Hao Ren [a,c], Xiao-Ping Liao [a,c], Liang Chen [d,**], Jian Sun [a,c,*]

[a] *Lingnan Guangdong Laboratory of Modern Agriculture, National Risk Assessment Laboratory for Antimicrobial Resistance of Animal Original Bacteria, South China Agricultural University, Guangzhou, PR China*

[b] *Guangdong Provincial Key Laboratory of Utilization and Conservation of Food and Medicinal Resources in Northern Region, Henry Fok School of Biology and Agriculture, Shaoguan University, Shaoguan, 512005, PR China*

[c] *Guangdong Provincial Key Laboratory of Veterinary Pharmaceutics Development and Safety Evaluation, South China Agricultural University, Guangzhou, 510642, PR China*

[d] *Department of Pharmacy Practice, School of Pharmacy and Pharmaceutical Sciences, University at Buffalo, Buffalo, NY, 14214, USA*

ARTICLE INFO

Keywords:
Antimicrobial resistance
Waterborne polyurethane
Conjugation inhibitor
IncX4
Mcr-1

ABSTRACT

Plasmid-mediated conjugative transfer of antibiotic resistance genes (ARGs) within the human and animal intestine represents a substantial global health concern. linoleic acid (LA) has shown promise in inhibiting conjugation *in vitro*, but its *in vivo* effectiveness in the mammalian intestinal tract is constrained by challenges in efficiently reaching the target site. Recent advancements have led to the development of waterborne polyurethane nanoparticles for improved drug delivery. In this study, we synthesized four waterborne polyurethane nanoparticles incorporating LA (WPU@LA) using primary raw materials, including N-methyldiethanolamine, 2,2'-(piperazine-1,4-diyl) diethanol, isophorone diisocyanate, castor oil, and acetic acid. These nanoparticles, identified as $WPU_{0.89}$@LA, $WPU_{0.99}$@LA, $WPU_{1.09}$@LA, and $WPU_{1.19}$@LA, underwent assessment for their pH-responsive release property and biocompatibility. Among these, $WPU_{0.99}$@LA displayed superior pH-responsive release properties and biocompatibility towards Caco-2 and IPEC-J2 cells. In a mouse model, a dosage of 10 mg/kg/day $WPU_{0.99}$@LA effectively reduced the conjugation of IncX4 plasmids carrying the mobile colistin resistance gene (*mcr-1*) by more than 45.1-fold. *In vivo* toxicity assessment demonstrated that 10 mg/kg/day $WPU_{0.99}$@LA maintains desirable biosafety and effectively preserves gut microbiota homeostasis. In conclusion, our study provides crucial proof-of-concept support, demonstrating that $WPU_{0.99}$@LA holds significant potential in controlling the spread of antibiotic resistance within the mammalian intestine.

Abbreviations: AMR, Antimicrobial resistance; HGT, Horizontal gene transfer; GTAs, Phage-like gene transfer agents; ARGs, Antibiotic resistance genes; LA, Linoleic acid; WPU, Waterborne polyurethane; MDEA, N-methyldiethanolamine; CO, Castor oil; MEK, Methyl ethyl ketone; HEP, 2,2'-(piperazine-1,4-diyl) diethanol; IPDI, Isophorone diisocyanate; DBTDL, Dibutyltin dilaurate; AcOH, Acetic acid; ACN, Acetonitrile; LB, Luria-Bertani; EMB, Eosin Methylene Blue; FTIR, Fourier-transform infrared spectroscopy; TEM, Transmission electron microscopy; HPLC, High-performance liquid chromatography; H&E, Hematoxylin and eosin; DLC, Drug loading content; EE, Encapsulation efficiency; DLE, Drug loading efficiency; OTUs, Operational taxonomic units; PCoA, Principal coordinates analysis; WPU@LA, Waterborne polyurethane nanoparticles incorporating LA; ^{1}H NMR, H proton magnetic resonance; GPC, Gel permeation chromatography; THF, Tetrahydrofuran; PBS, Phosphate-buffered saline; SGF, Simulated gastric fluid; SIF, Simulated intestinal fluid.

* Corresponding author. Guangdong Provincial Key Laboratory of Veterinary Pharmaceutics Development and Safety Evaluation, South China Agricultural University, Guangzhou, 510642, PR China

** Corresponding author.

E-mail addresses: liangch@buffalo.edu (L. Chen), jiansun@scau.edu.cn (J. Sun).

[1] Gong Li and Lu Han are co-first authors of the article.

https://doi.org/10.1016/j.mtbio.2024.101181
Received 20 February 2024; Received in revised form 10 July 2024; Accepted 3 August 2024
Available online 10 August 2024
2590-0064/© 2024 The Authors. Published by Elsevier Ltd. This is an open access article under the CC BY-NC license (http://creativecommons.org/licenses/by-nc/4.0/).

1. Introduction

Antimicrobial resistance (AMR) poses a significant challenge by limiting the effectiveness of antimicrobial agents, impacting both human and animal health [1,2]. This issue is exacerbated by horizontal gene transfer (HGT) among diverse microorganisms [3–5]. Bacteria employ various pathways for HGT, including phage-mediated transduction, transformation through 'naked' DNA, plasmid-mediated conjugation, and mechanisms involving vesicles, nanotubes, and phage-like gene transfer agents (GTAs) [6]. Among these pathways, conjugation is recognized as the most prevalent mechanism [7–9]. For example, naturally occurring plasmids like IncI2, IncX4, and IncX3 increasingly carry antibiotic resistance genes (ARGs) such as *mcr-1* for colistin, $bla_{\text{NDM-1}}$ for carbapenem, and *tet(*X4) for tigecycline [10–12], impacting the treatment of Gram-negative bacterial infections. These plasmids, carrying ARGs, transfer through conjugation between different bacteria, leading to the global dissemination and spread of ARGs. The mammalian gut, known for its diverse microbial population, acts as a reservoir for genetic exchange, strongly linked to the widespread occurrence of conjugation events involving ARGs [13]. Consequently, preventing ARG conjugation, particularly in the mammalian gut, is crucial to mitigate the spread of AMR.

Conjugation involves the transfer of DNA through donor cell-formed conjugative pili to recipient cells [8]. Conjugation of ARGs hinders antibiotic effectiveness, emphasizing its significance in controlling AMR. To tackle this issue, various natural products and small molecules have been developed as conjugation inhibitors. Examples include free nitrous acid, azidothymidine, capsaicin, gingerol analogues, Fe_2O_3@-MoS_2, and abacavir [14–19], but many of these have either shown toxicity or lack *in vivo* testing. Additionally, both Ripoll-Rozada et al. and our previous study have demonstrated that linoleic acid (LA) inhibits the conjugative transfer of IncW, IncH, IncF, IncI, IncL/M and IncX plasmids by suppressing the TrwD ATPase (VirB11 homologue) [20,21].

LA, which is essential for human or animal bodies, is absorbed in the small intestine under acidic pH conditions (pH ~ 2) [22]. However, the challenge arises when considering the normal colon and cecum, which maintain a slightly neutral pH (6.0–7.2) [23]. These regions serve as primary colonization sites for bacteria in the intestinal tract and are key locations for plasmid conjugative transfer. Unfortunately, LA is unable to reach the colon and cecum before its absorption in the small intestine, thereby hindering its potential to inhibit plasmid conjugation in these critical areas. Consequently, the limited pharmacokinetic properties of LA constrain its broader *in vivo* application in conjugation inhibition.

To enhance LA production in the colon and cecum, Peng et al. devised a strategy by constructing a bioactive *Lactobacillus casei* strain $LC^{+\text{ mcra}}$ by inserting the *mcra* (myosin cross-reactive antigen) gene into the bacterial genome, which promotes the conversion of conjugated LA [24]. On the other hand, when considering drug administration methods, intestinal-based drug delivery is regarded as the preferred approach [25]. Within this context, waterborne polyurethane (WPU), a synthetic high molecular weight polymer, emerges as a versatile material class with applications ranging from coatings to healthcare [26,27]. Recent studies have shown that the integration of N-methyldiethanolamine (MDEA), featuring tertiary amines, plays a pivotal role in the development of pH-responsive polyurethanes [28]. The tertiary amines present in the MDEA segment are widely recognized for their ability to undergo protonation, leading to the formation of an ionic state [29,30]. Consequently, when exposed to acetic acid, the polyurethane with the MDEA segment undergoes ionization, resulting in the formation of zwitterionic polyurethanes. Moreover, a satisfactory nanocarrier usually requires low toxicity [31]. Notably, these zwitterionic polyurethanes have gained significant attention due to their remarkable biocompatibility [32].

This study introduces a novel nanoparticle-based system known as $WPU_{0.99}$@LA, demonstrating its versatility and responsiveness in releasing LA. The effectiveness and safety of this nanocarrier have been robustly established and validated through *in vivo* models. These findings strongly emphasize the promising potential of $WPU_{0.99}$@LA for future applications in inhibiting the spread of AMR within the mammalian intestine.

2. Methods

2.1. Chemicals and bacteria

Castor oil (CO) was purchased from Guangzhou Xinye Co., Ltd. (Guangzhou, China). Linoleic acid (LA), N-methyldiethanolamine (MDEA), and methyl ethyl ketone (MEK) were obtained from Shanghai Rhawn Co., Ltd. (Shanghai, China). 2,2'-(piperazine-1,4-diyl) diethanol (HEP) was obtained from Shanghai Aladdin Reagent Co., Ltd. (Shanghai, China). Isophorone diisocyanate (IPDI) was supplied by Guangzhou Wengjiang Chemical Reagent Co., Ltd. (Guangzhou, China). Dibutyltin dilaurate (DBTDL) was purchased from Fuchen Reagent (Tianjin, China). Acetic acid (AcOH) and phosphoric acid (H_3PO_4) were acquired from Guangzhou Chemical Reagent Factory (Guangzhou, China). Acetonitrile (ACN) was sourced from Shanghai Macklin Biochemical Technology Co., Ltd (Shanghai, China). Human intestinal epithelial cells (Caco-2) and the intestinal porcine enterocyte cell line (IPEC-J2) were procured from Dojindo Chemical Technology (Shanghai, China). Dulbecco's modified Eagle's medium (DMEM, Gibco) and fetal bovine serum (FBS, Gibco) were obtained from Nobimpex Biotechnology (Shanghai, China). Mueller Hinton (MH) broth, Luria-Bertani (LB) broth, LB agar, and Eosin Methylene Blue (EMB) agar were purchased from Guangzhou Huankai Microbial Technology (Guangzhou, China). Streptomycin sulfate and polymyxin sulfate were procured from Beijing Pubo Biotechnology Co., Ltd. (Beijing, China). Antibiotics used for screening and selection procedures were added at the following concentrations (μg/mL): streptomycin sulfate (STR, 2000) and polymyxin sulfate (CS, 2).

Donor strains employed in this study were *E. coli* MQCSZ4GFP, which harbors the conjugative IncX4 plasmid pCSZ4-sfGFP with colistin resistance (*mcr-1*), and a non-conjugative plasmid pMQ expressing mCherry fluorescence protein and LacIq [33]. pCSZ4-sfGFP is a derivative of the clinical IncX4 *mcr-1*-harboring plasmid pCSZ4 [34], and was tagged with the green fluorescent protein (sfGFP) downstream a lacI repressor. *E. coli* C600-lux (streptomycin resistance) was genetically modified by chromosomally tagging with gene cluster *lux*CDABE encoding constitutive bioluminescence. Consequently, donor cells exhibited red fluorescence but GFP expression was inhibited due to the presence of LacIq. Upon the transfer of the pCSZ4-sfGFP plasmid into *E. coli* C600-lux (referred to as the transconjugant), GFP expression became possible without the *lacI* suppression.

2.2. Characterization

Fourier-transform infrared spectroscopy (FTIR) was conducted using a Thermo Fisher Nicolet IS10 FTIR spectrophotometer (Thermo Fisher, Waltham, MA, USA). The H proton magnetic resonance (^{1}H NMR) spectra were recorded on a Bruker AV 600M spectrometer (Karlsruhe, Germany). Gel permeation chromatography (GPC) tests were performed in tetrahydrofuran (THF) solutions at 35 °C with an elution rate of 1.0 mL/min using a Waters 1525 system equipped with a Waters 2414 detector (Burlington, MA, USA). The system was calibrated using polystyrene standards ranging from 200 to 500,000 g/mol. Zeta potential and particle sizes were determined using a Zeta-sizer Nano ZSE instrument (Malvern, Worcestershire, UK). Transmission electron microscopy (TEM) measurements were carried out with an FEI/Talos L120C transmission electron microscope (Thermo Fisher, Pittsburgh, PA, USA) operating at an acceleration voltage of 100 kV. High-performance liquid chromatography (HPLC) measurements were performed with a Waters 2695 instrument (Waters, Milford, MA, USA). Colony images were

captured using the IVIS Lumina LT Series III system (PerkinElmer, Waltham, MA, USA). Histological sections were stained with hematoxylin and eosin (H&E) and observed using a Nikon TE2000U optical microscope (Tokyo, Japan) [35].

2.3. Preparation of WPU and WPU@LA

The representative synthetic route of WPU and WPU@LA is depicted in Fig. 1A. Specifically, a dried double-necked flask was used to introduce CO (3.25 g), IPDI (3.32 g), and HEP (0.4 g), which were then stirred at 78 °C (130–170 r/min) for 10 min to achieve a homogeneous dispersion. The OH group ratio of CO: MDEA: HEP: IPDI was maintained at 1:0.89 (0.99/1.09/1.19):2.15 (2.25/2.35/2.45). Subsequently, 20 μL of DBTDL was added as a catalyst. After 10 min, an appropriate amount of MDEA was added to the solution. MEK (30 mL) was then added to the system and allowed to react for 2 h, followed by cooling the solution to room temperature. Next, AcOH was introduced into the polyurethane chain to counterbalance the presence of free COOH, while being stirred for 30 min.

To synthesize various WPU@LA, 2.35 g of LA was incorporated into the solution. Subsequently, the stirring rate was increased to 300 r/min, and the prepolymer was dispersed in 90 mL of deionized water for 2 h. The successful preparation of both WPU and WPU@LA was achieved through the elimination of MEK in the emulsion via vacuum distillation. Furthermore, 5 mg of WPU@LA was dissolved in 2 mL of methanol, sonicated until fully dissolved, and then filtered through a 0.22 μm microporous membrane. The drug loading content (DLC), encapsulation efficiency (EE), and drug loading efficiency (DLE) of LA were quantitatively determined using HPLC with an Agilent Eclipse XDB-C18 column (4.6 mm × 250 mm, 5 μm) and a mobile phase consisting of acetonitrile and 0.05 % H_3PO_4 (v/v = 10:90) at a flow rate of 1.0 mL/min, maintained at 30 °C, and monitored at 203 nm [36]. DLC (%) and DLE (%) were calculated as described in a previous article [37]. Encapsulation efficiency was calculated as follows: Encapsulation efficiency (%) = (Actual drug loaded)/(Theoretical drug loaded) * 100 [38].

2.4. The LA release rate in vitro

The release amount of LA from WPU@LA *in vitro* was tested according to a dialysis method [37]. Briefly, the release medium contained a phosphate-buffered saline (PBS) solution, 30 % ethanol, and 0.5 % sodium dodecyl sulfate, adjusted to pH = 2.0, 5.8, or 7.4 with hydrochloric acid. 0.5 g of WPU@LA was transferred into dialysis bags (MWCO 3.5 kDa) and suspended in 100 mL of release medium at 37 °C, stirred at 120 rpm. At 0, 0.5, 1, 2, 4, 6, 8, 10, 12, 24, 48, and 96 h post dialysis, 2 mL aliquots were taken for the determination of released LA, measured using a Waters 2695 instrument, and monitored at 203 nm.

2.5. In vitro biocompatibility assay

Caco-2 and IPEC-J2 cells were seeded in 24-well culture plates (1.0×10^5 cells per well) and allowed to adhere for 18 h. Samples of different WPU@LAs were added to each well at final concentrations of 400, 200, 100, 50, 25, 12.5, and 0 μg/mL and incubated for 12 h 10 μL of cell counting Kit-8 (CCK-8) was added to the medium and incubated at 37 °C, 5 % carbon dioxide in the dark for 2 h, and the solution absorbance was measured at 450 nm. Cell viability (%) was calculated using the equation: $(A_{sample}/A_{control}) \times 100$ %, where A_{sample} represents the absorbance of cells treated with the samples, and $A_{control}$ represents the absorbance of the untreated cells [38]. Cell viability was also assessed using a live and dead cell staining kit for Caco-2 and IPEC-J2 cells. These cells were incubated at 37 °C for 24 h, washed with sterile PBS, and then 250 μL of detection buffer containing 0.1 % Calcein-AM/PI was added. The plate was incubated at 37 °C for 30 min, and cell images were observed using a fluorescence microscope [39,40].

2.6. Stability

The stability of $WPU_{0.99}$@LA nanoparticles was evaluated under simulated gastric and intestinal conditions (Hu et al., 2016). Simulated gastric fluid (SGF) and simulated intestinal fluid (SIF) solutions were prepared according to the Chinese Pharmacopoeia (2015) [37]. Briefly, 1 mL of freshly prepared nanoparticles was added to 9 mL of SGF (pH 2) or SIF (pH 6.8), followed by incubation at 37 °C for 6 h [41]. Particle size and zeta potential were measured after each incubation.

2.7. Animal

C57BL/6J mice (SPF, 6 weeks, female) were housed at the Laboratory Animal Center of Southern Medical University, Guangzhou, China. Animal care was conducted in accordance with the guidelines of the American Association for Accreditation of Laboratory Animal Care criteria (2022c045). The mice were allowed to acclimate for 7 days prior to experimentation. All animal experiments were carried out in compliance with the institution's guidelines for animal use and the Guide for the Care and Use of Laboratory Animals at the Laboratory Animal Center of South China Agricultural University (Guangzhou, China).

2.8. In vivo conjugation experiments

All mice were divided into four groups, each consisting of eight mice. Prior to the experiment, all mice were administered STR through oral gavage (200 μL, 5 mg/mL) and drinking water (5 mg/mL) for three days to eliminate colonization resistance. Following this pretreatment, all mice were intragastrically administered a mixture of donor *E. coli* MQCSZ4GFP and recipient *E. coli* C600-lux, with a concentration of approximately 10^8 CFU. Subsequently, the mice were further treated via daily gavage of 10 mg/kg $WPU_{0.99}$@LA, 8 mg/kg $WPU_{0.99}$@LA, or 2 mg/kg LA into the intestinal tract, with the control group receiving an equal volume of sterile water. Fecal samples were obtained on days 1, 2, 3, 5, and 7, and subsequently homogenized by vortexing. The bacterial populations were evaluated through selective plating on EMB agar, enabling the identification of recipient bacteria (STR2000) and transconjugants (STR2000+CS2). The presence of *mcr-1* in the transconjugants was confirmed by PCR and sequencing. The reaction mixture (25 μL) contained 12.5 μL Green Taq MIX (Novizan, Nanjing, China), 2 μL of each primer, 1 μL DNA template, and 9.5 μL nuclease-free water. The PCR procedure was performed using the following reaction conditions: initial denaturation at 98 °C for 3 min followed by 30 cycles of 95 °C for 10 s, 56 °C for 30 s and 72 °C for 30 s, with a final extension at 72 °C for 5 min. The primers for *mcr-1* were GCGTGATGCCAGTTTGCTTA (mcr-F) and GCACATCGACGGCGTATTC (mcr-R). The conjugation frequency was determined by dividing the number of detected transconjugants by the total count of recipients. The conjugation rate was determined by the number of mice with transconjugants in the feces per the total number of mice in each group.

2.9. In vivo biocompatibility assay

For acute toxicity, mice were intravenously injected with 0.2 mL of $WPU_{0.99}$@LA at doses of 5000 mg/kg according to the Guidelines of Animal Drug Acute Toxicity Study (the Center for Veterinary Drug Evaluation of Ministry of Agriculture, 2012) [42]. The time of death was recorded daily for 2 weeks [43]. Then, uninfected mice were randomly assigned to two groups (n = 5/group) for a 2-week treatment period via oral gavage: $WPU_{0.99}$@LA (10 mg/kg/day) and a control group receiving sterile water. The mice were weighed and monitored daily throughout the study. After 2 weeks of $WPU_{0.99}$@LA or sterile water administration, the mice were euthanized. Liver, spleen, duodenum, kidney, stomach, and colon tissues were collected and fixed overnight in 4 % (v/v) PBS-buffered paraformaldehyde. Subsequently, the tissues

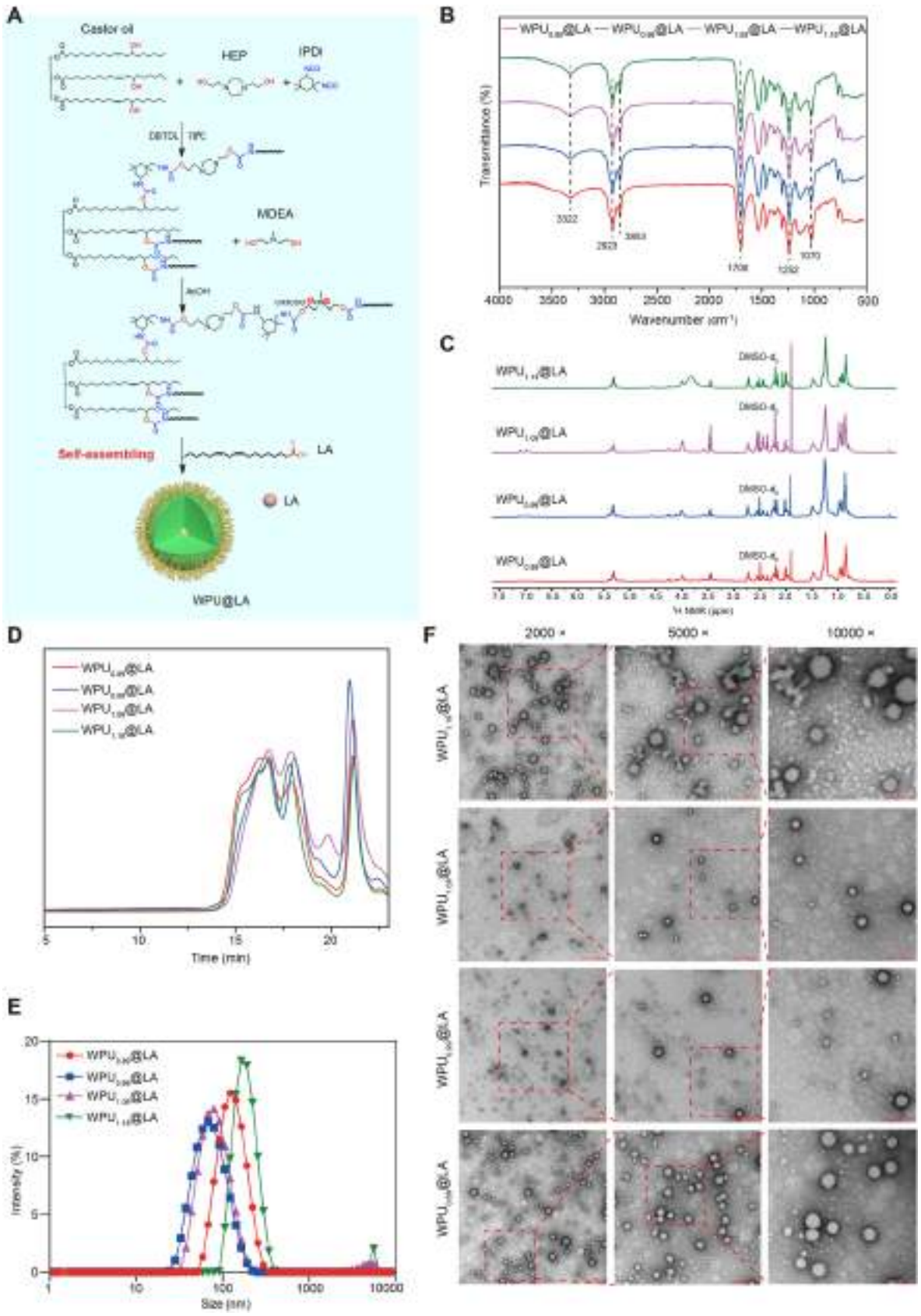


Fig. 1. Synthesis and characterization of WPU, WPU@LA nanomaterials. (A) Schematic of the synthesis of WPU@LA nanomaterials. **(B)** FTIR spectrum, **(C)** ^{1}H NMR, **(D)** GPC, **(E)** particle size distribution and **(F)** TEM images, respectively, of four WPU@LAs. HEP, 2,2'-(piperazine-1,4-diyl) diethanol. IPDI, isophorone diisocyanate. DBTDL, dibutyltin dilaurate. MDEA, N methyldiethanolamine. AcOH, acetic acid. LA, linoleic acid, scale bar: 500 nm, 200, and 100 nm, respectively.

were embedded in paraffin, cut into 5 μm sections, stained with H&E, and observed using Nikon TE2000U optical microscopy (Tokyo, Japan) [35,44]. 16S rRNA sequencing was performed following the procedures outlined in a previous study [45].

2.10. Statistical analysis

Statistical analyses and data visualization were conducted using a two-tailed Student's t-test, Kruskal-Wallis test, or Tukey's test with one-way ANOVA (Prism 8.0, GraphPad Software Inc., San Diego, CA, USA). Statistical significance was indicated as follows: * for $p < 0.05$.

3. Results and discussion

3.1. Synthesis and characterization of WPU and WPU@LA nanomaterials

To create a pH-responsive WPU system, we employed MDEA, HEP, IPDI, CO, and AcOH for synthesizing hydrophilic and hydrophobic structures to encapsulate LA (Fig. 1A). MDEA acted as an internal emulsifying agent, influencing emulsification [46]. Increasing MDEA proportions shifted the solution appearance from translucent to milky white, indicating enhanced emulsification efficiency (Table 1). Within WPU carriers, nucleophilic addition reactions occurred between hydroxyl groups in CO, HEP, and MDEA with isocyanate groups in IPDI, forming polyurethane with urethane bonds. Specifically, CO's long fatty acid chain served as the soft segment, providing material flexibility, while HEP and MDEA acted as hard segments, with HEP being pH-responsive [47]. The NCO groups on IPDI acted as crosslinkers, forming polymer chains [48]. By optimizing material proportions, aqueous polyurethane WPU@LA with varying MDEA concentrations (0.89, 0.99, 1.09, and 1.19) were synthesized with respective yields of 87.8 % (w/w), 92.1 % (w/w), 75.2 % (w/w), and 86.4 % (w/w), respectively (Table 1). Fourier-transform infrared (FTIR) spectrum exhibited typical features of WPU at 3321 cm^{-1} (-N-H-), 1252 cm^{-1} (-C-N-), 1700 cm^{-1} (-C=O), and 1070 cm^{-1} (-C-O-C-) (Fig. 1B), confirming reaction between reactant hydroxyl and isocyanate groups to form polyurethane with urethane functional groups containing amino formate.

As shown in Fig. 1C, H NMR spectra peaks at δ5.32 ppm are attributed to the carbon-carbon double bonds of the fatty acid chains from castor oil. New peaks appear at δ3.99 and δ3.44 ppm, corresponding to the proton signals of the ethanoyloxy and acetoxy groups (OCH_2 and OCH) in the esters formed from the esterification of HEP, MDEA, and CO with IPDI. Molecular weight by GPC analysis showed number-average molecular weights of four WPU@LAs as 8407 (PDI = 1.47), 7102 (PDI = 1.37), 6334 (PDI = 1.27), and 8103 (PDI = 1.38) g/mol, respectively (Fig. 1D and Table S1). The high molecular weights of the obtained WPU@LAs could be beneficial for the formation of supramolecular polymeric materials [37]. WPU@LAs exhibited diameters ranging from 68.1 nm to 164.0 nm (Fig. 1E). TEM images further confirmed the spherical morphology of the WPU@LAs (Fig. 1F). Zeta potential of WPU@LA nanoparticles ranged from 23.0 to 52.0 mV (Table 1), indicating a cationic polymer. Together, these results confirm the successful preparation of WPU@LA nanoparticles.

3.2. WPU@LA nanomaterials exhibit promising pH-responsive LA release capability

To investigate the pH-responsive release of LA from various WPU@LAs, solutions with pH values of 2.0, 5.8, and 7.4 were prepared to simulate conditions in the gastrointestinal tract. As illustrated in Fig. 2, minimal release was observed at lower pH (pH = 2), with increased release correlating with higher hydroxide ion concentrations in the medium. The cohesive assembly and release behavior of cationic WPUs are influenced by their similar structures and electrostatic interactions. Hence, monomers with multiple hydroxyl groups (e.g., CO) and positively charged monomers like HEP and MDEA were deliberately chosen. IPDI was slightly in excess during stepwise copolymerization in a butanone solution, decisions driven by the physical properties of WPU. The pH variations trigger conformational changes in microspheres due to positively charged HEP, thereby modulating the amount of released LA [49]. Notably, increasing MDEA ratio significantly enhanced LA release. This can be attributed to MDEA acting as a chain extender. Higher MDEA content reduces cationic WPU chain length, diminishing cross-linking and accelerating release rates [50]. These findings robustly underscore the promising pH-responsive LA release capabilities of the four cationic WPU@LAs.

3.3. In vitro cytotoxicity of WPU@LA

Before considering *in vivo* application, addressing the biosafety of the system is paramount. To assess their suitability for *in vivo* use, we initially evaluated the cytotoxicity of four WPU@LAs using Caco-2 and IPEC-J2 cell lines, commonly employed for *in vitro* cytotoxicity assessments [51,52]. Cell viability was assessed by exposing Caco-2 and IPEC-J2 cells to WPU@LA concentrations ranging from 12.5 to 400 μg/mL. Viability levels remained above 90 % after treatment with $WPU_{0.89}$@LA, $WPU_{0.99}$@LA, and $WPU_{1.19}$@LA at concentrations from 12.5 to 200 μg/mL. However, viability dropped to 32.98 % with 200 μg/mL of WPU1.09@LA for Caco-2 cells (Fig. 3A). Similarly, for IPEC-J2 cells, viability was above 90 % with 200 μg/mL $WPU_{0.99}$@LA, whereas viability significantly decreased in the other three groups. Notably, the 200 μg/mL $WPU_{1.09}$@LA group exhibited the lowest cell viability, at only 6.99 % (Fig. 3B). Additionally, live/dead cell staining for Caco-2 and IPEC-J2 at 200 μg/mL indicated minimal toxicity for $WPU_{0.99}$@LA (Fig. 3C and Fig. S1). Given its lower cytotoxic effect and superior release properties, $WPU_{0.99}$@LA was selected for subsequent experiment.

3.4. $WPU_{0.99}$@LA improves the inhibition of conjugation of mcr-1-harboring IncX4 plasmid in vivo

As emulsions undergo digestion in gastrointestinal conditions, the stability determines how quickly they digest [53]. To explore their potential as oral delivery vehicles, the stability of $WPU_{0.99}$@LA under simulated gastric (SGF) and intestinal (SIF) conditions was determined, respectively. As shown in Fig. S2, minimal changes in particle size and

Table 1
Fundamental characteristics of $WPU_{0.99}$ and WPU@LA nanoparticles.

Nanoparticle	Functional OH (castor oil)	HEP	MDEA	NCO (IPDI)	Appearance	Z-average size (nm)	Zeta potential (mV)	Solids content	Drug loading efficiency	Encapsulation efficiency
$WPU_{0.89}$@LA	1	0.25	0.89	2.15	Translucent	122.2	23	20.7 %	14.16 %	87.8 %
$WPU_{0.99}$@LA	1	0.25	0.99	2.25	Translucent	68.1	52	22.1 %	16.40 %	92.1 %
$WPU_{1.09}$@LA	1	0.25	1.09	2.35	Oyster white	78.8	27.6	19.3 %	13.16 %	75.2 %
$WPU_{1.19}$@LA	1	0.25	1.19	2.45	Oyster white	164.0	33.1	18.7 %	15.88 %	86.4 %
$WPU_{0.99}$	1	0.25	0.99	2.25	Translucent	15.7	15.1	16.8 %	0 %	–

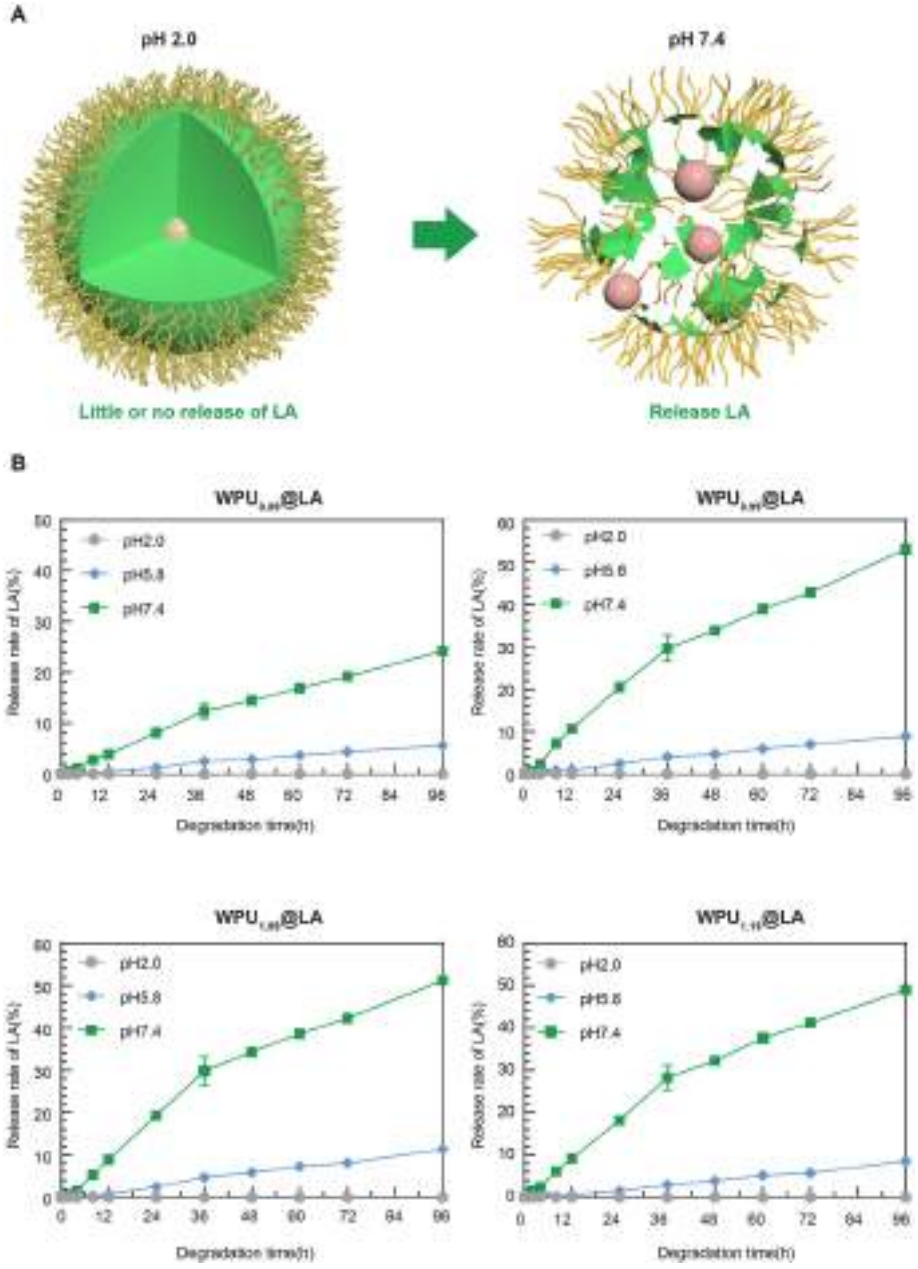


Fig. 2. WPU@LA nanomaterials exhibit promising pH-responsive LA release capability. (A) Schematic of the release of LA from nanoparticle $WPU_{0.89}$@LA, $WPU_{0.99}$@LA, $WPU_{1.09}$@LA and $WPU_{1.19}$@LA under different pH conditions. **(B)** LA release profiles of $WPU_{0.89}$@LA, $WPU_{0.99}$@LA, $WPU_{1.09}$@LA, and $WPU_{1.19}$@LA within 96 h.

zeta potential were observed in SGF, indicating that $WPU_{0.99}$@LA remains stable under gastric condition. However, prolonged incubation in SIF led to a continuous increase in zeta potential and gradual enlargement of particle size, indicating poorer stability of $WPU_{0.99}$@LA under intestinal condition. This underscores our targeted delivery approach to ensure the predominant release of LA in the intestinal environment.

The gut harbors trillions of densely colonizing bacteria that actively combat pathogens, a phenomenon commonly known as "colonization resistance" [54]. Colonization resistance limits the colonization of donor and recipient bacteria in the gut and the subsequent transfer of plasmids [55,56]. To evaluate the efficacy of $WPU_{0.99}$@LA *in vivo* on plasmid conjugation, we initially treated mice with streptomycin to reduce intestinal microbiota, rendering mice susceptible to colonization by exogenous donor and recipient (Fig. 4A). As expected, Fig. 4B shows a significantly reduced colonization level of Enterobacteriaceae (below detection limits) after one day of streptomycin treatment, indicating abnormal changes in intestinal flora amounts and microbiota destruction. Conjugation experiments employed E. coli MQCSZ4GFP as the donor and E. coli C600-lux as the recipient. E. coli MQCSZ4GFP exhibited red fluorescent, while *E. coli* C600-lux expressed bioluminescent luciferase. Transconjugants displayed both green fluorescence and luciferase activity (Fig. 4C), facilitating clear observation of conjugation events. Colony imaging and PCR results confirmed that the IncX4 plasmid pCSZ4-sfGFP could undergo conjugative transfer within the mammalian gut (Fig. 4D–F).

Based on pre-experiment results, both 50 mg/kg $WPU_{0.99}$@LA and 10 mg/kg $WPU_{0.99}$@LA reduced conjugation rates in the *in vivo* experiment (data not shown). To explore potential factors mediating the inhibition of conjugation, we synthesized $PU_{0.99}$ and conducted a subsequent *in vivo* experiment (Table 1). Mice were administered with 10 mg/kg $WPU_{0.99}$@LA, 8 mg/kg $WPU_{0.99}$, 2 mg/kg LA, or sterile water, respectively. Within the first three days post-infection, the conjugation

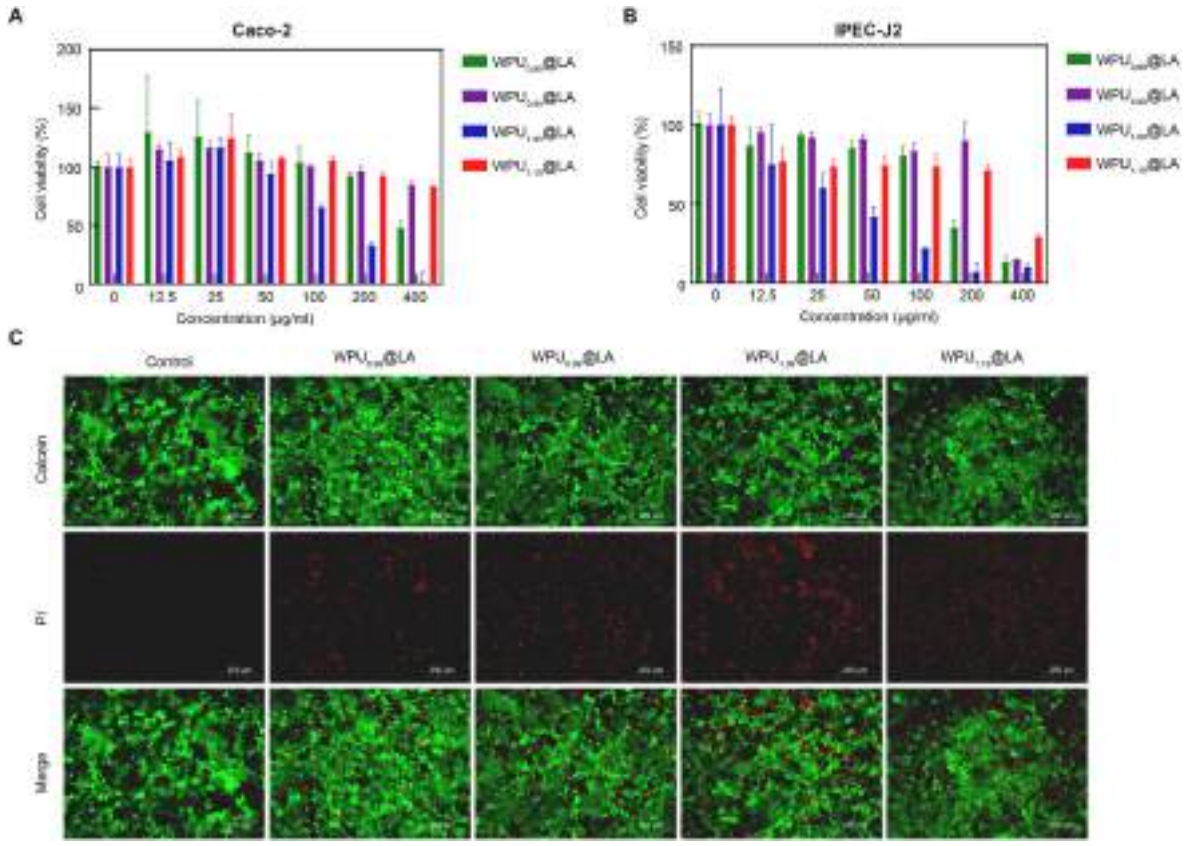


Fig. 3. ***In vitro*** **cytotoxicity of WPU@LAs.** Cell proliferation rate (%) of Caco-2 cells **(A)** and IPEC-J2 cells **(B)** after the treatment with $WPU_{0.89}$@LA, $WPU_{0.99}$@LA, $WPU_{1.09}$@LA and $WPU_{1.19}$@LA nanoparticles for 24 h. **(C)** Live/dead cell staining of Caco-2 cells using 100 μg/ml test samples. scale bar: 250 μm.

rates for the control group were 100 %, 100 %, and 75 %, respectively. In contrast, for the $WPU_{0.99}$@LA group, rates were 100 %, 37.5 %, and 25 %, respectively (Fig. 4G). Conjugation rates in the $WPU_{0.99}$ and LA groups were similar to those in the control group. Similarly, compared to the control group, on day 1, the conjugation frequency in the $WPU_{0.99}$ group decreased by 3.3-fold ($p < 0.05$), and in the $WPU_{0.99}$@LA group, it decreased by 3.0-fold ($p < 0.05$). However, no conjugation inhibition was observed in the samples collected in the $WPU_{0.99}$ group on day 2. Meanwhile, compared to the control group, the conjugation frequency in the $WPU_{0.99}$@LA group decreased by 45.1-fold ($p < 0.05$) (Fig. 4H).

The aforementioned findings highlight the potential of $WPU_{0.99}$@LA in reducing *in vivo* plasmid transfer, indicating its efficacy in mitigating plasmid dissemination within living organisms. Specifically, $WPU_{0.99}$@LA could effectively deliver LA to the site of plasmid conjugation. LA exerts inhibitory effects on VirB11 activity and the expression of its associated genes [20,21]. This inhibition can potentially lower ATP levels, thereby hindering plasmid transfer. Consequently, the inhibitory effect of $WPU_{0.99}$@LA can be attributed to the synergy between LA and the responsive-release $WPU_{0.99}$ carrier.

3.5. *$WPU_{0.99}$@LA demonstrates excellent biocompatibility*

As conjugation inhibitors act preventively without directly triggering therapeutic responses, their practical application requires administration in the mammalian intestine, where plasmid conjugation occurs [57]. Therefore, the conjugation inhibitor must demonstrate favorable biosafety upon entering the human or animal body through the digestive system [57,58]. Initially, an acute toxicity assay was conducted to evaluate the safety of $WPU_{0.99}$@LA *in vivo*. The results indicated that the LD_{50} value for $WPU_{0.99}$@LA in C57BL/6J mice exceeded 5000 mg/kg, with no deaths observed among the 10 mice tested (Fig. S3).

Subsequently, treatment biosafety was evaluated by monitoring changes in body weight and examining organ tissue sections using H&E staining (Fig. 5A). Throughout the experiment, mice receiving 10 mg/kg/day $WPU_{0.99}$@LA did not exhibit significant differences in body weight compared to those receiving sterile water (Fig. 5B). Since organs involved in digestion and metabolism often encounter and accumulate chemicals [59]. We pathologically examined the liver, kidney, spleen, stomach, duodenum, and colon of treated mice using H&E staining. Fig. 5C shows that no damage or inflammation was evident in these organs of mice treated with $WPU_{0.99}$@LA. These findings underscore the excellent biosafety profile of $WPU_{0.99}$@LA, confirming its suitability for *in vivo* use in conjugation inhibition.

3.6. *$WPU_{0.99}$@LA maximally maintains the gut microbiota homeostasis*

The composition of the microbiota in the mammalian gut is intricately linked to both health and disease [60,61]. To assess the impact of $WPU_{0.99}$@LA exposure on the gut microbiota of mice, we conducted 16S rRNA gene sequencing. A total of 294 operational taxonomic units (OTUs) were identified across all samples from the biosafety assay, with 185 unique OTUs in the control group and 151 in the $WPU_{0.99}$@LA group (Fig. 6A). α-diversity was assessed using the Chao1 and Shannon indexes, revealing no significant difference between the two groups [62]. Principal Coordinates Analysis (PCoA) based on Unweighted_Unifac and Bray-Curtis distance indicated a tendency of separation between the two groups (Fig. 6B–F), suggesting differences in the overall structure of gut microbiota [63]. At the phylum level, 8 phyla were detected in all samples, including Bacteroidetes, Firmicutes, Actinobacteria, Verrucomicrobia, Proteobacteria, TM7, Tenericutes, and Deferribacteres (Fig. 6G). Predominantly, Bacteroidetes, Firmicutes, Actinobacteria, and Verrucomicrobia were observed among the gut microbiota from all tested animals. The Firmicutes/Bacteroidetes ratio is an important parameter for evaluating the distribution of gut microbiota

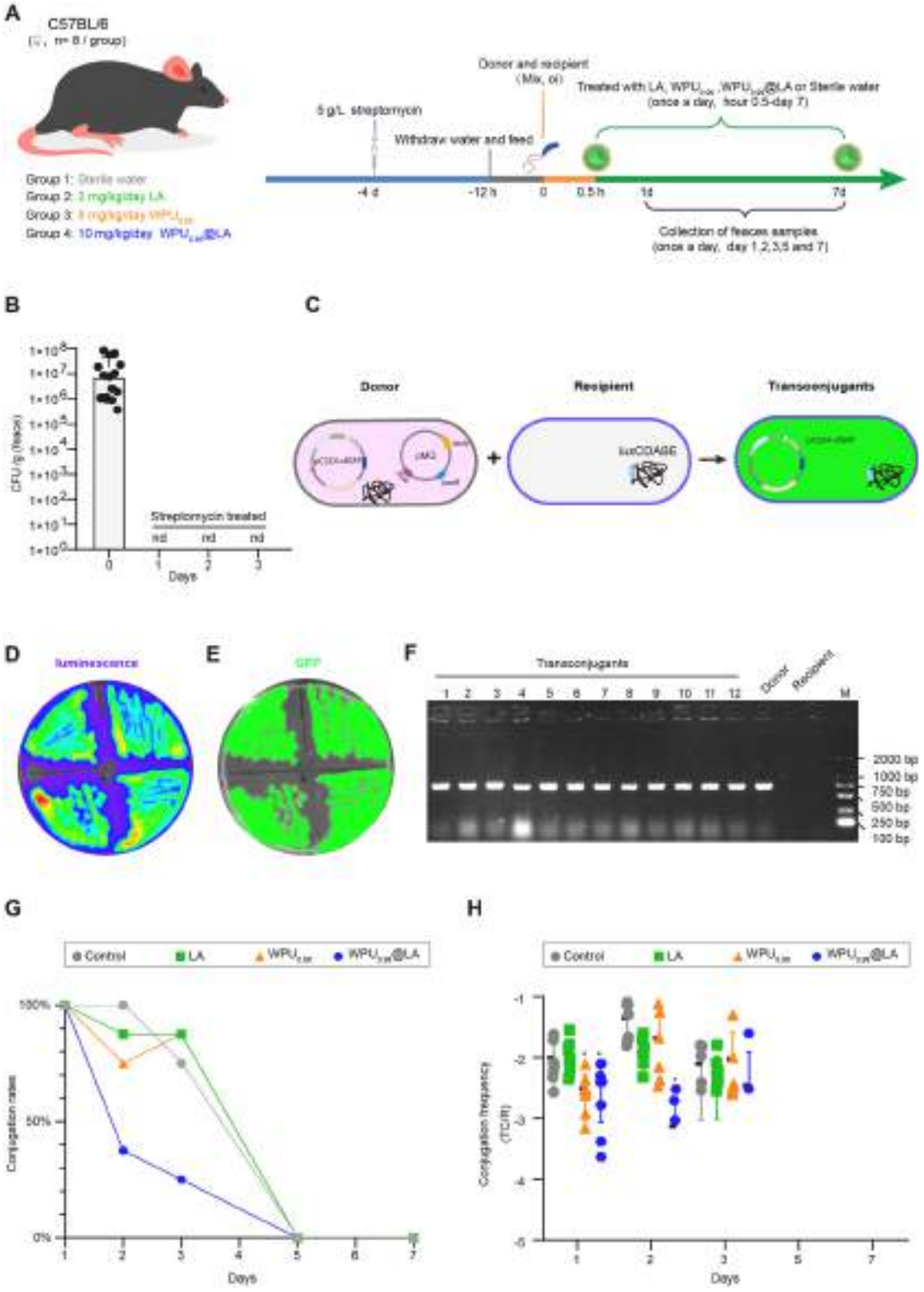


Fig. 4. $WPU_{0.99}$@LA improves the inhibition of conjugation of *mcr-1*-harboring IncX4 plasmid *in vivo*. **(A)** The study protocol including streptomycin pretreatment, donor and recipient inoculation, and mice with the following treatments: sterile water, 2 mg/kg/day LA, 8 mg/kg/day $WPU_{0.99}$ and 10 mg/kg/day $WPU_{0.99}$@LA. **(B)** Enterobacteriaceae depletion followed by CFU counts from feces of mice treated with 5 g/L streptomycin. **(C)** Development of fluorescence-based strains to monitor transfer of plasmid *in vivo*. Isolated transconjugants were plated on selective media and grown at 37 °C for 24 h. (D) Representative bioluminescence images of transconjugants in the bioluminescence channel. **(E)** Representative green fluorescence (GFP) images of transconjugants in the GFP channel. **(F)** Colony PCR for the *mcr-1* gene using mcr-F and mcr-R as specific primers. Line1-12: PCR product for transconjugants colony; Line13, PCR product for donor (*E. coli* MQCSZ4GFP); Line13, PCR product for recipient (*E. coli* C600-lux). **(G)** Conjugation rates and **(H)** Conjugation frequency in response to sterile water, 2 mg/kg/day LA, 8 mg/kg/day $WPU_{0.99}$ and 10 mg/kg/day $WPU_{0.99}$@LA. Filled icons show individual values for each dataset. Bar graphs represent the average and error bars the standard deviation of the data set. n = 8, *, $p < 0.05$.

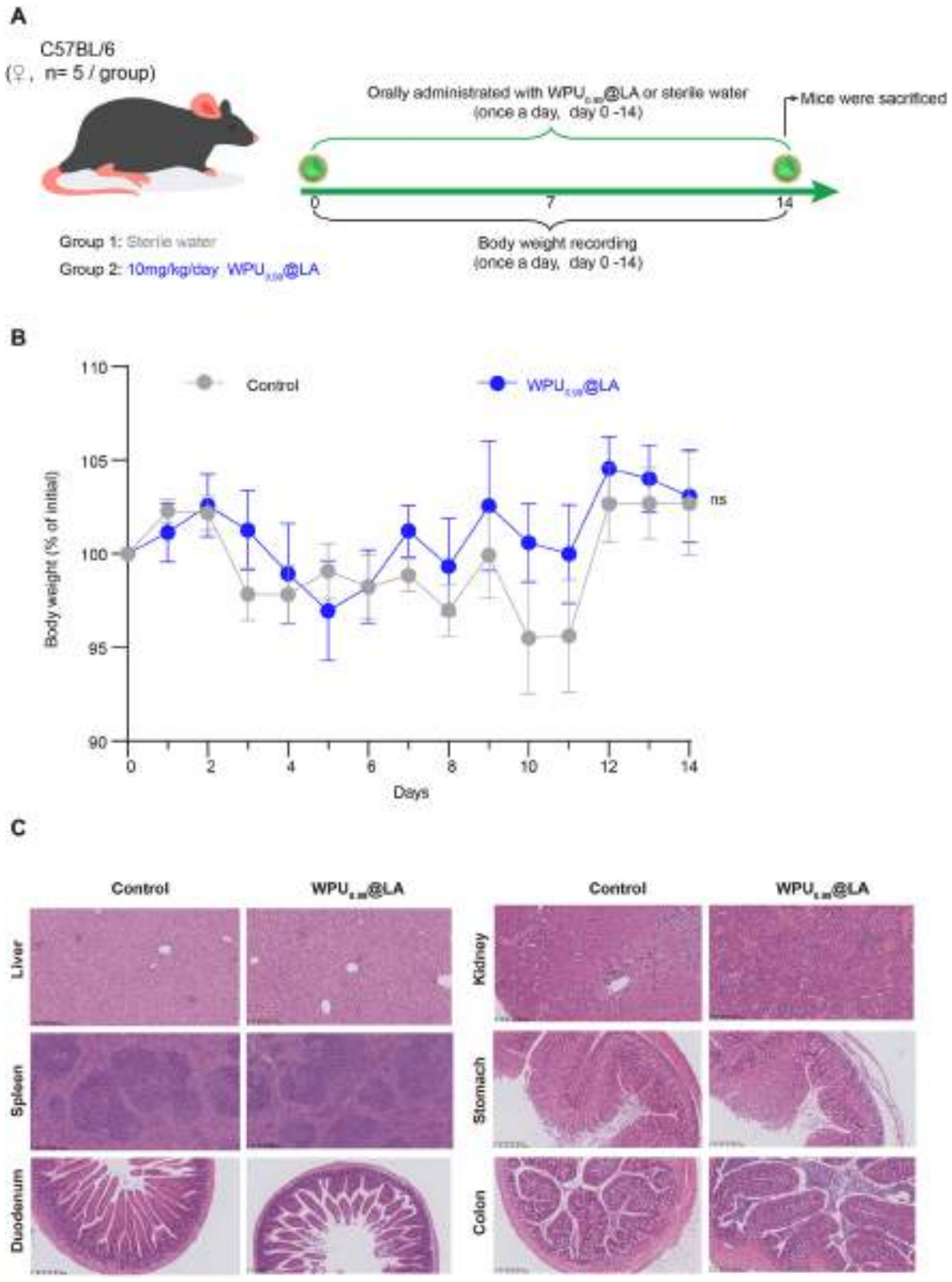


Fig. 5. $WPU_{0.99}$@LA demonstrates excellent biocompatibility. (A) Schematic illustration of the workflow of animal experiments. **(B)** Body weight alteration of mice received the sterile water and $WPU_{0.99}$@LA. **(C)** Pathological examination of liver, kidney, spleen, stomach, duodenum and colon of mice received sterile water and WPU0.99@LA, scale bar: 250 μm. n = 5, *, $p < 0.05$.

[64]. Firmicutes/Bacteroidetes ratio and the relative abundance of Bacteroidota, Firmicutes, Actinobacteria, Verrucomicrobia, and Proteobacteria did not significantly differ between the $WPU_{0.99}$@LA and control group (Fig. 6H–N). These findings suggest that $WPU_{0.99}$@LA maintains gut microbiota homeostasis effectively.

Despite these findings, our study has several limitations. Firstly, our research solely focused on the inhibitory effect of the $WPU_{0.99}$@LA nanoparticle on the IncX4 plasmid. Additionally, we investigated the

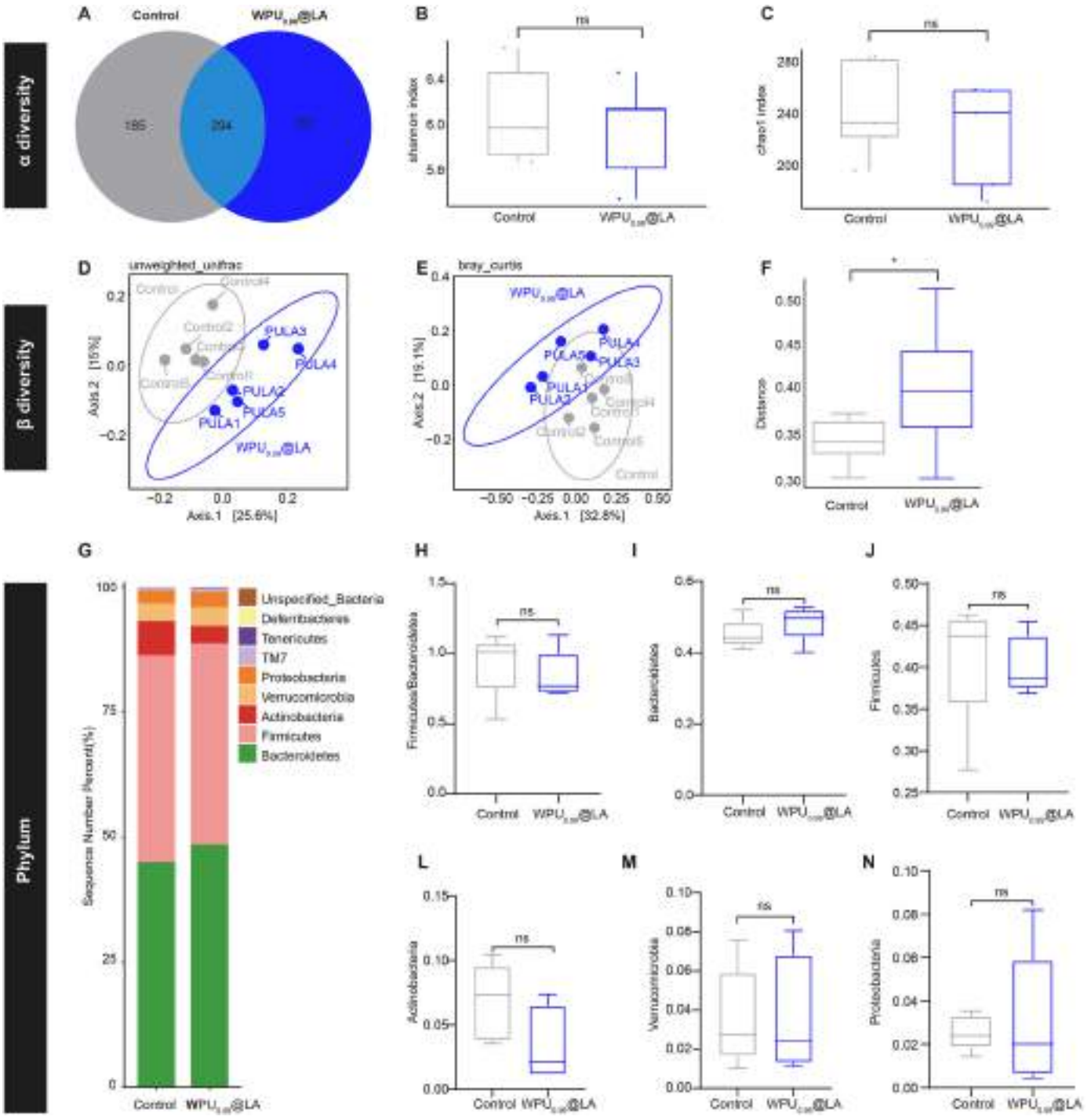


Fig. 6. $WPU_{0.99}$@LA maximally maintains the gut microbiota homeostasis. Operational taxonomic units (OTUs) **(A)**, Shannon index **(B)**, chao1 index **(C)**, Unweighted UniFrac principal coordinate analysis (PCA) **(D)**, Bray Curtis **(E)**, Bray Curtis distances **(F)** of the microbial composition for two groups. **(G)** The relative abundance of cecal bacteria at the phylum level. The Firmicutes/Bacteroidota ratio **(H)**, the relative abundance of cecal Bacteroidota **(I)**, Firmicutes **(J),** Actinobacteria **(L)**, Verrucomicrobia **(M)** and Proteobacteria **(N).** n = 5 mice/group. *, $p < 0.05$.

plasmid conjugation inhibition effect of $WPU_{0.99}$@LA in a mouse model with disrupted gut microbiota. Future studies should broaden the scope of investigation by exploring the inhibitory effects of $WPU_{0.99}$@LA nanoparticles on a diverse range of AMR plasmids *in vivo*. Additionally, examining the conjugation inhibition efficacy of $WPU_{0.99}$@LA in animal models with intact gut microbiota would enhance the translational relevance of our findings. Addressing these aspects will contribute to a more comprehensive understanding of the potential applications of $WPU_{0.99}$@LA in combating antimicrobial resistance. Nevertheless, this study provides robust proof of concept evidence, supporting that $WPU_{0.99}$@LA hold significant potential in controlling the spread of antibiotic resistance within the mammalian intestine.

4. Conclusions

In summary, the $WPU_{0.99}$@LA nanoparticle was engineered as a pH-responsive polyurethane system, showcasing its capability for the precise delivery of LA. This innovative nanoparticle demonstrated

effectiveness in combating the HGT of ARG-bearing plasmids within the mammalian intestine. Overall, $WPU_{0.99}$@LA exhibited a superior safety profile and offers insights for mitigating the spread of AMR *in vivo*.

Ethics approval

Animal experimentation was approved by the by the ethics Committee of the Laboratory Animal Center of South China Agricultural University (Guangzhou, China), approval number 2020B041.

Consent for publication

Not applicable.

CRediT authorship contribution statement

Gong Li: Writing – original draft, Validation, Methodology, Investigation, Funding acquisition, Data curation. **Lu Han:** Writing – original draft, Software, Investigation. **Li-Juan Xia:** Methodology, Investigation. **Ang Gao:** Investigation. **Zhi-Peng Li:** Investigation. **Shi-Ying Zhou:** Methodology, Investigation. **Lei Wan:** Methodology, Investigation. **Yao Deng:** Investigation. **Tian-Hong Zhou:** Investigation. **Xin-Yi Lu:** Investigation. **Yang Luo:** Validation, Investigation. **Dun-Sheng Liang:** Validation, Methodology, Investigation, Formal analysis. **Gui-Ting Wu:** Investigation. **Sheng-Qiu Tang:** Funding acquisition. **Xin-Lei Lian:** Software, Methodology. **Hao Ren:** Writing – review & editing, Supervision. **Xiao-Ping Liao:** Supervision, Project administration. **Liang Chen:** Writing – review & editing, Visualization, Validation. **Jian Sun:** Writing – review & editing, Validation, Supervision, Project administration, Funding acquisition, Conceptualization.

Declaration of competing interest

The authors declare that they have no known competing financial interests or personal relationships that could have appeared to influence the work reported in this paper.

Data availability

Data will be made available on request.

Acknowledgements

This work was supported by National key research and development program of China (2022YFD1800400), the Foundation for Innovative Research Groups of the National Natural Science Foundation of China (32121004), Local Innovative and Research Teams Project of Guangdong Pearl River Talents Program (2019BT02N054), Guangdong provincial key research and development program (2023B0202150001), National key research and development program of China (2022YFD1802100), Laboratory of Lingnan Modern Agriculture Project (NT2021006), Double first-class discipline promotion project (2023B10564003), the 111 Project (D20008), Guangdong Major Project of Basic and Applied Basic Research (2020B0301030007) and the China Postdoctoral Science Foundation (2023M741221).

Appendix A. Supplementary data

Supplementary data to this article can be found online at https://doi.org/10.1016/j.mtbio.2024.101181.

References

[1] L.-R. Jp, F.-M. A, A. L-L, B. P-E, G. C-P, S.-A. O, Prevention of infective endocarditis and bacterial resistance to antibiotics: a brief review, Spec. Care Dent. : official publication of the American Association of Hospital Dentists, the Academy of Dentistry for the Handicapped, and the American Society for Geriatric Dentistry 39 (6) (2019) 603–609.
[2] F. Nd, T. N, M. L, L. Cl, Antibiotic resistance in pacific island countries and territories: a systematic scoping review, Antibiotics (Basel, Switzerland) 8 (1) (2019).
[3] P.-I. A, S. Id, H.-E. G, et al., Horizontally acquired homologs of xenogeneic silencers: modulators of gene expression encoded by plasmids, phages and genomic islands, Genes 11 (2) (2020).
[4] L. Na, C. Ads, Horizontal transfer of antibiotic resistance genes in clinical environments, Can. J. Microbiol. 65 (1) (2019) 34–44.
[5] H. K, M. H, J. J, J. E, S. A, S. D, Role of horizontal gene transfer in the development of multidrug resistance in Haemophilus influenzae, mSphere 5 (1) (2020).
[6] B.J. Arnold, I.T. Huang, W.P. Hanage, Horizontal gene transfer and adaptive evolution in bacteria, Nat. Rev. Microbiol. 20 (4) (2022) 206–218.
[7] J.P.J. Hall, M.A. Brockhurst, E. Harrison, Sampling the mobile gene pool: innovation via horizontal gene transfer in bacteria, Philosophical transactions of the Royal Society of London Series B, Biological sciences 372 (1735) (2017).
[8] I.L. Brito, Examining horizontal gene transfer in microbial communities, Nat. Rev. Microbiol. 19 (7) (2021) 442–453.
[9] M. Hashimoto, H. Hasegawa, S. Maeda, High temperatures promote cell-to-cell plasmid transformation in Escherichia coli, Biochem. Biophys. Res. Commun. 515 (1) (2019) 196–200.
[10] D. Yong, M.A. Toleman, C.G. Giske, et al., Characterization of a new metallo-beta-lactamase gene, *bla*$_{NDM-1}$, and a novel erythromycin esterase gene carried on a unique genetic structure in *Klebsiella pneumoniae* sequence type 14 from India, Antimicrobial agents and chemotherapy 53 (12) (2009) 5046–5054.
[11] Y.Y. Liu, Y. Wang, T.R. Walsh, et al., Emergence of plasmid-mediated colistin resistance mechanism MCR-1 in animals and human beings in China: a microbiological and molecular biological study, Lancet Infect. Dis. 16 (2) (2016) 161–168.
[12] J. Sun, C. Chen, C.Y. Cui, et al., Plasmid-encoded tet(X) genes that confer high-level tigecycline resistance in Escherichia coli, Nature microbiology 4 (9) (2019) 1457–1464.
[13] R.S. McInnes, G.E. McCallum, L.E. Lamberte, W. van Schaik, Horizontal transfer of antibiotic resistance genes in the human gut microbiome, Curr. Opin. Microbiol. 53 (2020) 35–43.
[14] M. Buckner, M. Ciusa, R. Meek, et al., HIV drugs inhibit transfer of plasmids carrying extended-spectrum β-lactamase and carbapenemase genes, mBio 11 (1) (2020).
[15] H. Huang, J. Liao, X. Zheng, Y. Chen, H. Ren, Low-level free nitrous acid efficiently inhibits the conjugative transfer of antibiotic resistance by altering intracellular ions and disabling transfer apparatus, Water Res. 158 (2019) 383–391.
[16] M.M.C. Buckner, M.L. Ciusa, L.J.V. Piddock, Strategies to combat antimicrobial resistance: anti-plasmid and plasmid curing, FEMS Microbiol. Rev. 42 (6) (2018) 781–804.
[17] H. Wang, H. Qi, M. Zhu, et al., MoS(2) decorated nanocomposite: Fe(2)O(3)@MoS(2) inhibits the conjugative transfer of antibiotic resistance genes, Ecotoxicol. Environ. Saf. 186 (2019) 109781.
[18] M.M.C. Buckner, M.L. Ciusa, R.W. Meek, et al., HIV drugs inhibit transfer of plasmids carrying extended-spectrum β-lactamase and carbapenemase genes, mBio 11 (1) (2020), https://doi.org/10.1128/mbio.03355-19.
[19] B.O. Oyedemi, E.M. Kotsia, P.D. Stapleton, S. Gibbons, Capsaicin and gingerol analogues inhibit the growth of efflux-multidrug resistant bacteria and R-plasmids conjugal transfer, J. Ethnopharmacol. 245 (2019) 111871.
[20] G. Li, L. Xia, S. Zhou, et al., Linoleic acid and α-linolenic acid inhibit conjugative transfer of an IncX4 plasmid carrying *mcr-1*, J. Appl. Microbiol. 130 (6) (2021) 1893–1901.
[21] J. Ripoll-Rozada, Y. García-Cazorla, M. Getino, et al., Type IV traffic ATPase TrwD as molecular target to inhibit bacterial conjugation, Mol. Microbiol. 100 (5) (2016) 912–921.
[22] C.W. Ko, J. Qu, D.D. Black, P. Tso, Regulation of intestinal lipid metabolism: current concepts and relevance to disease, Nat. Rev. Gastroenterol. Hepatol. 17 (3) (2020) 169–183.
[23] N.G. Kotla, S. Rana, G. Sivaraman, et al., Bioresponsive drug delivery systems in intestinal inflammation: state-of-the-art and future perspectives, Adv. Drug Deliv. Rev. 146 (2019) 248–266.
[24] M. Peng, Z. Tabashsum, P. Patel, et al., Prevention of enteric bacterial infections and modulation of gut microbiota with conjugated linoleic acids producing Lactobacillus in mice, Gut Microb. 11 (3) (2019) 433–452.
[25] B. Ye, D.R. van Langenberg, Mesalazine preparations for the treatment of ulcerative colitis: are all created equal? World J. Gastrointest. Pharmacol. Therapeut 6 (4) (2015) 137–144.
[26] D.B. Ju, J.C. Lee, S.K. Hwang, C.S. Cho, H.J. Kim, Progress of polysaccharide-contained polyurethanes for biomedical applications, Tissue engineering and regenerative medicine 19 (5) (2022) 891–912.
[27] M.H.S. Mangal, S. Bose, T. Banerjee, Innovations in applications and prospects of non-isocyanate polyurethane bioplastics, Biopolymers (2023) e23568.
[28] Y. Wang, X. Li, G. Wu, et al., Precise control of drug release from dually responsive poly (ether urethane) nanoparticles, RSC advances 3 (33) (2013) 13859–13868.
[29] R. Liu, Y. Chen, H. Fan, Design, characterization, dyeing properties, and application of acid-dyeable polyurethane in the manufacture of microfiber synthetic leather, Fibers Polym. 16 (2015) 1970–1980.
[30] K. Chen, R. Liu, C. Zou, et al., Linear polyurethane ionomers as solid–solid phase change materials for thermal energy storage, Solar energy materials and solar cells 130 (2014) 466–473.

[31] F. Liu, D. He, Y. Yu, L. Cheng, S. Zhang, Quaternary ammonium salt-based cross-linked micelles to combat biofilm, Bioconjugate Chem. 30 (3) (2019) 541–546.
[32] S. Fu, H. Ren, Z. Ge, H. Zhuo, S. Chen, Shape memory polyurethanes based on zwitterionic hard segments, Polymers 9 (10) (2017) 465.
[33] G. Li, T. Long, S. Zhou, et al., CRISPR-AMRtracker: a Novel Toolkit to Monitor the Antimicrobial Resistance Gene Transfer in Fecal Microbiota, 2023.
[34] J. Sun, L.X. Fang, Z. Wu, et al., Genetic analysis of the IncX4 plasmids: implications for a unique pattern in the mcr-1 acquisition, Sci. Rep. 7 (1) (2017) 424.
[35] R. Lu, X. Zhou, K. Peng, et al., High-density dynamic bonds cross-linked hydrogel with tissue adhesion, highly efficient self-healing behavior, and NIR photothermal antibacterial ability as dressing for wound repair, Biomacromolecules 25 (4) (2024) 2486–2496.
[36] Z.Z.A. B, H.W. A, C.Y. A, et al., Qualitative and quantitative analysis of linoleic acid in polygonati rhizoma, Digital Chinese Medicine 3 (3) (2020) 180–187.
[37] L. Han, X.W. Liu, T. Zang, et al., H(2)S responsive PEGylated poly (lipoic acid) with ciprofloxacin for targeted therapy of Salmonella, J. Contr. Release : official journal of the Controlled Release Society 351 (2022) 896–906.
[38] Y. Yu, P. Li, C. Zhu, N. Ning, S. Zhang, G.J. Vancso, Multifunctional and recyclable photothermally responsive cryogels as efficient platforms for wound healing, Adv. Funct. Mater. 29 (35) (2019) 1904402.
[39] L. Han, T. Zang, L. Tan, et al., Self-assembly of H(2)S-responsive nanoprodrugs based on natural rhein and geraniol for targeted therapy against *Salmonella* Typhimurium, J Nanobiotechnology 21 (1) (2023) 483.
[40] D. He, Y. Yu, F. Liu, et al., Quaternary ammonium salt-based cross-linked micelle templated synthesis of highly active silver nanocomposite for synergistic anti-biofilm application, Chem. Eng. J. 382 (2020) 122976.
[41] S. Hu, T. Wang, M.L. Fernandez, Y. Luo, Development of tannic acid cross-linked hollow zein nanoparticles as potential oral delivery vehicles for curcumin, Food Hydrocolloids 61 (2016) 821–831.
[42] Center for Veterinary Drug Evaluation MoA, Compilation of Guidelines of Veterinary Drug Research Technology (2006–2011), China Chemical Industry Press, Beijing, 2012.
[43] P. Jing, Y. Luo, Y. Chen, J. Tan, C. Liao, S. Zhang, Aspirin-loaded cross-linked lipoic acid nanodrug prevents postoperative tumor recurrence by residual cancer cell killing and inflammatory microenvironment improvement, Bioconjug Chem 34 (2) (2023) 366–376.
[44] P. Li, W. She, Y. Luo, et al., One-pot, self-catalyzed synthesis of self-adherent hydrogels for photo-thermal, antimicrobial wound treatment, J. Mater. Chem. B 9 (1) (2021) 159–169.
[45] A.D. Sklirou, M. Ralli, M. Dominguez, I. Papassideri, A.L. Skaltsounis, I. P. Trougakos, Hexapeptide-11 is a novel modulator of the proteostasis network in human diploid fibroblasts, Redox Biol. 5 (2015) 205–215.
[46] H. Daemi, M. Barikani, M. Barmar, Highly stretchable nanoalginate based polyurethane elastomers, Carbohydr. Polym. 95 (2) (2013) 630–636.
[47] J.P.P. de Morais, I.K.C. Pacheco, A. Filho, et al., Polyurethane derived from castor oil monoacylglyceride (Ricinus communis) for bone defects reconstruction: characterization and in vivo testing, J. Mater. Sci. Mater. Med. 32 (4) (2021) 39.
[48] Y. Xia, Z. Zhang, M.R. Kessler, B. Brehm-Stecher, R.C. Larock, Antibacterial soybean-oil-based cationic polyurethane coatings prepared from different amino polyols, ChemSusChem 5 (11) (2012) 2221–2227.
[49] L. Wang, W. Cao, Y. Yi, H.P. Xu, Dual redox responsive coassemblies of diselenide-containing block copolymers and polymer lipids, Langmuir 30 (19) (2014) 5628–5636.
[50] H. Liang, Q. Lu, M. Liu, et al., UV absorption, anticorrosion, and long-term antibacterial performance of vegetable oil based cationic waterborne polyurethanes enabled by amino acids, Chem. Eng. J. 421 (2021) 127774.
[51] M. Wang, S.K. You, H.K. Lee, et al., Development and evaluation of docetaxel-phospholipid complex loaded self-microemulsifying drug delivery system: optimization and in vitro/ex vivo studies, Pharmaceutics 12 (6) (2020).
[52] C. Yu, P. Lu, S. Liu, et al., Efficiency of deoxynivalenol detoxification by microencapsulated sodium metabisulfite assessed via an *in vitro* bioassay based on intestinal porcine epithelial cells, ACS Omega 6 (12) (2021) 8382–8393.
[53] M. Zhang, X. Li, L. Zhou, W. Chen, E. Marchioni, Protein-based high internal phase pickering emulsions: a review of their fabrication, composition and future perspectives in the food industry, Foods 12 (3) (2023).
[54] F. Spragge, E. Bakkeren, M.T. Jahn, et al., Microbiome diversity protects against pathogens by nutrient blocking, Science 382 (6676) (2023) eadj3502.
[55] K. Neil, N. Allard, F. Grenier, V. Burrus, S. Rodrigue, Highly efficient gene transfer in the mouse gut microbiota is enabled by the Incl2 conjugative plasmid TP114, Commun. Biol. 3 (1) (2020) 523.
[56] B. Stecher, R. Denzler, L. Maier, et al., Gut inflammation can boost horizontal gene transfer between pathogenic and commensal Enterobacteriaceae, Proceedings of the National Academy of Sciences of the United States of America 109 (4) (2012) 1269–1274.
[57] M. Getino, R. Fernandez-Lopez, C. Palencia-Gandara, et al., Tanzawaic acids, a chemically novel set of bacterial conjugation inhibitors, PLoS One 11 (1) (2016) e0148098.
[58] S.-T. Yang, Y. Liu, Y.-W. Wang, A. Cao, Biosafety and bioapplication of nanomaterials by designing protein–nanoparticle interactions, Small 9 (9–10) (2013) 1635–1653.
[59] H. Ren, Y. Pan, J. Zhong, et al., An antibiotic-destructase-activated Fenton-like catalyst for synergistic removal of tetracycline residues from aquatic environment, Chem. Eng. J. 459 (2023) 141576.
[60] C. Kunz, S. Kuntz, S. Rudloff, Intestinal flora, Advances in experimental medicine and biology 639 (2009) 67–79.
[61] M. Tramontano, S. Andrejev, M. Pruteanu, et al., Nutritional preferences of human gut bacteria reveal their metabolic idiosyncrasies, Nature microbiology 3 (4) (2018) 514–522.
[62] Z. He, Y. Ma, S. Yang, et al., Gut microbiota-derived ursodeoxycholic acid from neonatal dairy calves improves intestinal homeostasis and colitis to attenuate extended-spectrum β-lactamase-producing enteroaggregative *Escherichia coli* infection, Microbiome 10 (1) (2022) 79.
[63] F. Pan, L. Zhang, M. Li, et al., Predominant gut *Lactobacillus murinus* strain mediates anti-inflammaging effects in calorie-restricted mice, Microbiome 6 (1) (2018) 54.
[64] C. Brandscheid, F. Schuck, S. Reinhardt, et al., Altered gut microbiome composition and tryptic activity of the 5xFAD alzheimer's mouse model, J Alzheimers Dis 56 (2) (2017) 775–788.

Check for updates

ORIGINAL RESEARCH

Acquisition of a novel conjugative multidrug-resistant hypervirulent plasmid leads to hypervirulence in clinical carbapenem-resistant *Klebsiella pneumoniae* strains

Gong Li[1,2,#], Ling Jia[1,2,#], Lei Wan[1,2], Lijuan Xia[1,2], Ang Gao[1,2], Runshi Yang[3], Ruanyang Sun[1,2], Minge Wang[1,2], Juan Du[1,2], Xinlei Lian[1,2], Rongmin Zhang[1,2], Liangxing Fang[1,2], Xiaoping Liao[1,2], Yahong Liu[1,2], Bao-Tao Liu[4,*], and Jian Sun[1,2,*]

Edited by Liang Yang, Southern University of Science and Technology, China; Received January 31, 2023; Accepted July 13, 2023; Published online September 28, 2023

Abstract

The co-occurrence of plasmid-mediated multidrug resistance and hypervirulence in epidemic carbapenem-resistant *Klebsiella pneumoniae* has emerged as a global public health issue. In this study, an ST23 carbapenem-resistant hypervirulent *K. pneumoniae* (CR-HvKP) strain VH1-2 was identified from cucumber in China and harbored a novel hybrid plasmid pVH1-2-VIR. The plasmid pVH1-2-VIR carrying both virulence and multidrug-resistance (MDR) genes was likely generated through the recombination of a virulence plasmid and an IncFIIK conjugative MDR plasmid in clinical ST23 18622 isolated from a sputum sample. The plasmid pVH1-2-VIR exhibited the capacity for transfer to the clinical ST11 carbapenem-resistant *K. pneumoniae* (CRKP) strain via conjugation assay. Acquisition of pVH1-2-VIR plasmid directly converted a CRKP into CR-HvKP strain characterized by hypermucoviscosity, heightened virulence for *Galleria mellonella* larvae, and increased colonization ability in the mouse intestine. The emergence of such a hybrid plasmid may expedite the spread of CR-HvKP strains, posing a significant risk to human health.

Keywords: conjugative virulence plasmid; CR-HvKP; hybrid plasmid; *Klebsiella pneumoniae*; ST23

Impact statement

An ST23 carbapenem-resistant and hypervirulent *K. pneumoniae* (CR-HvKP) strain VH1-2 was detected from cucumber in China. VH1-2 was observed to possess a hybrid virulence plasmid, pVH1-2-VIR, which may have arisen from the recombination of a virulence plasmid and an IncFIIK conjugative MDR plasmid in clinical ST23 18622 from a sputum sample. The hypervirulent plasmid pVH1-2-VIR was proficient in conjugative transfer to clinical ST11 CRKP, leading to an escalation in virulence and colonization levels. The appearance of such plasmids can be worrisome, which necessitates vigilant observation of their prevalence in the food chain.

INTRODUCTION

Klebsiella pneumoniae is a significant constituent of the human gut microbiota, yet it also serves as a prominent causative agent of invasive nosocomial infections including pyogenic liver abscesses that pose a substantial clinical treatment across the globe, particularly in Asia[1]. Clinical *K. pneumoniae* strains have undergone a transformation into hypervirulent *K. pneumoniae* (HvKP) (initially detected in Taiwan, China in 2002) and carbapenem-resistant *K. pneumoniae* (CRKP), both of which are currently prevalent in Asia[2–4]. Infection by HvKP strains is the cause of

[1]State Key Laboratory for Animal Disease Control and Prevention, South China Agricultural University, Guangzhou, China. [2]Guangdong Provincial Key Laboratory of Veterinary Pharmaceutics Development and Safety Evaluation, South China Agricultural University, Guangzhou, China. [3]Department of Pathogen Biology and Microbiology, Zhejiang University School of Medicine, Hangzhou, China. [4]College of Veterinary Medicine, Qingdao Agricultural University, Qingdao, China.

* **Correspondence:** Bao-Tao Liu, liubaotao-1986@163.com; Jian Sun, jiansun@scau.edu.cn

[#]Gong Li and Ling Jia contributed equally to this study.

DOI: 10.1002/mlf2.12086

This is an open access article under the terms of the Creative Commons Attribution License, which permits use, distribution and reproduction in any medium, provided the original work is properly cited.

mLife | WILEY

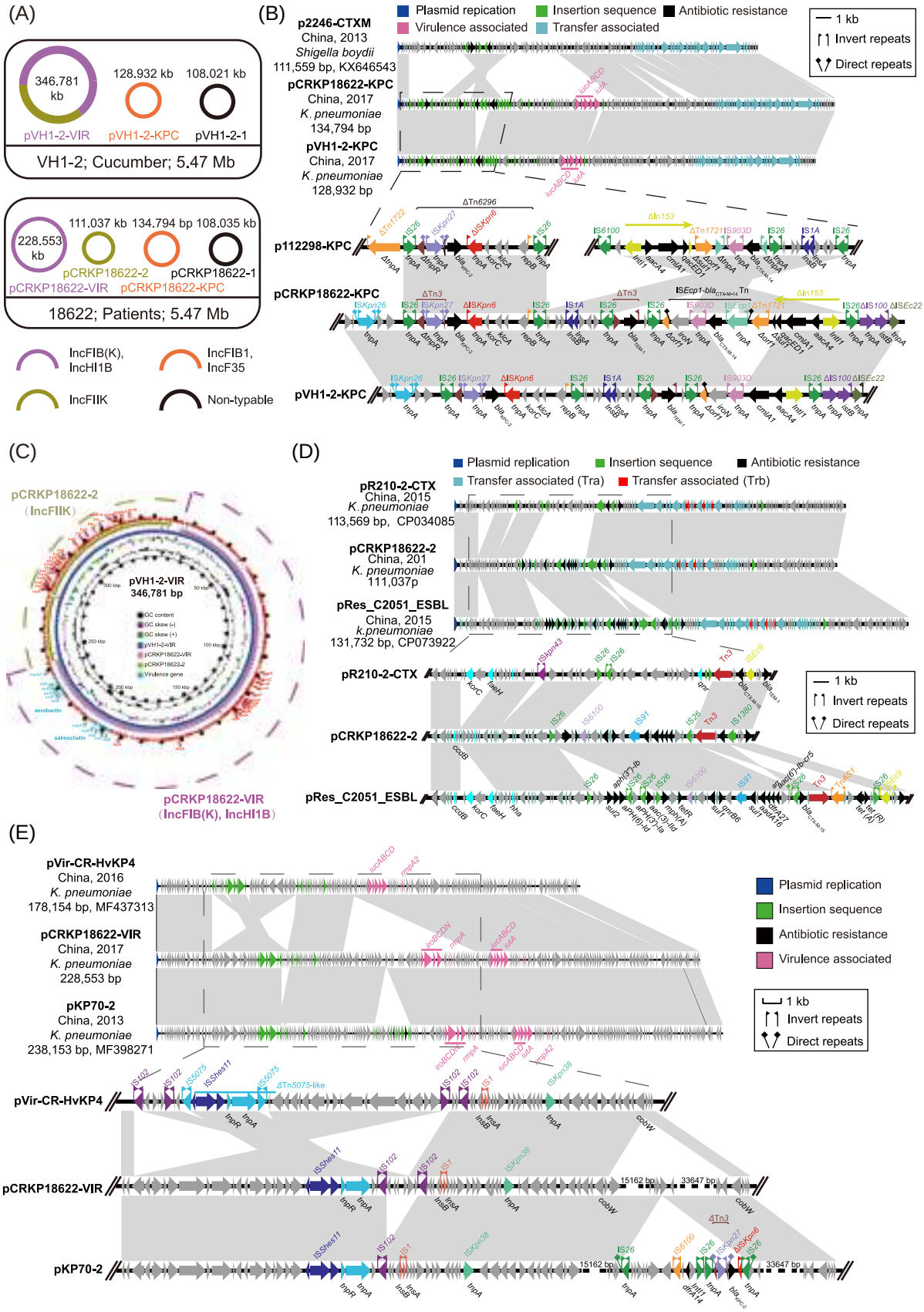


FIGURE 1 (Continued)

2770100x, 2023, 3, Downloaded from https://onlinelibrary.wiley.com/doi/10.1002/mlf2.12086 by South China Agricultural, Wiley Online Library on [06/10/2023]. See the Terms and Conditions (https://onlinelibrary.wiley.com/terms-and-conditions) on Wiley Online Library for rules of use; OA articles are governed by the applicable Creative Commons License

significant life-threatening liver abscesses or pneumonia thereby resulting in a high morbidity and mortality[5]. CRKP strains are responsible for the majority of (70%–90%) clinical carbapenem-resistant *Enterobacteriaceae* (CRE) infections in several countries including China[6]. This has resulted in untreatable or difficult-to-treat infections and poses a pressing public health concern globally. Fortunately, most HvKP strains as of now are susceptible to antibiotic therapy.

A significant threat to animal and human health is the acquisition of a carbapenemase-encoding plasmid by an HvKP strain, which results in a carbapenem-resistant HvKP (CR-HvKP)[7,8]. A fatal outbreak caused by ST11 CR-HvKP strains carrying a pLVPK-like hypervirulence plasmid was reported in China[3] and subsequent CR-HvKP infections have been documented[9,10]. It was recently discovered that the integration of carbapenemase gene bla_{KPC-2} into an HvKP virulence plasmid, along with the capsular polysaccharide (CPS) regulator *rmpA2*, had resulted in the emergence of hyper-resistance and hyper-virulence phenotypes[8]. Fortunately, this plasmid was determined to be nontransferable even though it was mobilizable. A recent discovery in China revealed the insertion of a transposon element carrying$bla_{CTX-M-24}$ into a pLVPK-like hypervirulence plasmid in an ST23 CR-HvKP[11]. However, the nonconjugative characteristic of pLVPK-like virulence plasmids has constrained the dissemination levels of CR-HvKP. The greatest concern, however, is a hybrid virulence plasmid that is conjugative. Moreover, composite pLVPK and IncFIB plasmid has been detected in a clinical *Klebsiella variicola* isolate, suggesting a potential for increased dissemination of CR-HvKP[12]. All previously reported CR-HvKP strains have been isolated solely from hospitalized patients with no instances from animals, environment, or retail food.

The current safety status of the food chain has attracted significant public attention due to contamination risks and its potential to act as a reservoir for antibiotic resistance genes (ARGs). Numerous studies have reported a high prevalence of antibiotic-resistant bacteria in the global food chain, particularly in retail[13–15]. CRE are also frequently detected in retail meat with some new isolates carrying both bla_{NDM} type carbapenemases and the mobilized colistin resistance gene *mcr-1*[16]. The safety of fresh vegetables has also become a growing concern due to the rising number of foodborne disease outbreaks linked to contaminated vegetables. These infections are often caused by bacteria exhibiting hyper-resistance and hyper-virulence phenotypes, such as Shiga toxin-producing *Escherichia coli* (STEC), which encoded ESBL in sprouts in Germany in 2011[17]. In our previous study, two CRKP isolates were found in ready-to-eat vegetables but the virulence potential of these isolates is currently unknown[18].

The current study presents novel findings on the identification of a conjugative virulence plasmid (undergone hybridization) with a conjugative IncFII MDR plasmid (isolated from cucumber). Acquisition of this virulence plasmid was observed to understand the level of virulence and intestinal colonization.

RESULTS

Genome sequence analysis of *K. pneumoniae* strains VH1-2 and 18622

Between May and November 2017, the CR-HvKP ST23 strains 18622 and VH1-2 were obtained from an inpatient sputum sample and cucumber, respectively, in the Qingdao region of Shandong province, China. These strains exhibited highly similar pulsed-field gel electrophoresis (PFGE) patterns (Figure S1). ARG and virulence gene analysis indicated a significant degree of relatedness between strain 18622 and VH1-2 (Table S1). Altogether, these findings indicate that VH1-2 and 18622 are phylogenetically closely related.

Whole genome sequencing (WGS) analysis of the genomes of these two strains revealed the presence of three and four plasmid types in VH1-2 and 18622, respectively (Figure 1A). Isolate 18622 contained bla_{KPC-2} on an F35:A-:B1 type plasmid pCRKP18622-KPC (134,794 bp, Genbank Accession No. CP027866), which carried *aac(6′)-Ib*, bla_{TEM-1B}, $bla_{CTX-M-14}$, *aac(6′)-Ib-cr*, *cmlA1*, and *iucABCD-iutA*. Notably, isolate VH1-2 from cucumber contained a highly similar bla_{KPC-2}-bearing F35:A-:B1 type plasmid. The backbone of both bla_{KPC-2}-bearing plasmids was organized similar to plasmid p2246-CTXM (Genbank Accession No. KX646543) carrying $bla_{CTX-M-14}$ from *Shigella boydii*. The primary component of the multidrug-resistant (MDR) region on pCRKP18622-KPC was bla_{KPC-2} and $bla_{CTX-M-14}$. The bla_{KPC-2} was located in the ΔTn*6296* that inserted at a site downstream of IS*Kpn26* in both strains 18622 and VH1-2 and differed from the site in p112298-KPC (Genbank Accession No. NZ_KP987215). The $bla_{CTX-M-14}$ transposition unit was flanked by 5 bp direct repeats (DRs) at both ends, located downstream of bla_{KPC-2} and inserted on a reverse ΔTn*1721* on plasmid pCRKP18622-KPC. However, the $bla_{CTX-M-14}$ transposition unit was truncated and further disrupted by ΔIn*153* and IS*26* elements on plasmid pVH1-2-KPC, resulting in the minor differences between pVH1-2-KPC and pCRKP18622-KPC (Figure 1B).

Numerous virulence genes were identified on the plasmids in both strains and VH1-2 possessed *rmpA*, *iroBCDN*, *iucABCD-iutA*, and *rmpA2* on a 346,781 bp IncHI1B-FIIK2-FIB(K)

Figure 1. Genome sequence analysis of *Klebsiella pneumoniae* strains VH1-2 and 18622. (A) Species, sources, and chromosome sizes of the CRKP isolates. (B) Comparison of plasmids pCRKP18622-KPC, pVH1-2-KPC, and p112298-KPC. (C) Circular comparison of plasmid pVH1-2-VIR, pCRKP18622-VIR, and pCRKP18622-2. The plasmid pVH1-2-VIR located at the innermost circle was used as the reference plasmid to perform sequence alignment with BLASTn by the BRIG software. Genetic regions associated with virulence are highlighted in cyan. (D) Linear alignment of complete plasmid sequences of pR210-2-CTX, pCRKP18622-2, and pRes_C2051_ESBL. Genes are denoted by arrows and colored based on function classification. Shaded regions denote shared regions of homology (95% nucleotide identity). (E) Linear alignment of complete plasmid sequences of pVir-CR-HvKP4, pCRKP18622-VIR, and pKP70-2.

2770100x, 2023, 3, Downloaded from https://onlinelibrary.wiley.com/doi/10.1002/mlf2.12086 by South China Agricultural, Wiley Online Library on [06/10/2023]. See the Terms and Conditions (https://onlinelibrary.wiley.com/terms-and-conditions) on Wiley Online Library for rules of use; OA articles are governed by the applicable Creative Commons License

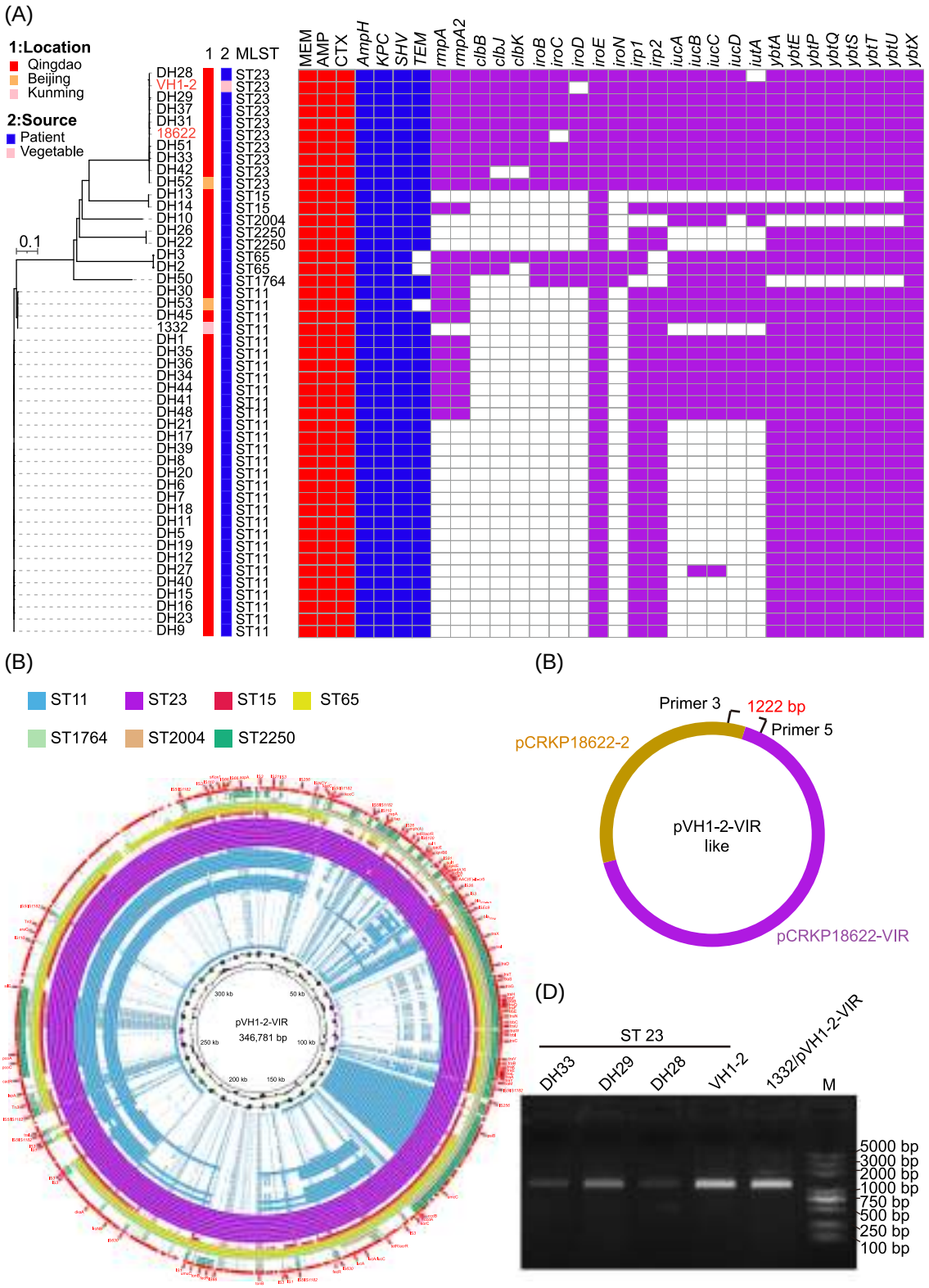


Figure 2. Prevalence of pVH1-2-VIR-like plasmids. (A) Phylogenetic structures, MLST, antibiotic resistance phenotypes, ARGs, and virulence genes of CRKP isolates. Isolate location and sources are indicated. Red and blue squares represent positivity for resistance phenotypes and resistance genes, respectively. Purple squares represent positivity for virulence genes. AMP, ampicillin; CTX, cefotaxime; MEM, meropenem. (B) Sequence alignment of virulence plasmids harboring *rmpA* and *rmpA2* in the 23 clinical CR-HvKP strains of different STs used in this study. The 346.781 kb virulence plasmid pVH1-2-VIR found in this study is used as a reference and genetic regions associated with virulence are highlighted in green. (C) Schematic depicting for investigating potential pVH1-2-VIR-like plasmids. Primers 3 and 5 were used to amplify hybrid regions. (D) PCR confirmed the presence of the pVH1-2-VIR-like plasmids in CRKP isolates. CRKP, carbapenem-resistant *K. pneumoniae*.

2770100x, 2023, 3, Downloaded from https://onlinelibrary.wiley.com/doi/10.1002/mlf2.12086 by South China Agricultural, Wiley Online Library on [06/10/2023]. See the Terms and Conditions (https://onlinelibrary.wiley.com/terms-and-conditions) on Wiley Online Library for rules of use; OA articles are governed by the applicable Creative Commons License

plasmid designated as pVH1-2-VIR, which also carried ARGs for β-lactams ($bla_{CTX\text{-}M\text{-}15}$, $bla_{TEM\text{-}1C}$), fluoroquinolones (*qnrB6, aac (6′)-Ib-crcr*), aminoglycosides (*aadA16*), rifampicin (*arr-3*), sulfonamides (*sul1*), macrolide (*mph*(A)), and trimethoprim (*dfrA27*). Interestingly, the virulence plasmid pVH1-2-VIR covered all the regions of both the IncFIIK resistance plasmid (pCRKP18622-2) and the IncFIB(K)-IncHI1B virulence plasmid (pCRKP18622-VIR) and carried the ARGs *aadA16*, $bla_{CTX\text{-}M\text{-}15}$, $bla_{TEM\text{-}1C}$, *aac(6′)-Ib-cr*, *qnrB6*, *mph(A)*, *arr-3*, *sul1*, *dfrA27* as well as virulence genes *iucABCD-iutA*, *iroBCDN*, *rmpA*, and *rmpA2*, respectively (Table S1). Moreover, sequence comparisons indicated that the virulence plasmid pVH1-2-VIR was formed by the fusion of pCRKP18622-2 and pCRKP18622-VIR carried by strain 18622 (Figure 1C).

The backbone of plasmids pR210-2-CTX (Genbank Accession No. CP034085) and pRes-C2051-ESBL (Genbank Accession No. CP073922) from *K. pneumoniae* in the GenBank database were similar to pCRKP18622-2, especially for pRes-C2051-ESBL. Compared with pCRKP18622-2, the plasmid pRes-C2051-ESBL was inserted with a 5036 bp *hp-korc-hp-fesH-hp* fragment and a 9221 bp MDR region mediated by IS*26* in two identical directions. In particular, a 10,971 bp tetracycline resistance gene region flanked by Tn*AS1* and IS*26* in two opposite directions was inserted in plasmid pRes-C2051-ESBL (Figure 1D). The conjugative transfer regions including *tra* and *trb* genes were identified in the plasmid pCRKP18622-2 and pVH1-2-VIR (Figure 1C,D).

An identical multidrug resistance region (MRR) of 29,479 bp containing $bla_{CTX\text{-}M\text{-}15}$, *aac (6′)-Ib-cr* and *qnrB6* as well as another six ARGs were found in both pVH1-2-VIR and pCRKP18622-2 and both harbored virulence genes *iucABCD-iutA*, *iroBCDN*, *rmpA*, and *rmpA2*. In the GenBank database, there was no highly similar plasmid to pVH1-2-VIR whereas pKP70-2 (Genbank Accession No. MF398271) from a clinical CR-HvKP isolate in China showed the highest similarity to pCRKP18622-VIR in this study. The minor differences between these two plasmids were two unique regions and a segment of 3645 bp franked by two IS*102* in the same orientation was inserted in pCRKP18622-VIR. Furthermore, an MDR region of 14,780 bp flanked by two IS*26* elements containing 8 bp DRs (CTAAAATT) in the same orientation was inserted between the backbone region in pKP70-2, suggesting that the insertion of this MDR region into the virulence plasmid pCRKP18622-VIR was mediated by IS*26* to form pKP70-2 (Figure 1E).

Prevalence of pVH-2-VIR-like plasmids

To investigate the prevalence of such virulence plasmid, we retrospectively screened 45 clinical CRKP strains collected from Qingdao, Beijing, and Kunming in China in 2017–2018. All the 45 clinical CRKP strains that carried $bla_{KPC\text{-}2}$ and 23 (51.11%) possessed the virulence plasmids harboring *rmpA* and *rmpA2*. Both the CRKP isolates (1742 and 1743) from Beijing were CR-HvKP, possessing *rmpA* and *rmpA2*, and 21/45 (46.67%) clinical CRKP strains were classified as CR-HvKP. WGS analysis indicated that five different ST types were present in the 23 clinical CR-HvKP strains, among which ST11 (10 strains) and ST23 (10 strains) were the most prevalent (Figure 2A). We also found that all ST11 and ST1764 CR-HvKP strains lacked the *clbA-S* virulence gene cluster, which was found in all examined ST23 and ST65 clinical CR-HvKP strains. Of note, all 23 CR-HvKP strains carried the gene cluster *iucABCD-iutA*, which was also located in the virulence plasmid pVH1-2-VIR harboring *rmpA2*, and genes *ybtA/E/P/Q/S/T/U/X* were found in 42 clinical CRKP strains (Figure 2A).

Owing to its hybrid nature encompassing both the virulence plasmid pCRKP18622-VIR and resistance plasmid pCRKP18622-2, the 346.781 kb virulence plasmid pVH1-2-VIR was aligned to pVH1-2-VIR in 47 CR-HvKP strains of varying STs. A retrospective analysis of clinical records revealed that the plasmid contigs within the ST23 strains covered nearly all regions of pVH1-2-VIR (Figure 2B) indicating that CR-HvKP from patients exhibited similarity with those from ready-to-eat vegetables.

To further investigate the prevalence of the pVH1-2-VIR-like plasmid, two pairs of primers were designed to target the hybrid region for PCR amplification and sequencing (Figure 2C). The results of the PCR amplification and sequencing confirmed that four ST23 isolates from hospital patients in Qingdao, Shandong province, China (DH33, DH29, DH28, and VH1-2) were positive for the hybrid region (Figure 2D). This indicated that the occurrence of pVH1-2-VIR-like virulence plasmids was not limited to VH1-2 but was also present in other clinical ST23 CRKP strains.

The pVH1-2-VIR plasmid contributes to hypervirulence in clinical ST11 CRKP

Given that ST11 has been the predominant CRKP type in China and the majority of ST11 CRKP strains are not hypervirulent, conjugation experiments were conducted to assess the potential hazard of the pVH1-2-VIR plasmid using a clinical ST11 strain as the recipient. The results of the conjugation experiments demonstrated that the pVH1-2-VIR plasmid was transmissible to ST11 CRKP1332 from VH1-2 at a conjugative frequency of $2.2 \pm 0.56 \times 10^{-6}$. Of note, the transconjugant 1332 demonstrated resistance to amikacin while remaining susceptible to rifampicin whereas VH1-2 exhibited resistance to rifampicin but remained susceptible to amikacin. MIC tests demonstrated that the acquisition of pVH1-2-VIR resulted in resistance to amikacin and rifampicin, indicating the successful transfer of pVH1-2-VIR into strain 1332. Additionally, both 1332/pVH1-2-VIR and 1332 exhibited comparable susceptibilities to meropenem, rifampicin, fosfomycin, gentamicin, ciprofloxacin, tetracycline, and doxycycline (Tables S2 and S3).

Interestingly, the growth curves of the transconjugant 1332/pVH1-2-VIR and donor were indistinguishable (Figure 3A). This indicated that the introduction of pVH1-2-VIR plasmid did not alter the normal growth of donor 1332. Moreover, since plasmids can introduce fitness costs to their hosts, we performed a quantitative evaluation of the fitness

2770100x, 2023, 3, Downloaded from https://onlinelibrary.wiley.com/doi/10.1002/mlf2.12086 by South China Agricultural, Wiley Online Library on [06/10/2023]. See the Terms and Conditions (https://onlinelibrary.wiley.com/terms-and-conditions) on Wiley Online Library for rules of use; OA articles are governed by the applicable Creative Commons License

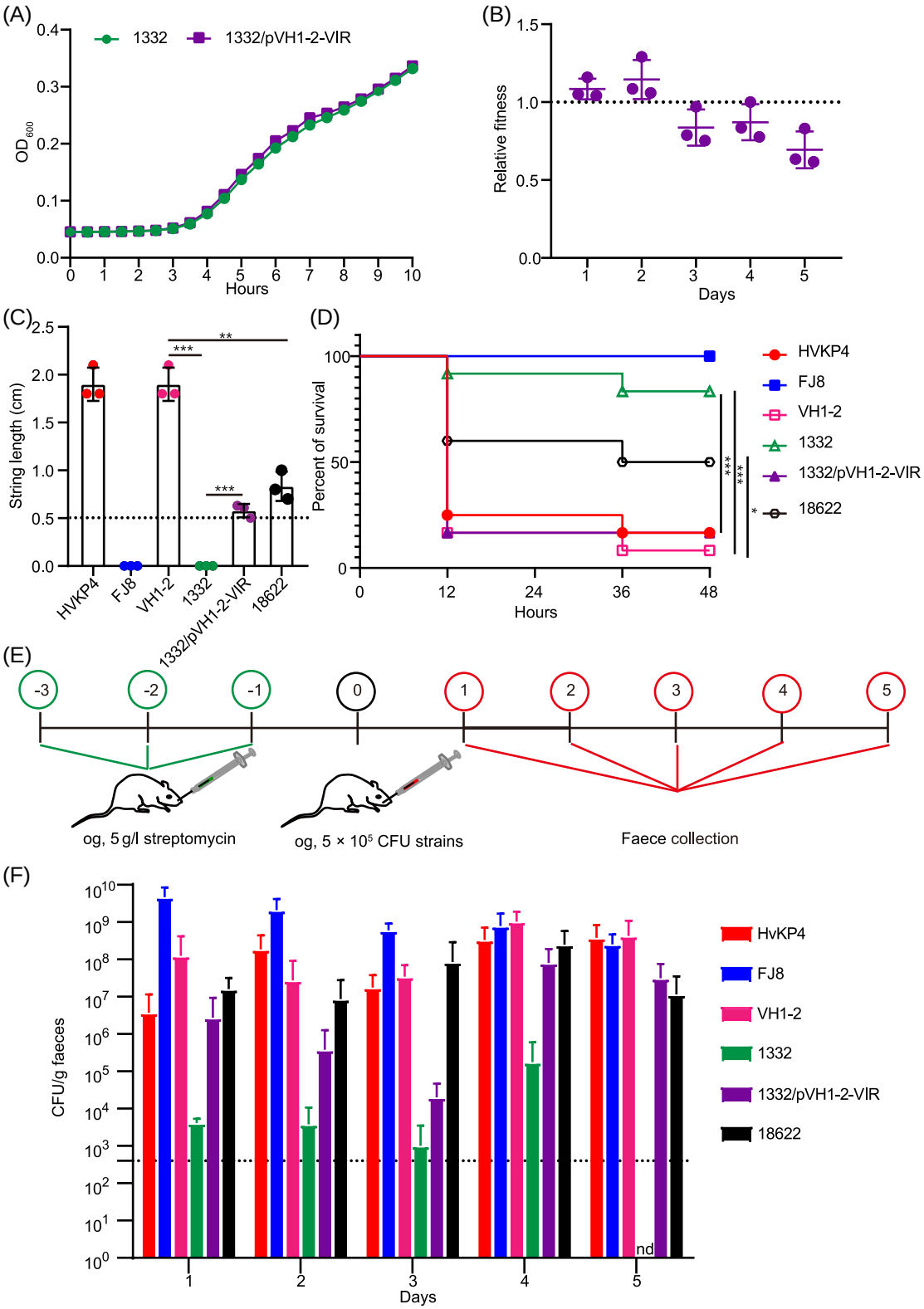


Figure 3. The pVH1-2-VIR plasmid contributes to hypervirulence to clinical ST11 CRKP. (A) Growth curve of 1332 and 1332/pVH1-2-VIR ($n = 3$). (B) Relative fitness of pVH1-2-VIR plasmid carrying clones compared with pVH1-2-VIR-free clones obtained by competition assays. Bars represent normalized relative fitness after subtracting the effect of pVH1-2-VIR ($n = 3$). (C) String length observed in tested CRKP isolates ($n = 3$). (D) Virulence potential of CRKP isolates tested in a *Galleria mellonella* infection model. Survival of mice infected with 5×10^5 CFU of each *Klebsiella pneumoniae* at 48 h is shown ($n = 12$). (E) Experimental setup for the intestinal colonization assay. (F) Colonization levels of CRKP isolates in feces at Days 1 to 5 after infection ($n = 6$). $^*p < 0.05$; $^{**}p < 0.01$; $^{***}p < 0.001$. CFU, colony-forming unit; CRKP, carbapenem-resistant *K. pneumoniae*; nd, not detected.

2770100x, 2023, 3, Downloaded from https://onlinelibrary.wiley.com/doi/10.1002/mlf2.12086 by South China Agricultural, Wiley Online Library on [06/10/2023]. See the Terms and Conditions (https://onlinelibrary.wiley.com/terms-and-conditions) on Wiley Online Library for rules of use; OA articles are governed by the applicable Creative Commons License

costs linked to pVH1-2-VIR carriage. We carried out a competition between isogenic 1332/pVH1-2-VIR and 1332 clones. However, the outcomes of these assays indicated that pVH1-2-VIR introduced only minor fitness costs (Figure 3B).

The virulence potentials of strains 18622, VH1-2, 1332, and 1332/pVH1-2-VIR were also assessed through viscous string assay and the *G. mellonella* larvae survival assay. Plasmid HVKP4 was used as a hyper-virulence control and FJ8 as a low-virulence control[18]. We found that both FJ8 and 1332 generated viscous string <0.5 cm, indicating a low-mucoviscous phenotype. In contrast, HVKP4, 18622, VH1-2, and 1332/pVH1-2-VIR exhibited a higher degree of mucoviscosity with strings >0.5 cm compared to the low-virulence control FJ8 (Figure 3C). The virulence potential using *G. mellonella* larvae indicated that inoculation with 5×10^5 CFU of VH1-2 strain resulted in a mortality of 91.67% at 48 h and this surpassed that of the hypervirulent control strain HVKP4 (83.33% mortality) and was significantly higher than the low-virulence control strain FJ8 (0% mortality).

The inoculation of *G. mellonella* larvae with 5.0×10^5 CFU 1332/pVH1-2-VIR resulted in a mortality rate of 83.33% at 48 h and was comparable to that of HVKP4 but higher than that of 1332 (12.67%, $p < 0.001$). These findings provide further evidence that the acquisition of the pVH1-2-VIR plasmid by the ST11 CRKP strain 1332 facilitated its transformation into a hypervirulent strain. In contrast, strain 18622 displayed a lower degree of mucoviscosity ($p < 0.01$) and mortality (50%, $p < 0.05$) compared to VH1-2, suggesting that its virulence level may be lower than that of the VH1-2 strain (Figure 3D).

The process of gastrointestinal colonization plays a crucial role in the development of healthcare-associated infections caused by *K. pneumoniae* strains[19]. To assess the colonization potential of CRKP strains, a streptomycin-treated mouse model was utilized. Interestingly, despite the seemingly low virulence of strain FJ8, its colonization level was found to be significantly high in the mouse model. Specifically, infection with either 5×10^5 VH1-2 or 1332/pVH1-2-VIR at 5 days postinfection (dpi) resulted in a colonization level of 4.28×10^8 and 3.12×10^7 CFU/g, respectively. However, CRKP strain 1332 was not detected in the feces at 5 dpi. The data indicated that the presence of a pVH1-2-VIR plasmid in 1332 resulted in an elevated level of colonization whereas 18622 demonstrated a slightly lower level of colonization compared to VH1-2 (Figure 3E).

DISCUSSION

The incidence of CR-HvKP strains has been on the rise, particularly in China[12,20]. Previous reports have indicated that the carbapenemase gene bla_{KPC-2} and virulence genes *rmpA/rmpA2* were typically situated on separate plasmids in most of CR-HvKP strains[3,21]. Plasmids carrying bla_{KPC-2}, for example pVH1-2-KPC, were frequently found to be transferable[6,22]. Whereas hypervirulence plasmids, for example pLVPK-like plasmids, often lacked conjugative regions like *tra*[20]. These findings prompted the hypothesis that hypervirulent plasmids present in clinical HvKP strains lacked conjugative properties. Consequently, the formation of CR-HvKP was believed to primarily occur via conjugative bla_{KPC-2} plasmid acquisition from HvKP strains. Although pLVPK-like virulence plasmids were initially deemed nonconjugative, a recent investigation revealed that virulence plasmids could mobilize independently or in conjunction with a helper plasmid at a lower rate[23]. Furthermore, the nonconjugative virulence plasmid could be supplied with transfer functions from a conjugative plasmid during conjugation and mobilize at a higher frequency[24].

Previous reports have indicated that ARGs, such as bla_{CTX-M}[11] and bla_{KPC-2}[8], are colocated on pLVPK-like plasmids. However, these plasmids are devoid of conjugative regions. In contrast to previously identified virulence plasmids, a novel conjugative virulence plasmid was recently identified in *K. variicola*, which integrated a 100 kb virulence fragment into a conjugative IncFIB plasmid. This plasmid was capable of being transferred to various *Klebsiella* strains via conjugation but did not harbor any ARGs[12]. In scattered clinical CRKP strains, 11 virulence plasmids were identified that were potentially capable of conjugation and contained the transfer region of plasmid IncFII, that is, *tra* genes. In addition, most of these plasmids also harbored ARGs[25,26] while only two have been demonstrated to be transferable. Recently, a conjugative hybrid plasmid of 479 kb was reported in a clinical ST15 CR-HvKP in China. This plasmid shared regions from a 290 kb virulence plasmid and a conjugative MDR plasmid (188 kb), both of which are present in another clinical ST15 CR-HvKP[27].

There have been recent increases in the incidence of foodborne illnesses caused by contaminated vegetables. This is compounded by the presence of hypervirulent MDR organisms in ready-to-eat vegetables and poses a significant food safety concern. The current study aims to characterize a CR-HvKP strain associated with foodborne transmission. We identified an ST23 CR-HvKP strain from cucumber that harbored a 347 kb conjugative hybrid virulence plasmid. This plasmid was likely formed through the recombination of a virulence plasmid (228 kb) and an IncFIIK conjugative MDR plasmid (111 kb) present in clinical ST23 CRKP strains. The virulence plasmid (pVH1-2-VIR) contained IncFIIK, IncFIB(K), and IncHI1B replicons as well as transfer regions *tra* and *trb*. These three types of Inc plasmids are predominantly distributed among *Enterobacteriaceae*, including *E. coli*, *K. pneumoniae*, *Shigella flexneri*, and *Salmonella enterica Typhimurium*[28–30]. Our conjugation assays demonstrated the transferability of the pVH1-2-VIR plasmid to the widely prevalent clinical ST11 CRKP strain. Our conjecture is that these virulence plasmids have the potential to directly disseminate among bacterial pathogens, especially *Enterobacteriaceae*, resulting in the simultaneous expression of phenotypic carbapenem resistance and high-level virulence. This could pose a significant threat to human health through the food chain. To the best of our knowledge, this is the first documented

2770100x, 2023, 3, Downloaded from https://onlinelibrary.wiley.com/doi/10.1002/mlf2.12086 by South China Agricultural, Wiley Online Library on [06/10/2023]. See the Terms and Conditions (https://onlinelibrary.wiley.com/terms-and-conditions) on Wiley Online Library for rules of use; OA articles are governed by the applicable Creative Commons License

report of this type of particularly hypervirulent MDR plasmid, particularly in the context of the food chain.

The ST23 clonal group is associated with hypervirulence and has been identified as a prevalent ST in clinical *K. pneumoniae* across several countries including China[31]. Examination of virulence genes in CR-HvKP revealed that all ST23 CR-HvKP strains contained nearly all virulence genes, resulting in heightened virulence compared to other STs. This finding further supports the notion that ST23 clonal group members are highly virulent. In addition, our findings indicated that CR-HvKP strains (specifically ST23 VH1-2) that possess virulence plasmids containing CPS regulatory genes, exhibit greater virulence than CRKP strains lacking such plasmids. This was indicated quantitively here using *G. mellonella* assays. The hypervirulent potential of the foodborne strain VH1-2 and its virulence plasmid transconjugant was assessed using the string test, a widely used method for identifying HvKP strains[31]. The results confirmed that VH1-2 and its transconjugants exhibited high levels of virulence and provided additional evidence that the acquisition of a conjugative hypervirulent plasmid by ST11 1332 contributed to the observed increase in virulence.

The cocarriage of ARGs and virulence factors within a singular virulence vector can facilitate the concurrent transmission of both traits, thereby promoting the rapid emergence and dissemination of multidrug-resistant hypervirulent *K. pneumoniae* (MDR HvKP) strains[32]. Our results of colonization assay further confirmed that the acquisition of the virulence plasmid could augment mammalian colonization, thereby posing an unprecedented threat to human health via the food chain. Notably, VH1-2 exhibited a greater degree of virulence and colonization relative to 18622, suggesting that the fusion of the two plasmids enhanced not only virulence but also bacterial colonization. However, the underlying mechanisms remain unclear and require further investigation.

In brief, this study delineated the emergence of an infrequent conjugative MDR hypervirulent plasmid in an ST23 CR-HvKP strain isolated from fresh cucumber. This conjugative plasmid has the potential to directly disseminate into human CRKP and contribute to augmented virulence and colonization, thereby posing an unparalleled risk to human health through the food chain. The emergence of conjugative MDR hypervirulent plasmids in pathogens found in ready-to-eat food is a concerning trend and it is imperative to closely monitor the prevalence of such plasmids among clinical strains and the food chain.

MATERIALS AND METHODS

Bacterial strains antimicrobial susceptibility testing and PFGE typing

In 2017–2018, a total of 47 isolates were obtained from inpatient sputum and cucumber samples in Qingdao ($n = 44$), Beijing ($n = 2$), and Kunming ($n = 1$), China. The agar dilution method was used to determine the minimum inhibitory concentrations (MIC) for meropenem, cefotaxime, ampicillin, fosfomycin, amikacin, ciprofloxacin, gentamicin, tetracycline, trimethoprim/sulfamethoxazole, rifampicin, and florfenicol. The results were interpreted in accordance with the Clinical and Laboratory Standards Institute (CLSI) guidelines. Broth microdilution method was used to examine the MIC of tigecycline. *E. coli* ATCC 25922 was used as a quality control strain. Clonal relationships of VH1-2 and 18622 were investigated using PFGE of *Xba*I-digested genomic DNA as previously described[33].

WGS and phylogenetic analysis

WGS was conducted on 47 selected isolates using the Illumina MiSeq system (Illumina), and the paired-end Illumina reads were assembled using SPAdes v3.6.2[34]. ARG was identified via ResFinder 3.1 (https://cge.cbs.dtu.dk/services/ResFinder/) while transposon and insertion sequence (IS) elements were predicted using ISfinder (https://www-is.biotoul.fr). The prediction of virulence genes was facilitated with the Virulence Factor Database (http://www.mgc.ac.cn/VFs/). The genome was annotated through the Prokaryotic Genome Annotation Pipeline server. The BLASTn algorithm, integrated in BLAST ring image generator (BRIG) Version 0.95 was employed for sequence comparisons and map generation[35]. In addition, EasyFig. 2.1 (BLASTn, default setting) was utilized for the linear comparison of plasmids[36].

Identification of pVH1-2-VIR-like plasmid

The CRKP isolates were screened for the presence of pVH1-2-VIR-like hybrid plasmid using primers F3: 5′-GCACTCCG GAATACATACTGATG-3′, F5: 5′-GCAAAAAGGGCGTGAACT TCAGG-3′. The samples were run with the following PCR program: 95°C 3 min, 95°C 15 s–55°C 15 s–72°C 1 min for 30 cycles, 72°C 5 min. The presence of the targeted gene was confirmed by Sanger sequencing.

Conjugation experiments

The conjugation experiments were conducted following previously established protocols with minor modifications[37]. Specifically, the donor VH1-2 (ST23, rifampicin-resistant) and recipient *K. pneumoniae* 1332 (ST11, amikacin-resistant) were each inoculated into 5 ml of LB broth at a concentration of 10^8 colony-forming units (CFU)/ml and incubated at 37°C. After 6 h of liquid mating, the mixed suspension was subjected to serial dilutions and plated on selective media as follows: (1) LB agar supplemented with rifampicin (128 μg/ml) and amikacin (64 μg/ml) for the enumeration of transconjugants; (2) LB agar containing amikacin (64 μg/ml) for the calculation of recipient cells. The identity of transconjugants was confirmed by PCR assays and ERIC-PCR[38]. Conjugative frequency was calculated as: $\gamma = T/R$, T and R represent the number of transconjugants and recipients per milliliter, respectively[39]. The experiment was performed in triplicate.

Growth curves

The bacterial cells of *K. pneumoniae* 1332 and 1332/pVH1-2-VIR were cultured overnight and subsequently adjusted to a concentration of 5×10^5 CFU/ml with LB broth. The cultures

2770100x, 2023, 3, Downloaded from https://onlinelibrary.wiley.com/doi/10.1002/mlf2.12086 by South China Agricultural, Wiley Online Library on [06/10/2023]. See the Terms and Conditions (https://onlinelibrary.wiley.com/terms-and-conditions) on Wiley Online Library for rules of use; OA articles are governed by the applicable Creative Commons License

were then incubated at 37°C with shaking at 180 rpm. Growth curves were generated by measuring the optical density at 600 nm for a duration of 10 h utilizing an EnSight Multimode Microplate Reader (PerkinElmer). Prism 8 software (GraphPad) was employed to construct the growth curves.

Competition assay

The *K. pneumoniae* 1332 and 1332/pVH1-2-VIR strains were cultured overnight, washed, and resuspended in LB broth. Subsequently, the cultures were combined in a 1:1 ratio and inoculated at a 1:100 dilution. The resulting mixtures were incubated at 37°C for 1, 2, 3, 4, and 5 days. Following incubation, LB agar supplemented with or without rifampicin (128 μg/ml) was utilized to plate dilutions of the bacterial mixture, enabling differentiation between the rifampicin-resistant 1332/pVH1-2-VIR and 1332 strains. Relative fitness was calculated as the ratio of Malthusian parameters $W = \log_{10}(1332/\text{pVH1-2-VIR}_{end}/1332/\text{pVH1-2-VIR}_{start})/\log_{10}(1332_{end}/1332_{start})$ as previously described[40]. Three independent competition experiments were performed to calculate the Malthusian parameters.

String tests

The methodology for the string test was executed in accordance with the previously published protocol[5]. All CRKP isolates were cultured on agar plates supplemented with 5% sheep blood and incubated at 37°C for one night. The hypermucoviscous phenotype was identified by observing the formation of a viscous string measuring greater than 5 mm in length generated by pulling a single colony upwards using a standard inoculation loop.

The *Galleria mellonella* infection assay

The *G. mellonella* infection assay was conducted in accordance with the methodology outlined in a previous study[41]. Each group was comprised of a sample population of 12 larvae weighing 300 ± 50 mg. All CRKP isolates were cultured in LB broth and harvested during the exponential phase. Following a wash with sterile phosphate-buffered saline (PBS), 10 μl of 5×10^5 CFU bacterial cells were administered via injection into the rear left proleg of the larvae. The survival rate of the *G. mellonella* larvae was monitored and recorded at regular 12 h intervals over a period of 48 h. Survival was analyzed using the Kaplan–Meier method and implemented with Prism 8.0 (GraphPad).

Mouse colonization assay

Female BALB/c SPF mice (8 weeks old, weighing 20 ± 2 g) were utilized for colonization assays. All mice were housed in the Laboratory Animal Center of Southern Medical University in Guangzhou, China. To overcome colonization resistance, the mice were pretreated with 200 μl streptomycin (5 g/l) via intragastric gavage for 3 consecutive days. The CRKP strains were experimentally introduced as previously described[42]. *K. pneumoniae* strains were cultured overnight, washed, and adjusted to a concentration of 5×10^7 CFU/ml with sterile PBS. The mice were subjected to oral gavage with 200 μl of 5×10^5 CFU bacterial cells following which their feces were collected on Days 1 to 5 post-CRKP administration. The level of colonization was assessed by plating on LB agar with 100 μg/ml ampicillin and quantifying CRKP CFU in fecal samples. The colonization assay was conducted in accordance with the guidelines stipulated in the Guide for the Care and Use of Laboratory Animals at the Laboratory Animal Center of South China Agricultural University.

Statistical analysis

Statistical analysis was performed using the software GraphPad Prism version 8.0. The significance of differences ($p < 0.05$) was determined using the unpaired *t* test with a two-tailed nonparametric analysis.

ACKNOWLEDGMENTS

This study was supported in part by the Foundation for Innovative Research Groups of the National Natural Science Foundation of China (32121004), Local Innovative and Research Teams Project of Guangdong Pearl River Talents Program (2019BT02N054), Laboratory of Lingnan Modern Agriculture Project (NT2021006), Guangdong Major Project of Basic and Applied Basic Research (grant 2020B0301030007), Innovation Team Project of Guangdong University (2019KCXTD001), the 111 Project (grant D20008), Natural Science Foundation of Shandong Province of China (ZR2022MC001), and the Scientific and Technological Projects of Qingdao (19-6-1-94-nsh). The hyper-virulence strain HVKP4 and low-virulence strain FJ8 were kindly gifted by Professor Rong Zhang, Zhejiang University.

AUTHOR CONTRIBUTIONS

Gong Li: Investigation (lead); methodology (equal); software (equal); validation (equal); visualization (lead); writing—original draft (lead). **Ling Jia**: Data curation (equal); formal analysis (equal); methodology (equal); validation (supporting); visualization (equal). **Lei Wan**: Investigation (supporting). **Lijuan Xia**: Investigation (supporting); methodology (supporting). **Ang Gao**: Methodology (supporting). **Runshi Yang**: Investigation (supporting); validation (supporting); visualization (supporting). **Ruanyang Sun**: Methodology (supporting). **Minge Wang**: Data curation (supporting); formal analysis (supporting); validation (supporting); visualization (supporting). **Juan Du**: Formal analysis (supporting); validation (supporting). **Xinlei Lian**: Software (supporting). **Rongmin Zhang**: Software (supporting); visualization (supporting). **Liangxing Fang**: Writing—review and editing (supporting). **Xiaoping Liao**: Supervision (supporting). **Yahong Liu**: Funding acquisition (equal); project administration (equal); supervision (lead). **Bao-Tao Liu**: Conceptualization (equal); data curation (equal); funding acquisition (supporting); methodology (supporting); project administration (supporting); resources (equal); validation (lead); writing—original draft (equal); writing—review and editing (equal). **Jian Sun**: Conceptualization (equal); funding acquisition (equal); project administration (equal); resources (supporting);

2770100x, 2023, 3, Downloaded from https://onlinelibrary.wiley.com/doi/10.1002/mlf2.12086 by South China Agricultural, Wiley Online Library on [06/10/2023]. See the Terms and Conditions (https://onlinelibrary.wiley.com/terms-and-conditions) on Wiley Online Library for rules of use; OA articles are governed by the applicable Creative Commons License

validation (equal); writing—original draft (equal); writing—review and editing (lead).

ETHICS STATEMENT

Animal experimentation was approved by the Ethics Committee of the Laboratory Animal Center of South China Agricultural University (Guangzhou, China), approval number 2022C16.

CONFLICT OF INTERESTS

The authors declare no conflict of interests.

DATA AVAILABILITY

All sequencing data have been deposited in GenBank under BioProject accession number PRJNA885955.

SUPPORTING INFORMATION

Additional Supporting Information for this article can be found online at https://doi.org/10.1002/mlf2.12086.

ORCID

Jian Sun http://orcid.org/0000-0002-4209-7555

REFERENCES

1 Meatherall BL, Gregson D, Ross T, Pitout JDD, Laupland KB. Incidence, risk factors, and outcomes of *Klebsiella pneumoniae* bacteremia. *Am J Med*. 2009;122:866–73.

2 Liu YM, Li BB, Zhang YY, Zhang W, Shen H, Li H, et al. Clinical and molecular characteristics of emerging hypervirulent *Klebsiella pneumoniae* bloodstream infections in mainland China. *Antimicrob Agents Chemother*. 2014;58:5379–85.

3 Gu D, Dong N, Zheng Z, Lin D, Huang M, Wang L, et al. A fatal outbreak of ST11 carbapenem-resistant hypervirulent *Klebsiella pneumoniae* in a Chinese hospital: a molecular epidemiological study. *Lancet Infect Dis*. 2018;18:37–46.

4 Lee CR, Lee JH, Park KS, Jeon JH, Kim YB, Cha CJ, et al. Antimicrobial resistance of hypervirulent *Klebsiella pneumoniae*: epidemiology, hypervirulence-associated determinants, and resistance mechanisms. *Front Cell Infect Microbiol*. 2017;7:483.

5 Shon AS, Bajwa RPS, Russo TA. Hypervirulent (hypermucoviscous) *Klebsiella pneumoniae*: a new and dangerous breed. *Virulence*. 2013;4:107–18.

6 Zhang R, Liu L, Zhou H, Chan EW, Li J, Fang Y, et al. Nationwide surveillance of clinical carbapenem-resistant *Enterobacteriaceae* (CRE) strains in China. *EBioMedicine*. 2017;19:98–106.

7 Dong N, Sun Q, Huang Y, Shu L, Ye L, Zhang R, et al. Evolution of carbapenem-resistant serotype K1 hypervirulent *Klebsiella pneumoniae* by acquisition of $bla_{(VIM-1)}$-bearing plasmid. *Antimicrob Agents Chemother*. 2019;63:01056-19.

8 Dong N, Lin D, Zhang R, Chan EW, Chen S. Carriage of bla_{KPC-2} by a virulence plasmid in hypervirulent *Klebsiella pneumoniae*. *J Antimicrob Chemoth*. 2018;73:3317–21.

9 Du P, Zhang Y, Chen C. Emergence of carbapenem-resistant hypervirulent *Klebsiella pneumoniae*. *Lancet Infect Dis*. 2018;18:23–4.

10 Wong MHY, Shum HP, Chen JHK, Man MY, Wu A, Chan EWC, et al. Emergence of carbapenem-resistant hypervirulent *Klebsiella pneumoniae*. *Lancet Infect Dis*. 2018;18:24.

11 Shen D, Ma G, Li C, Jia X, Qin C, Yang T, et al. Emergence of a multidrug-resistant hypervirulent *Klebsiella pneumoniae* sequence type 23 strain with a rare $bla_{(CTX-M-24)}$-harboring virulence plasmid. *Antimicrob Agents Chemother*. 2019;63:e02273-18.

12 Yang X, Wai-Chi Chan E, Zhang R, Chen S. A conjugative plasmid that augments virulence in *Klebsiella pneumoniae*. *Nat Microbiol*. 2019;4:2039–43.

13 Xie M, Lin D, Chen K, Chan EWC, Yao W, Chen S. Molecular characterization of *Escherichia coli* strains isolated from retail meat that harbor bla_{CTX-M} and *fosA3* genes. *Antimicrob Agents Chemother*. 2016;60:2450–5.

14 Casella T, Nogueira MCL, Saras E, Haenni M, Madec JY. High prevalence of ESBLs in retail chicken meat despite reduced use of antimicrobials in chicken production, France. *Int J Food Microbiol*. 2017;257:271–5.

15 Hayashi W, Ohsaki Y, Taniguchi Y, Koide S, Kawamura K, Suzuki M, et al. High prevalence of blaCTX-M-14 among genetically diverse *Escherichia coli* recovered from retail raw chicken meat portions in Japan. *Int J Food Microbiol*. 2018;284:98–104.

16 Zhang Q, Lv L, Huang X, Huang Y, Zhuang Z, Lu J, et al. Rapid increase in carbapenemase-producing *Enterobacteriaceae* in retail meat driven by the spread of the $bla_{(NDM-5)}$-carrying IncX3 plasmid in China from 2016 to 2018. *Antimicrob Agents Chemother*. 2019;63:e00573-19.

17 Buchholz U, Bernard H, Werber D, Böhmer MM, Remschmidt C, Wilking H, et al. German outbreak of *Escherichia coli* O104:H4 associated with sprouts. *N Engl J Med*. 2011;365:1763–70.

18 Dong N, Liu L, Zhang R, Chen K, Xie M, Chan EWC, et al. An IncR plasmid harbored by a hypervirulent carbapenem-resistant *Klebsiella pneumoniae* strain possesses five tandem repeats of the $bla_{(KPC-2)::NTE(KPC)-Id}$ fragment. *Antimicrob Agents Chemother*. 2019;63:e01775-18.

19 Osbelt L, Wende M, Almási É, Derksen E, Muthukumarasamy U, Lesker TR, et al. *Klebsiella oxytoca* causes colonization resistance against multidrug-resistant *K. pneumoniae* in the gut via cooperative carbohydrate competition. *Cell Host Microbe*. 2021;2911:1663–79.

20 Yang X, Dong N, Chan EWC, Zhang R, Chen S. Carbapenem resistance-encoding and virulence-encoding conjugative plasmids in *Klebsiella pneumoniae*. *TIM*. 2021;29:65–83.

21 Zhao Q, Feng Y, Zong Z. Conjugation of a hybrid plasmid encoding hypervirulence and carbapenem resistance in *Klebsiella pneumoniae* of sequence type 592. *Front Microbiol*. 2022;13:852596.

22 Liu BT, Zhang XY, Wan SW, Hao JJ, Jiang RD, Song FJ. Characteristics of carbapenem-resistant *Enterobacteriaceae* in ready-to-eat vegetables in China. *Front Microbiol*. 2018;9:1147.

23 Xu Y, Zhang J, Wang M, Liu M, Liu G, Qu H, et al. Mobilization of the nonconjugative virulence plasmid from hypervirulent *Klebsiella pneumoniae*. *Genome Med*. 2021;13:119.

24 Xie M, Chen K, Ye L, Yang X, Xu Q, Yang C, et al. Conjugation of virulence plasmid in clinical *Klebsiella pneumoniae* strains through formation of a fusion plasmid. *Adv Biosyst*. 2020;4:1900239.

25 Lam MMC, Wyres KL, Wick RR, Judd LM, Fostervold A, Holt KE, et al. Convergence of virulence and MDR in a single plasmid vector in MDR *Klebsiella pneumoniae* ST15. *J Antimicrob Chemother*. 2019;74:1218–22.

26 Turton J, Davies F, Turton J, Perry C, Payne Z, Pike R. Hybrid resistance and virulence plasmids in "High-Risk" clones of *Klebsiella pneumoniae*, including those carrying $bla_{(NDM-5)}$. *Microorganisms*. 2019;7:326.

27 Li R, Cheng J, Dong H, Li L, Liu W, Zhang C, et al. Emergence of a novel conjugative hybrid virulence multidrug-resistant plasmid in extensively drug-resistant *Klebsiella pneumoniae* ST15. *Int J Antimicro Ag*. 2020;55:105952.

28 de Toro M, Garcilláon-Barcia MP, De La Cruz F. Plasmid diversity and adaptation analyzed by massive sequencing of *Escherichia coli* plasmids. *Microbiol Spectrum*. 2014;2:31.

29 Liebert CA, Hall RM, Summers AO. Transposon Tn*21*, flagship of the floating genome. *Microbiol Mol Biol Rev*. 1999;63:507–22.

30 Sherburne CK. The complete DNA sequence and analysis of R27, a large IncHI plasmid from *Salmonella typhi* that is temperature sensitive for transfer. *Nucleic Acids Res*. 2000;28:2177–86.

31 Russo TA, Olson R, Fang CT, Stoesser N, Miller M, MacDonald U, et al. Identification of biomarkers for differentiation of hypervirulent *Klebsiella pneumoniae* from classical *K. pneumoniae*. *J Clin Microbiol*. 2018;56:e00776-18.

32 Yang X, Dong N, Liu X, Yang C, Ye L, Chan EWC, et al. Co-conjugation of virulence plasmid and KPC plasmid in a clinical *Klebsiella pneumoniae* strain. *Front Microbiol*. 2021;12:739461.

33 Gautom RK. Rapid pulsed-field gel electrophoresis protocol for typing of *Escherichia coli* O157:H7 and other gram-negative organisms in 1 day. *J Clin Microbiol*. 1997;35:2977–80.

2770100x, 2023, 3, Downloaded from https://onlinelibrary.wiley.com/doi/10.1002/mlf2.12086 by South China Agricultural, Wiley Online Library on [06/10/2023]. See the Terms and Conditions (https://onlinelibrary.wiley.com/terms-and-conditions) on Wiley Online Library for rules of use; OA articles are governed by the applicable Creative Commons License

34 Bankevich A, Nurk S, Antipov D, Gurevich AA, Dvorkin M, Kulikov AS, et al. SPAdes: a new genome assembly algorithm and its applications to single-cell sequencing. *J Comput Biol*. 2012;19:455–77.

35 Alikhan NF, Petty NK, Ben Zakour NL, Beatson SA. BLAST ring image generator (BRIG): simple prokaryote genome comparisons. *BMC Genomics*. 2011;12:402.

36 Sullivan MJ, Petty NK, Beatson SA. Easyfig: a genome comparison visualizer. *Bioinformatics*. 2011;27:1009–10.

37 Neil K, Allard N, Grenier F, Burrus V, Rodrigue S. Highly efficient gene transfer in the mouse gut microbiota is enabled by the Incl(2) conjugative plasmid TP114. *Commun Biol*. 2020;3:523.

38 de Bruijn FJ. Use of repetitive (repetitive extragenic palindromic and enterobacterial repetitive intergeneric consensus) sequences and the polymerase chain reaction to fingerprint the genomes of *Rhizobium meliloti* isolates and other soil bacteria. *Appl Environ Microbiol*. 1992;58:2180–7.

39 Gama JA, Zilhão R, Dionisio F. Conjugation efficiency depends on intra and intercellular interactions between distinct plasmids: plasmids promote the immigration of other plasmids but repress co-colonizing plasmids. *Plasmid*. 2017;93:6–16.

40 Hall JPJ, Wright RCT, Harrison E, Muddiman KJ, Wood AJ, Paterson S, et al. Plasmid fitness costs are caused by specific genetic conflicts enabling resolution by compensatory mutation. *PLoS Biol*. 2021; 19:e3001225.

41 McLaughlin MM, Advincula MR, Malczynski M, Barajas G, Qi C, Scheetz MH. Quantifying the clinical virulence of *Klebsiella pneumoniae* producing carbapenemase *Klebsiella pneumoniae* with a *Galleria mellonella* model and a pilot study to translate to patient outcomes. *BMC Infect Dis*. 2014;14:31.

42 Bohnhoff M, Drake BL, Miller CP. Effect of streptomycin on susceptibility of intestinal tract to experimental *Salmonella* infection. *Exp Biol Med*. 1954;86:132–7.

How to cite this article: Li G, Jia L, Wan L, Xia L, Gao A, Yang R, et al. Acquisition of a novel conjugative multidrug-resistant hypervirulent plasmid leads to hypervirulence in clinical carbapenem-resistant *Klebsiella pneumoniae* strains. *mLife*. 2023;2:317–327. https://doi.org/10.1002/mlf2.12086

© 2023 The Authors. *mLife* published by John Wiley & Sons Australia, Ltd. on behalf of Institute of Microbiology, Chinese Academy of Sciences.

2770100x, 2023, 3, Downloaded from https://onlinelibrary.wiley.com/doi/10.1002/mlf2.12086 by South China Agricultural, Wiley Online Library on [06/10/2023]. See the Terms and Conditions (https://onlinelibrary.wiley.com/terms-and-conditions) on Wiley Online Library for rules of use; OA articles are governed by the applicable Creative Commons License

Microbiology Spectrum

| Microbial Pathogenesis | Research Article

Mechanisms of gastrointestinal toxicity in neuromyelitis optica spectrum disorder patients treated with mycophenolate mofetil: insights from a mouse model and human study

Gong Li,[1,2,3] Li-Juan Xia,[1,3] Ya-Qing Shu,[4] Lei Wan,[1,3] Qiao Huang,[5] Xiao-Yu Ma,[4] Hai-Yi Zhang,[1,3] Zi-Jian Zheng,[1,3] Xi-Ran Wang,[1,3] Shi-Ying Zhou,[1,3] Ang Gao,[1,3] Hao Ren,[1,3] Xin-Lei Lian,[1,3] Dan Xu,[1,3] Sheng-Qiu Tang,[2] Xiao-Ping Liao,[1,3] Wei Qiu,[4] Jian Sun[1,3]

AUTHOR AFFILIATIONS See affiliation list on p. 13.

ABSTRACT Mycophenolate mofetil (MMF) is commonly utilized for the treatment of neuromyelitis optica spectrum disorders (NMOSD). However, a subset of patients experience significant gastrointestinal (GI) adverse effects following MMF administration. The present study aims to elucidate the underlying mechanisms of MMF-induced GI toxicity in NMOSD. Utilizing a vancomycin-treated mouse model, we compiled a comprehensive data set to investigate the microbiome and metabolome in the GI tract to elucidate the mechanisms of MMF GI toxicity. Furthermore, we enrolled 17 female NMOSD patients receiving MMF, who were stratified into non-diarrhea NMOSD and diarrhea NMOSD (DNM) groups, in addition to 12 healthy controls. The gut microbiota of stool samples was analyzed using 16S rRNA gene sequencing. Vancomycin administration prevented weight loss and tissue injury caused by MMF, affecting colon metabolomes and microbiomes. Bacterial β-glucuronidase from Bacteroidetes and Firmicutes was linked to intestinal tissue damage. The DNM group showed higher alpha diversity and increased levels of Firmicutes and Proteobacteria. The β-glucuronidase produced by Firmicutes may be important in causing gastrointestinal side effects from MMF in NMOSD treatment, providing useful information for future research on MMF.

IMPORTANCE Neuromyelitis optica spectrum disorder (NMOSD) patients frequently endure severe consequences like paralysis and blindness. Mycophenolate mofetil (MMF) effectively addresses these issues, but its usage is hindered by gastrointestinal (GI) complications. Through uncovering the intricate interplay among MMF, gut microbiota, and metabolic pathways, this study identifies specific gut bacteria responsible for metabolizing MMF into a potentially harmful form, thus contributing to GI side effects. These findings not only deepen our comprehension of MMF toxicity but also propose potential strategies, such as inhibiting these bacteria, to mitigate these adverse effects. This insight holds broader implications for minimizing complications in NMOSD patients undergoing MMF therapy.

KEYWORDS neuromyelitis optica spectrum disorders, mycophenolate mofetil, gastrointestinal toxicity, multi-omics, colitis

Neuromyelitis optica spectrum disorder (NMOSD) is a central nervous system autoimmune disease characterized by inflammation affecting the optic nerve and spinal cord either concurrently or sequentially (1, 2). NMOSD can lead to paralysis, blindness, and potentially respiratory failure (3). Mycophenolate mofetil (MMF) is a commonly utilized immunosuppressant that has demonstrated efficacy in treating NMOSD. However, the use of MMF is often hindered by significant gastrointestinal (GI) side effects, thereby limiting its high-dose and long-term administration (4). Enhanced

Editor Jinxin Liu, Nanjing Agricultural University, Nanjing, China

Address correspondence to Wei Qiu, qiuwei@mail.sysu.edu.cn, or Jian Sun, jiansun@scau.edu.cn.

Gong Li, Li-Juan Xia, and Ya-Qing Shu contributed equally to this article. The order of authors was determined by the alphabetical order of their first name.

The authors declare no conflict of interest.

Received 28 December 2023
Accepted 28 May 2024
Published 25 June 2024

Copyright © 2024 Li et al. This is an open-access article distributed under the terms of the Creative Commons Attribution 4.0 International license.

Downloaded from https://journals.asm.org/journal/spectrum on 25 June 2024 by 125.88.24.103.

comprehension of the pathogenesis of GI toxicity associated with MMF could potentially pave the way for novel therapeutic approaches and more efficacious interventions.

MMF is an orally administered prodrug of mycophenolic acid (MPA) known for its efficacy as a reversible, non-competitive inhibitor of inosine monophosphate dehydrogenase within the purine synthesis pathway (5). Its therapeutic benefits primarily stem from its selective inhibition of T- and B-lymphocyte proliferation. The GI toxicity associated with MMF is multifaceted and has been extensively studied using various methodologies, including molecular (6), cellular (7, 8), and whole-animal (5, 9) approaches, in an effort to elucidate the comprehensive disease networks implicated in MMF-induced toxicity. Specifically, research has indicated that the gut microbiota may influence MMF metabolism through the activity of gut bacterial β-glucuronidase (BGUS), which can counteract hepatic glucuronidation, a crucial pathway for xenobiotic elimination. While these studies have yielded valuable findings, the precise mechanisms underlying MMF toxicity in patients with NMOSD remain to be elucidated.

The utilization of sequencing technologies in the fields of medicine and biology has produced data across various levels, encompassing transcriptome, microbiome, and metabolome, collectively constituting a "multi-omics" strategy (10). Recent researchers have shown that the integration of omics data sets can result in a more thorough comprehension of intestinal diseases. For example, a comprehensive examination of gut microbiota and whole transcriptome profiling data utilizing the dextran sodium sulfate/azoxymethane mouse model of inflammatory colorectal cancer indicated enhancements in sphingolipid signaling and the anti-inflammatory lipoarabinomannan biosynthetic pathway (11). Mars et al. identified subset-specific mechanisms associated with irritable bowel syndrome through the analysis of metagenomic and metabolomic data (12). Therefore, multi-omic investigations enable the elucidation of disease mechanisms.

The primary objective of this study was to investigate the mechanism of MMF GI toxicity in NMOSD utilizing a multi-omics approach. Initially, an MMF-induced colitis mouse model was established, followed by the collection of a multi-omic data set through microbiome and metabolome analyses comparing mice with and without colitis. This data set was then utilized to elucidate the associations between metabolite abundance and microbial abundance. The gut microbiomes of NMOSD patients receiving MMF treatment were subsequently analyzed to investigate a potential association between gut microbiomes and MMF-induced gastrointestinal toxicity. These studies collectively offer a comprehensive understanding of the dysregulated signaling pathways involved in MMF-induced GI toxicity and highlight a promising therapeutic strategy for its management.

MATERIALS AND METHODS

Strains, chemicals, reagents, and deposited data

The strains, chemicals, and reagents utilized in this study are detailed in Table S1. *Escherichia coli* strains were cultivated under aerobic conditions at 37°C in Luria–Bertani (LB) broth or on LB agar. Anaerobic culturing was exclusively conducted on brain–heart infusion agar or broth as described by Li et al. (13).

Animal experiments

Female C57BL/6 mice, aged 6 weeks, were subjected to animal experiments conducted at the laboratory animal center of South China Agricultural University in Guangzhou, China. The animals were maintained in accordance with the guidelines for the Care and Use of Laboratory Animals. The mouse feed was enriched with MMF at a concentration of 0.563% (wt/wt), and mouse sampling was conducted in accordance with established protocols (5).

Downloaded from https://journals.asm.org/journal/spectrum on 25 June 2024 by 125.88.24.103.

Histology of mouse tissue

Mice were utilized as the providers of livers, spleens, colon, and cecum, which were subsequently fixed in 4% paraformaldehyde for a period of 24 hours. Subsequently, the organs were embedded in paraffin longitudinally. The tissues were sliced into longitudinal sections measuring 4 µm in thickness, which were then subjected to histological examination through staining with hematoxylin and eosin (H&E).

Metabolome profiling

The extraction of metabolites, liquid chromatography with tandem mass spectrometry (LC-MS/MS) analysis, data processing, and statistical analysis were conducted according to the methods described by Liu et al. (14) and carried out by Biotree, Shanghai, China. In brief, metabolites present in colon content were analyzed using LC-MS/MS with a 0.3 annotation cutoff. A total of 8,332 peaks were identified, with 372 metabolites remaining after de-noising based on the standard deviation in control colon content samples. The final data set included peak numbers, sample names, and normalized peak areas, which were then imported into the SIMCA 15.0.2 software for further analysis. The data underwent scaling and logarithmic transformation, following the previously described methods (15).

Microbiome 16S rRNA gene sequencing, alignment, and analysis

Microbial DNA was extracted from fecal samples of patients with NMOSD using the E.Z.N.A. Stool DNA Kit (Omega Bio-tek, Norcross, GA, USA) in accordance with the manufacturer's protocol. The V3-V4 DNA region was amplified by PCR using the 338F_806R primer set. The PCR amplicons were purified according to the manufacturer's instructions after extraction from a 2% agarose gel (Axygen Biosciences, Union City, CA, USA). Paired-end sequencing was conducted on an Illumina MiSeq platform, and sequencing, alignment, and analysis were performed by Microeco Tech (Shenzhen, China).

MALDI-TOF MS^{BGUS} assay

The matrix-assisted laser desorption ionization time-of-flight mass spectrometry (MALDI-TOF MS)^{BGUS} assays were conducted with slight modifications to the established protocol (16, 17). Bacterial cultures were standardized to a uniform concentration, resuspended in 0.9% NaCl solution with MPAG at a final concentration of 100 µg/mL, and incubated at 37°C for 4 hours. Subsequently, the samples were centrifuged at 4,000 × *g* for 5 minutes, and the resulting supernatants were applied onto MSP 384 target polished steel plates (Shimadzu, Kyoto, Japan) and air-dried at room temperature. Following this, 1 µL of the matrix [α-cyano-4-hydroxycinnamic acid (HCCA), Sigma-Aldrich, St. Louis, MO, USA] was applied and allowed to dry at room temperature for 10 minutes. The internal calibration standard for the mass spectrometer was the HCCA polymer ($[2M + H]^+$, m/z 379). Mass spectra were collected utilizing a Shimadzu performance mass spectrometer and Shimadzu Biotech MALDI-MS software in positive linear ion mode within the range of 200–900 Da. The parameters set are as follows: ion source 1, 20 kV; ion source 2, 2.62 kV; lens, 6 kV; pulsed ion extraction, 114 ns; electronic gain, enhanced; mode, low range; mass range selection, 300–800 Da; laser frequency, 50 Hz; digitizer trigger level, 2,500 mV; laser attenuator, 25%; laser range, 40%. Seven hundred fifty shots were acquired per position for each spectrum. Peak ratios for MPA($[M + Na]^+$) at m/z 343 ± 1.0 and MPAG($[M + Na]^+$) at m/z 519 ± 1.0 were used to assess BGUS activity (18).

The *ex vivo* procedure utilized in this study involved the utilization of freshly collected fecal pellets from mice and live gut bacteria obtained through mechanical homogenization of extracted intestinal segments, as detailed in a previous study (19). The assays included the incorporation of 4% (vol/vol) live gut bacteria, which were subsequently subjected to anaerobic incubation with 100 µM vancomycin (VAN) using microbiome profile (MiPro) media to simulate an *in vivo* microbial environment (13). The control

Downloaded from https://journals.asm.org/journal/spectrum on 25 June 2024 by 125.88.24.103.

group received double-distilled water as the vehicle control. The specimens underwent a 20-hour incubation period, followed by centrifugation of the cultured gut microbiome samples at 4,000 × *g* for 1 minute. Subsequently, the samples were washed twice with 0.9% NaCl solution and resuspended in 90 µL of the same solution. Following this, 10 µL of MPAG at a concentration of 100 µg/mL was introduced to the gut microbiome samples and incubated for an additional hour. Following centrifugation at 4,000 × *g* for 5 minutes, the supernatants were subsequently removed, and 1 µL of the samples was utilized for MALDI-TOF MS analysis. All experiments were conducted using three independent bacterial cultures.

Cell culture and experimental design

The murine colon cancer cell lines (MC38) were cultured in culture flasks at 37°C with 5% CO_2 and 95% humidity in dulbecco's modified eagle medium (DMEM) supplemented with 10% fetal bovine serum (FBS) and 1% penicillin/streptomycin, following standard methods outlined by Qasim et al. (20). MC38 cells were established and treated with MPA at concentrations of 5, 10, and 50 µM, or DMSO (control), for 72 hours. Subsequently, real-time PCR, Western blot, and immunofluorescence experiments were conducted.

Expression analysis

Total RNAs were extracted from MC38 cells in each experimental group utilizing the Trizol method as outlined in a previous study (20). Subsequently, 1 µg of RNA from each group was reverse-transcribed into cDNA for gene expression analysis via real-time PCR. The housekeeping gene GADPH was chosen as the internal reference. Data analysis was conducted using the comparative Ct method, with primer sequences provided in Table S2.

Western blot

Whole-cell lysates were prepared from each group using protein lysis buffer, and the protein concentration was quantified using a bicinchoninic acid kit. Subsequently, 20 µg of protein sample was subjected to electrophoresis on a 10% sodium dodecyl sulfate-polyacrylamide gel. Following the transfer of the samples onto a polyvinylidene difluoride membrane (Millipore), they were blocked with 5% skim milk in 1× Tris-buffered saline with Tween for 1 hour at room temperature. Subsequently, the membranes were exposed to monoclonal rabbit anti-mouse antibodies (GAPDH, 1:2,000; CLDN2, 1:1,000) overnight at 4°C, followed by incubation with horseradish peroxidase (HRP) -conjugated secondary antibody (1:5,000) for 1 hour. The signals were visualized using an ECL chemiluminescent kit.

Immunofluorescence assay

MC38 cells were evenly distributed in 24-well plates and exposed to either MPA or DMSO for a period of 72 hours. Subsequently, the cells were fixed in a freshly prepared solution of 4% paraformaldehyde in phosphate buffered saline (PBS) for a duration of 15 minutes. Following permeabilization with 0.5% Triton X-100 in PBS for 15 minutes and blocking with 10% goat serum at 37°C for 1 hour, the sections were subjected to overnight incubation with primary antibody (CLDN2, 1:200) at 4°C. After rinsing with PBS, the sections underwent a 30-minute incubation with a 488-conjugated secondary antibody at room temperature. The results were then examined using laser scanning confocal microscopy (Leica, TCS SP8).

Patient enrollment

A total of 17 female patients diagnosed with NMOSD and receiving MMF therapy (0.5 g MMF orally, twice a day for long-term therapy) at the Third Affiliated Hospital of Sun Yat-sen University in Guangzhou, China, were included in this study. The primary

Downloaded from https://journals.asm.org/journal/spectrum on 25 June 2024 by 125.88.24.103.

inclusion criteria encompassed the following: (i) a clinical diagnosis of NMOSD based on clinical characteristics as outlined by Kalari et al. (21), (ii) patients aged between 30 and 70 years, and (iii) an Expanded Disability Status Scale (EDSS) score not exceeding 8.0. Patients meeting any of the subsequent exclusion criteria were not considered: (i) recent administration of antibiotics or probiotics within the preceding 3 months; (ii) emergency treatment, such as plasmapheresis or intravenous methylprednisolone, for acute recurrence within the previous month; and (iii) concurrent presence of diabetes mellitus, systemic autoimmune diseases, or other neurological disorders.

Stool samples were obtained from female participants (n = 12) in both the NMOSD patient and healthy control groups. Clinical data, including follow-up time, relapses, EDSS score, and the presence of diarrhea symptoms, were collected. Subsequently, the 17 individuals were categorized into two groups: the diarrhea NMOSD (DNM) group, characterized by patients with diarrhea symptoms and elevated EDSS scores, and the non-diarrhea NMOSD (NM) group, consisting of patients without diarrhea symptoms.

Statistical analysis

Statistical analysis and graphing were conducted using unpaired Student's t-test or Mann–Whitney U test. Significant differences among three or more groups were assessed using one-way ANOVA with Bonferroni's multiple comparisons test (Prism 8.0, GraphPad Software Inc., San Diego, CA, USA). Compounds with variable importance in projection values greater than 1.0 and two-tailed Student's t-test P-values less than 0 were considered statistically significant. Statistical significance was defined as $^{*}P < 0.05$, $^{**}P < 0.01$, and $^{***}P < 0.001$.

RESULTS

Vancomycin effectively prevented GI toxicity associated with MMF

The gut microbiota has been implicated in the development of inflammatory processes in the gastrointestinal tract (11, 22). In this investigation, a bacterial disruption mouse model was employed by administering vancomycin through drinking water (Fig. 1A). It was observed that the body weights of mice in the MMF group significantly decreased compared to the control group, with this effect not observed when vancomycin was pre-administered with MMF (VM group) ($P < 0.0001$) (Fig. 1B). The weights of the heart, liver, spleen, and kidney in mice from the MMF group exhibited a significant decrease when compared to those in the control group ($P < 0.05$). Vancomycin demonstrated a significant preventive effect on these symptoms ($P < 0.05$; Fig. S1). Additionally, vancomycin significantly mitigated the colonic shortening observed in colitis-induced mice treated with MMF ($P < 0.0001$) (Fig. 1C).

The examination of liver and spleen tissue histopathology in control and MMF-treated mice did not show any notable abnormalities (Fig. S2). However, MMF treatment resulted in significant disruption of cecal and colon tissue architecture, characterized by mucosal and submucosal erosion, loss of intestinal crypt structure, and extensive infiltration of inflammatory cells. Co-administration of vancomycin with MMF prevented this tissue damage in the VM group (Fig. 1D). Control mice treated with vancomycin alone did not exhibit significant differences in body weights, cecum and colon tissue destruction, and organ weights compared to untreated control mice. These findings indicate the potential importance of vancomycin in mitigating GI toxicity induced by MMF.

Vancomycin significantly modified the metabolomic profile of the colon in mice treated with MMF

In order to investigate the disparities in metabolic profiles between the MMF and VM groups, we conducted a thorough analysis of colon content samples through metabolomic profiling. Our findings revealed distinct clustering of colon metabolite content among the control, MMF, and VM groups through principal component analysis (PCA).

Downloaded from https://journals.asm.org/journal/spectrum on 25 June 2024 by 125.88.24.103.

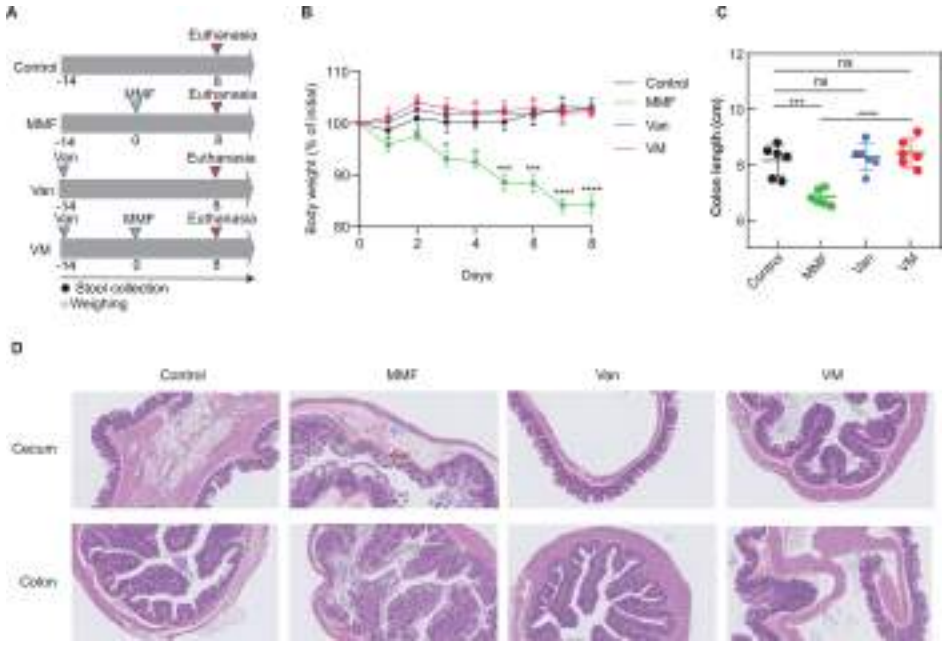


FIG 1 Vancomycin effectively prevented GI toxicity associated with MMF. (A) The experimental setup utilized in the MMF mouse model included the administration of MMF, VAN, and a combination of VAN and MMF (VM). (B) Mouse body weights. (C) Colon length. (D) Representative cecum and colon tissues were stained with H&E at 100× magnification for the specified groups. Mild edema in the submucosa was indicated by blue arrows, while inflammatory cell infiltration in tissues was indicated by red arrows. Data are presented as the mean ± standard deviation (n = 6 mice per group). Statistical significance was denoted as $^{*}P < 0.05$, $^{**}P < 0.01$, $^{***}P < 0.001$, and $^{****}P < 0.0001$.

The results suggest that all samples fell within the 95% confidence interval based on Hotelling's *T*-squared ellipse analysis (Fig. 2A).

Ten metabolic pathways were found to be significantly altered by MMF treatment based on their impact scores. These pathways included linoleic acid metabolism (1.000); methane metabolism (0.400); glycine, serine, and threonine metabolism (0.238); histidine metabolism (0.145); aminoacyl-tRNA biosynthesis (0.129); porphyrin and chlorophyll metabolism (0.083); vitamin B6 metabolism (0.078); arginine and proline metabolism (0.044); purine metabolism (0.043); and cysteine and methionine metabolism (0.025) as shown in Fig. 2B. Furthermore, the analysis identified 64 endogenous metabolites that exhibited significant variations in the colon content samples (Fig. 2C).

Additionally, 23 metabolic pathways demonstrated a high degree of responsiveness to gut bacterial disruption induced by vancomycin. These pathways encompassed ubiquinone and other terpenoid-quinone biosynthesis (1); D-glutamine and D-glutamate metabolism (1); linoleic acid metabolism (1); alpha-linolenic acid metabolism (1); valine, leucine, and isoleucine biosynthesis (0.667); alanine, aspartate, and glutamate metabolism (0.516); and phenylalanine, tyrosine, and tryptophan biosynthesis (0.500) (Fig. 2D). In this categorization, we have delineated 36 metabolites that exhibit differential regulation in response to the perturbation of gut microbiota, such as MPA (Fig. 2E), 4-hydroxyproline (Fig. 2F), pyridoxine (Fig. 2G), abscisic acid (Fig. 2H), α-tocopherol (Fig. 2I), and linoleic acid (Fig. 4J). After exposure to MMF on day 8, elevated levels of MPA were observed in the MMF group (61.21 ± 47.93) compared to controls (0.06 ± 0.03, $P < 0.05$). Pre-administration of vancomycin (Group VM) resulted in a reduction of MPA levels (25.37 ± 3.13, $P < 0.05$). Additionally, levels of 4-hydroxyproline, pyridoxine, abscisic acid, α-tocopherol, and linoleic acid were significantly decreased in the MMF group ($P < 0.05$) and increased in the VM group ($P < 0.01$). These findings suggest that perturbation of gut microbiota leads to changes in metabolite concentrations within the gastrointestinal tract.

Downloaded from https://journals.asm.org/journal/spectrum on 25 June 2024 by 125.88.24.103.

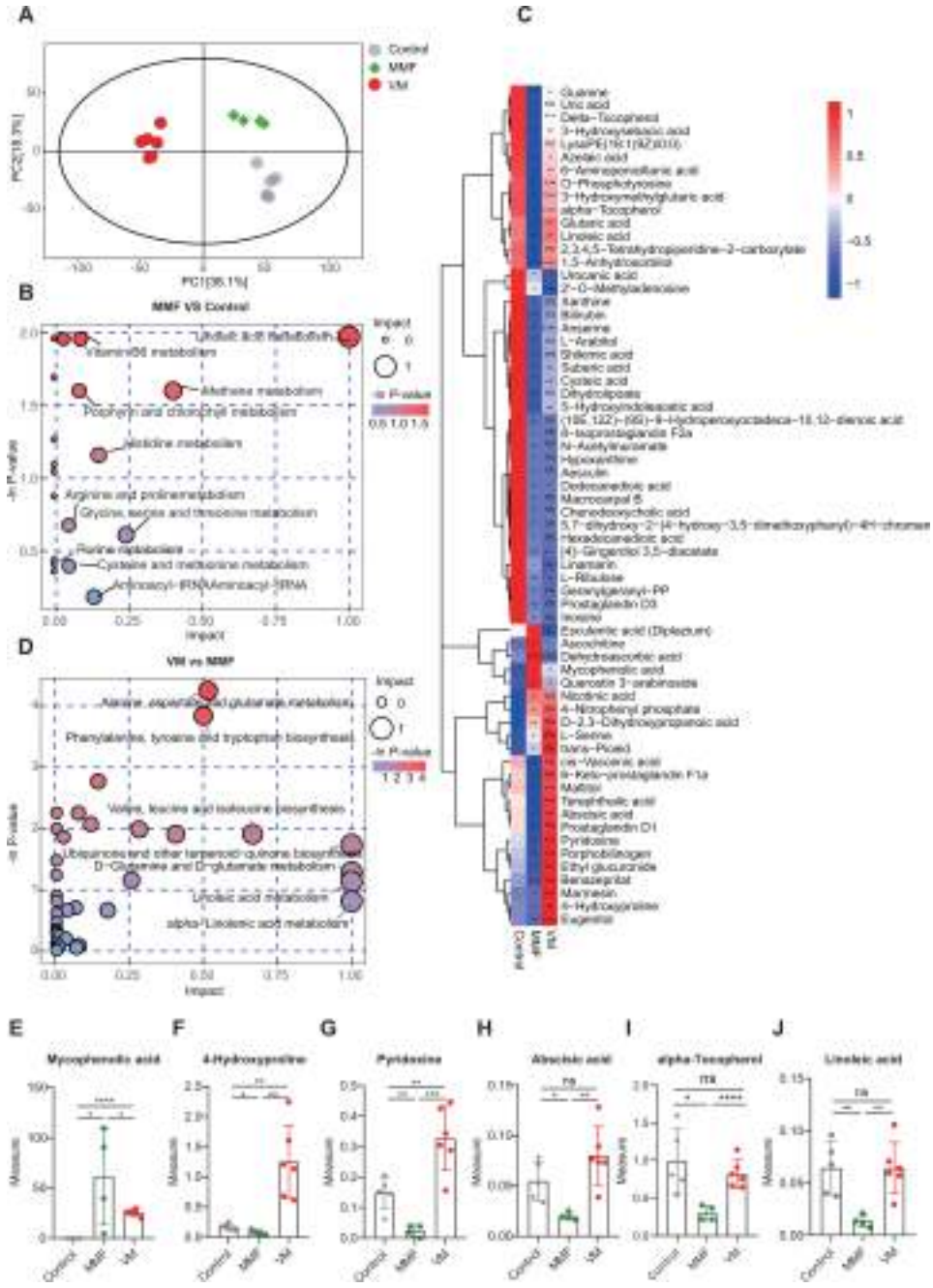


FIG 2 Vancomycin significantly modified the metabolomic profile of the colon in mice treated with MMF. (A) PCA of metabolites in the colons of the experimental mice. (B) Differential metabolic pathways between the MMF group and control mice. (C) Heatmap of the differential metabolites found in colon content samples. (D) Differential metabolic pathways between the VM versus MMF mice. The levels of specific metabolites in the colon contents of the indicated mice. (E) Mycophenolic acid, (F) 4-hydroxyproline, (G) pyridoxine, (H) abscisic acid, (I) α-tocopherol, and (J) linoleic acid. n = 4–6 mice/group. $^{*}P < 0.05$, $^{**}P < 0.01$, $^{***}P < 0.001$, and $^{****}P < 0.0001$.

Gut bacteria are required for MMF GI toxicity

The composition of gut microbiota in our experimental mice was determined through the analysis of fecal samples using the 16S rRNA gene sequencing method. The results revealed that 17 operational taxonomic units (OTUs) were present in all control, MMF-treated, and VM groups, while 129, 148, and 24 OTUs were uniquely present in each group, respectively (Fig. 3A). The alpha diversity, as measured by the Shannon index, of

Downloaded from https://journals.asm.org/journal/spectrum on 25 June 2024 by 125.88.24.103.

the MMF group was comparable to that of the control groups, whereas the VM group displayed lower alpha diversity compared to both the controls and the MMF group (Fig. 3B). Beta diversity was evaluated through PCA on unweighted UniFrac distance matrices, which indicated that the overall composition of the MMF gut microbiota closely resembled that of the control group. Conversely, the VM group led to the development of a distinct phylogenetic microbiota (Fig. 3C).

Analysis at the phylum level did not yield any notable distinctions between the MMF and control groups (Fig. 3D). Conversely, the administration of vancomycin (VM group) resulted in a reduction in the abundance of Bacteroidetes ($P < 0.05$), Firmicutes ($P < 0.01$), TM7 ($P < 0.05$), and Actinobacteria ($P < 0.01$), while facilitating the proliferation of Verrucomicrobia ($P < 0.001$) and Proteobacteria ($P < 0.01$) (Fig. 3F through J).

Significant differences were observed in the abundance of genus *Clostridium* ($P < 0.05$) between the MMF and VM, with the former showing enrichment. Additionally, the abundance of *Bacteroides* ($P < 0.001$), *Clostridium* ($P < 0.001$), and *Ruminococcus* ($P < 0.01$) was notably decreased in the VM group compared to controls. Conversely, *Akkermansia* ($P < 0.001$) and *Parabacteroides* ($P < 0.0001$) showed significant enrichment (Fig. 3K through P). These findings suggest a potential association between gut microbiota composition and MMF-induced GI toxicity.

Correlation between the microbiota and MPA after MMF treatment

The activities of BGUS have been shown to catalyze the conversion of phenyl-beta-D-glucuronide (MPAG) to MPA, as depicted in Fig. 4A, resulting in GI side effects commonly associated with MMF administration (23). Furthermore, our observations indicate that MPA upregulates the expression of the gut barrier-related *cldn2* gene and CLDN2 protein in a model using MC38 cells, as illustrated in Fig. 4A; Fig. S3A through C. BGUS enzymes possess distinctive active site structures and exhibit unique substrate processing functions, as reported in studies by Little et al. and Ervin et al. (24, 25). Therefore, we posited that only a restricted set of enzymes would have the ability to metabolize MPAG. In order to investigate the primary bacteria involved in MPA metabolism, we conducted an analysis of the associations between the microbiota and MPA at the species level.

Initially, a MALDI-TOF MS^{BGUS} method was developed using MALDI-TOF MS (Fig. 4B) for MPAG metabolism research. Peaks corresponding to MPAG ($[M + Na]^+$, 519 ± 1.0 m/z) and the metabolite MPA ($[M + Na]^+$, 343 ± 1.0 m/z) were manually identified, and their intensities were documented (Fig. S4). Furthermore, a strain overexpressing the BGUS gene (*uidA*) (*E. coli* DH10BΔ*uidA*::pZE-*uidA*) was introduced to validate the reliability of the method. The findings indicated a reduction in the peak of MPAG and a concomitant elevation in the peak of MPA in both the *E. coli* DH10B and *E. coli* DH10BΔ*uidA*::pZE-*uidA* cohorts. Within the DH10BΔ*uidA*::pZE-*uidA* cohort, the transformation of the substrate (MPAG) into the product (MPA) was complete. Conversely, no analogous occurrence was noted in the *E. coli* DH10BΔ*uidA* group. Subsequently, an *ex vivo* culture model was implemented to confirm the impact of vancomycin on BGUS activity. Our findings indicated that vancomycin decreased the MS ratio [MPA/(MPAG + MPA)] by 2.32-fold compared to the control group ($P < 0.01$, Fig. 4D), providing additional evidence that vancomycin diminishes the MPAG processing capacity of the gut microbiota. Consequently, the MALDI-TOF MS^{BGUS} assay method demonstrates a degree of reliability.

The 16S rRNA gene sequencing analysis revealed the presence of 12 species belonging to the Bacteroidetes and Firmicutes phyla in the microbiomes of mice. Subsequent investigation of these species for their ability to convert MPAG to MPA enzymatically showed that 10 strains exhibited varying degrees of MPAG metabolism (with a range of one- to ninefold increase). However, *C. perfringens* ATCC 13124 and *C. comes* ATCC 27758 were unable to perform this conversion, as illustrated in Fig. 4E. The findings suggest that the presence of Bacteroidetes and Firmicutes members plays a significant role in the toxicity of MMF through the conversion to MPA in the context of metabolic diversity within the bacterial population.

Downloaded from https://journals.asm.org/journal/spectrum on 25 June 2024 by 125.88.24.103.

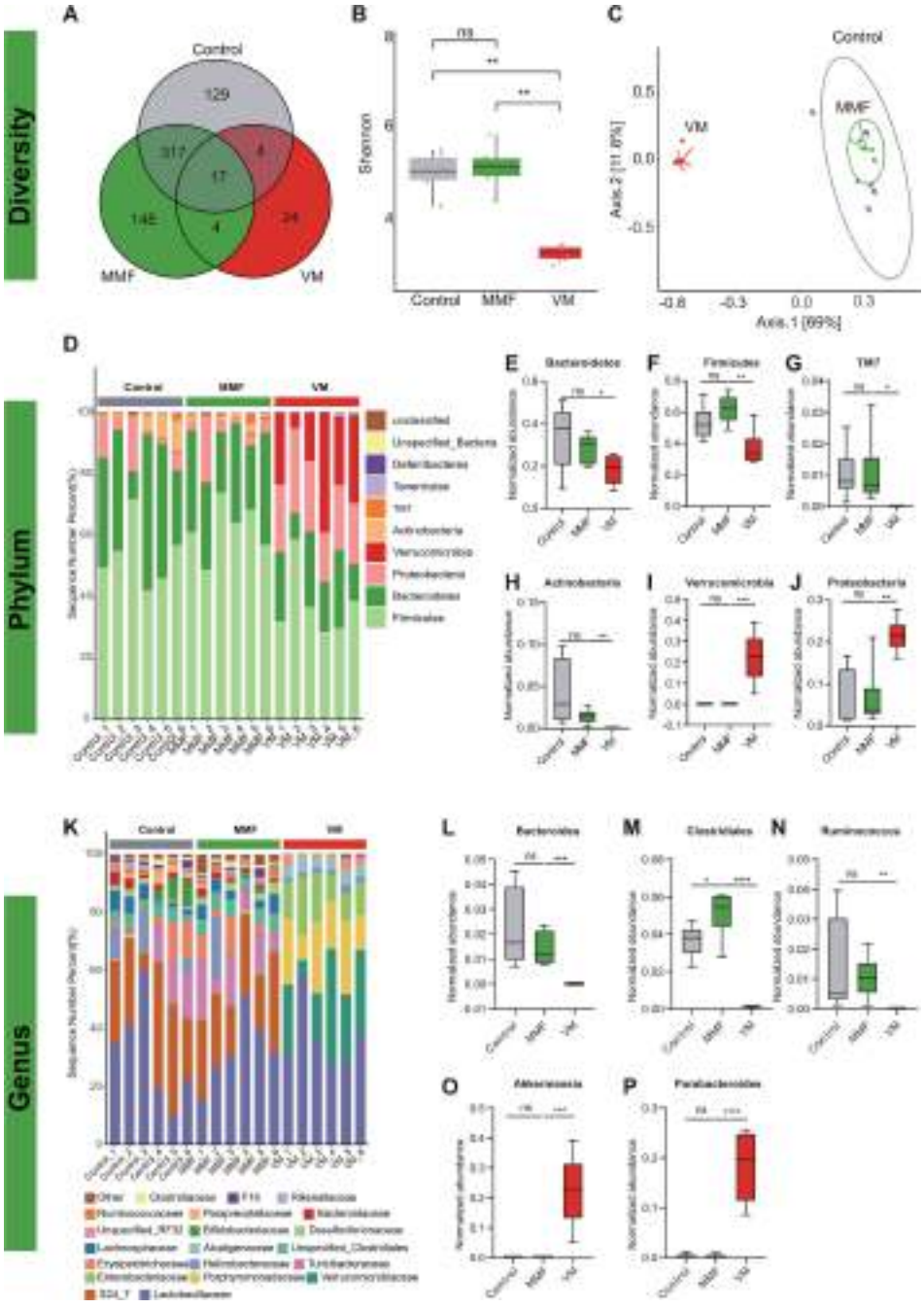


FIG 3 Gut bacteria are required for MMF GI toxicity. Bacterial taxonomic groups in feces from experimental mouse groups. (A) OTU and (B) Shannon index. (C) Unweighted UniFrac PCA of the microbial composition for all groups. (D) Phylum level composition of the gut microbiota. Relative abundance of the phyla (E) Bacteroidetes, (F) Firmicutes, (G) TM7, (H) Actinobacteria, (I) Verrucomicrobia, and (J) Proteobacteria. (K) Composition at the genus level. (L) *Bacteroides*, (M) *Clostridiales*, (N) *Ruminococcus*, (O) *Akkermansia,* and (P) *Parabacteroides*. $^{*}P < 0.05$, $^{**}P < 0.01$, $^{***}P < 0.001$, and $^{****}P < 0.0001$. $n = 6$ mice/group.

The gut microbiota of diarrheal NMOSD patients were structurally and compositionally altered

To investigate the potential relationship between MMF-induced diarrhea in NMOSD patients and the composition of their gut microbiota, we conducted a profiling analysis of the gut microbiota in NMOSD patients. Participants were categorized into the DNM or

Downloaded from https://journals.asm.org/journal/spectrum on 25 June 2024 by 125.88.24.103.

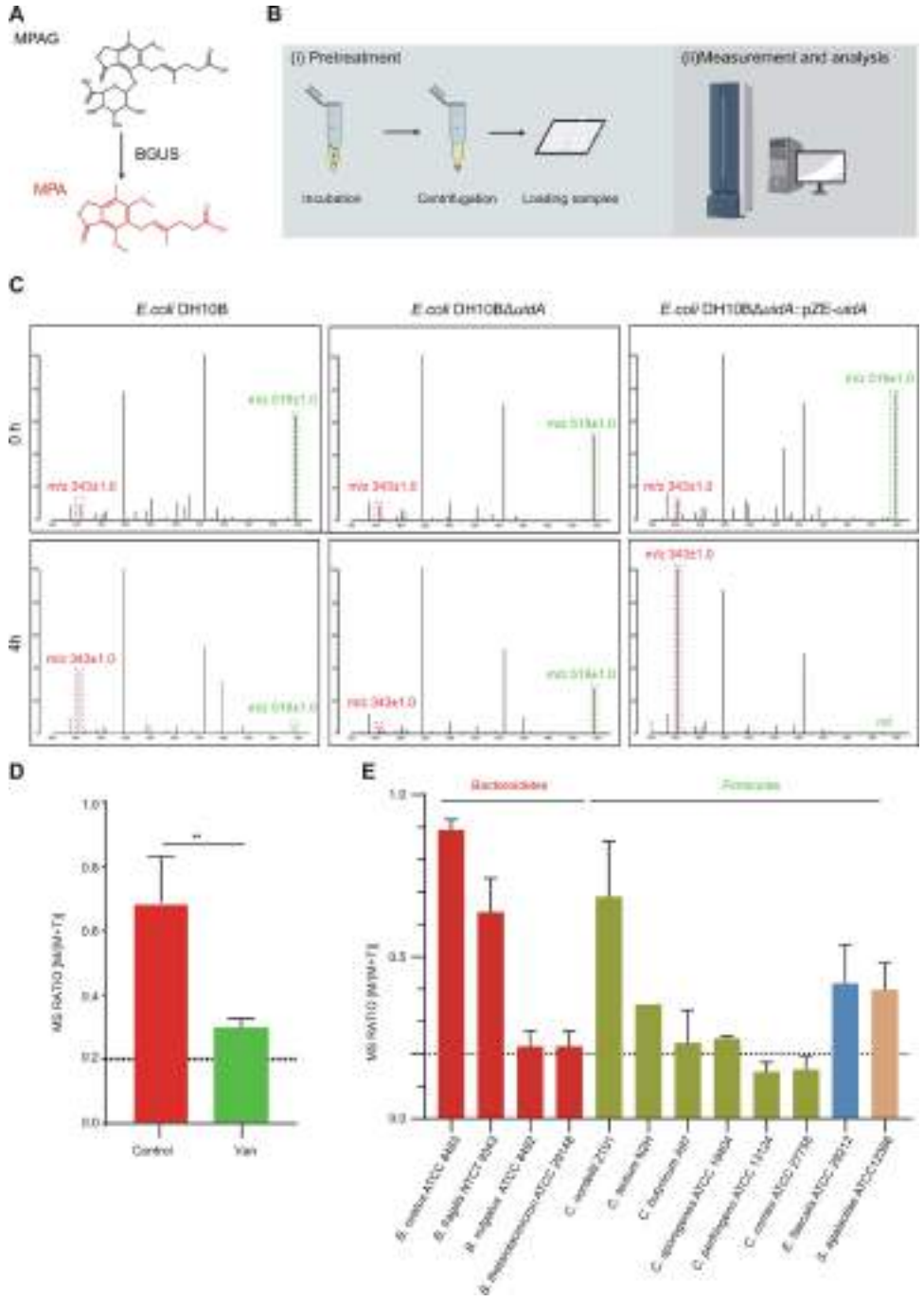


FIG 4 Correlation between the microbiota and MPA after MMF treatment. (A) MPAG metabolism by BGUS. (B) Experimental flow of the MALDI-TOF MS^{BGUS} assay. (C) Representative MALDI-TOF MS spectra of MALDI-TOF MS^{BGUS} assays after 4-hour incubation with DH10B, DH10BΔ*uidA*, and DH10BΔ*uidA*::pZE-*uidA*, respectively. Peaks of MPA (343 ± 1.0 m/z) are indicated by dashed red lines, while peaks of MPAG (519 ± 1.0 m/z) are denoted by dashed green lines. (D) Effects of vancomycin on MPAG processing in an *ex vivo* model. (E) Comparison of MPAG metabolism abilities among different Bacteroidetes and Firmicutes species. $^{**}P < 0.01$.

NM groups based on their responses to MMF treatment and were compared to a healthy control group (HC) to assess the potential impact of gut microbiota on diarrhea in NMOSD patients receiving MMF treatment (Fig. 5A).

Downloaded from https://journals.asm.org/journal/spectrum on 25 June 2024 by 125.88.24.103.

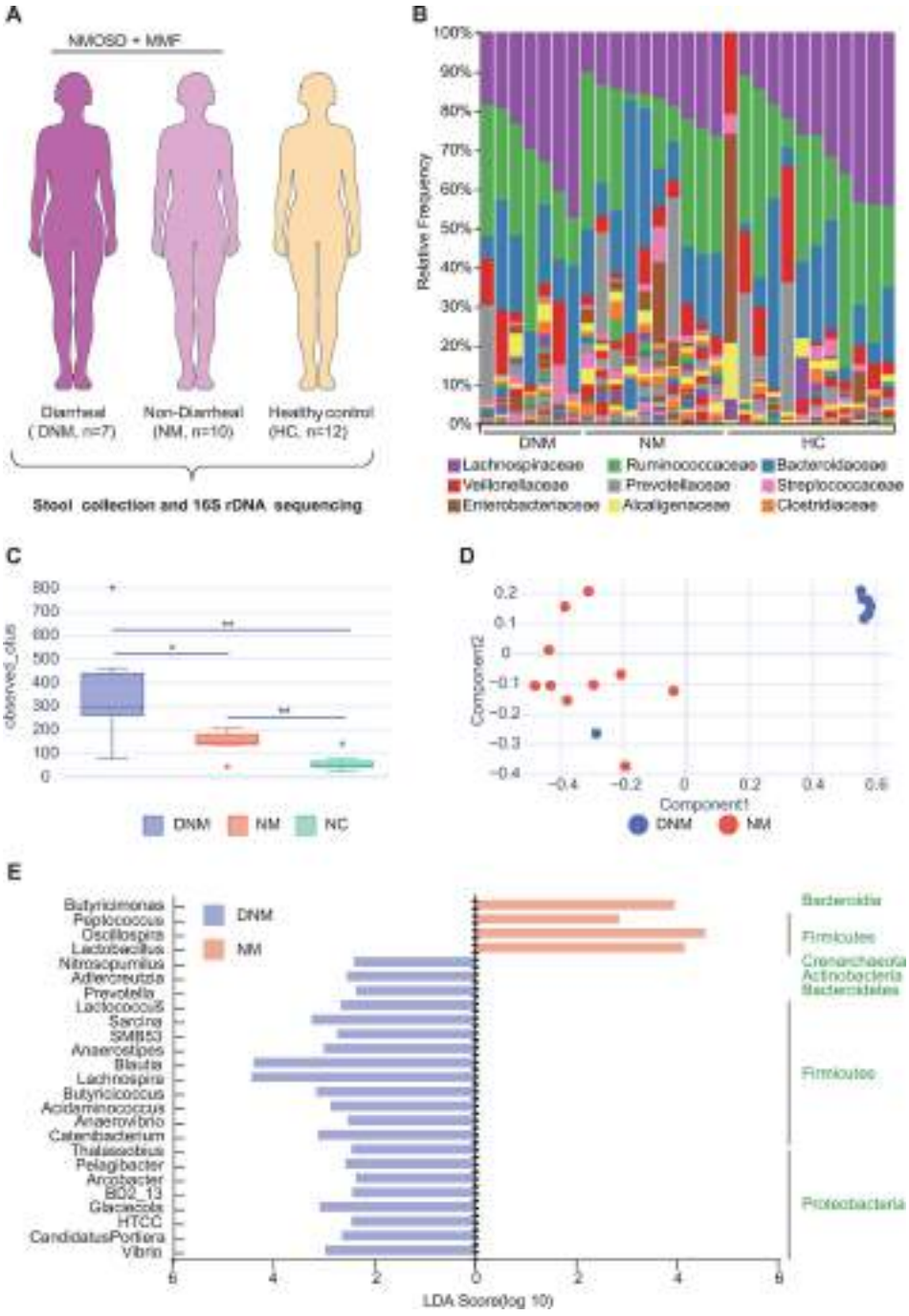


FIG 5 The gut microbiota of diarrheal NMOSD patients were structurally and compositionally altered. (A) The study cohort. (B) Composition of the gut microbiome from fecal samples at the family level between NMOSD and HCs. (C) OTUs observed in the groups. (D) Non-metric multidimensional scaling (NMDS) profile of gut microbial diversity. (E) LEfSe analysis showing taxa associated with DNM and NM patients. $n = 7$ for DNM group. $n = 10$ for NM group and $n = 12$ for HC group. $^{*}P < 0.05$. $^{**}P < 0.01$.

The microbial composition was assessed through genus-level unsupervised hierarchical OTU clustering, revealing notable distinctions between DNM and NM patients (Fig. 5B). Analysis of microbial alpha diversity, as determined by observed OTUs, indicated significantly higher diversity in the DNM group compared to both the NM ($P < 0.05$) and HC ($P < 0.01$) groups (Fig. 5C). Beta diversity was assessed using NMDS based on Jaccard metrics. The study revealed notable variations in the gut microbial community of MMF-treated NMOSD patients with and without diarrhea, as evidenced by phylogenetic

Downloaded from https://journals.asm.org/journal/spectrum on 25 June 2024 by 125.88.24.103.

tree-based distances (Fig. 5D). Subsequent analysis at the taxonomic level, using linear discriminant analysis effect size (LEfSe) , identified 21 genera with significant differences in abundance between the two groups. Specifically, *Lachnospira* and *Blautia* were found to be increased in patients with diarrhea, while *Butyricimonas*, *Peptococcus*, *Oscillospira*, and *Lactobacillus* showed decreased levels (Fig. 5D). The primary bacterial phyla observed in DNM samples were Firmicutes and Proteobacteria, as shown in Fig. 5E. These results collectively suggest that there was an increase in alpha diversity, along with a higher abundance of Firmicutes, Proteobacteria, and Bacteroidetes in the DNM group compared to the NM group. Overall, these findings indicate that the gut microbiota's structure and composition may play a role in influencing the intestinal toxicity of MMF.

DISCUSSION

MMF has been recognized as a potent immunosuppressant commonly employed in the management of NMOSD and various other medical conditions, yet its therapeutic efficacy is hindered by GI toxicity (26, 27). Existing literature suggests that the GI toxicity of MMF may be attributed to an exaggerated inflammatory reaction and dysbiosis of the gut microbiota, although the precise underlying mechanisms remain elusive (5, 28).

In our previous study, we observed a male-to-female ratio of approximately 1:10 among NMOSD patients in Asian countries, indicating a notably higher prevalence of NMOSD in females compared to males (29). Given the significant impact of gender on gut microbiota composition (30), our study focused on analyzing the gut microbiota of females and utilized female mice as the experimental model. In contrast to our research, Flannigan et al. conducted a study utilizing a male C57BL/6 mouse model and determined that the gut microbiota significantly contributes to MMF toxicity. Hence, this phenomenon should remain consistent regardless of the gender of the mice. The administration of MMF resulted in significant colitis characterized by weight loss, colon shortening, and colonic tissue damage in mice. Notably, treatment with vancomycin mitigated these effects, consistent with previous research findings, thereby implicating the gut microbiome in mediating MMF-induced toxicity (5).

The dextran sulfate sodium-induced colitis model has yielded valuable insights into the metabolic aspects of the gut microbiome disorder (31, 32), whereas the establishment of an MMF-induced colitis model has been less extensive. In our study, we employed non-targeted metabolomics to identify notable variations in gut metabolites resulting from MMF administration, which were found to be modifiable with vancomycin treatment. Specifically, vancomycin was observed to significantly decrease MPA levels while increasing the levels of 4-hydroxyproline, pyridoxine, abscisic acid, α-tocopherol, and linoleic acid in the intestinal environment. A significant amount of research has established a connection between these compounds and the mitigation of colitis (33). For example, patients with ulcerative colitis and Crohn's disease exhibit notably lower levels of linolenic acid compared to non-inflamed individuals and control subjects (34). These findings align with our MMF-induced colitis model, indicating that the levels of these five distinct metabolites can be influenced by vancomycin treatment, suggesting a correlation with the microbiome.

The microbiome data indicated comparable composition and abundance between the MMF and control groups, with the VM group exhibiting lower Shannon and PCA indices. Specifically, vancomycin administration resulted in decreased abundance of Bacteroides and Clostridiales, which are prominent genera within the gut microenvironment (35). The BGUS activity can catalyze the conversion of the MPA glucuronidated derivative MPAG to release the parent compound MPA within the GI tract (5). MALDI-TOF MS is considered to be a convenient, efficient, expeditious, consistent, and easily obtainable tool in microbiology laboratories when contrasted with alternative mass spectrometry techniques that are combined with gas or liquid chromatography (36, 37). In a prior investigation, a MALDI-Tet(X)-plus method was devised to promptly and dependably identify Tet(X)-producing Gram-negative bacteria (17, 38). Hence, a MALDI-TOF MS^{BGUS} method was developed to investigate the conversion of MPAG to

Downloaded from https://journals.asm.org/journal/spectrum on 25 June 2024 by 125.88.24.103.

MPA by BGUS enzymes expressed in Bacteroidetes and Firmicutes. This study represents the first direct confirmation of MPAG metabolism by various bacterial species using MALDI-TOF MS. Additionally, a significantly higher microbial richness and diversity were observed in DNM patients compared to NM and HC subjects, suggesting increased BGUS activity in DNM patients. These findings may contribute to elevated MPA levels in the gastrointestinal tract.

The findings of this study offer compelling evidence that bacteria within the Bacteroidetes and Firmicutes phyla, capable of producing BGUS, are able to convert MPAG to MPA, leading to disruptions in intestinal homeostasis and reductions in levels of various metabolites. This process contributes to GI toxicity in patients with NMOSD. Inhibiting BGUS activity using natural and synthetic small molecules has been shown to alleviate GI toxicity induced by irinotecan (CPT11) (39–41). Therefore, the use of BGUS inhibitors may have potential applications in preventing GI toxicity associated with MMF treatment. However, our study was constrained by the need for further experimental validation of BGUS activity in patients with DNM and NM. Additionally, it would be beneficial to include a comparative analysis of the transcriptional levels of the BGUS gene across various species to enhance the credibility of our findings.

Conclusions

In conclusion, our study demonstrates that the BGUS produced by Bacteroidetes and Firmicutes are capable of metabolizing MPAG into MPA, leading to disturbances in gut homeostasis and contributing to GI toxicity in patients with NMOSD. By conducting a thorough examination of the gut microbiota and intestinal metabolites, we have deduced this interaction and observed similar findings in a mouse model of MMF toxicity. Targeting the inhibition of BGUS may represent a promising strategy for preventing MMF-induced GI toxicity.

ACKNOWLEDGMENTS

We thank Hangzhou Zhongmei Huadong Pharmaceutical for their help with grant support.

This work was supported by the Foundation for Innovative Research Groups of the National Natural Science Foundation of China (32121004), Local Innovative and Research Teams Project of Guangdong Pearl River Talents Program (2019BT02N054), Guangdong Major Project of Basic and Applied Basic Research (2020B0301030007), Laboratory of Lingnan Modern Agriculture Project (NT2021006), 111 Center (D20008), China Postdoctoral Science Foundation (2023M741221), and Double First-Class Discipline Promotion Project (2023B10564003).

J.S. and W.Q. contributed to the conception and design drafting of the work. G.L., L.J.X., Y.Q-S., L.W., Q.H., X.Y.M., H.Y.Z., Z.J.Z., S.Y.Z., and A.G. contributed to the acquisition of data. G.L., L.J.X., X.R.W., X.L.L., and D.X. contributed to the analysis of data. S.Q.T., X.P.L., and Y.H.L. supervised the project. G.L. wrote the manuscript. H.R., W.Q., and J.S. revised the manuscript. All authors read and approved the final manuscript.

AUTHOR AFFILIATIONS

[1]Lingnan Guangdong Laboratory of Modern Agriculture, National Risk Assessment Laboratory for Antimicrobial Resistance of Animal Original Bacteria, South China Agricultural University, Guangzhou, China
[2]Guangdong Provincial Key Laboratory of Utilization and Conservation of Food and Medicinal Resources in Northern Region, Henry Fok School of Biology and Agriculture, Shaoguan University, Shaoguan, China
[3]Guangdong Provincial Key Laboratory of Veterinary Pharmaceutics Development and Safety Evaluation, South China Agricultural University, Guangzhou, China
[4]Department of Neurology, The Third Affiliated Hospital of Sun Yat-sen University, Guangzhou, China

Downloaded from https://journals.asm.org/journal/spectrum on 25 June 2024 by 125.88.24.103.

[5]Department of Neurology, Zhaoqing No. 2 People's Hospital, Zhaoqing, China

AUTHOR ORCIDs

Li-Juan Xia http://orcid.org/0009-0001-4449-1943
Xiao-Ping Liao https://orcid.org/0000-0002-4654-5837
Wei Qiu http://orcid.org/0000-0002-0880-958X
Jian Sun http://orcid.org/0000-0002-4209-7555

DATA AVAILABILITY

The raw sequence data from the fecal microbiota in this paper were uploaded to the Sequence Read Archive (SRA) data (https://www.ncbi.nlm.nih.gov/sra) under accession number PRJNA976489. The original serum metabolite data were also deposited in the MetaboLights database under accession number MTBLS4392.

ETHICS APPROVAL

The study was approved by the Ethics Committee of the Third Affiliated Hospital of Sun Yat-sen University ([2020]02-016-01), and all patients signed informed consent. Animal experimentation was approved by the Ethics Committee of the laboratory animal center of South China Agricultural University (Guangzhou, China), approval number 2020B041.

ADDITIONAL FILES

The following material is available online.

Supplemental Material

Supplemental material (Spectrum04307-23-s0001.docx). Fig. S1 to S4; Tables S1 and S2.

REFERENCES

1. Borisow N, Mori M, Kuwabara S, Scheel M, Paul F. 2018. Diagnosis and treatment of NMO spectrum disorder and MOG-encephalomyelitis. Front Neurol 9:888. https://doi.org/10.3389/fneur.2018.00888
2. Poupart J, Giovannelli J, Deschamps R, Audoin B, Ciron J, Maillart E, Papeix C, Collongues N, Bourre B, Cohen M, Wiertlewski S, Outteryck O, Laplaud D, Vukusic S, Marignier R, Zephir H, NOMADMUS study group. 2020. Evaluation of efficacy and tolerability of first-line therapies in NMOSD. Neurology 94:e1645–e1656. https://doi.org/10.1212/WNL.0000000000009245
3. Sellner J, Boggild M, Clanet M, Hintzen RQ, Illes Z, Montalban X, Du Pasquier RA, Polman CH, Sorensen PS, Hemmer B. 2010. EFNS guidelines on diagnosis and management of neuromyelitis optica. Eur J Neurol 17:1019–1032. https://doi.org/10.1111/j.1468-1331.2010.03066.x
4. Huang Q, Wang J, Zhou Y, Yang H, Wang Z, Yan Z, Long Y, Yin J, Feng H, Li C, Lu Z, Hu X, Qiu W. 2018. Low-dose mycophenolate mofetil for treatment of neuromyelitis optica spectrum disorders: a prospective multicenter study in South China. Front Immunol 9:2066. https://doi.org/10.3389/fimmu.2018.02066
5. Taylor MR, Flannigan KL, Rahim H, Mohamud A, Lewis IA, Hirota SA, Greenway SC. 2019. Vancomycin relieves mycophenolate mofetil-induced gastrointestinal toxicity by eliminating gut bacterial β-glucuronidase activity. Sci Adv 5:eaax2358. https://doi.org/10.1126/sciadv.aax2358
6. Ohmann EL, Burckart GJ, Brooks MM, Chen Y, Pravica V, Girnita DM, Zeevi A, Webber SA. 2010. Genetic polymorphisms influence mycophenolate mofetil-related adverse events in pediatric heart transplant patients. J Heart Lung Transplant 29:509–516. https://doi.org/10.1016/j.healun.2009.11.602
7. Khan N, Binder L, Pantakani DVK, Asif AR. 2017. MPA modulates tight junctions' permeability via Midkine/PI3K pathway in Caco-2 cells: a possible mechanism of leak-flux diarrhea in organ transplanted patients. Front Physiol 8:438. https://doi.org/10.3389/fphys.2017.00438
8. Heischmann S, Christians U. 2018. Validation of the cell line LS180 as a model for study of the gastrointestinal toxicity of mycophenolic acid. Xenobiotica 48:433–441. https://doi.org/10.1080/00498254.2017.1329567
9. Flannigan KL, Taylor MR, Pereira SK, Rodriguez-Arguello J, Moffat AW, Alston L, Wang X, Poon KK, Beck PL, Rioux KP, Jonnalagadda M, Chelikani PK, Galipeau HJ, Lewis IA, Workentine ML, Greenway SC, Hirota SA. 2018. An intact microbiota is required for the gastrointestinal toxicity of the immunosuppressant mycophenolate mofetil. J Heart Lung Transplant 37:1047–1059. https://doi.org/10.1016/j.healun.2018.05.002
10. Subramanian I, Verma S, Kumar S, Jere A, Anamika K. 2020. Multi-omics data integration, interpretation, and its application. Bioinform Biol Insights 14:1177932219899051. https://doi.org/10.1177/-1177932219899051
11. Sakai K, De Velasco MA, Kura Y, Nishio K. 2021. Transcriptome profiling and metagenomic analysis help to elucidate interactions in an inflammation-associated cancer mouse model. Cancers (Basel) 13:3683. https://doi.org/10.3390/cancers13153683
12. Mars RAT, Yang Y, Ward T, Houtti M, Priya S, Lekatz HR, Tang X, Sun Z, Kalari KR, Korem T, et al. 2020. Longitudinal multi-omics reveals subset-specific mechanisms underlying irritable bowel syndrome. Cell 182:1460–1473. https://doi.org/10.1016/j.cell.2020.08.007
13. Li L, Abou-Samra E, Ning Z, Zhang X, Mayne J, Wang J, Cheng K, Walker K, Stintzi A, Figeys D. 2019. An *in vitro* model maintaining taxon-specific functional activities of the gut microbiome. Nat Commun 10:4146. https://doi.org/10.1038/s41467-019-12087-8
14. Liu Q, Li B, Li Y, Wei Y, Huang B, Liang J, You Z, Li Y, Qian Q, Wang R, Zhang J, Chen R, Lyu Z, Chen Y, Shi M, Xiao X, Wang Q, Miao Q, Fang J-Y,

Downloaded from https://journals.asm.org/journal/spectrum on 25 June 2024 by 125.88.24.103.

Gershwin ME, Lian M, Ma X, Tang R. 2022. Altered faecal microbiome and metabolome in IgG4-related sclerosing cholangitis and primary sclerosing cholangitis. Gut 71:899–909. https://doi.org/10.1136/gutjnl-2020-323565
15. Zhou L, Wang D, Zhou H. 2021. Metabolic profiling of two medicinal piper species. S Afr J Bot 139:281–289. https://doi.org/10.1016/j.sajb.2021.03.007
16. Sugimoto Y, Camacho FR, Wang S, Chankhamjon P, Odabas A, Biswas A, Jeffrey PD, Donia MS. 2019. A metagenomic strategy for harnessing the chemical repertoire of the human microbiome. Science 366:eaax9176. https://doi.org/10.1126/science.aax9176
17. Zheng ZJ, Cui ZH, Diao QY, Ye XQ, Zhong ZX, Tang T, Wu SB, He HL, Lian XL, Fang LX, Wang XR, Liang LJ, Liu YH, Liao XP, Sun J. 2022. MALDI-TOF MS for rapid detection and differentiation between Tet(X)-producers and non-Tet(X)-producing tetracycline-resistant Gram-negative bacteria. Virulence 13:77–88. https://doi.org/10.1080/21505594.2021.2018768
18. Dortet L, Tandé D, de Briel D, Bernabeu S, Lasserre C, Gregorowicz G, Jousset AB, Naas T. 2018. MALDI-TOF for the rapid detection of carbapenemase-producing Enterobacteriaceae: comparison of the commercialized MBT STAR-Carba IVD Kit with two in-house MALDI-TOF techniques and the RAPIDEC CARBA NP. J Antimicrob Chemother 73:2352–2359. https://doi.org/10.1093/jac/dky209
19. Ronda C, Chen SP, Cabral V, Yaung SJ, Wang HH. 2019. Metagenomic engineering of the mammalian gut microbiome *in situ*. Nat Methods 16:167–170. https://doi.org/10.1038/s41592-018-0301-y
20. Qasim M, Rahman H, Ahmed R, Oellerich M, Asif AR. 2014. Mycophenolic acid mediated disruption of the intestinal epithelial tight junctions. Exp Cell Res 322:277–289. https://doi.org/10.1016/j.yexcr.2014.01.021
21. Kalari KR, Nair AA, Bhavsar JD, O'Brien DR, Davila JI, Bockol MA, Nie J, Tang X, Baheti S, Doughty JB, Middha S, Sicotte H, Thompson AE, Asmann YW, Kocher J-PA. 2014. MAP-RSeq: Mayo Analysis Pipeline for RNA sequencing. BMC Bioinformatics 15:224. https://doi.org/10.1186/1471-2105-15-224
22. Yue S-J, Qin Y-F, Kang A, Tao H-J, Zhou G-S, Chen Y-Y, Jiang J-Q, Tang Y-P, Duan J-A. 2021. Total flavonoids of glycyrrhiza uralensis alleviates irinotecan-induced colitis via modification of gut microbiota and fecal metabolism. Front Immunol 12:628358. https://doi.org/10.3389/fimmu.2021.628358
23. Kodawara T, Masuda S, Yano Y, Matsubara K, Nakamura T, Masada M. 2014. Inhibitory effect of ciprofloxacin on beta-glucuronidase-mediated deconjugation of mycophenolic acid glucuronide. Biopharm Drug Dispos 35:275–283. https://doi.org/10.1002/bdd.1894
24. Little MS, Pellock SJ, Walton WG, Tripathy A, Redinbo MR. 2018. Structural basis for the regulation of β-glucuronidase expression by human gut Enterobacteriaceae. Proc Natl Acad Sci U S A 115:E152–E161. https://doi.org/10.1073/pnas.1716241115
25. Ervin SM, Hanley RP, Lim L, Walton WG, Pearce KH, Bhatt AP, James LI, Redinbo MR. 2019. Targeting regorafenib-induced toxicity through inhibition of gut microbial β-glucuronidases. ACS Chem Biol 14:2737–2744. https://doi.org/10.1021/acschembio.9b00663
26. Kharfan-Dabaja M, Mhaskar R, Reljic T, Pidala J, Perkins JB, Djulbegovic B, Kumar A. 2014. Mycophenolate mofetil versus methotrexate for prevention of graft-versus-host disease in people receiving allogeneic hematopoietic stem cell transplantation. Cochrane Database Syst Rev 2014:CD010280. https://doi.org/10.1002/14651858.CD010280.pub2
27. Broen JCA, van Laar JM. 2020. Mycophenolate mofetil, azathioprine and tacrolimus: mechanisms in rheumatology. Nat Rev Rheumatol 16:167–178. https://doi.org/10.1038/s41584-020-0374-8
28. Bhattacharya S, Stoleru G, Patel P, Abutaleb A, Stashek K, Cross RK. 2022. Characterization of mycophenolate mofetil gastrointestinal toxicity and risk factors for severe disease and poor prognosis. Inflamm Bowel Dis 28:811–814. https://doi.org/10.1093/ibd/izab254
29. Fu Y, Bi J, Yan Y, Sun X, Li K, Kim SY, Han SM, Zhou L, Li R, Huang Q, Wang N, Lin A, Kim HJ, Qiu W. 2023. Rapid immunodot AQP4 assay for neuromyelitis optica spectrum disorder. JAMA Neurol 80:1105–1112. https://doi.org/10.1001/jamaneurol.2023.2974
30. Santos-Marcos JA, Haro C, Vega-Rojas A, Alcala-Diaz JF, Molina-Abril H, Leon-Acuña A, Lopez-Moreno J, Landa BB, Tena-Sempere M, Perez-Martinez P, Lopez-Miranda J, Perez-Jimenez F, Camargo A. 2019. Sex differences in the gut microbiota as potential determinants of gender predisposition to disease. Mol Nutr Food Res 63:e1800870. https://doi.org/10.1002/mnfr.201800870
31. Liu F, Yao Y, Lu Z, Zhang Q, Liu C, Zhu C, Lin C. 2021. 5-Hydroxy-4-methoxycanthin-6-one alleviates dextran sodium sulfate-induced colitis in rats via regulation of metabolic profiling and suppression of NF-κB/p65 signaling pathway. Phytomedicine 82:153438. https://doi.org/10.1016/j.phymed.2020.153438
32. Hong Z-S, Xie J, Wang X-F, Dai J-J, Mao J-Y, Bai Y-Y, Sheng J, Tian Y. 2022. Moringa oleifera lam peptide remodels intestinal mucosal barrier by inhibiting JAK-STAT activation and modulating gut microbiota in colitis. Front Immunol 13:924178. https://doi.org/10.3389/fimmu.2022.924178
33. Ji Y, Dai Z, Sun S, Ma X, Yang Y, Tso P, Wu G, Wu Z. 2018. Hydroxyproline attenuates dextran sulfate sodium-induced colitis in mice: involvment of the NF-κB signaling and oxidative stress. Molecular Nutrition Food Res 62. https://doi.org/10.1002/mnfr.201800494
34. Pearl DS, Masoodi M, Eiden M, Brümmer J, Gullick D, McKeever TM, Whittaker MA, Nitch-Smith H, Brown JF, Shute JK, Mills G, Calder PC, Trebble TM. 2014. Altered colonic mucosal availability of n-3 and n-6 polyunsaturated fatty acids in ulcerative colitis and the relationship to disease activity. J Crohns Colitis 8:70–79. https://doi.org/10.1016/j.crohns.2013.03.013
35. Axarlis K, Daskalaki MG, Michailidou S, Androulaki N, Tsoureki A, Mouchtaropoulou E, Kolliniati O, Lapi I, Dermitzaki E, Venihaki M, Kousoulaki K, Argiriou A, Marsni ZE, Tsatsanis C. 2021. Diet supplementation with fish-derived extracts suppresses diabetes and modulates intestinal microbiome in a murine model of diet-induced obesity. Mar Drugs 19:268. https://doi.org/10.3390/md19050268
36. Šebela M. 2022. Biomolecular profiling by MALDI-TOF mass spectrometry in food and beverage analyses. Int J Mol Sci 23:13631. https://doi.org/10.3390/ijms232113631
37. Sarvestani HK, Ramandi A, Getso MI, Razavyoon T, Javidnia J, Golrizi MB, Saboor-Yaraghi AA, Ansari S. 2022. Mass spectrometry in research laboratories and clinical diagnostic: a new era in medical mycology. Braz J Microbiol 53:689–707. https://doi.org/10.1007/s42770-022-00715-3
38. Cui CY, He Q, Jia QL, Li C, Chen C, Wu XT, Zhang XJ, Lin ZY, Zheng ZJ, Liao XP, Kreiswirth BN, Liu YH, Chen L, Sun J. 2021. Evolutionary trajectory of the Tet(X) family: critical residue changes towards high-level tigecycline resistance. mSystems 6:e00050-21. https://doi.org/10.1128/mSystems.00050-21
39. Yue B, Gao R, Lv C, Yu Z, Wang H, Geng X, Wang Z, Dou W. 2021. Berberine improves irinotecan-induced intestinal mucositis without impairing the anti-colorectal cancer efficacy of irinotecan by inhibiting bacterial beta-glucuronidase. Front Pharmacol 12:774560. https://doi.org/10.3389/fphar.2021.774560
40. Kong R, Liu T, Zhu X, Ahmad S, Williams AL, Phan AT, Zhao H, Scott JE, Yeh L-A, Wong STC. 2014. Old drug new use--amoxapine and its metabolites as potent bacterial beta-glucuronidase inhibitors for alleviating cancer drug toxicity. Clin Cancer Res 20:3521–3530. https://doi.org/10.1158/1078-0432.CCR-14-0395
41. Bhatt AP, Pellock SJ, Biernat KA, Walton WG, Wallace BD, Creekmore BC, Letertre MM, Swann JR, Wilson ID, Roques JR, Darr DB, Bailey ST, Montgomery SA, Roach JM, Azcarate-Peril MA, Sartor RB, Gharaibeh RZ, Bultman SJ, Redinbo MR. 2020. Targeted inhibition of gut bacterial beta-glucuronidase activity enhances anticancer drug efficacy. Proc Natl Acad Sci U S A 117:7374–7381. https://doi.org/10.1073/pnas.1918095117

Downloaded from https://journals.asm.org/journal/spectrum on 25 June 2024 by 125.88.24.103.

Journal of Applied Microbiology

Journal of Applied Microbiology ISSN 1364-5072

ORIGINAL ARTICLE

Linoleic acid and α-linolenic acid inhibit conjugative transfer of an IncX4 plasmid carrying *mcr-1*

G. Li[1,2], L.-J. Xia[1,2], S.-Y. Zhou[1,2], X.-R. Wang[1,2], C.-Y. Cui[1,2], Y.-Z. He[1,2], X.-Y. Diao[1,2], M. Liu[1,2], X.-L. Lian[1,2], B.N. Kreiswirth[3,4], Y.-H. Liu[1,2,5], X.-P. Liao[1,2,5], L. Chen[3,4] and J. Sun[1,2,5]

1 National Risk Assessment Laboratory for Antimicrobial Resistance of Animal Original Bacteria, South China Agricultural University, Guangzhou, China
2 Guangdong Provincial Key Laboratory of Veterinary Pharmaceutics Development and Safety Evaluation, South China Agricultural University, Guangzhou, P. R. China
3 Center for Discovery and Innovation, Hackensack Meridian Health, Nutley, NJ, USA
4 Hackensack Meridian School of Medicine, Seton Hall University, Nutley, NJ, USA
5 Lingnan Guangdong Laboratory of Modern Agriculture, Guangzhou, China

Keywords
conjugation, IncX4, *mcr-1*, unsaturated fatty acids, T4SS.

Correspondence
Jian Sun, National Risk Assessment Laboratory for Antimicrobial Resistance of Animal Original Bacteria, College of Veterinary Medicine, South China Agricultural University, Guangzhou, P. R. China.
E-mail: jiansun@scau.edu.cn.

2020/1433: received 10 July 2020, revised 19 September 2020 and accepted 1 October 2020

doi:10.1111/jam.14885

Abstract

Aims: The aim of this study was to determine the effects of unsaturated fatty acids on clinical plasmids.
Methods and Results: Two unsaturated fatty acids, linoleic acid (LA) and α-linolenic acid (ALA) at final concentration 0, 0·03, 0·3 and 3 mmol l^{-1}, respectively, were used to assess the effects on conjugative transfer of a *mcr-1*-harbouring plasmid pCSZ4 (IncX4) in conjugation experiment. The inhibitory mechanisms were analysed by molecular docking and the gene expression of *virB11* was quantitated by qRT-PCR. Target plasmid diversity was carried out by TrwD/VirB11 homology protein sequence prediction analysis. Our results showed that LA and ALA inhibit plasmid pCSZ4 transfer by binding to the amino acid residues (Phe124 and Thr125) of VirB11 with dose-dependent effects. The expression levels of *virB11* gene were also significantly inhibited by LA and ALA treatment. Protein homology analysis revealed a wide distribution of TrwD/VirB11-like genes among over 37 classes of plasmids originated from both Gram-negative and Gram-positive bacteria.
Conclusions: This study demonstrates representing a diversity of plasmids that may be potentially inhibited by unsaturated fatty acids.
Significance and Impact of the Study: Our work reported here provides additional support for application of curbing the spread of multiple plasmids by unsaturated fatty acids.

Introduction

The global spread of antibiotic resistance genes (ARG) poses a significant threat to public health (Chen *et al.* 2019; McInnes *et al.* 2020). To treat infections caused by multidrug-resistant (MDR) pathogens, focus has been shifted to the polymyxins (colistin and polymyxin B), a class of cationic polypeptide antibiotics typically reserved as the last line of defence (Sun *et al.* 2018; Zając *et al.* 2019; Tang *et al.* 2020). Unfortunately, this last-resort antibiotic has been challenged by the emergence and global spread of the plasmid-mediated mobile colistin resistance genes (e.g. *mcr-1*) (Liu *et al.* 2016; Sun *et al.* 2018).

Currently, different strains carrying *mcr-1* have been isolated (Farzana *et al.* 2019; Zhang *et al.* 2019). Furthermore, diversified plasmids can act as plasmid vectors for the dissemination of the *mcr-1* in Enterobacteriaceae. Among them, IncX4 plasmid is the most common *mcr-1*-harbouring plasmid vector, having a significantly high self-transferable frequencies (~10^{-1} to ~10^{-4})

(Matamoros *et al.* 2017). The *mcr-1*-harbouring IncX4 plasmids are widespread in various species (*Escherichia coli*, *Salmonella enterica* and *Klebsiella pneumoniae*) from different origins of human, animals and animal products, in many countries, in particular China, Denmark and United Kingdom (Sun *et al.* 2017).

Inhibiting plasmids transfer has been proposed to be an effective approach in limiting the spread of ARGs (Graf *et al.* 2019). Previous studies showed that unsaturated fatty acids can inhibit the conjugation of IncW plasmids, through the binding to the essential plasmid transfer related ATPase TrwD, which, in turn, limits the pilus biogenesis and DNA translocation (Ripoll-Rozada *et al.* 2016; Getino and de la Cruz 2018). However, previous studies have focused on some laboratory plasmids like R388 (IncW) and few studies have investigated the effects of unsaturated fatty acids on clinical plasmids, such as the *mcr-1*-harbouring IncX4 plasmids with high transfer rates. Although VirB11 traffic ATPase encoded on IncX4 plasmids was reported as the homolog of TrwD (Ripoll-Rozada *et al.* 2013), there is a paucity of experimental data to corroborate.

In this study, we examined the inhibitory effects of two unsaturated fatty acids, linoleic acid (LA, 18:2n-6) and α-linolenic acid (ALA, 18:3n-3), on the conjugative transfer of an IncX4 plasmid pCSZ4. We used molecular docking to explore the binding of unsaturated fatty acids to ATPase TrwD of IncX4 plasmid, and evaluated the effects of unsaturated fatty acids on the expression of *trwD*/*virB11* gene. Lastly, we explored the target plasmid diversity of unsaturated fatty acids based on the TrwD/VirB11 protein sequence homology detection.

Materials and methods

Bacterial strains

Donor strain *E. coli* CSZ4 was isolated from food animals in Guangdong province, China (Sun *et al.* 2017), which harbours a plasmid pCSZ4 (GenBank accession number KX711706) containing *mcr-1* gene that confers resistance to colistin. This plasmid belongs to the transferable plasmid of IncX4. The presence of IncX4 plasmid was tested by PCR using specific primers (Table 1). Streptomycin-resistant *E. coli* C600 was used as the recipient strain of conjugation experiments. Antibiotics, used for screening and selection, were added at the concentrations of 2 mg l^{-1} for colistin and 2000 mg l^{-1} for streptomycin. Linoleic acid (18:2n-6) and ALA (18:3n-3) were obtained from Shanghai Yien Chemical Technology (Shanghai, China). Dimethyl sulfoxide (DMSO) was purchased from Solarbio (Beijing, China).

Conjugation assay

Broth mating procedure of conjugation experiment was conducted according to the previous study with minor modifications (Huang *et al.* 2019). First, both donor and recipient strains were cultured to middle exponential phase at 37°C in Luria-Bertani (LB) broth, supplemented with appropriate antibiotics. Second, the cultures were washed three times with LB broth and adjusted to the same OD_{600} of ~0·5. Third, 0·495 ml of donor and recipient cultures were mixed with ratio of 1 : 1. Subsequently, 0·01 ml of LA or ALA solutions was added to the mixture to get different final concentrations of 0·03, 0·3 and 3 mmol l^{-1}, respectively. 0·01 ml DMSO was used as negative controls (0 mmol l^{-1}). Lastly, the mixtures were gently vortexed and incubated at 37°C for 4 h without shaking.

After 4 h of incubation, the cultures were mixed, diluted and plated on LB solid medium containing appropriate antibiotics. Transconjugants were selected by plates contained 2 mg l^{-1} colistin and 2000 mg l^{-1} streptomycin, while the plates for donor or recipient selection contained 2 mg l^{-1} colistin and 2000 mg l^{-1} streptomycin, respectively. In addition, donors and recipients were also plated on plates with 2 mg l^{-1} colistin and 2000 mg l^{-1} streptomycin, to rule out of possibility of spontaneous mutations. Plates were incubated at 37°C for 18–24 h and the colonies were enumerated and confirmed by PCR to examine *mcr-1* gene. Conjugation frequency was expressed as the number of transconjugants per output donor. All the experiments were conducted in triplicate.

Molecular docking analysis

The VirB11 molecular structure was generated using the *Brucella suis* VirB11 (2gza.pdb) as the template. LA and ALA structures were obtained from the ZINC database (http://zinc.docking.org) and prepared for docking. Files containing the atomic coordinate of the VirB11 model and the LA or ALA were submitted to the AutoDock 4·2 server and blind molecular docking (Ripoll-Rozada *et al.* 2016; Shen *et al.* 2018).

The mRNA expression analysis

The donor strain *E. coli* CSZ4 was inoculated separately into LB broth containing 0 or 0·3 mmol l^{-1} concentrations of LA or ALA (Qiu *et al.* 2012; Wang *et al.* 2019). After 4-h incubation, the total RNA in each system was extracted using the E.Z.N.A Bacterial RNA Kit (Omega, Norcross, GA) following the manufacturer's instructions. Next, RNA was transcribed to cDNA by reverse

Table 1 Complete list of primers used in this study

Gene	Primer	5′–3′	Product size	Reference
mcr-1	mcr1-F	GCGTGATGCCAGTTTGCTTA	672 bp	Present study
	mcr1-R	GCACATCGACGGCGTATTC		
VirB11	VirB11-F	TGATGGCATCTTTTGCCGAGG	178 bp	Present study
	VirB11-R	TCCGGCTCTATCATAACAGCAG		
X4	X4-F	AGCAAACAGGGAAAGGAGAAGACT	570 bp	Present study
	X4-R	TACCCCAAATCGTAACCTG		
16S rRNA	16S rRNA-F	CCTACGGGAGGCAGCAG	194 bp	19
	16S rRNA-R	ATTACCGCGGCTGCTGG		

transcription polymerase chain reaction (RT-PCR) using M-MLV First Strand cDNA Synthesis Kit (Omega). Real-time PCR was carried out using ChamQ Universal SYBR qPCR Master Mix (Vazyme, Nanjing, China) on a Light-Cycler® 96 instrument (Roche, Mannheim, German). The relative quantification method was used to quantify the *virB11* gene of the plasmid pCSZ4 by ΔΔCt method (Livak and Schmittgen 2001). 16S rRNA was used as an internal control to normalize total RNA yields (Qiu *et al.* 2012). Denaturation step at 95°C for 30 s, and 45 cycles of denaturation for 10 s at 95°C, primer annealing for 30 s at 58°C and extension for 30 s at 72°C. Melt curve analysis was performed in all reactions to confirm the amplification of correct product. All experiments were repeated three times as independent biological replicates.

Building of TrwD/VirB11 hidden Markov models

Sequence database homology searching is one of the most crucial applications of computational molecular biology (Eddy 2011). Particularly, probabilistic inference methods based on profile hidden Markov models (profile HMMs) HMM approaches facilitated a hierarchical classification of proteins (Feldgarden *et al.* 2019). For TrwD and VirB11 separately, homologous protein sequences were selected using BLASTP with a coverage cut-off of 90% and an identity cut-off of 50% (Lavigne *et al.* 2008). The homologous protein sequences were performed multiple sequence alignment using MUSCLE with default parameters (Edgar 2004a, 2004b). For training profile HMMs, the *hmmbuild* module as a part of HMMER3 packages was using with default parameters (Eddy 2009; Skewes-Cox *et al.* 2014).

Homologous proteins prediction of plasmid database

The TrwD profile HMMs and VirB11 profile HMMs were using against an comprehensive plasmid databases contains 10 892 complete plasmid sequences (Brooks *et al.* 2019) using *hmmsearch* function of HMMER3 with default parameters, and the plasmids sequences contain annotated homologous proteins were extracted from the database for the following plasmid typing.

Plasmid replicon typing

The TrwD/VirB11 homologous proteins carried plasmids mentioned above were typing using BLASTN against the PlasmidFinder database downloaded from Center for Genomic Epidemiology (https://cge.cbs.dtu.dk/) with an e-value cut-off at 1e-5.

Statistical analysis

Statistical analysis was performed using GraphPad Prism 8 software. All data were obtained from at least three independent experiments and presented as means ± SD. In the in vitro studies, unpaired *t* test between two groups or one-way ANOVA among multiple groups were used to calculate *P* values.

Results

Linoleic acid (LA) and α-linolenic acid efficiently inhibit conjugal transfer of plasmid pCSZ4

In this study, we tested the effects of two unsaturated fatty acids, LA and ALA, on the conjugal transfer of *mcr-1*-harbouring IncX4 plasmid pCSZ4. Compared to control group (without LA or ALA treatment), the conjugation frequency did not show significant change ($P > 0{\cdot}05$) in response to 0·03 mmol l^{-1} LA. However, when the LA concentrations increased to 0·3 and 3 mmol l^{-1}, the conjugation frequency decreased 10 ($P < 0{\cdot}05$) and 100 folds ($P < 0{\cdot}001$), respectively (Fig. 1a). Results showed a correlation between log concentration of LA and percent inhibition ($R^2 = 0{\cdot}8697$). The results indicated that LA had a dose-dependent response (from 0·03 to 3 mmol l^{-1}) on the inhibition of the conjugation transfer of plasmid pCSZ4.

We also evaluated the effects of LA on the growth of donor and recipient strains during conjugation. The

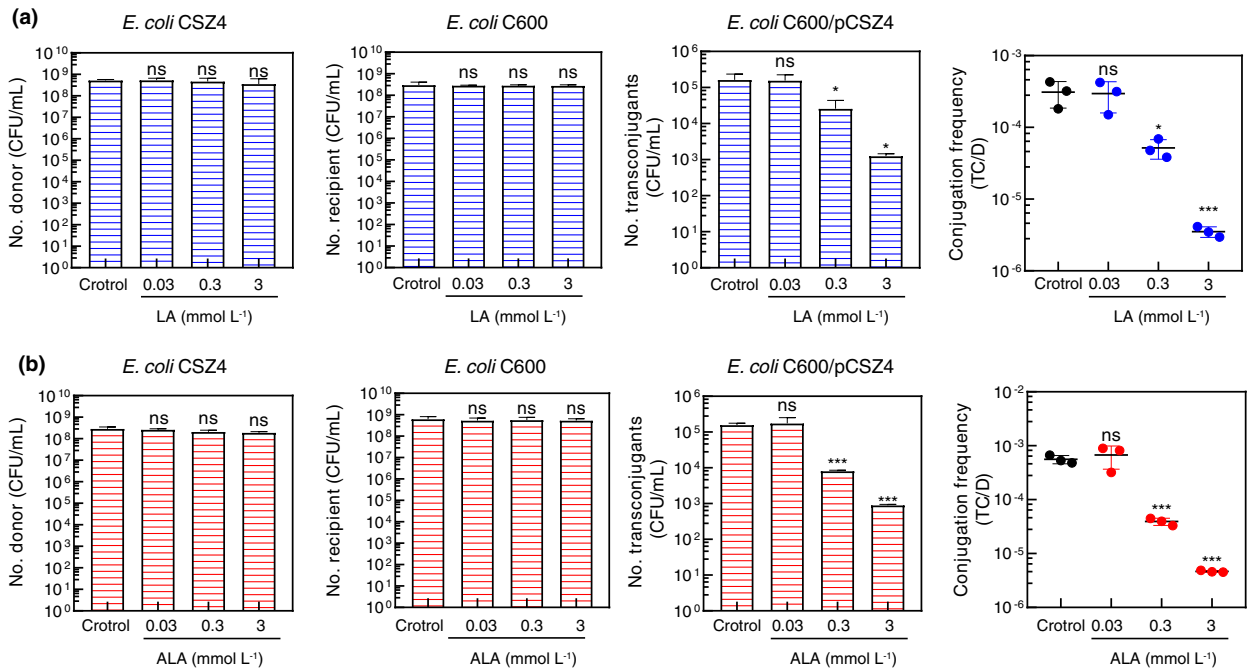


Figure 1 Effects of unsaturated fatty acids on conjugative transfer of pCSZ4 (IncX4). Effects of linoleic acid (LA, a) and α-linolenic acid (ALA, b) on donor, recipient, transconjugants numbers and the conjugation frequency. Conjugation efficiency (Tc/D) was calculated by the numbers of transconjugants (Tc)/donor numbers (D). Each point represents the result of one independent experiment. Horizontal and vertical bars represent the mean ± SD of each group (ns $P > 0{\cdot}05$; $*P < 0{\cdot}05$, $**P < 0{\cdot}01$, $***P < 0{\cdot}001$). All data were plotted using Graphpad Prism 8. [Colour figure can be viewed at wileyonlinelibrary.com]

results showed that 0·3 and 3 mmol l^{-1} LA slightly inhibited the growth of donors, but the difference was not significant ($P > 0{\cdot}05$) (Fig. 1a). The recipient was not affected by LA treatment ($P > 0{\cdot}05$). Our results indicated that the reduced conjugative transfer frequency was due to the inhibition of plasmid transfer but not because of the growth inhibition of the donor or recipient strains by LA.

α-linolenic acid was found to have the similar effects on the inhibition of plasmid pCSZ4 conjugal transfer (Fig. 1b). Results showed a correlation between log concentration of ALA and percent inhibition ($R^2 = 0{\cdot}7886$). These results indicated that two unsaturated fatty acids ALA and LA both are able to inhibit conjugal transfer of *mcr-1*-harbouring IncX4 plasmid pCSZ4.

Unsaturated fatty acids bind VirB11

To understand the binding of IncX4 plasmid VirB11 ATPases and unsaturated fatty acids, we then performed molecular docking analysis using VirB11 ATPases as receptor, LA and ALA as the ligand (Fig. 2). The bonding site of LA and ALA is a pocket composed of NTD and liner as previous report (Ripoll-Rozada *et al.* 2016). LA and ALA could form hydrogen bonds with amino acid residues (Phe124 and Thr125) and show a high affinity with VirB11 protein. These interactions are predicted to result in decreased VirB11 activity including inhibition of its ATPase activity that would compromise plasmid conjugation (Ripoll-Rozada *et al.* 2016).

Linoleic acid (LA) and α-linolenic acid inhibit transcriptional expression of *virB11* gene

Type IV traffic ATPase TrwD was found to be the molecular target of bacterial conjugation inhibit by unsaturated fatty acids (Ripoll-Rozada *et al.* 2016). We then evaluated the expressions of *virB11* gene under LA and ALA treatment. When donor was treated with 0·3 mmol l^{-1} LA or ALA, the expression of *virB11* gene was significantly inhibited by >50%, compared with the control (Fig. 3), which indicated unsaturated fatty acids inhibit conjugation not only by affecting VirB11 activity with hydrogen bond but also inhibiting transcriptional expression of *virB11* gene.

Target plasmids diversity of unsaturated fatty acids inhibition

This study and the results from the others suggested that TrwD/VirB11 may be one of the key plasmid conjugation inhibitory targets by unsaturated fatty acids

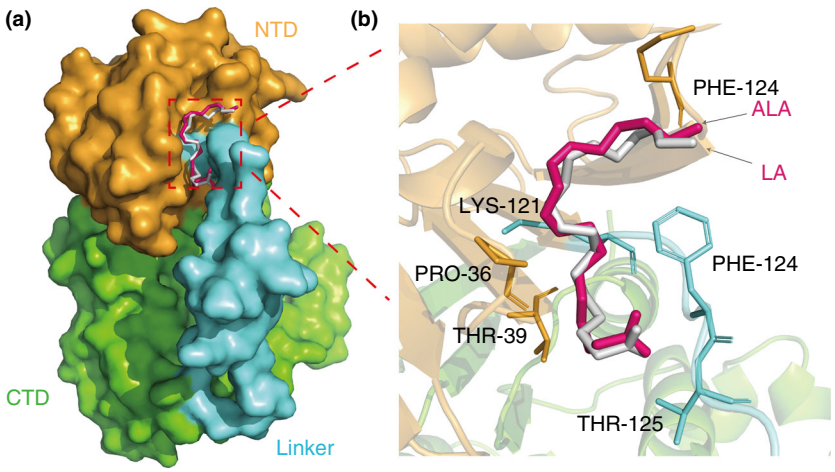


Figure 2 Blind docking of LA and ALA into the molecular model of VirB11. (a) Surface structure of VirB11 containing an LA and ALA-loaded tunnel. Blind docking predictions between a molecular model of monomeric VirB11 and LA (grey) and ALA (claret) ligands were performed using the Autodock 4·2 server. The N-terminal domain (NTD) is shown in orange and the C-terminal domain (CTD) in green connected via a blue linker. (b) An enlarged view of LA (grey) and ALA (claret) bonding cavity in VirB11. [Colour figure can be viewed at wileyonlinelibrary.com]

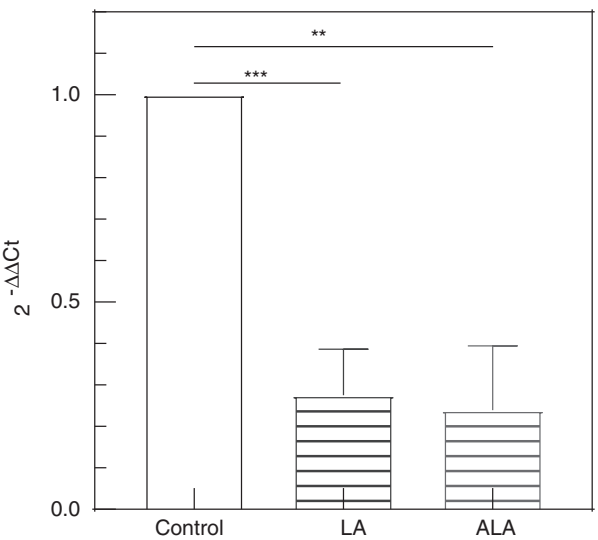


Figure 3 Effects of two unsaturated fatty acids on the mRNA expressions of *virB11* gene. Error bars represent standard error of the means. *$P < 0{\cdot}05$, **$P < 0{\cdot}01$. All data were plotted using Graphpad Prism 8. [Colour figure can be viewed at wileyonlinelibrary.com]

(Ripoll-Rozada *et al.* 2016). We then explored the distribution of TrwD/VirB11 homologous proteins among different plasmid groups to reveal the target plasmid diversity of unsaturated fatty acids inhibition.

We build TrwD/VirB11 HMMs by homologous protein sequences of TrwD and VirB11 separately, and we predicted homologous proteins of a comprehensive plasmid databases contain 10 892 complete plasmid sequences plasmid databases. The TrwD/VirB11 homologous proteins carried plasmids mentioned above were typing. Among them, in total 984 plasmid sequences (9·03%) which including 984 carried TrwD/VirB11-like protein genes as shown in Fig. 4. The typing results showed the presence of TrwD/VirB11-like protein gene sequences in 37 different plasmid groups (Fig. 4). Of these, the TrwD/VirB11-like proteins originated from Gram-negative bacteria were commonly found IncX1 (17·21%), IncX3 (11·10%), IncA/C (10·71%), IncI2 (9·95%), IncN (9·57%), IncFIB (9·31%), IncFII (9·31%), IncX4 (8·29%). IncI1 (8·04%) and IncP (4·59%) plasmid groups. In addition, TrwD/VirB11-like protein sequences were also found in some plasmid types from Gram-positive bacteria, harbouring rep12 (2·55%), rep3 (2·55%) and repUS7 (0·38%) replicons. Our study suggested the wide distribution of TrwD/VirB11-like protein genes among various plasmid sequences. The conjugation transfer of these plasmids may likewise be inhibited by unsaturated fatty acids through the interference of TrwD/VirB11 function, which deserves further studies.

Discussion

Antibiotic resistance in bacteria has been documented as a major global public health concern (Chukwu *et al.* 2019; Scheenstra *et al.* 2019). The prevalence of antibiotic resistance against conventional antibiotics is increasing dramatically and we are about to enter the post-antibiotic era (Scheenstra *et al.* 2019). The cause for this phenomenon is the rapid evolution and adaptation of bacteria to antimicrobial selection pressures, which mainly through the acquisition of AMR genes by horizontal

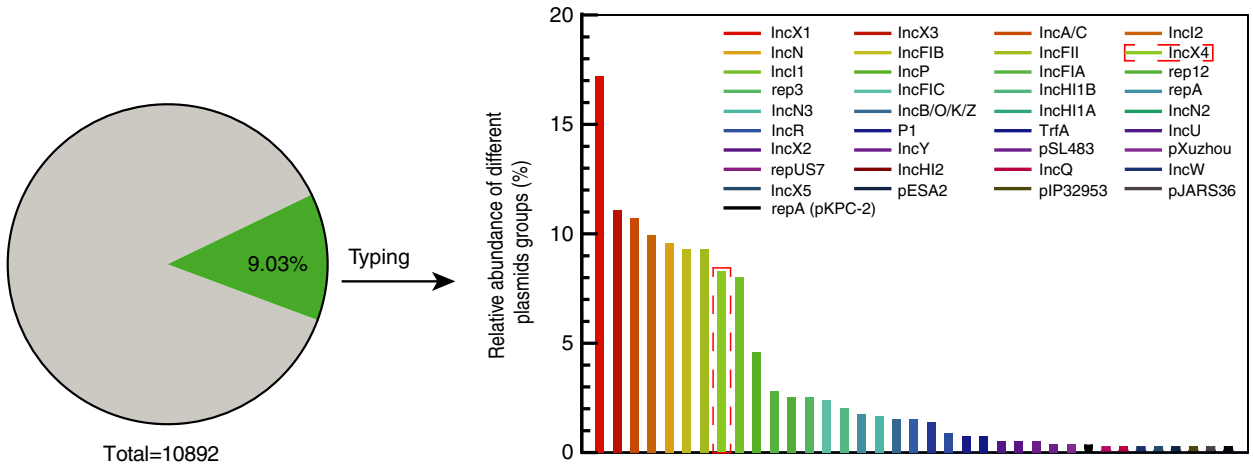


Figure 4 Target plasmids diversity of unsaturated fatty acids inhibition. The TrwD profile HMMs and VirB11 profile HMMs were using against an comprehensive plasmid databases contains 10 892 complete plasmid sequences using *hmmsearch* function of HMMER3 with default parameters, and the plasmids sequences contain annotated homologous proteins were extracted from the database for the following plasmid replicon typing using BLASTN against the PlasmidFinder database downloaded from Center for Genomic Epidemiology(https://cge.cbs.dtu.dk/) with an e-value cut-off at 1e-5 using BioEdit sequence Alignment Editor Software. The dashed line represents the relative abundance of IncX4 plasmid type tested in this study. Relative abundance of the different plasmid groups carrying TrwD/VirB11-like protein genes were plotted with GraphPath Prism software 8.0. Inc, incompatibility group. [Colour figure can be viewed at wileyonlinelibrary.com]

transfer (Guynet *et al.* 2011). Horizontal transfer of conjugative resistance plasmids served as a major mechanism of acquired resistance in bacteria, especially for Gram-negative pathogens.

There is an urgent need to explore timely and effective strategies to cope with this challenge. Plasmid conjugation inhibition has even been proposed as a tool in the fight against antibiotic resistance (Fernandez-Lopez *et al.* 2005; Graf *et al.* 2019). In this study, two unsaturated fatty acids, LA and ALA, were evaluated against the conjugative transfer of IncX4 plasmid pCSZ4 *in vitro*. Our experimental results showed effective inhibition of LA and ALA on conjugative transfer of plasmid pCSZ4. To the best of our knowledge, this is the first study of the effects of unsaturated fatty acids on IncX4 plasmid.

Type IV traffic ATPase TrwD was found as molecular target to inhibit bacterial conjugation (Ripoll-Rozada *et al.* 2016). While VirB11 orthologue TrwD is structurally related to a large family of ATPases commonly associated with macromolecular trafficking systems, including type II secretion systems, type IV pilus systems and archaeal flagellar biogenesis systems. This activity is stimulated by lipid *in vitro*, consistent with the affinity of these ATPases for membranes *in vivo* (Christie *et al.* 2017). In addition, VirB11 is the ATPases for pilus biogenesis and DNA translocation of IncX4 plasmid.

Our molecular docking analysis showed that both LA and ALA mainly bind at the pocket of NTD and linker, which inhibits movement of the NTD over the CTD, and in return interferes VirB11 ATPase activity, therefore compromising plasmid conjugation. This result is consistent with (or similar to) previous molecular docking analysis on IncW plasmid TrwD protein (Ripoll-Rozada *et al.* 2016; Graf *et al.* 2019). In addition, our qRT-PCR results indicated that LA and ALA significantly inhibited the gene expressions of *trwD*/*virB11*, suggesting that unsaturated fatty acids can not only interfere the TrwD/VirB11 protein structure but also inhibit the gene expressions, which collectively affect the ATPase synthesis in bacteria and, in turn, limit pilus biogenesis and DNA translocation. This downregulation of *virB11*gene expression by LA and ALA interference could have resulted from acid stress because the cells responded to acidic environment by shutting down the ATP synthesis pathways (Broadbent *et al.* 2010).

Moreover, VirB11 is part of the type IV secretory system (T4SS) in Gram-negative and Gram-positive bacteria, and contribute to virulence and antimicrobial resistance transfer between different bacteria including pathogens (Sutten *et al.* 2010; Rossetti *et al.* 2017). This suggests that virulence transfer among bacteria may be curbed by unsaturated fatty acids.

TrwD/VirB11 protein homology sequence analysis revealed 37 classes of plasmids, originated from both Gram-negative and Gram-positive bacteria, contained *trwD/virB11*-like genes, which served as putative inhibitory targets by unsaturated fatty acids. Of which, the major plasmid types included IncX1 (17·21%), IncX3

(11·10%), IncA/C (10·71%), IncI2 (9·95%), IncN (9·57%), IncFIB (9·31%), IncFII (9·31%), and IncX4 (8·29%). IncI1 (8·04%) and IncP (4·59%) are plasmid groups. The inhibited effect of unsaturated fatty acid 2-HAD to IncFI and IncFII plasmids has been demonstrated before (Getino *et al.* 2015). However, it is worth noting that this literature has indicated that plasmids (IncN and IncP) were not significantly affected even at 0·4 mmol l^{-1} of unsaturated fatty acid 2-HAD(Getino *et al.* 2015). Contrary to this view, another literature showed that LA at 3 mmol l^{-1} effectively inhibit conjugation of the plasmid pCT, which encodes an ATPase TrbB originated from plasmid RP4 (Inc P) (Buckner *et al.* 2020). This difference is likely to be due to different compounds and concentrations in two literature. TrwD/VirB11 was not more widely spread among some Inc groups of plasmids in our study, the low sequence homology is likely a major contributing factor to the lower plasmid targets.

Notably, some of these 37 plasmid groups have been significantly associated with the horizontal spread of antimicrobial resistance genes in various species. For example, IncX3 type plasmids have been linked to the spread of carbapenemase gene bla_{NDM}, dispersed across the 'one-health' ecosystem: environment, livestock and human (Liu *et al.* 2017; Pulss *et al.* 2017; Cai *et al.* 2019; Nigg *et al.* 2019). $bla_{CTX\text{-}M\text{-}15}$-harbouring IncFII type plasmids attributed to clinical success of *E. coli* epidemic ST131 strains (Partridge *et al.* 2011) and bla_{KPC}-harbouring IncN plasmids were associated with the early spread of KPC in the Northeastern United States (Eilertson *et al.* 2017). Future studies are needed to evaluate whether unsaturated fatty acids can serve as broad spectrum conjugative transfer inhibitory agents against a variety of clinical MDR plasmids.

Our study has some limitations. First, as a first step towards the understanding the inhibitory effects of unsaturated fatty acids on clinically important plasmids, we only studied a single *mcr-1*-harbouring IncX4 plasmid pCSZ4. Other clinically relevant plasmids, harbouring different resistance genes, should be examined in the future. Second, our study has been focused on the interference of unsaturated fatty acids on the plasmid transfer gene *trwD/virB11*. The result cannot rule out the possibility that unsaturated fatty acids may also interfere with other plasmid or chromosome encoded genes. Lastly, previous research suggested that presented toxic levels of LA to five different human-derived cells, bacteria and fungus species were above threshold (Getino *et al.* 2016), which makes it potential use in mammalian. However, our results only showed that conjugal transfer of IncX4 plasmid pCSZ4 can be effectively inhibited by unsaturated fatty acids *in vitro*, further studies are needed to evaluate the *in vivo* inhibitory effects of these unsaturated fatty acids.

Taken together, our study descried the first time of conjugative transfer inhibitory effects of unsaturated fatty acids, LA and ALA, on a *mcr-1*-harbouring IncX4 plasmid. Our results suggested that inhibitory effects of unsaturated fatty acids were likely associated the structure interference and expression inhibition of transfer-related *trwD/virB11* gene. Protein homology analysis revealed the wide spread of *trwD/virB11*-like genes in various plasmids from numerous bacterial species. Further studies are needed to explore whether unsaturated fatty acids can act as broad-spectrum conjugal transfer inhibitory agents against other clinical MDR plasmids and examined the inhibitory effects *in vivo* models.

Acknowledgements

This work was supported by National Natural Science Foundation of China (31972735), the National Key Research and Development Program of China (2016YFD0501300), the Program for Innovative Research Team in the University of Ministry of Education of China (IRT_17R39), the 111 Project (D20008), and in part supported by the National Institute of Allergy and Infectious Diseases (R01AI090155 and R21AI135250 to B.N.K).

Conflict of Interests

None declared.

References

Broadbent, J., Larsen, R., Deibel, V. and Steele, J. (2010) Physiological and transcriptional response of Lactobacillus casei ATCC 334 to acid stress. *J Bacteriol* **192**, 2445–2458.

Brooks, L., Kaze, M. and Sistrom, M. (2019) A curated, comprehensive database of plasmid sequences. *Microbiol Resour Announc* **8**, e01325-18.

Buckner, M., Ciusa, M., Meek, R., Moorey, A., McCallum, G., Prentice, E., Reid, J., Alderwick, L. *et al.* (2020) HIV drugs inhibit transfer of plasmids carrying extended-spectrum β-lactamase and carbapenemase genes. *MBio* **11**(1), https://doi.org/10.1128/mBio.03355-19.

Cai, Y., Chen, C., Zhao, M., Yu, X., Lan, K., Liao, K., Guo, P., Zhang, W. *et al.* (2019) High prevalence of metallo-β-lactamase-producing *Enterobacter cloacae* from three tertiary hospitals in China. *Front Microbiol* **10**, 1610.

Chen, C., Cui, C.Y., Zhang, Y., He, Q., Wu, X.T., Li, G., Liao, X.P., Kreiswirth, B.N. *et al.* (2019) Emergence of mobile tigecycline resistance mechanism in *Escherichia coli* strains from migratory birds in China. *Emerg Microbes Infect* **8**, 1219–1222.

Christie, P.J., Gomez Valero, L. and Buchrieser, C. (2017) Biological diversity and evolution of type IV secretion systems. *Curr Top Microbiol Immunol* **413**, 1–30.

Chukwu, M.O., Luther King Abia, A., Ubomba-Jaswa, E., Obi, L. and Dewar, J.B. (2019) Characterization and phylogenetic analysis of *Campylobacter* species isolated from paediatric stool and water samples in the Northwest Province, South Africa. *Int J Environ Res Public Health* **16**, 2205.

Eddy, S.R. (2009) A new generation of homology search tools based on probabilistic inference. *Genome inform Int Conf Genome Inform* **23**, 205–211.

Eddy, S.R. (2011) Accelerated profile HMM searches. *PLoS Comput Biol* **7**, e1002195.

Edgar, R.C. (2004a) MUSCLE: a multiple sequence alignment method with reduced time and space complexity. *BMC Bioinform* **5**, 113.

Edgar, R.C. (2004b) MUSCLE: multiple sequence alignment with high accuracy and high throughput. *Nucleic Acids Res* **32**, 1792–1797.

Eilertson, B., Chen, L., Chavda, K.D. and Kreiswirth, B.N. (2017) Genomic characterization of two KPC-producing *Klebsiella* isolates collected in 1997 in New York City. *Antimicrob Agents Chemother* **61**, e02458-16.

Farzana, R., Jones, L.S., Rahman, M.A., Toleman, M.A., Sands, K., Portal, E., Boostrom, I., Kalam, M.A. *et al.* (2019) Emergence of mcr-1 mediated colistin resistant *Escherichia coli* from a hospitalized patient in Bangladesh. *J Infect Dev Count* **13**, 773–776.

Feldgarden, M., Brover, V., Haft, D.H., Prasad, A.B., Slotta, D.J., Tolstoy, I., Tyson, G.H., Zhao, S. *et al.* (2019) Validating the AMRFinder tool and resistance gene database by using antimicrobial resistance genotype-phenotype correlations in a collection of isolates. *Antimicrob Agents Chemother* **63**, 11.

Fernandez-Lopez, R., Machón, C., Longshaw, C.M., Martin, S., Molin, S., Zechner, E.L., Espinosa, M., Lanka, E. *et al.* (2005) Unsaturated fatty acids are inhibitors of bacterial conjugation. *Microbiology* **151**, 3517–3526.

Getino, M. and de la Cruz, F. (2018) Natural and artificial strategies to control the conjugative transmission of plasmids. *Microbiology Spectr* **6**, MTBP-0015-2016.

Getino, M., Fernandez-Lopez, R., Palencia-Gandara, C., Campos-Gomez, J., Sanchez-Lopez, J.M., Martinez, M., Fernandez, A. and de la Cruz, F. (2016) Tanzawaic acids, a chemically novel set of bacterial conjugation inhibitors. *PLoS One* **11**, e0148098.

Getino, M., Sanabria-Ríos, D.J., Fernández-López, R., Campos-Gómez, J., Sánchez-López, J.M., Fernández, A., Carballeira, N.M. and de la Cruz, F. (2015) Synthetic fatty acids prevent plasmid-mediated horizontal gene transfer. *MBio* **6**, https://doi.org/10.1128/mBio.01032-15.

Graf, F.E., Palm, M., Warringer, J. and Farewell, A. (2019) Inhibiting conjugation as a tool in the fight against antibiotic resistance. *Drug Dev Res* **80**, 19–23.

Guynet, C., Cuevas, A., Moncalian, G. and de la Cruz, F. (2011) The stb operon balances the requirements for vegetative stability and conjugative transfer of plasmid R388. *PLoS Genet* **7**, e1002073.

Huang, H., Liao, J., Zheng, X., Chen, Y. and Ren, H. (2019) Low-level free nitrous acid efficiently inhibits the conjugative transfer of antibiotic resistance by altering intracellular ions and disabling transfer apparatus. *Water Res* **158**, 383–391.

Lavigne, R., Seto, D., Mahadevan, P., Ackermann, H.W. and Kropinski, A.M. (2008) Unifying classical and molecular taxonomic classification: analysis of the Podoviridae using BLASTP-based tools. *Res Microbiol* **159**, 406–414.

Liu, Y.Y., Wang, Y., Walsh, T.R., Yi, L.X., Zhang, R., Spencer, J., Doi, Y., Tian, G. *et al.* (2016) Emergence of plasmid-mediated colistin resistance mechanism MCR-1 in animals and human beings in China: a microbiological and molecular biological study. *Lancet Infect Dis* **16**, 161–168.

Liu, Z., Wang, Y., Walsh, T.R., Liu, D., Shen, Z., Zhang, R., Yin, W., Yao, H. *et al.* (2017) Plasmid-mediated novel bla (NDM-17) gene encoding a carbapenemase with enhanced activity in a sequence type 48 *Escherichia coli* Strain. *Antimicrob Agents Chemother* **61**, e02233-16.

Livak, K.J. and Schmittgen, T.D. (2001) Analysis of relative gene expression data using real-time quantitative PCR and the 2(-Delta Delta C(T)) Method. *Methods* **25**, 402–408.

Matamoros, S., van Hattem, J.M., Arcilla, M.S., Willemse, N., Melles, D.C., Penders, J., Vinh, T.N., Thi Hoa, N. *et al.* (2017) Global phylogenetic analysis of *Escherichia coli* and plasmids carrying the mcr-1 gene indicates bacterial diversity but plasmid restriction. *Sci Rep* **7**, 15364.

McInnes, R.S., McCallum, G.E., Lamberte, L.E. and van Schaik, W. (2020) Horizontal transfer of antibiotic resistance genes in the human gut microbiome. *Curr Opin Microbiol* **53**, 35–43.

Nigg, A., Brilhante, M., Dazio, V., Clément, M., Collaud, A., Gobeli Brawand, S., Willi, B., Endimiani, A. *et al.* (2019) Shedding of OXA-181 carbapenemase-producing *Escherichia coli* from companion animals after hospitalisation in Switzerland: an outbreak in 2018. *Eurosurveillance* **24**, 1900071.

Partridge, S.R., Zong, Z. and Iredell, J.R. (2011) Recombination in IS26 and Tn2 in the evolution of multiresistance regions carrying blaCTX-M-15 on conjugative IncF plasmids from *Escherichia coli*. *Antimicrob Agents Chemother* **55**, 4971–4978.

Pulss, S., Semmler, T., Prenger-Berninghoff, E., Bauerfeind, R. and Ewers, C. (2017) First report of an *Escherichia coli* strain from swine carrying an OXA-181 carbapenemase and the colistin resistance determinant MCR-1. *Int J Antimicrob Agents* **50**, 232–236.

Qiu, Z., Yu, Y., Chen, Z., Jin, M., Yang, D., Zhao, Z., Wang, J., Shen, Z. *et al.* (2012) Nanoalumina promotes the horizontal transfer of multiresistance genes mediated by

plasmids across genera. *Proc Natl Acad Sci USA* **109**, 4944–4949.

Ripoll-Rozada, J., García-Cazorla, Y., Getino, M., Machón, C., Sanabria-Ríos, D., de la Cruz, F., Cabezón, E. and Arechaga, I. (2016) Type IV traffic ATPase TrwD as molecular target to inhibit bacterial conjugation. *Mol Microbiol* **100**, 912–921.

Ripoll-Rozada, J., Zunzunegui, S., de la Cruz, F., Arechaga, I. and Cabezón, E. (2013) Functional interactions of VirB11 traffic ATPases with VirB4 and VirD4 molecular motors in type IV secretion systems. *J Bacteriol* **195**, 4195–4201.

Rossetti, C.A., Drake, K.L., Lawhon, S.D., Nunes, J.S., Gull, T., Khare, S. and Adams, L.G. (2017) Systems biology analysis of temporal in vivo *Brucella melitensis* and bovine transcriptomes predicts host: pathogen protein-protein interactions. *Front Microbiol* **8**, 1275.

Scheenstra, M.R., van den Belt, M., Tjeerdsma-van Bokhoven, J.L.M., Schneider, V.A.F., Ordonez, S.R., van Dijk, A., Veldhuizen, E.J.A. and Haagsman, H.P. (2019) Cathelicidins PMAP-36, LL-37 and CATH-2 are similar peptides with different modes of action. *Sci Rep* **9**, 4780.

Shen, C., Wang, Z., Yao, X., Li, Y., Lei, T., Wang, E., Xu, L., Zhu, F. *et al.* (2018) Comprehensive assessment of nine docking programs on type II kinase inhibitors: prediction accuracy of sampling power, scoring power and screening power. *Brief Bioinform* https://doi.org/10.1093/bib/bby103.

Skewes-Cox, P., Sharpton, T.J., Pollard, K.S. and DeRisi, J.L. (2014) Profile hidden Markov models for the detection of viruses within metagenomic sequence data. *PLoS One* **9**, e105067.

Sun, J., Fang, L.X., Wu, Z., Deng, H., Yang, R.S., Li, X.P., Li, S.M., Liao, X.P. *et al.* (2017) Genetic analysis of the incx4 plasmids: implications for a unique pattern in the mcr-1 acquisition. *Sci Rep* **7**, 424.

Sun, J., Zhang, H., Liu, Y.H. and Feng, Y. (2018) Towards understanding MCR-like colistin resistance. *Trends Microbiol* **26**, 794–808.

Sutten, E.L., Norimine, J., Beare, P.A., Heinzen, R.A., Lopez, J.E., Morse, K., Brayton, K.A., Gillespie, J.J. *et al.* (2010) Anaplasma marginale type IV secretion system proteins VirB2, VirB7, VirB11, and VirD4 are immunogenic components of a protective bacterial membrane vaccine. *Infect Immun* **78**, 1314–1325.

Tang, B., Chang, J., Zhang, L., Liu, L., Xia, X., Hassan, B.H., Jia, X., Yang, H. *et al.* (2020) Carriage of distinct mcr-1-harboring plasmids by unusual serotypes of *Salmonella*. *Adv Biosyst* **4**, 1900219.

Wang, Y., Lu, J., Mao, L., Li, J., Yuan, Z., Bond, P.L. and Guo, J. (2019) Antiepileptic drug carbamazepine promotes horizontal transfer of plasmid-borne multi-antibiotic resistance genes within and across bacterial genera. *ISME J* **13**, 509–522.

Zając, M., Sztromwasser, P., Bortolaia, V., Leekitcharoenphon, P., Cavaco, L.M., Ziętek-Barszcz, A., Hendriksen, R.S. and Wasyl, D. (2019) Occurrence and characterization of mcr-1-positive *Escherichia coli* isolated from food-producing animals in Poland, 2011–2016. *Front Microbiol* **10**, 1753.

Zhang, H., Zong, Z., Lei, S., Srinivas, S., Sun, J., Feng, Y., Huang, M. and Feng, Y. (2019) A genomic, evolutionary, and mechanistic study of MCR-5 action suggests functional unification across the MCR family of colistin resistance. *Adv Sci* https://doi.org/10.1002/advs.201900034.

BMC Neurology

RESEARCH

Open Access

Integrative analysis of purine metabolites and gut microbiota in patients with neuromyelitis optica spectrum disorders after mycophenolate mofetil treatment

Gong Li[1†], Xiaoyu Ma[2†], Lijuan Xia[1], Ran Wei[1], Xiran Wang[1], Cang Li[1], Yuge Wang[3], Limin He[1], Hao Ren[1], Jian Sun[1*] and Wei Qiu[3*]

Abstract

Background Neuromyelitis optica spectrum disorder (NMOSD) is a recurring inflammatory demyelinating disease that is commonly observed in Asian countries like China. Prior investigations have shown that mycophenolate mofetil (MMF) with better biocompatibility compared to azathioprine (AZA), and can prevent relapses of NMOSD, but the efficacy was controversially reported in different NMOSD cases. We aimed to explore the factors that weaken efficacy of MMF in NMOSD.

Methods A total of 34 NMOSD patients treated with MMF were prospectively enrolled and grouped according to the therapeutic efficacy as effective group (EG, n = 23) versus less-effective group (LEG, n = 11). The purine metabolites were profiled in serum samples and gut microbiota was analyzed using 16S rRNA sequencing with stool samples from the same patients.

Results Purine salvage pathway (PSP) metabolites (inosine, hypoxanthine, xanthine, guanine and uric acid) in the serum of NMOSD patients were elevated in the LEG compared to EG ($p < 0.05$). Additionally, the richness and microbial diversity of gut microbiota was found to be similar between EG and LEG patients. However, LEG patients had increased presence of *Clostridium* and *Synergistes* but decreased abundance of the *Coprococcus* genus.

Conclusions The PSP metabolites and composition of the gut microbiota were changed between patients with or without optimal clinical response after MMF treatment. This may help us to understand the pharmacodynamics of MMF in NMOSD.

Keywords Neuromyelitis Optica Spectrum Disorders, Mycophenolate Mofetil, Gut Microbiota, Therapeutic Efficacy, PSP Metabolites

[†]Gong Li and Xiaoyu Ma are co-first authors of the article.

*Correspondence:
Jian Sun
jiansun@scau.edu.cn
Wei Qiu
qiuwei@mail.sysu.edu.cn

[1]College of veterinary medicine, South China Agricultural University, Guangzhou, China
[2]Department of Neurology, The Second Hospital of Shandong University, Jinan 250033, China
[3]Department of Neurology, The Third Affiliated Hospital of Sun Yat-sen University, No. 600 Tianhe Road, Guangzhou 510630, China

© The Author(s) 2023. **Open Access** This article is licensed under a Creative Commons Attribution 4.0 International License, which permits use, sharing, adaptation, distribution and reproduction in any medium or format, as long as you give appropriate credit to the original author(s) and the source, provide a link to the Creative Commons licence, and indicate if changes were made. The images or other third party material in this article are included in the article's Creative Commons licence, unless indicated otherwise in a credit line to the material. If material is not included in the article's Creative Commons licence and your intended use is not permitted by statutory regulation or exceeds the permitted use, you will need to obtain permission directly from the copyright holder. To view a copy of this licence, visit http://creativecommons.org/licenses/by/4.0/. The Creative Commons Public Domain Dedication waiver (http://creativecommons.org/publicdomain/zero/1.0/) applies to the data made available in this article, unless otherwise stated in a credit line to the data.

Introduction

Neuromyelitis optica spectrum disorders (NMOSD) is a severe, disabling autoimmune disease of the central nervous system (CNS) characterized by its association with serum anti-aquaporin-4 antibodies (AQP4-IgG) [1–4]. Clinically, NMOSD results in a range of syndromes of varied severities including recurrent paralysis, blindness and brain syndromes [5]. Immunosuppressive therapies including administration of azathioprine (AZA) and mycophenolate mofetil (MMF) in addition to the new B cell- and complement-targeted therapies are the current NMOSD treatments aimed at relapse prevention [6, 7], with MMF demonstrating better tolerability compared to AZA [8]. MMF is a prodrug whose active metabolite mycophenolic acid (MPA) inhibits inosine monophosphate dehydrogenase (IMPDH) and suppresses the de novo synthesis of guanine nucleotides in rapidly-proliferating cells such as T and B lymphocytes [9, 10]. MMF/MPA treatments significantly and comprehensively lower the levels of baseline purine metabolites in intestinal cell models as well as in patients [11, 12]. However, previous studies have shown mixed efficacy of MMF in treating NMOSD, the proportion of recurrence-free patients in NMOSD is 46–73%, the Expanded Disability Status Scale (EDSS) score decreased or stabilized in 83–91% of patients [6, 13–15].

Our laboratory recently demonstrated that the gut microbiomes of healthy individuals can be distinguished from NMOSD patients. In particular, the degree of *Streptococcus* spp. colonization was significantly and positively correlated with disease severity [16]. Other studies have demonstrated strong associations between several *Clostridium* spp. and NMOSD development [17, 18]. These studies linked dynamic interactions of the host gut microbiota to NMOSD. However, it is not known whether NMOSD therapies such as MMF administration are also influenced by the gut microbiota and whether the gut microbiota has a role in the efficacy of these therapies.

In the current study, we performed metabolic profiling and microbiome analysis on samples collected from NMOSD patients. This may not only help us to understand the pharmacodynamics of MMF but may also reveal the reasons of therapeutic effect.

Materials and methods

Reagents and chemicals

Inosine, hypoxanthine, xanthine, guanine and uric acid were obtained from MedChemExpress (Shanghai, China) and were prepared as 1000 ppm methanol stocks. NaOH 10 mM was used as necessary to increase solubility. Acetonitrile was purchased from Macklin (Shanghai, China).

Patient enrollment

The study group included 34 NMOSD patients who had received MMF therapy (0.5 g MMF orally, twice a day for long term therapy) at the Third Affiliated Hospital of Sun Yat-sen University (Guangzhou, China). The primary inclusion criteria were (1) clinical diagnosis of NMOSD and seropositive for AQP4-IgG [19, 20]; (2) patients aged 15–65 and (3) an Kurtzke Expanded Disability Status Scale (EDSS) score ≤ 8.0. Patients who met any of the following key criteria were excluded: (1) treatment with antibiotics or probiotics within the last 3 months; (2) emergency treatment such as plasmapheresis or intravenous methylprednisolone for acute recurrence within the last 1 month; (3) Concurrent disease with diabetes mellitus, systemic autoimmune diseases or other neurological diseases.

Stool and serum samples were taken from the patient that received MMF treatment at least for 3 months. Stool samples were taken in the morning. Serum samples were taken for 0.5, 1 and 2 h after receiving MMF in the early morning. Clinical data was collected included relapses, follow-up time and EDSS score. The 34 participants were divided into two groups: patients with no relapse were classified into the effective group (EG). Patients who relapsed after 3 months of MMF treatment were treated as the less-effective group (LEG). This study was approved by the ethics Committee of the Third Affiliated Hospital of Sun Yat-sen University ([2020]02-016-01) and all patients signed informed consent.

HPLC-MS/MS analysis

Serum sample processing and HPLC-UV–MS/MS analysis were performed as previously described with minor modifications [21]. In brief, chromatographic separations were conducted using a Shimadzu LC-30AD series HPLC system (Shimadzu, Kyoto, Japan) with an Frulic N column (AZYP, LLC, Arlington, USA). Analytes were eluted at a flow rate of 0.4 mL/min using a gradient of phase A (0.2% formic acid) and phase B (0.2% formic acid in acetonitrile) as follows: 0–0.5 min, 80% B; 0.5–4.5 min, 50% B; 4.5–8 min, 80% B. The eluates were monitored by UV at 254 nm and MS detection in parallel. The injection volume as 5 μL, and the column temperature was maintained at 23 °C. MS detection was performed using an AB Sciex Triple Quad 5500 (AB Sciex, Toronto, Canada).

Microbiome 16S rRNA gene sequencing, alignment and analysis

Microbial DNA was extracted from fecal samples of NMOSD patients using the E.Z.N.A. Stool DNA Kit (Omega Bio-Tek, Norcross, GA, USA) according to the manufacturer's protocol. Extracted DNA was qualitatively and quantitatively analyzed by gel electrophoresis and ultraviolet spectroscopy before sequencing.

Thereafter, bacterial 16S rDNA V3–V4 regions were amplified using primers 341 F and 806R (Illumina, San Diego, CA, USA). The resulting amplicons were sequenced using the Illumina NovaSeq 6000 platform (Guangdong Longsee Biomedical, Foshan, China).

Statistical analyses

The data were expressed as the mean ± standard deviation (SD). A unpaired parametric t-test was performed for comparison of the two groups using Prism v8.0 software (GraphPad, San Diego, CA, USA). A p value of 0.05 was considered to be statistically significant.

Results

Clinical characteristics

A total of 34 NMOSD patients who had received MMF therapy were recruited. All patients were diagnosed with NMOSD according to clinical diagnosis and seropositive for AQP4-IgG [19]. Immunotherapies such as MMF or AZA typically require 3–6 months to reach a milestone of stable effectiveness [22]. Hence, all the recurrences we recorded in this study occurred after 6 months of MMF use. The acute treatment guideline for NMOSD involves high-dose steroid therapy, follow with a gradual reduction in steroid usage and long-term maintenance [22–25]. Throughout the steroid treatment process, patients were gradually tapered to a maintenance dose of 8 mg methylprednisolone or 10 mg prednisone every other day or 5 mg prednisone once daily during the remission phase. As 4 mg methylprednisolone is equal to 5 mg prednisone, they all use similar doses of steroids. And in the remission stage, they all didn't use other immunotherapy to prevent relapse currently and previously.

Our group of NMOSD patients were analyzed according to their clinical responses to MMF therapies and grouped according to responders (EG) and less-responders (LEG). The clinical characteristics of the patients are shown in Table 1. Significant differences in relapse times ($p<0.001$) and EDSS after MMF ($p=0.005$) were observed between EG and LEG patients.

Table 1 Clinical parameters in NMOSD patients according to response to MMF

Variables	EG (n = 23)	LEG (n = 11)	*p* value
Relapse times	0	2.00 ± 0.89	< 0.001
Age (years)	39.95 ± 12.20	47.45 ± 11.76	0.106
Gender (male: female)	5:18	1:10	0.638
Follow-up time (months)	21.00 ± 14.34	37 ± 20.27	0.060
EDSS before MMF	4.00 ± 0.86	3.5 ± 1.06	0.228
EDSS after MMF	3.00 ± 1.06	4.0 ± 1.30	0.005

Purine salvage pathway metabolites are maintained at high levels in LEG patients

We examined purine metabolites whose biosynthesis is targeted by MMF(MPA) in the serum of recruited patients (Fig. 1A-B). Interestingly, we found distinct differences in the abundance of the purine salvage pathway (PSP) metabolites inosine, hypoxanthine, xanthine, guanine and uric acid (UA) for the patients that responded to MMF therapy (EG) and non-responders (LEG). These 5 PSP metabolites were all elevated in the serum of LEG patients. In particular, inosine, hypoxanthine, xanthine and guanine were significantly ($p<0.05$) decreased in EG patients 1 h after receiving the MMF. At 2 h following MMF intervention, inosine levels reached the level of significance ($p<0.05$) and were also lower in EG patients (Fig. 1C-G). The observations indicated a negative correlation between the MMF therapeutic response and PSP metabolite levels in serum of patients.

Altered gut microbiota in NMOSD patients by their responses to MMF therapy

Previous studies have indicated that the gut microbiota participates in the development and pathogenesis of NMOSD [16–18, 26]. The gut microbiota was profiled for each patient using 16 S rRNA sequencing. The microbial richness (operational taxonomic units, OTUs and Chao1 indices) and microbial diversity (Shannon and Simpson indices) were similar between EG and LEG patients (Fig. 2A-D). β diversity was assessed using principal-coordinate analysis (PCA) based on weighted UniFrac metrics and the results again indicated no compositional alterations between the microbiota of the patients in the two groups (Fig. 2E).

Since no structural shifts were observed among the patients in the response to MMF, we extended our taxonomic comparisons. The microbial compositions of each group were compared using the 20 most-abundant operational taxonomic units OUT at the genus level. Overall, *Bacteroides* dominated in both EG and LEG patients while the other dominate genera including *Faecalibacterium*, *Roseburia* and *Megamonas*, rarely exceeded 30% of all sequences (Fig. 2F). Interestingly, LEfSe analysis indicated that the abundance of *Clostridium* and *Synergistes* had significantly increased for EG and corresponded to a significant decline in abundance of the *Coprococcus* genus in LEG (Fig. 2G). These results indicated that overall, the gut microbiota stayed compositionally stable in the MMF therapy while the abundance of 3 bacterial genera were significantly altered.

Discussion

NMOSD pathogenesis has been linked to the activity of microbiota [26, 27]. Long-term MMF therapy is widely used in immunological and NMOSD diseases although

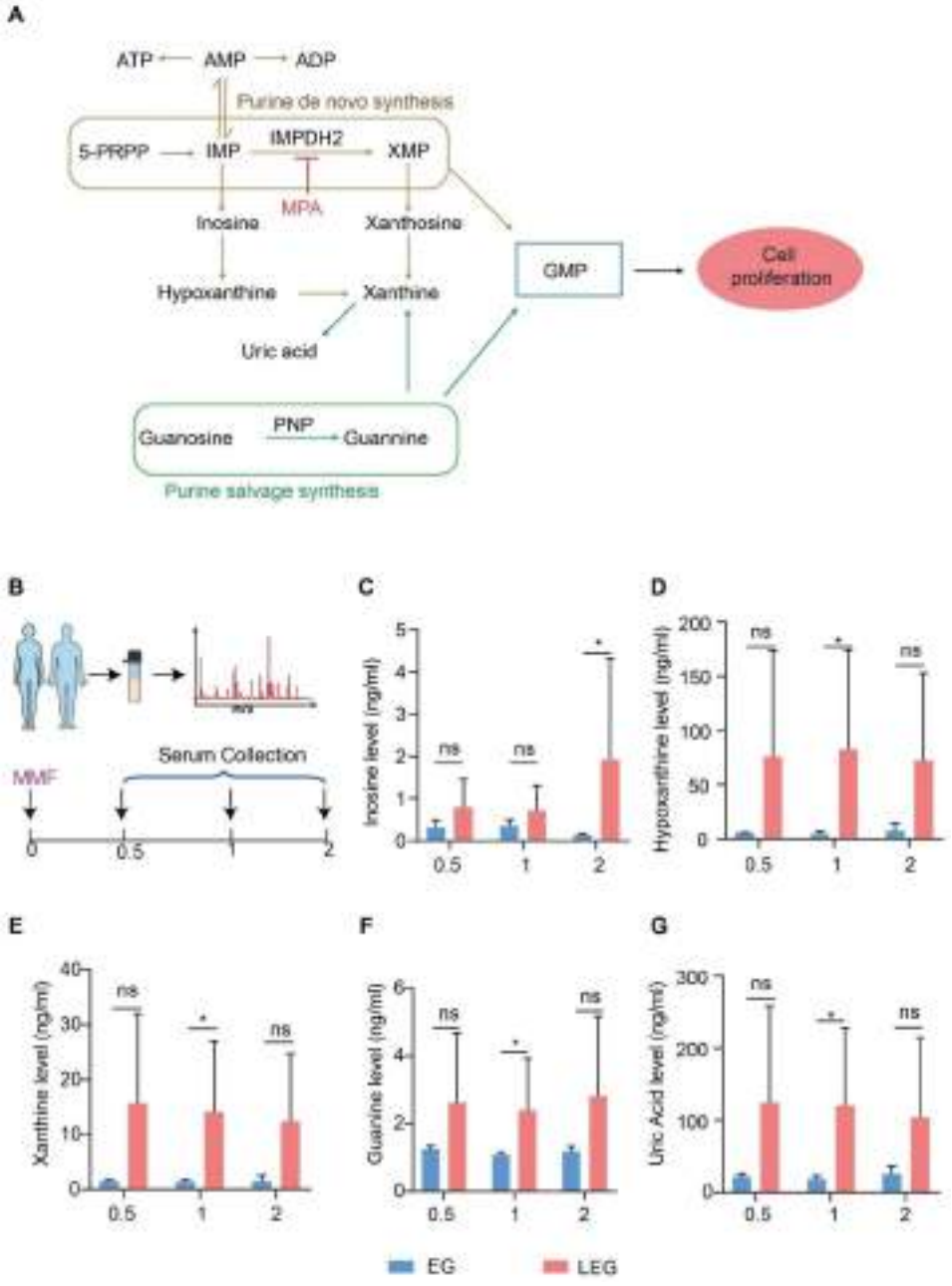


Fig. 1 Purine salvage pathway metabolites are maintained at high levels in LEG patients. (**A**) Schematic of the de novo and salvage pathways of purine synthesis. (**B**) Serum collection point for the experiments. Quantification of the levels of (**C**) Inosine (**D**) Hypoxanthine (**E**) Xanthine (**F**) Guanine and (**G**) Uric acid. *$p < 0.05$

not all patients display the optimal clinical response. Whether the microbiota is also involved in the therapeutic response to the drugs against NMOSD has not been previously investigated. In this study, our findings first showed that the purine metabolites and composition of the gut microbiota were changed.

The NMOSD patients may experience pathogenesis of different level that influenced by various factors such as disease duration, comorbidities, prior disease-modifying treatment (DMT), and their baseline magnetic resonance imaging (MRI) status. However, NMOSD exacerbation is often reported to be associated with recurrences rather than a gradual progression, typically manifesting as a "cliff-like" exacerbation followed by incomplete recovery [6]. Consequently, the worsening of NMOSD appears to have little correlation with disease duration [7]. Based on our pre-survey, all patients recruited in our study had no histories for other DMT. Since the MMF has been primarily considered to target the relapses of NMOSD, we

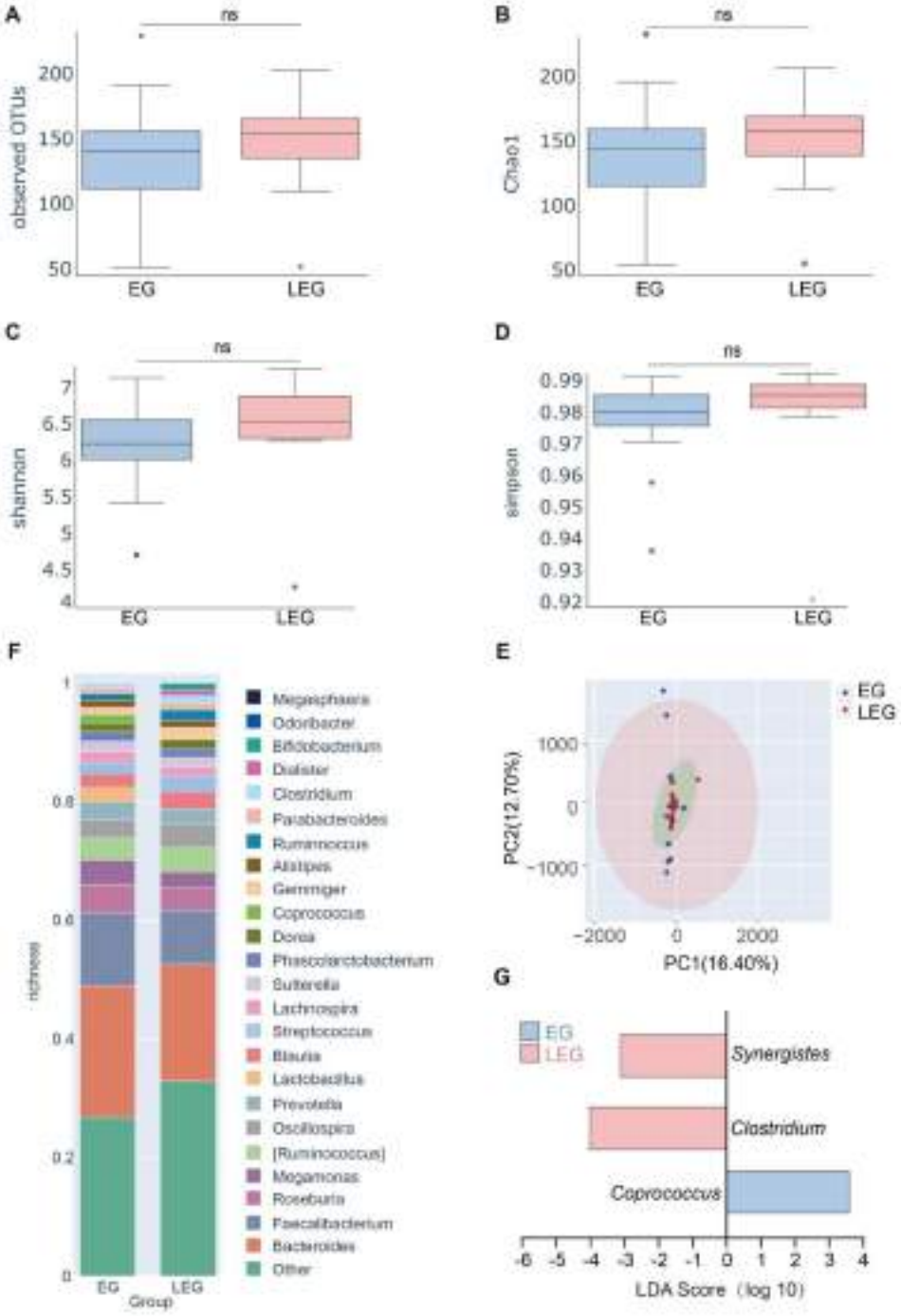


Fig. 2 Altered gut microbiota in NMOSD patients by their responses to MMF therapy. (**A**) Observed OTUs. (**B**) Chao1 index. (**C**) Shannon index. (**D**) Simpson index of the gut microbiota in EG and LEG samples. (**E**) Principal component analysis. (**F**) Composition of the gut microbiota at the genus levels in fecal samples in EG and LEG samples. (**G**) LEfSe (Linear discriminant analysis effect size) analysis showing taxa associated with therapeutic response of MMF. n = 23 for effective group (EG) and n = 11 for less-effective group (LEG). *$p < 0.05$

assessed failed responses of patients to MMF by examining recurrences and the EDSS.

The assessment of the effectiveness of MMF primarily relies on the area under the plasma concentration-time curve from 0 to 12 h (AUC_{0-12}) as the principal parameter. However, while the AUC_{0-12} of the MPA concentration-time curve exhibits a strong correlation with pharmacological effects, its measurement proves to be arduous in a clinical setting. Several clinical trials have demonstrated that the predicted value of the AUC

from 0 to 2 h (AUC_{0-2}) can effectively evaluate the AUC from 0 to 12 h [28, 29]. Considering the challenges associated with sampling during clinical practice, we have chosen to employ three specific time points (0.5, 1, and 2 h) to represent the aforementioned parameter. We found that the levels of four PSP metabolites, including inosine, hypoxanthine, xanthine and guanine were significantly decreased in EG patients 1 h after receiving the MMF compared to LEG patients. MMF was originally designed to inhibit GMP and GTP synthesis. However, GTP synthesis is also coupled to purine *de novo* synthesis via PRPP availability that is regulated by the rapamycin complex 1 (mTORC1) [30]. Thus, other purines and in particular the PSP metabolites should be suppressed by the presence of MMF. In support of this, previous studies have demonstrated that levels of PSP metabolites levels in serum or plasma elevated in patients with CNS disease [31, 32]. Similarly, UA levels were mildly elevated in NMOSD patients during relapse compared with patients with a good prognosis [33].These findings coupled with our results potentially indicated that selected PSP metabolites might be used to distinguish the therapeutic efficacy of MMF in NMOSD patients.

A key factor for the poor response to MMF therapy in NMOSD patients has been linked to host genetic polymorphisms. For instance, single nucleotide polymorphisms (SNPs) in the genes encoding the MPA metabolizing enzyme UDP-glucuronosyltransferase 1–9 (UGT1A9) or the molecular targets (IMPDH1 and IMPDH2) are linked to a weakened drug responsiveness of individual patients [19, 30, 34]. In addition to SNP differences, the metabolic capacity of gut microbiota also actively participates in the utilization and metabolism of MMF e.g. through β-glucuronidase (GUS) enzymes expressed by gut commensals [35–37]. We profiled the microbiomes of NMOSD patients that were grouped according to their therapeutic responses to MMF therapy. Out of expectation, significant changes were not found in the microbial richness and diversity in the MMF non-responders compared to responders in this study. This implied a minor impact of the established host microbiome on the therapeutic response to MMF.

Currently, numerous studies have demonstrated that patients with NMOSD undergo substantial alterations in the composition of their gut microbiota following administration of immunotherapy drugs. Cree et al. observed a noteworthy proliferation of *Clostridium perfringens* in NMOSD patients treated with rituximab, in comparison to a control group [38]. In a separate study, Junli Gong et al. revealed a decrease in the relative abundance of the *Streptococcus* genus following treatment with immunosuppressants (MMF and AZA), when compared to an untreated group [39]. These findings suggest a potential association between the enrichment of *C. perfringens* and *Streptococcus* in NMOSD and the development of the disease. In this study, the abundance of *Clostridium* and *Synergistes* had significantly increased for EG patients and corresponded to a significant decline in abundance of the *Coprococcus* genus in LEG patients. *Clostridium* in the Firmicutes phylum was related to the AQP4-IgG–associated NMOSD [17, 18]. Moreover, the genus *Coprococcus* includes species that are strong butyrate producers [40–42] so that one possible explanation for our results is that they alleviate the syndromes of NMOSD by butyrate-dependent anti-inflammatory effects as well as having a negative effect on IL-17 A expression [43, 44]. A recent study also spotlighted this genus, whose abundance sharply reduced in NMOSD patients in comparison with the health control [45]. Hence, the existing *Coprococcus* species might be beneficial microbes to patients with NMOSD and ameliorate its symptoms by curtailing the levels of pro-inflammatory cytokines. This is an encouraging finding, and further investigation is needed to identify the mechanism adopted by *Coprococcus* couple with MMF to suppress the process of NMOSD development.

However, there are several limitations for this study. First, the absence of criteria for assessing the effectiveness of NMOSD treatment may weaken our conclusion. Our analysis based on relapse frequency and EDSS as criteria may introduce inherent bias into our findings. Second, the limited sampling size restricts our capacity to establish comprehensive conclusive remarks. Also, this precluded the consideration of baseline MRI status and general complications.

Future investigations would incorporate a comprehensive categorization of patients' conditions, which is beneficial to better understand NMOSD.

Conclusions

In this study, altered PSP metabolites and composition of the gut microbiota were observed between NMOSD patients with or without optimal clinical response after MMF treatment. Poor clinical response might be the increased abundance of *Clostridium* and *Synergistes* and decreased relative abundances of the genera *Coprococcus.* Our data might help to understand the pharmacodynamics of MMF in the aspect of the gut-brain axis. Furthermore, in view of the fact that MMF is so widely used in NMOSD, further studies investigating the mechanism of this *Coprococcus in* NMOSD are needed.

Abbreviations

MMF	Mycophenolate Mofetil
NMOSD	Neuromyelitis Optica Spectrum Disorders
EG	Effective Group
LEG	Less-Effective Group
PSP	Purine Salvage Pathway
MPA	Mycophenolic Acid
AQP4-IgG	Anti-Aquaporin-4 Antibodies
EDSS	Expanded Disability Status Scale

SNPs	Single Nucleotide Polymorphisms:UGT1A9:UDP-Glucuronosyltransferase 1–9
IMPDH	Inosine Monophosphate Dehydrogenase
SNP	Single Nucleotide Polymorphisms
GUS	β-glucuronidase
CNS	Central Nervous System

Acknowledgements
We thank Hangzhou Zhongmei Huadong Pharmaceutical for their help with grant support.

Author contributions
GL, XYM, LJX, RW, CL, LMH contributed to the acquisition of data, GL, XRW, YGW contributed to the analysis of data. GL, XYM, and HR contributed to the drafting of the work. JS and WQ contributed to the conception and design drafting of the work. All authors read and approved the final manuscript.

Funding
This work was supported by grants from the National Natural Science Foundation of China (81771300, 81971140), Natural Science Foundation of Guangdong Province (2020A1515010053) and the Guangdong Major Project of Basic and Applied Basic Research (2020B0301030007) .

Data availability
The raw sequence data from the fecal microbiota in this paper were uploaded to the Sequence Read Archive (SRA) data (https://www.ncbi.nlm.nih.gov/sra) under accession number PRJNA813001.

Declarations

Ethics approval and consent to participate
All procedures performed in studies involving human participants were in accordance with the ethical standards and with the Helsinki declaration. And this study was approved by the ethics Committee of the Third Affiliated Hospital of Sun Yat-sen University ([2020]02-016-01). Written informed consent was obtained from all of patients or their relatives and healthy controls (or their parent or legal guardian in the case of children under 18).

Consent for publication
Not applicable.

Competing interests
The authors declare no competing interests.

Received: 2 December 2022 / Accepted: 8 December 2023
Published online: 16 December 2023

References

1. Lucchinetti C, Guo Y, Popescu B, Fujihara K, Itoyama Y, Misu T. The pathology of an autoimmune astrocytopathy: lessons learned from neuromyelitis optica. Brain Pathol. 2014;24 1:83–97. https://doi.org/10.1111/bpa.12099.
2. Mader S, Kümpfel T, Meinl E. Novel insights into pathophysiology and therapeutic possibilities reveal further differences between AQP4-IgG- and MOG-IgG-associated Diseases. Curr Opin Neurol. 2020;33 3:362–71. https://doi.org/10.1097/wco.0000000000000813.
3. Bennett JL, Costello F, Chen JJ, Petzold A, Biousse V, Newman NJ, et al. Optic neuritis and autoimmune optic neuropathies: advances in diagnosis and treatment. Lancet Neurol. 2023;22 1:89–100. https://doi.org/10.1016/s1474-4422(22)00187-9.
4. Fu Y, Bi J, Yan Y, Sun X, Li K, Kim SY, et al. Rapid Immunodot AQP4 assay for Neuromyelitis Optica Spectrum Disorder. JAMA Neurol. 2023;80 10:1105–12. https://doi.org/10.1001/jamaneurol.2023.2974.
5. Wingerchuk DM, Banwell B, Bennett JL, Cabre P, Carroll W, Chitnis T, et al. International consensus diagnostic criteria for neuromyelitis optica spectrum disorders. Neurology. 2015;85(2):177–89. https://doi.org/10.1212/wnl.0000000000001729.
6. Huang Q, Wang J, Zhou Y, Yang H, Wang Z, Yan Z, et al. Low-dose mycophenolate mofetil for Treatment of Neuromyelitis Optica Spectrum Disorders: a prospective Multicenter Study in South China. Front Immunol. 2018;9:2066. https://doi.org/10.3389/fimmu.2018.02066.
7. Wingerchuk D, Weinshenker B. Neuromyelitis Optica. Curr Treat Options Neurol. 2008;10(1):55–66. https://doi.org/10.1007/s11940-008-0007-z.
8. Yong HYF, Burton JM. A Clinical Approach to existing and emerging therapeutics in Neuromyelitis Optica Spectrum Disorder. Curr Neurol Neurosci Rep. 2023;23 9:489–506. https://doi.org/10.1007/s11910-023-01287-x.
9. Allison A. Mechanisms of action of mycophenolate mofetil. Lupus. 2005;2–8. https://doi.org/10.1191/0961203305lu2109oa.
10. Allison AC, Eugui EM. The design and development of an immunosuppressive drug, mycophenolate mofetil. Springer Semin Immunopathol. 1993;14 4:353–80. https://doi.org/10.1007/bf00192309.
11. Moreno Planas J, Cuervas-Mons Martinez V, Rubio Gonzalez E, Gomez Cruz A, Lopez-Monclus J, Sánchez-Turrion V et al. Mycophenolate mofetil can be used as monotherapy late after liver transplantation. American journal of transplantation: official journal of the American Society of Transplantation and the American Society of Transplant Surgeons. 2004;4 10:1650–5; https://doi.org/10.1111/j.1600-6143.2004.00556.x.
12. Heischmann S, Dzieciatkowska M, Hansen K, Leibfritz D, Christians U. The immunosuppressant mycophenolic acid alters nucleotide and lipid metabolism in an intestinal cell model. Sci Rep. 2017;7:45088. https://doi.org/10.1038/srep45088.
13. Montcuquet A, Collongues N, Papeix C, Zephir H, Audoin B, Laplaud D, et al. Effectiveness of mycophenolate mofetil as first-line therapy in AQP4-IgG, MOG-IgG, and seronegative neuromyelitis optica spectrum disorders. Mult Scler. 2017;23 10:1377–84. https://doi.org/10.1177/1352458516678474.
14. Huh SY, Kim SH, Hyun JW, Joung AR, Park MS, Kim BJ, et al. Mycophenolate mofetil in the treatment of neuromyelitis optica spectrum disorder. JAMA Neurol. 2014;71 11:1372–8. https://doi.org/10.1001/jamaneurol.2014.2057.
15. Jacob A, Matiello M, Weinshenker BG, Wingerchuk DM, Lucchinetti C, Shuster E, et al. Treatment of neuromyelitis optica with mycophenolate mofetil: retrospective analysis of 24 patients. Arch Neurol. 2009;66 9:1128–33. https://doi.org/10.1001/archneurol.2009.175.
16. Gong J, Qiu W, Zeng Q, Liu X, Sun X, Li H et al. Lack of short-chain fatty acids and overgrowth of opportunistic pathogens define dysbiosis of neuromyelitis optica spectrum disorders: a Chinese pilot study. Multiple sclerosis (Houndmills, Basingstoke, England). 2019;25 9:1316–25; https://doi.org/10.1177/1352458518790396.
17. Pandit L, Cox L, Malli C, D'Cunha A, Rooney T, Lokhande H, et al. Clostridium bolteae is elevated in neuromyelitis optica spectrum disorder in India and shares sequence similarity with AQP4. Neurology(R) Neuroimmunol Neuroinflammation. 2021;8(1). https://doi.org/10.1212/nxi.0000000000000907.
18. Cree B, Spencer C, Varrin-Doyer M, Baranzini S, Zamvil S. Gut microbiome analysis in neuromyelitis optica reveals overabundance of Clostridium perfringens. Ann Neurol. 2016;80 3:443–7. https://doi.org/10.1002/ana.24718.
19. Wingerchuk D, Banwell B, Bennett J, Cabre P, Carroll W, Chitnis T, et al. International consensus diagnostic criteria for neuromyelitis optica spectrum disorders. Neurology. 2015;85(2):177–89. https://doi.org/10.1212/wnl.0000000000001729.
20. Benard-Seguin E, Costello F. Optic neuritis: current challenges in diagnosis and management. Curr Opin Neurol. 2023;36 1:10–8. https://doi.org/10.1097/wco.0000000000001128.
21. Lu JJ, Jia BJ, Yang L, Zhang W, Dong X, Li P, et al. Ultra-high performance liquid chromatography with ultraviolet and tandem mass spectrometry for simultaneous determination of metabolites in purine pathway of rat plasma. J Chromatogr B Analyt Technol Biomed Life Sci. 2016;1036–1037:84–92. https://doi.org/10.1016/j.jchromb.2016.09.023.
22. Trebst C, Jarius S, Berthele A, Paul F, Schippling S, Wildemann B, et al. Update on the diagnosis and treatment of neuromyelitis optica: recommendations of the Neuromyelitis Optica Study Group (NEMOS). J Neurol. 2014;261(1):1–16. https://doi.org/10.1007/s00415-013-7169-7.
23. Sellner J, Boggild M, Clanet M, Hintzen RQ, Illes Z, Montalban X, et al. EFNS guidelines on diagnosis and management of neuromyelitis optica. Eur J Neurol. 2010;17 8:1019–32. https://doi.org/10.1111/j.1468-1331.2010.03066.x.
24. Kimbrough DJ, Fujihara K, Jacob A, Lana-Peixoto MA, Leite MI, Levy M, et al. Treatment of Neuromyelitis Optica: review and recommendations. Mult Scler Relat Disord. 2012;1 4:180–7. https://doi.org/10.1016/j.msard.2012.06.002.
25. Wingerchuk DM, Lennon VA, Lucchinetti CF, Pittock SJ, Weinshenker BG. The spectrum of neuromyelitis optica. Lancet Neurol. 2007;6 9:805 – 15; doi: 10.1016/s1474-4422(07)70216-8.

26. Carnero Contentti E, Correale J. Association between Infections, the microbiome, vaccination, and neuromyelitis optica spectrum disorder. Mult Scler. 2023;29(4–5):492–501. https://doi.org/10.1177/13524585221113272.
27. Cui C, Ruan Y, Qiu W. Potential role of the gut microbiota in neuromyelitis optica spectrum disorder: implication for intervention. J Clin Neuroscience: Official J Neurosurgical Soc Australasia 2020;82 Pt B:193–9; https://doi.org/10.1016/j.jocn.2020.11.011.
28. Pawinski T, Durlik M, Szlaska I, Urbanowicz A, Majchrnak J, Gralak B. Comparison of mycophenolic acid pharmacokinetic parameters in kidney transplant patients within the first 3 months post-transplant. J Clin Pharm Ther. 2006;31 1:27–34. https://doi.org/10.1111/j.1365-2710.2006.00713.x.
29. Pillans PI, Rigby RJ, Kubler P, Willis C, Salm P, Tett SE, et al. A retrospective analysis of mycophenolic acid and cyclosporin concentrations with acute rejection in renal transplant recipients. Clin Biochem. 2001;34 1:77–81. https://doi.org/10.1016/s0009-9120(00)00196-x.
30. Emmanuel N, Ragunathan S, Shan Q, Wang F, Giannakou A, Huser N, et al. Purine nucleotide availability regulates mTORC1 activity through the Rheb GTPase. Cell Rep. 2017;19 13:2665–80. https://doi.org/10.1016/j.celrep.2017.05.043.
31. Lazzarino G, Amorini A, Petzold A, Gasperini C, Ruggieri S, Quartuccio M, et al. Serum compounds of Energy Metabolism Impairment are related to disability, Disease Course and Neuroimaging in multiple sclerosis. Mol Neurobiol. 2017;54 9:7520–33. https://doi.org/10.1007/s12035-016-0257-9.
32. Kuračka L, Kalnovičová T, Kucharská J, Turčáni P. Multiple sclerosis: evaluation of purine nucleotide metabolism in central nervous system in association with serum levels of selected fat-soluble antioxidants. Multiple Scler Int. 2014;2014:759808. https://doi.org/10.1155/2014/759808.
33. Shu Y, Li H, Zhang L, Wang Y, Long Y, Li R, et al. Elevated cerebrospinal fluid uric acid during relapse of neuromyelitis optica spectrum disorders. Brain and Behavior. 2017;7(1):e00584. https://doi.org/10.1002/brb3.584.
34. Wei Y, Wu D, Chen Y, Dong C, Qi J, Wu Y, et al. Population pharmacokinetics of mycophenolate mofetil in pediatric patients early after liver transplantation. Front Pharmacol. 2022;13:1002628. https://doi.org/10.3389/fphar.2022.1002628.
35. Taylor M, Flannigan K, Rahim H, Mohamud A, Lewis I, Hirota S, et al. Vancomycin relieves mycophenolate mofetil-induced gastrointestinal toxicity by eliminating gut bacterial β-glucuronidase activity. Sci Adv. 2019;5 8:eaax2358. https://doi.org/10.1126/sciadv.aax2358.
36. Simpson JB, Sekela JJ, Graboski AL, Borlandelli VB, Bivins MM, Barker NK, et al. Metagenomics combined with activity-based proteomics point to gut bacterial enzymes that reactivate mycophenolate. Gut Microbes. 2022;14(1:2107289). https://doi.org/10.1080/19490976.2022.2107289.
37. Khan MH, Onyeaghala GC, Rashidi A, Holtan SG, Khoruts A, Israni A, et al. Fecal β-glucuronidase activity differs between hematopoietic cell and kidney transplantation and a possible mechanism for disparate dose requirements. Gut Microbes. 2022;14(1:2108279). https://doi.org/10.1080/19490976.2022.2108279.
38. Cree BA, Spencer CM, Varrin-Doyer M, Baranzini SE, Zamvil SS. Gut microbiome analysis in neuromyelitis optica reveals overabundance of Clostridium perfringens. Ann Neurol. 2016;80 3:443–7. https://doi.org/10.1002/ana.24718.
39. Gong J, Qiu W, Zeng Q, Liu X, Sun X, Li H, et al. Lack of short-chain fatty acids and overgrowth of opportunistic pathogens define dysbiosis of neuromyelitis optica spectrum disorders: a Chinese pilot study. Mult Scler. 2019;25 9:1316–25. https://doi.org/10.1177/1352458518790396.
40. Liu C, Du P, Cheng Y, Guo Y, Hu B, Yao W, et al. Study on fecal fermentation characteristics of aloe polysaccharides in vitro and their predictive modeling. Carbohydr Polym. 2021;256:117571. https://doi.org/10.1016/j.carbpol.2020.117571.
41. Maier L, Pruteanu M, Kuhn M, Zeller G, Telzerow A, Anderson EE, et al. Extensive impact of non-antibiotic Drugs on human gut bacteria. Nature. 2018;555 7698:623–8. https://doi.org/10.1038/nature25979.
42. Nikolova VL, Smith MRB, Hall LJ, Cleare AJ, Stone JM, Young AH. Perturbations in Gut Microbiota Composition in Psychiatric disorders: a review and Meta-analysis. JAMA Psychiatry. 2021;78 12:1343–54. https://doi.org/10.1001/jamapsychiatry.2021.2573.
43. Huang S, Mao J, Zhou L, Xiong X, Deng Y. The imbalance of gut microbiota and its correlation with plasma inflammatory cytokines in pemphigus vulgaris patients. Scand J Immunol. 2019;90 3:e12799. https://doi.org/10.1111/sji.12799.
44. Yeh N, Hsu C, Tsai T, Chiu H. Gut Microbiome in Psoriasis is perturbed differently during secukinumab and Ustekinumab Therapy and Associated with response to treatment. Clin Drug Investig. 2019;39 12:1195–203. https://doi.org/10.1007/s40261-019-00849-7.
45. Shi Z, Qiu Y, Wang J, Fang Y, Zhang Y, Chen H, et al. Dysbiosis of gut microbiota in patients with neuromyelitis optica spectrum disorders: a cross sectional study. J Neuroimmunol. 2020;339:577126. https://doi.org/10.1016/j.jneuroim.2019.577126.

Publisher's Note

Springer Nature remains neutral with regard to jurisdictional claims in published maps and institutional affiliations.

证书号第4045937号

发明专利证书

发明名称：一种监测细菌生长的设备及监测方法

发 明 人：孙坚;李龚;刘雅红;廖晓萍;于洋;熊雁琼;姜雨微

专 利 号：ZL 2016 1 0375781.1

专利申请日：2016年05月30日

专利权人：华南农业大学

地 址：510642 广东省广州市天河区五山路483号

授权公告日：2020年10月23日　　授权公告号：CN 107460119 B

国家知识产权局依照中华人民共和国专利法进行审查，决定授予专利权，颁发发明专利证书并在专利登记簿上予以登记。专利权自授权公告之日起生效。专利权期限为二十年，自申请日起算。

专利证书记载专利权登记时的法律状况。专利权的转移、质押、无效、终止、恢复和专利权人的姓名或名称、国籍、地址变更等事项记载在专利登记簿上。

局长
申长雨

2020年10月23日

其他事项参见续页

证书号第4301676号

发明专利证书

发明名称：一种荧光菌株E.coli C600及构建方法与应用

发　明　人：孙坚;李龚;何玉张;苗媛媛;杨心怡;廖晓萍;刘雅红

专　利　号：ZL 2019 1 0355729.3

专利申请日：2019年04月29日

专利权人：华南农业大学

地　　址：510642 广东省广州市天河区五山路483号

授权公告日：2021年03月16日　　授权公告号：CN 110066820 B

国家知识产权局依照中华人民共和国专利法进行审查，决定授予专利权，颁发发明专利证书并在专利登记簿上予以登记。专利权自授权公告之日起生效。专利权期限为二十年，自申请日起算。

专利证书记载专利权登记时的法律状况。专利权的转移、质押、无效、终止、恢复和专利权人的姓名或名称、国籍、地址变更等事项记载在专利登记簿上。

局长
申长雨

2021年03月16日

其他事项参见续页

证书号第3912976号

发明专利证书

发明名称：基于mariner转座子构建自杀型质粒及耐药突变菌株的方法

发明人：孙坚;李龚;何玉张;刁晓苑;于泳鑫;刘雅红;廖晓萍

专利号：ZL 2019 1 0282837.2

专利申请日：2019年04月10日

专利权人：华南农业大学

地址：510642 广东省广州市天河区五山路483号

授权公告日：2020年07月31日　　授权公告号：CN 110079540 B

国家知识产权局依照中华人民共和国专利法进行审查，决定授予专利权，颁发发明专利证书并在专利登记簿上予以登记。专利权自授权公告之日起生效。专利权期限为二十年，自申请日起算。

专利证书记载专利权登记时的法律状况。专利权的转移、质押、无效、终止、恢复和专利权人的姓名或名称、国籍、地址变更等事项记载在专利登记簿上。

局长
申长雨

2020年07月31日

其他事项参见续页

证书号第4260282号

发明专利证书

发明名称：一株供体菌、其构建方法与应用以及质粒抑制剂筛选方法

发明人：孙坚;李龚;黄昊旻;邹文瑾;吉俊柔;刁晓苑;江颖琳
何玉张;廖晓萍;刘雅红

专利号：ZL 2019 1 0355278.3

专利申请日：2019年04月29日

专利权人：华南农业大学

地址：510642 广东省广州市天河区五山路483号

授权公告日：2021年02月19日　　授权公告号：CN 110129246 B

国家知识产权局依照中华人民共和国专利法进行审查，决定授予专利权，颁发发明专利证书并在专利登记簿上予以登记。专利权自授权公告之日起生效。专利权期限为二十年，自申请日起算。

专利证书记载专利权登记时的法律状况。专利权的转移、质押、无效、终止、恢复和专利权人的姓名或名称、国籍、地址变更等事项记载在专利登记簿上。

局长
申长雨

2021年02月19日

其他事项参见续页

证书号第4258417号

发明专利证书

发明名称：基于IS26插入序列构建能表达荧光的自杀型质粒及菌株的方法

发 明 人：孙坚;何玉张;李龚;刘苹;江颖琳;许金霞;刘雅红;廖晓萍

专 利 号：ZL 2019 1 0282847.6

专利申请日：2019年04月10日

专利权人：华南农业大学

地 址：510642 广东省广州市天河区五山路483号

授权公告日：2021年02月19日　　授权公告号：CN 110117605 B

国家知识产权局依照中华人民共和国专利法进行审查，决定授予专利权，颁发发明专利证书并在专利登记簿上予以登记。专利权自授权公告之日起生效。专利权期限为二十年，自申请日起算。

专利证书记载专利权登记时的法律状况。专利权的转移、质押、无效、终止、恢复和专利权人的姓名或名称、国籍、地址变更等事项记载在专利登记簿上。

局长
申长雨

2021年02月19日

其他事项参见续页

证书号第4148521号

发明专利证书

发明名称：基于ISAp11插入序列构建能表达荧光的自杀型质粒及菌株的方法

发明人：孙坚;何玉张;李龚;郭亚亚;王晓佩;刘雅红;廖晓萍

专利号：ZL 2019 1 0282838.7

专利申请日：2019年04月10日

专利权人：华南农业大学

地址：510642 广东省广州市天河区五山路483号

授权公告日：2020年12月11日　　授权公告号：CN 110129349 B

国家知识产权局依照中华人民共和国专利法进行审查，决定授予专利权，颁发发明专利证书并在专利登记簿上予以登记。专利权自授权公告之日起生效。专利权期限为二十年，自申请日起算。

专利证书记载专利权登记时的法律状况。专利权的转移、质押、无效、终止、恢复和专利权人的姓名或名称、国籍、地址变更等事项记载在专利登记簿上。

局长
申长雨

2020年12月11日

其他事项参见续页

证书号第6291447号

发明专利证书

发明名称：一种基于IncQ型质粒泛宿主的功能基因递送载体、构建方法和应用

发　明　人：孙坚;周士迎;龙腾飞;李龚;何玉张;万磊;黄紫蕾
刘雅红;廖晓萍

专　　利　　号：ZL 2022 1 0710412.9

专利申请日：2022年06月22日

专利权人：华南农业大学

地　　址：510000 广东省广州市天河区五山路483号

授权公告日：2023年09月01日　　授权公告号：CN 115109791 B

国家知识产权局依照中华人民共和国专利法进行审查，决定授予专利权，颁发发明专利证书并在专利登记簿上予以登记。专利权自授权公告之日起生效。专利权期限为二十年，自申请日起算。

专利证书记载专利权登记时的法律状况。专利权的转移、质押、无效、终止、恢复和专利权人的姓名或名称、国籍、地址变更等事项记载在专利登记簿上。

局长
申长雨

国家知识产权局
2023年09月01日

其他事项参见续页

证书号第6633272号

发明专利证书

发 明 名 称：一种抑制耐药质粒水平转移的复合材料及其制备方法和应用

发　明　人：孙坚;万磊;李龚;夏丽娟;韦然;周士迎

专　利　号：ZL 2022 1 0766494.9

专利申请日：2022年07月01日

专 利 权 人：华南农业大学

地　　址：510000 广东省广州市天河区五山路483号

授权公告日：2024年01月19日　　授权公告号：CN 115337296 B

国家知识产权局依照中华人民共和国专利法进行审查，决定授予专利权，颁发发明专利证书并在专利登记簿上予以登记。专利权自授权公告之日起生效。专利权期限为二十年，自申请日起算。

专利证书记载专利权登记时的法律状况。专利权的转移、质押、无效、终止、恢复和专利权人的姓名或名称、国籍、地址变更等事项记载在专利登记簿上。

局长
申长雨

国家知识产权局
2024年01月19日

其他事项参见续页

证书号第7157712号

专利公告信息

发明专利证书

发 明 名 称：肉桂酸在制备耐药质粒接合转移抑制剂中的应用

专 利 权 人：华南农业大学

地　　址：510000 广东省广州市天河区五山路483号

发　明　人：孙坚;高昂;万磊;夏丽娟;李龚

专　利　号：ZL 2023 1 0146808.X　　授权公告号：CN 116267932 B

专利申请日：2023年02月20日　　授权公告日：2024年07月02日

申请日时申请人：华南农业大学

申请日时发明人：孙坚;高昂;万磊;夏丽娟;李龚

国家知识产权局依照中华人民共和国专利法进行审查，决定授予专利权，并予以公告。

专利权自授权公告之日起生效。专利权有效性及专利权人变更等法律信息以专利登记簿记载为准。

局长
申长雨

国家知识产权局
2024年07月02日

证书号第7856278号

专利公告信息

发明专利证书

发明名称：一种靶向肠道菌群筛选影响黄嘌呤氧化酶活性药物的方法

专利权人：华南农业大学

地　　址：510000 广东省广州市天河区五山路483号

发 明 人：孙坚;韦然;李龚;仁昊;夏丽娟;万磊;刘雅红;廖晓萍

专 利 号：ZL 2022 1 0799165.4　　授权公告号：CN 115232855 B

专利申请日：2022年07月08日　　授权公告日：2025年04月04日

申请日时申请人：华南农业大学

申请日时发明人：孙坚;韦然;李龚;仁昊;夏丽娟;万磊;刘雅红;廖晓萍

国家知识产权局依照中华人民共和国专利法进行审查，决定授予专利权，并予以公告。

专利权自授权公告之日起生效。专利权有效性及专利权人变更等法律信息以专利登记簿记载为准。

局长
申长雨

国家知识产权局
2025年04月04日

荣誉证书

HONORARY CREDENTIAL

李 梦：

您的作品在中国畜牧兽医学会兽医药理毒理学分会第十六次学术会议中被遴选为优秀论文。

中国畜牧兽医学会兽医药理毒理学分会

二〇二一年十二月十六日

中国畜牧兽医学会 兽医药理毒理学分会

荣誉证书

HONORARY CREDENTIAL

李龚 同志：

您的报告在 2025 年中国畜牧兽医学会动物营养学分会第八届青年学者学术研讨会中被遴选为优秀报告。

特颁此证，以资鼓励。

中国畜牧兽医学会动物营养学分会

二〇二五年十一月

Erasmus MC, Rotterdam, Netherlands

Colleen Lau

Australian National University Research School of Population Health, Canberra, Australia

Fabian Lean

Royal Veterinary College, London, United Kingdom

Marc Leandri

Versailles Saint-Quentin-en-Yvelines University, Versailles, France

Gong Li

South China Agricultural University, Guangzhou, Guangdong, China

Jiahai Lu

Sun Yat-Sen University, Guangzhou, Guangdong, China

应用证明

项目名称	畜禽耐药病原菌传播机制与防控关键技术研究		
应用单位	广东广垦畜牧集团股份有限公司		
通讯地址	广州市天河区粤垦路607号力达广场A2栋		
联系人	李结	电话	13822287099
应用成果起止时间	2022年2月-2025年6月		

具体应用情况：

我司是由广东省农垦集团公司控股，以养殖业尤其是养猪业为主的全产业链集团，是农业产业化国家重点龙头企业。荣获全国首批“无公害农产品示范基地农场”和原农业部“生猪标准化示范场”荣誉称号。集团旗下沃而多原种猪场入选为“国家生猪核心育种场”，广前原种猪场入选为“广东省省级生猪核心育种场”及“国家非洲猪瘟无疫小区”。集团拥有多个粤港澳大湾区“菜篮子”生产基地和供港澳活猪饲养基地。

我公司是《畜禽耐药病原菌传播机制与防控关键技术研究》项目的主要应用单位，主要应用成果是耐药基因传播示踪系统监测耐药性传播。在长期的耐药性监测中发现耐药基因已经完成动物-环境-人跨界面的水平传播，但耐药基因跨界面传播的规律不得而知。为此，本项目建立了复杂微生物群中耐药基因传播示踪系统CRISPR-AMRtracker，基于该系统明确在耐药基因能够在复杂微生物群中的多种菌属中高效转移。相关技术在我司27个养殖场中进行推广应用，对遏制耐药基因的传播提供了良好指示作用，有效提升了动物产品的质量与国际竞争力。

广东广垦畜牧集团股份有限公司

2025年11月05日